Crumb rubber modified bitumen
Experimental characterization and modelling

Wang, H.

Important note
To cite this publication, please use the final published version (if applicable).
Please check the document version above.

CRUMB RUBBER MODIFIED BITUMEN

Experimental characterization and modelling

Haopeng Wang

Crumb rubber modified bitumen:

Experimental characterization and modelling

Haopeng WANG

Crumb rubber modified bitumen:

Experimental characterization and modelling

Dissertation

for the purpose of obtaining the degree of doctor

at Delft University of Technology

by the authority of the Rector Magnificus Prof.dr.ir. T. H. J. J. van der Hagen

chair of the Board for Doctorates

to be defended publicly on

Monday 27 September 2021 at 17.30 hours

by

Haopeng WANG

Master of Engineering in Highway & Railway Engineering

Southeast University, China

born in Huai'an, China

This dissertation has been approved by the

promotors: Prof.dr.ir. S.M.J.G. Erkens and Prof.dr. A. Scarpas

copromotor: Dr. X. Liu

Composition of doctoral committee:

Rector Magnificus	chairperson
Prof.dr.ir. S.M.J.G. Erkens	Delft University of Technology, promotor
Prof.dr. A. Scarpas	Delft University of Technology, promotor
Dr. X. Liu	Delft University of Technology, copromotor

Independent members:

Prof.dr. A. Bhasin	University of Texas at Austin
Prof.dr. K. Kaloush	Arizona State University
Prof.dr. G. Airey	University of Nottingham
Prof.dr.ir. E. Schlangen	Delft University of Technology

Reserve member:

Prof.dr. S. J. Picken	Delft University of Technology

Dedicated to my family

Acknowledgements

When I touched upon this research topic at the beginning of my PhD study, I thought I would spend several tough and boring years because rubber asphalt was a well-studied and well-established research direction in the pavement engineering community. For a very long time, I did not realize a wonderful journey was just begun. Many people have supported me in different ways during this journey and I very much appreciate it.

First and foremost, I owe enormous gratitude to my promotors Prof. Tom Scarpas and Prof. Sandra Erkens for their supervision and guidance. Tom offered me a wonderful opportunity to work on this challenging topic with a group of talented researchers. He not only provided me with advanced technical resources ("brainfoods") but also encouraged me to participate in the scientific community. His attitudes and spirits towards research have unconsciously influenced me in developing my own academic career. Although involving in my research halfway, Sandra could always point out the problems in my research with sharp and difficult questions. I am thankful for her assistance, fruitful discussions and faith.

Secondly, I would like to express my gratitude to my co-promotor as well as daily supervisor Dr. Xueyan Liu. Whenever I met problems in my research, Xueyan was the person I can always reach out to. He accompanied me in solving various issues I encountered during my study, from writing to publishing, from experiment to theory. I am grateful for his tremendous help and support.

I also would like to thank my Master supervisor Prof. Jun Yang at Southeast University for her continuous supports and care for both my study and life.

"If I have seen further, it is by standing on the shoulders of giants." My sincere thanks also go to all my colleagues in the pavement engineering section for their encouragement and support. I thank Katerina Varveri for her valuable comments on my research. I also thank Anupam Kumar and Cor Kasbergen for our discussions on mechanics and many other things during the countless coffee breaks. In particular, I want to thank my officemates Panos Apostolidis, my best Greek friend, and Hong Zhang for their valuable contributions to my research. Their extensive knowledge in physical chemistry and mechanics have inspired me throughout the research and made my PhD journey smooth.

It was also a great pleasure to work with Ruxin Jin, Peng Lin, Tianchi Tang, Zhaojie Sun, Lili Ma, Shisong Ren and Daniel Akinmade, to share the joys and worries. The secretaries and laboratory technicians of our section always provided a strong support network. I would like to thank Claudia Baltussen and Jacqueline Barnhoorn for tackling the administration issues. I am also thankful to Michèle van Aggelen and Marco Poot for helping me with the laboratory work.

"*Thy friendship makes us fresh*." I would like to thank my buddy, my brother, Dr. Guoyang Lu. The joy we had, the concern we shared, and the wine we drank, will eventually converge on the paths we have walked. I am also fortunate to have a group of lovely friends in Delft who have been supporting me and accompanying me in these years. Many thanks to Senlei Wang, Yunlong Guo, Pan Zhang, Cong Xiao, Xiuxiu Zhan, Jin Chang and many others for our lasting friendship.

Haopeng Wang 王昊鹏

August 2021 in Hong Kong

Contents

1

Introduction

1.1 Warm mix rubberized asphalt concrete

According to the European Environment Agency report in 2015, the transport sector contributed 25.8 % of the total European Union greenhouse gas (GHG) emissions (EEA 2017). With the Paris climate agreement taking effect, the global transport sectors have been facing growing international pressure on the reduction of GHG emission and fossil fuel consumption. In the Netherlands, to combat climate change, the Dutch government issued a highly ambitious Climate Law in 2019 (Directorate-General for Climate and Energy 2019). The Climate Law sets clear GHG emission reduction targets and introduces an innovative mechanism of an annual review to ensure that these targets are met by the Dutch government. Specifically, the Dutch government aims to (i) reduce the GHG emissions in the Netherlands by 49% by 2030 from 1990 levels, (ii) further achieve a 95% reduction of GHG emission by 2050, and (iii) realize 100% carbon neutral electricity in 2050.

Among the transport infrastructure, the road construction is always a large consumer of energy and resource. In view of this, developing sustainable paving technologies with fewer consumptions of resource and energy as well as fewer emissions of GHG while still meeting the demand for construction efficiency and improved pavement performance is a great concern for both transport agencies and the general public. This also coincides with the concept of global sustainable development (Mebratu 1998, Schleussner *et al.* 2016). According to a report from the Modified Asphalt Research Centre (Miller and Bahia 2009), a sustainable pavement may be defined as "*a pavement that minimizes environmental impacts through the reduction of energy consumption, natural resources and associated emissions while meeting all performance conditions and standards.*" Sustainable considerations in paving industry are not new, but in recent years, significant efforts are being made to realize the sustainability of pavement engineering in a more systematic and scientific way.

Meanwhile, with the development of transportation infrastructure and associated increase in the number of vehicles, approximately one billion of end-of-life tires (ELTs) are produced every year (WBCSD 2010). The rising environmental awareness has driven people to seek appropriate treatment and disposal of scrap tires, such as retreading, energy recovery and material recycling. In 2013, 96% of the waste tires (3.6 million tonnes) were recovered and recycled in the EU (Scott 2016), which confirms the EU as a leading role in the waste management. Material recycling is the most common means of managing ELTs in the EU and has been gaining more and more attention due to the lower processing costs and additional benefits (Sienkiewicz *et al.* 2012, Torretta *et al.* 2015). From a materials science point of view, the tire is made up of elastomeric compound, fabric and metal. The ELTs may be wastes for the tire industry, but they are still valuable raw materials for other applications. In civil engineering, bitumen modification with crumb rubber modifier (CRM) from ELTs, which is mainly the elastomeric compound, has been successfully applied in the paving industry since last century because of the economic benefits and environmental concerns (Lo Presti 2013). The rubberized asphalt concrete (RAC) technology not only solves the disposal issues of scrap tires but also improves the overall performance of asphalt pavements with add-on value (Shu and Huang 2014). Rubberized asphalt concrete has been proved to have improved aging resistance, greater resistance to fatigue/thermal cracking and rutting, lower noise generation, and high skid resistance. The above improved engineering performance eventually leads to improved durability and lower maintenance costs of asphalt pavements (Lo Presti 2013, Shu and Huang 2014). However, there are some concerns in using crumb rubber modified bitumen (CRMB) due to its high viscosity, such as poor pumpability, mixability and workability as

well as the high heat energy consumption during the production stage in the asphalt plant. In addition, due to the requirements of higher mixing and compaction temperatures, the production of rubberized asphalt mixtures increases GHG emissions and produces more asphalt fumes and volatile organic compounds (VOCs). The compromised work conditions for labors at the construction site of rubberized asphalt pavement are also criticized (Farshidi *et al.* 2013). Furthermore, if the compaction temperature is not high enough due to uncertain factors, the use of rubberized mixes will result in inadequate volumetric properties (i.e., higher air voids and uneven density distribution) and poor short-term and long-term performance (Akisetty 2008).

How to properly solve the above issues of rubberized asphalt concrete material has been concerned by pavement engineers for a long time until the appearance of warm mix asphalt (WMA) technology. Historically, the vast majority of highways and roads are constructed with hot mix asphalt (HMA). It is a consensus that the temperatures for the production of HMA, including manufacturing, transport and laying, should be roughly above 140 °C (Hurley and Prowell 2006). In order to reduce the GHG emission and the consumption of fossil fuels during the whole production and construction phase of asphalt concrete mixes, WMA has been proposed and implemented in asphalt paving technology without compromising the workability and mechanical performance of the material in comparison to HMA (Prowell D. *et al.* 2012). WMA are mixes that are manufactured and constructed at lower temperatures (100-140 °C) than HMA varying depending on the different utilized technologies. Besides the benefits of reduced emissions and energy consumption, WMA technologies also provide better working conditions, longer hauling distances, quicker turnover to traffic, an extended paving window, and less restrictions in non-attainment areas, as well as improved workability and compaction efficiency (Rubio *et al.* 2012).

Under these circumstances, coupling rubberized asphalt with warm mix technology will be of great significance. WMA technology is supposed to decrease mixing and compaction temperatures of the rubberized asphalt, making them comparable to or even lower than those of conventional HMAs (Hicks *et al.* 2010, Oliveira *et al.* 2013, Gandhi *et al.* 2014). Combining WMA with RAC technology not only reduces the production and compaction temperatures but also provides better working conditions with reduced odours and fumes. With synthesized properties of WMA and RAC, warm mix rubberized asphalt concrete (WarmRAC) is believed to be a promising and sustainable paving technology with many advantages, such as energy conservation, environmental protection, performance optimization and durability extension (Yu *et al.* 2017, Wang *et al.* 2018, Cao *et al.* 2019).

Previous studies have summarized the best practices and recent research findings on WarmRAC, including mix design, construction techniques, performance evaluation, recycling feasibility, and environmental and economic benefits (Wang *et al.* 2018). Based on the review and analysis, following conclusions and speculations can be drawn: (1) Generally, WarmRAC can use the same mix design methodology of conventional HMA with slight modifications, such as aggregate gradation, bitumen content, etc., based on specific WarmRAC product. (2) WMA technology is an aid to RAC pavement from the standpoint of construction. Construction techniques of conventional HMA with slight modifications can be successfully applied to WarmRAC. (3) The performance of WarmRAC is comparable to conventional HMA. Although there are some uncertainties of WarmRAC, it still meets the requirements or standards for typical HMA. (4) It is feasible to recycle WarmRAC using available technologies and equipment without adverse effects on environment and human beings. (5) WarmRAC can significantly reduce the emissions and energy consumption with insignificant negative impact on environment. Moreover, it is speculated that WarmRAC will maximize the additional value of waste tires, eliminating the

potential risks to environment under improper disposition. (6) Although WarmRAC has a higher initial cost than conventional HMA, it is believed to be more cost-effective based on the preliminary life cycle cost analysis.

As mentioned before, WarmRAC is a relatively new paving technology. The research findings to date about WarmRAC are positive and encouraged. Contractors continue to find new benefits from the use of WarmRAC. However, there remain a number of areas where additional evaluation, development, and research regarding WarmRAC are required. Further considerations are recommended as follows. (1) Both chemical and physical interaction mechanisms between bitumen and crumb rubber should be investigated for material selection and quality control. (2) The interactions between CRMB and WMA technology chemistry at various length scales (e.g., binder, mastic, mortar and mixture) should be further evaluated in terms of both performance and emission properties. (3) Long-term performance of WarmRAC should be documented and evaluated with the collaboration between different departments to realize its environmental, economic and social benefits. (4) A closer involvement of local and national government bodies with policies or regulations supporting will stimulate the development of this sustainable paving technology in both industry and academia. Education and training for related researchers, designers and workers are also required for the successful application of WarmRAC in asphalt pavements.

1.2 Research questions and objectives

Based on the literature review, it can be found that there is not a systematic methodology to characterize the complex properties of WarmRAC. The interaction mechanisms of the constituent materials are still unclear. The novelty and the main objective of this thesis is the development of chemo-physio-mechanical methodologies and test procedures for investigating the interaction mechanisms of the constituent materials and characterizing the performance of CRMB with WMA additives. In order to accomplish these objectives, a combination of dedicated laboratory tests and numerical modelling techniques will be utilized. Specifically, the following research questions (RQs) will be answered:

RQ1. What is the bitumen-rubber interaction mechanism?

RQ2. How to characterize the swelling process of rubber in bitumen, both experimentally and numerically?

RQ3. How to optimize the preparation procedure of CRMB?

RQ4. What are the effects of WMA additives on the properties of CRMB?

RQ5. What are the performance characteristics of CRMB containing WMA additives in terms of rutting, fatigue cracking, thermal cracking, aging, storage stability, etc.?

RQ6. How to predict the viscoelastic properties of CRMB, based on the answers to previous questions?

1.3 Thesis outline

This dissertation consists of eight chapters that intend to cover the most fundamental aspects of crumb rubber modified bitumen. Figure 1.1 presents the thesis structure. After the introductory chapter, a literature review on bitumen-rubber system is carried out to provide the theoretical basis of following chapters. Laboratory swelling tests of rubber in bitumen determines the

necessary parameters for the numerical rubber swelling model. With the further understanding of bitumen-rubber interaction mechanisms, both experimentally and numerically, the preparation procedures of CRMB are optimized and its chemo-physio-mechanical properties are characterized. Furthermore, long-term performance of binders, which are concerned by practitioners, are evaluated systematically. Micromechanical modeling utilizes the previous determined parameters of constituents and provides a robust prediction of the viscoelastic properties. Finally, main conclusions are summarized, and further research and practices are also recommended.
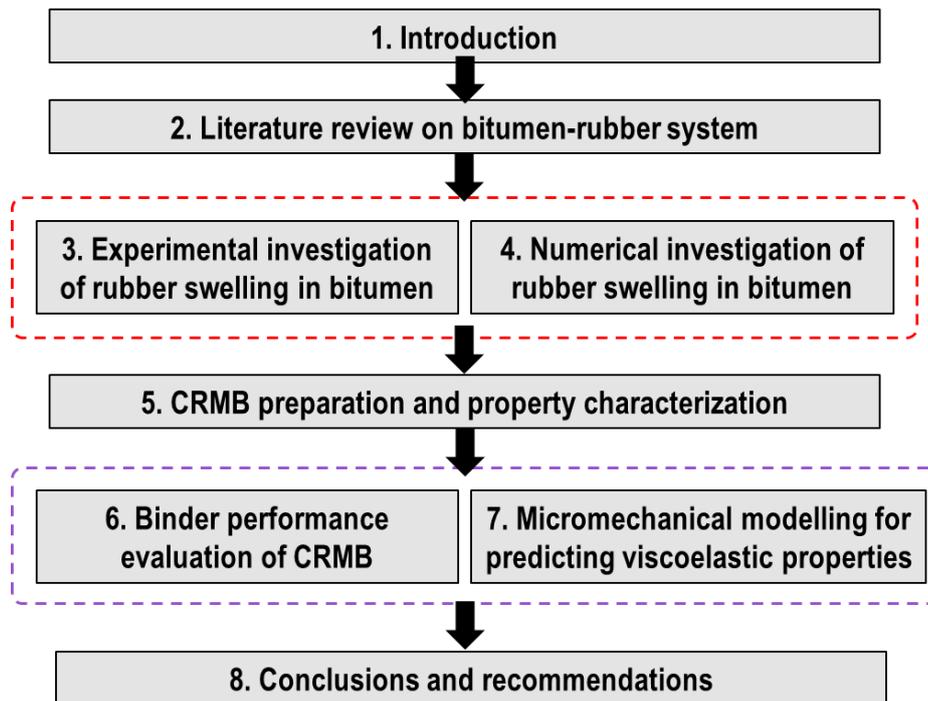
Figure 1.1 Thesis structure.

- Chapter 1 introduces the concept of warm-mix rubberized asphalt concrete. It also states the objectives of this research and provides the outline of this thesis.
- Chapter 2 focuses on a less discussed but crucial topic, namely, the interaction mechanisms between bitumen and rubber at different conditions from the viewpoint of polymer science by considering the thermodynamics and kinetics. It is an attempt to establish a theoretical framework for the rubber-bitumen interaction process as a tool to optimize the binder properties. (RQ1)
- Chapter 3 investigates the kinetics of bitumen diffusion into cylindrical rubber samples cut from scrap truck tires, the equilibrium swelling characteristics of rubber and the mechanical properties of rubber before and after swelling at different high temperatures. (RQ2)
- Chapter 4 develops a modeling methodology capable to simulate the rubber swelling process in bitumen. The mass diffusion and volume expansion phenomena of the rubber are incorporated in a multi-physics tool to predict the rubber swelling in bitumen. The model is calibrated with data generated from previous studies proving the reliability of the tool to evaluate the various influential factors on the design of rubberized bituminous materials with the desired properties and subsequently performance. (RQ2)

- Chapter 5 mainly includes two parts. The first part investigates the bitumen-rubber interaction at various mixing combinations of temperature and time to determine the optimized interaction condition. The second part investigates the binder rheological behaviour and its chemical interpretation from the perspective of activation energy and molecular weight distribution. (RQs 3&4)
- Chapter 6 systematically evaluates the long-term performance of CRMB containing warm-mix additives, i.e., high-temperature, low-temperature and fatigue performance, aging behaviours and storage stability. A unified DSR method is used to provide performance-related specifications for binders. (RQ 5)
- Chapter 7 consists of two stages. The first stage aims to examine the applicability and prediction accuracy of four common micromechanical models (the dilute model (DM), the Mori-Tanaka model (MTM), the self-consistent model (SCM), the generalized self-consistent model (GSCM)) for predicting the complex shear modulus of CRMB with different rubber contents. The second stage aims to further improve the prediction accuracy by amending the existing models or proposing new models. (RQ6)
- Chapter 8 concludes this thesis by providing a summary of findings and conclusions and giving an outlook for future research and practice to enable more successful and extensive applications of rubberized asphalt materials.

1.4 References

Akisetty, C., 2008. *Evaluation of warm asphalt additives on performance properties of crm binders and mixtures.* Clemson University.

Cao, R., Leng, Z., Yu, H. & Hsu, S.-C., 2019. Comparative life cycle assessment of warm mix technologies in asphalt rubber pavements with uncertainty analysis. *Resources, Conservation and Recycling,* 147, 137-144.

Directorate-General for Climate and Energy, 2019. National climate agreement of the netherlands. *In* Climate Department ed. The Hague.

Eea, 2017. Greenhouse gas emissions from transport. *In* European Environment Agency ed. Denmark: European Environment Agency.

Farshidi, F., Jones, D. & Harvey, J.T., 2013. *Warm-mix asphalt study: Evaluation of rubberized hot- and warm-mix asphalt with respect to emissions.* Davis, California, USA.

Gandhi, T., Wurst, T., Rice, C. & Milar, B., 2014. Laboratory and field compaction of warm rubberized mixes. *Construction and Building Materials,* 67, 285-290.

Hicks, R.G., Dingxin, C. & Teesdale, T., 2010. *Assessment of warm mix technologies for use with asphalt rubber paving applications.* California, USA.

Hurley, G.C. & Prowell, B.D., 2006. Evaluation of potential processes for use in warm mix asphalt. *Journal of the Association of Asphalt Paving Technologists,* 75 (4), 41-85.

Lo Presti, D., 2013. Recycled tyre rubber modified bitumens for road asphalt mixtures: A literature review. *Construction and Building Materials,* 49, 863-881.

Mebratu, D., 1998. Sustainability and sustainable development: Historical and conceptual review. *Environmental impact assessment review,* 18 (6), 493-520.

Miller, T.D. & Bahia, H.U., 2009. Sustainable asphalt pavements: Technologies, knowledge gaps and opportunities. Wisconsin, USA: Modified Asphalt Research Center.

Oliveira, J.R., Silva, H.M., Abreu, L.P. & Fernandes, S.R., 2013. Use of a warm mix asphalt additive to reduce the production temperatures and to improve the performance of asphalt rubber mixtures. *Journal of Cleaner Production,* 41, 15-22.

Prowell D., B., Hurley C., G. & Frank, B., 2012. *Warm mix asphalt: Best practice.* Lanham, MD, USA.

Rubio, M.C., Martínez, G., Baena, L. & Moreno, F., 2012. Warm mix asphalt: An overview. *Journal of Cleaner Production,* 24, 76-84.

Schleussner, C.-F., Rogelj, J., Schaeffer, M., Lissner, T., Licker, R., Fischer, E.M., Knutti, R., Levermann, A., Frieler, K. & Hare, W., 2016. Science and policy characteristics of the paris agreement temperature goal. *Nature Climate Change,* 6 (9), 827-835.

Scott, E., 2016. *End-of-life tyre report 2015.* Brussels, Belgium: Association, E.T.a.R.M.

Shu, X. & Huang, B.S., 2014. Recycling of waste tire rubber in asphalt and portland cement concrete: An overview. *Construction and Building Materials,* 67, 217-224.

Sienkiewicz, M., Kucinska-Lipka, J., Janik, H. & Balas, A., 2012. Progress in used tyres management in the european union: A review. *Waste Management,* 32 (10), 1742-51.

Torretta, V., Rada, E.C., Ragazzi, M., Trulli, E., Istrate, I.A. & Cioca, L.I., 2015. Treatment and disposal of tyres: Two eu approaches. A review. *Waste Management,* 45, 152-60.

Wang, H., Liu, X., Apostolidis, P. & Scarpas, T., 2018. Review of warm mix rubberized asphalt concrete: Towards a sustainable paving technology. *Journal of Cleaner Production,* 177, 302-314.

Wbcsd, 2010. *End-of-life tires: A framework for effective management systems.* Conches-Geneva, Switzerland.

Yu, H., Leng, Z., Zhou, Z., Shih, K., Xiao, F. & Gao, Z., 2017. Optimization of preparation procedure of liquid warm mix additive modified asphalt rubber. *Journal of Cleaner Production,* 141, 336-345.

2

Review on the Role of Thermodynamics and Kinetics in the Bitumen-Rubber System

2.1 Introduction of bitumen-rubber system

Crumb rubber is recycled rubber with a granular consistency produced from ELTs through removing the steel and tire cord (fluff) and mechanical grinding. Crumb rubber modifier (CRM), whose size is usually ranging from 0.075 mm to 4.75 mm, is the name originally utilized by the State of California Department of Transportation (2003) to identify rubber particles ground from ELTs for bitumen modification.

There are two primary methods of incorporating CRM into hot mix asphalt (HMA), which are generally referred to as dry process and wet process. In the dry process, CRM is mixed directly with the aggregate prior to introducing the required binder during hot-mix asphalt production. The CRM acts as a partial replacement of stone aggregates in the asphalt mixture. In the wet process, CRM is blended with bitumen and a predetermined reaction time is required before mixing the modified binder with aggregates. According to the different wet processing technologies (State of California Department of Transportation 2003, Lo Presti 2013, Shu and Huang 2014), rubberized asphalt has various technical terminologies, such as Asphalt Rubber (AR), Terminal Blend (TB), Crumb Rubber Modified Binder (CRMB), etc.

AR is defined as a blend of bitumen, recycled tire rubber and certain additives in which the minimum rubber content is 15% by weight of the total blend. The blend is reacted at high temperatures until sufficient swelling of rubber particles is achieved. TB is actually a preparation technique where finely ground CRMs are blended with hot bitumen at the refinery or at the binder storage and distribution terminal. CRMB is a general term to identify any bituminous binder modified via CRM. Rubberized asphalt concrete has been successfully applied in paving industries for decades thanks to the development of paving technologies (Lo Presti 2013). The incorporation of CRM into HMA improves the overall pavement performance and yields also intangible benefits, e.g., noise reduction, higher skid resistance (Wang *et al.* 2018). Most of these improvements are attributed to the interaction of crumb rubber and bitumen which leads to changes in binder composition and microstructure (Gawel *et al.* 2006, Attia and Abdelrahman 2009, Ghavibazoo and Abdelrahman 2013).

Previous researchers have done extensive literature reviews (Lo Presti 2013, Shu and Huang 2014, Wang *et al.* 2017a, Wang *et al.* 2017b, Wang *et al.* 2018) of rubberized asphalt regarding the production technology, mix design methodologies, performance characterization and specifications, storage and transport stability, construction technologies, environmental and economic impact assessment, etc. However, most of the conclusions drawn in the previous studies were based on laboratory tests and lack of fundamental explanations, which invariably limit their further application.

This chapter focuses on a less discussed but crucial topic, namely, the interaction mechanisms between bitumen and rubber at different conditions from the viewpoint of polymer science by considering thermodynamics and kinetics of rubber swelling in bitumen. It is an attempt to establish a theoretical framework for the rubber-bitumen interaction process as a tool to optimize the binder properties.

2.2 Chemistry of raw materials: bitumen and crumb rubber

2.2.1 Composition of bitumen

Bitumen is not a polymeric material but a complex mixture consisting of hydrocarbons of different size, polarity and aromaticity. It may also contain small amounts of heteroatoms, such as sulphur (0~9 wt.%), nitrogen (0~2 wt.%), oxygen (0~2 wt.%) and traces of metals (e.g., vanadium and nickel). The number-average molecular weight of bitumen generally ranges from 600 to 1500 Daltons and therefore, bitumen molecules cannot be considered as macromolecules in the polymeric sense. Given the highly complex molecular structure of bitumen, it is almost impossible to conduct detailed chemical analysis. Even though bitumen consists of a continuum of similar molecules, to facilitate classification and the understanding of its properties based on dominant molecular group types, bitumen molecules are generally classified into different molecular groups depending on their size and solubility in polar, aromatic or non-polar solvents.

The widely accepted SARA (saturates, aromatics, resins and asphaltenes) fractions, developed based on the selective adsorption-desorption (chromatographic) method (Lesueur 2009), are used to describe the relative quantities of these components in bitumen. The physiochemical properties of bitumen and the SARA fractions are compiled in Table 2.1 (Daly 2017). Bitumen can be described as a colloidal dispersion of high molecular weight asphaltene micelles in the low molecular weight maltenes (saturates, aromatics, resins) (Lesueur 2009). The solubility model is also often used to describe the chemistry of bitumen where the asphaltenes are dissolved in the maltenes rather than dispersed (Redelius 2004). The key aspect of the solubility model is that there is no gap in chemical properties between the fractions of bitumen which are considered as a continuous range of molecules with respect to size, polarity and aromaticity (Redelius and Soenen 2015). The colloidal structure and solubility parameter of bitumen influences its rheology and interactions with different polymers.

Table 2.1 Physiochemical properties of bitumen and the SARA fractions (Daly, 2017; Lesueur, 2009)

	Weight percentage (%)	H/C ratio	Molecular weight (g/mol)	Density at 20 °C (g/cm^3)	Solubility parameter (MPa$^{0.5}$)	T$_g$ (°C)	Solvent used for separation
Bitumen	100	1.5	600-1500	1.01-1.04	17.2-18.8	-20 (-40~5)	-
Saturates	5-15	1.9	470-880	0.9	15-17	-70	n-heptane
Aromatics	30-45	1.5	570-980	1	17-18.5	-20	toluene and toluene/methanol
Resins	30-45	1.4	780-1400	1.07	18.5-20	-	trichloroethylene
Asphaltenes	5-20	1.1	800-3500	1.15	17.6-21.7	-	n-heptane insoluble

2.2.2 Compositions of tire rubber

As mentioned before, the crumb rubber used for bitumen modification is recycled from waste tires. In order to fulfil their end-use properties, the composition of tires is very complex. Table 2.2 summarizes the detailed tire ingredients used for different vehicle types in the EU. Normally,

during the handling and shredding processes, the reinforcing wires and fibres are removed to produce a clean and highly consistent rubber material for bitumen modification.

Table 2.2 Composition comparison of different tires in the EU, adapted from (ETRMA, 2016)

Ingredients	Car type	Truck type	OTR type
Rubber/Elastomers	47%	45%	47%
Carbon black	21.5%	22%	22%
Metal	16.5%	25%	12%
Textile	5.5%	0%	10%
Zinc Oxide	1%	2%	2%
Sulphur	1%	1%	1%
Additives	7.5%	5%	6%

Note: OTR=off-the-road

In general, truck and off-the-road (OTR) tires contain higher proportions of natural rubber than passenger car tires. Natural rubber (NR) and synthetic rubber (SR) have different interactions with bitumen at the same conditions. This explains why the tire source can have considerable influence on the properties of CRMB binders (Frantzis 2004, Artamendi and Khalid 2006).

NR is industrially obtained from the latex of the tree called Hevea Brasiliensis and it is essentially a hydrocarbon polymer. The main constituent of NR is the polymer cis-1,4-polyisoprene with a molecular weight of 10^5 to 10^6 Daltons. As can be seen in Figure 2.1a, macromolecules of NR are long, regular, flexible and practically linear. In contrast, SR is any artificial rubber, synthesized from petroleum by-products through a polymerization process. The most common SR used in tire manufacturing is styrene-butadiene rubber (SBR) shown in Figure 2.1b derived from the copolymerization of styrene (C_8H_8) and butadiene (C_4H_6). The properties of SBR are influenced not only by the micro- and macrostructure of polymer chains, but also the styrene/butadiene ratio.

NR and SBR polymers used in tire manufacturing possess similar glass transition temperatures of approximately -70 °C (Burfield and Lim 1983). During polymer production, polymers are usually heated well above the glass transition temperature to allow casting, moulding and extrusion into desired forms. Considering that the typical tire moulding temperature is around 177 °C during the manufacturing process (Mark *et al.* 2013), it is common to observe the interaction/mixing temperature of rubber and bitumen is often chosen ranging from 180 to 220°C. In this temperature range, the polymer chains of rubber change from rigid glassy regions to flowable melt regions. Due to the high chain mobility of rubber, continuous phases of rubber network can be established in the bitumen matrix.

(a)
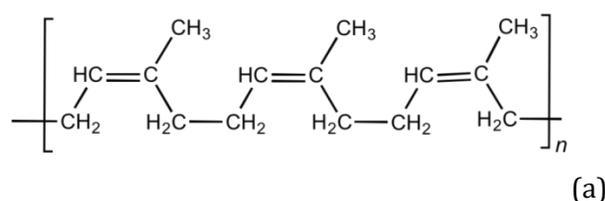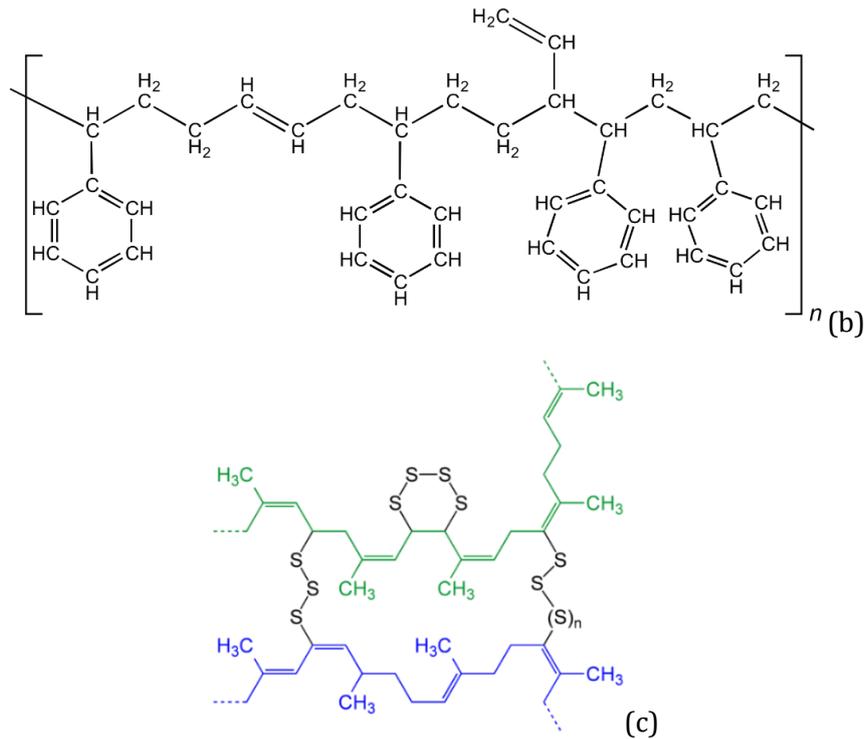
Figure 2.1 Chemical structure of (a) cis-polyisoprene, (b) copolymer SBR and (c) crosslinking after vulcanization, adapted from (Mark 2009).

To improve the durability and mechanical properties of rubber, vulcanization is applied to most rubber polymers by forming chemical crosslinks between individual polymer chains to create three-dimensional networks (Mark *et al.* 2013). The most commonly used curative during the vulcanization process is sulphur. Figure 2.1c shows the formation of crosslink between two strands (blue and green) of natural rubber after vulcanization with elemental sulphur (Mark 2009). Vulcanization can effectively increase the retractive force and reduce the amount of permanent deformation remaining after removal of the force.

During the tire rubber manufacturing process, various additives and ancillary substances necessary for vulcanization are added to improve the overall physical properties. Carbon black and amorphous silica are added into rubber as reinforcing fillers, which can significantly improve the anti-abrasion property and the material strength and hardness. Other additives, including activator accelerator (zinc oxide), coagulants, antioxidants, colour pigments, surfactants, softeners (oils), etc., are added in the tire manufacturing process to improve the tire properties and workability.

Thermogravimetric analysis (TGA) is a useful and reliable tool for material composition analysis (Cui *et al.* 1999). Figure 2.2 presents a typical TGA curve of a tire rubber sample. It provides quantitative and/or qualitative information about the main component and their concentrations in the sample based on the decomposition temperature and mass loss (Cui *et al.* 1999). As shown in Figure 2.2, the main components of tire rubber include oily and volatile substances, natural and synthetic rubber, inorganic fillers, carbon black and residual ash. TGA can also be used for monitoring the change of rubber during the bitumen-rubber interaction process (Ghavibazoo and Abdelrahman 2013).
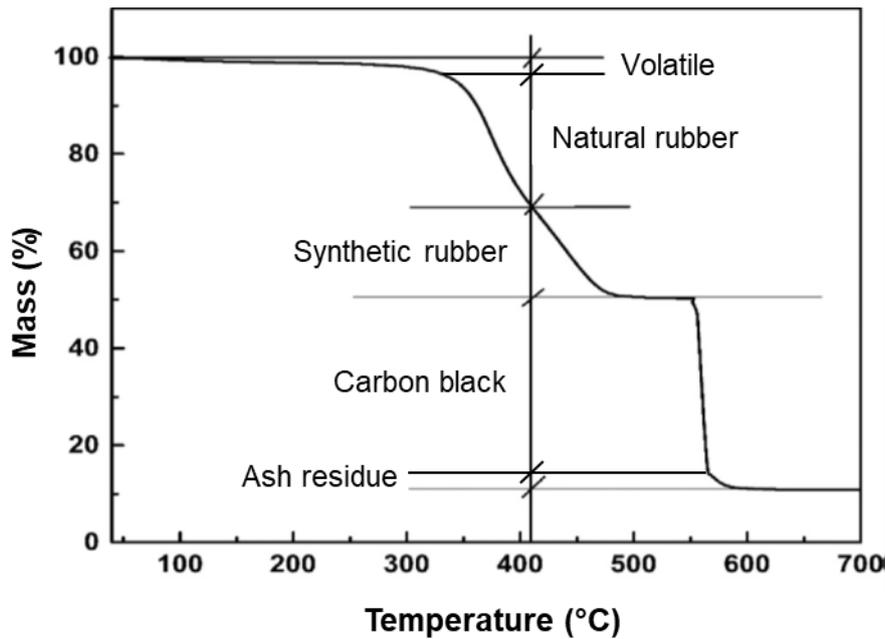
Figure 2.2 Typical TGA curve of crumb rubber from scrap tires

2.3 Bitumen-rubber system and interaction process

Typically, CRMB is produced by mixing bitumen and rubber at an elevated temperature for a certain period. The bitumen-rubber interaction controls the property development of CRMB and has great influence on binder transport and storage. There are two main stages which occur during the interaction process: rubber swelling and degradation (Abdelrahman and Carpenter 1999, Wang *et al.* 2017a).

2.3.1 Rubber swelling

Swelling of polymers is a volume expansion process of the polymeric network due to absorption of solvents. Uncrosslinked polymers, Figure 2.3a, when exposed to suitable solvents, can be easily swollen up and eventually may dissolve into the solvent. The dissolution aspects of this process will be discussed in the following section.

The dissolution of an uncrosslinked polymer into a solvent involves two phenomena, i.e., solvent diffusion-induced swelling and chain disentanglement (Tu and Ouano 1977). For crosslinked polymeric systems in which links between chains or segments are established, Figure 2.3b, because of the constraints of the network structure, the network might be swollen by absorbing solvents but the dissolution will hardly occur. Limited swelling is a characteristic property of polymers with network structures (Flory and Rehner Jr 1943). As clarified in the previous section, tire rubber contains a large portion of vulcanized/crosslinked polymers and a small portion of uncrosslinked polymers. Therefore, swelling of tire rubber in organic solvents is a partial dissolution process (Stroup-Gardiner *et al.* 1993, Artamendi and Khalid 2006). Depending on the compatibility between rubber and solvents, the swelling extent and dissolution rate may vary. When mixing rubber with bitumen at high temperatures, the light fractions of bitumen will diffuse into the rubber network and cause its swelling. The volume change of rubber particles and formation of gel layer adjacent to the rubber-bitumen interface reduces the inter-particle distance

and changes the component proportions of the remaining bitumen and, therefore, stiffens the composite material.

(a)   (b)

Figure 2.3 Schematic representation of the molecules of (a) the uncrosslinked polymer and (b) the crosslinked polymer (links are pictured as knots), adapted from (Mark et al. 2013).

2.3.2 Chemical degradation

Under severe interaction conditions (excessively high mixing temperature with high shear and long mixing times), rubber network degradation occurs. Even though the network structure formed by crosslinking prevents the dissolution of rubber molecules, the high thermal energy and shearing energy induced in the mixing process will destroy the crosslinking and hence the rubber network. This process involves the scission of disulfide bond (S-S), carbon–sulfur bond (C-S) and carbon-carbon bond (C-C), which eventually results in the breakage of crosslinked bonds and backbone chain bonds reducing thus the average molecular weight of rubber (Zanzotto and Kennepohl 1996). This degradation process is referred as devulcanization and depolymerization respectively (Abdelrahman and Carpenter 1999).

The average bond energies of different bonds are listed in Table 2.3 (Chemistry LibreTexts Library 2017). Based on the relative bond energies of S-S, C-S and C-C bonds (with the order of C-S < S-S < C-C), the S-S bond or C-S bond is less stable than C-C bond in the presence of chemical and thermal attacks. Therefore, the scission of S-S and S-C takes place earlier and destroys the network formed by crosslinking. That is why during the mixing process of bitumen-rubber blend at high temperatures, acrid smell from sulfoxide may be detected.

The rubber network degradation removes the constraints for the polymer chains. The free rubber polymer chains will eventually dissolve into bitumen. The mixing energy imposed by the mixer during interaction offers extra forces rather than diffusion, therefore accelerating the swelling process of rubber particles and enhancing the size-reduction effects. The chemical degradation of rubber networks is adverse to the mechanical property development of binders (Tang *et al.* 2016, Yao *et al.* 2016) but beneficial to improve the binder storage stability (Lo Presti *et al.* 2018).

Table 2.3 Average bond energies of chemical bonds typically in CRMB

Bond name	C-C	C-S	S-S
Bond energy (kJ/mol)	347	259	266

2.3.3 Exchange of other components

The previous two sub-sections discussed the behavior of rubber polymer when interacting with bitumen. However, in reality, tire rubber is a mixture of different components. During the bitumen-rubber interaction process, oily components, carbon black and some inorganic fillers bound to rubber are also released under high interaction temperatures and mixing forces. Considering the large proportion of these non-polymer components, the effects of their release into bitumen on the binder properties cannot be ignored. It was reported that these non-polymer components significantly influence the aging and rheological properties of CRMB (Ghavibazoo *et al.* 2015, Wang *et al.* 2019b).

2.3.4 Summary

The interaction stages of bitumen-rubber can be divided into four stages as shown in Figure 2.4 (Wang *et al.* 2017a). Stage 0: *Initial configuration*. Rubber particles are just immersed in the fluid bitumen. Stage 1: *Swelling phase*. Rubber particles start swelling by absorbing the light fractions of bitumen and form a gel layer adjacent to the bitumen-rubber interface. Stage 2: *Post-swelling and beginning of degradation*. The swelling of rubber particles continues. Meanwhile, chemical degradation takes place through the breakup of the crosslinked network and polymer chains. Swollen rubber particles are split into smaller ones due to the destruction of the network structure. Stage 3: *Degradation and complete dissolution*. The degradation of rubber particles continues progressing until they are completely dissolved into the bitumen matrix, which produces a homogenous binder.
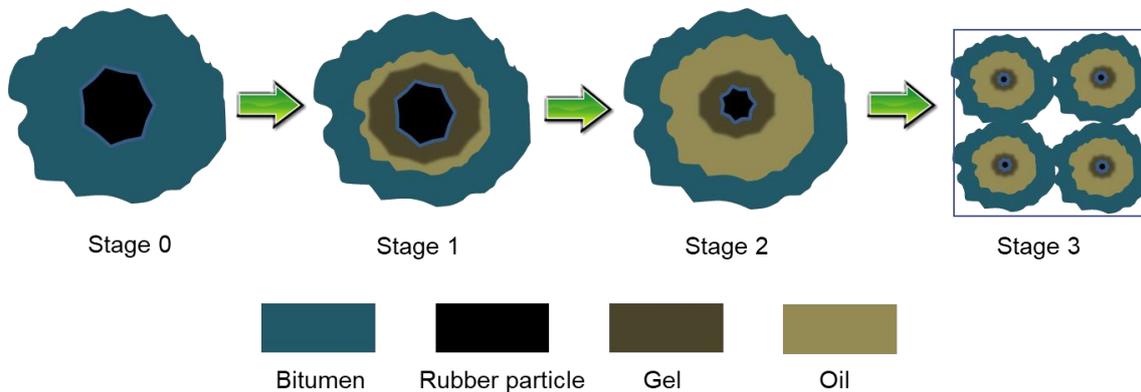
Figure 2.4 Interaction stages of bitumen and rubber adapted from (Wang et al. 2017a).

It is noteworthy that the different interaction stages may overlap. The degradation of rubber network enhances the absorption of light components from bitumen to the remaining rubber for swelling. In turn, swelling also speeds up the degradation rate of rubber. In reality, there is a swelling gradient of rubber from the outer layer to inner core.

2.4 Theoretical considerations of bitumen-rubber interaction

2.4.1 Relationship between bitumen-rubber interaction and polymer dissolution in solvents

Looking back to the interaction between bitumen and rubber, it has similarities as the polymer dissolution process but is not identical to each other. In the following analysis, bitumen is

generally considered as the low molecular weight solvent while rubber is a polymer with high molecular weight. The complex composition of the rubber material increases the complexity of the interaction mechanism with bitumen. The uncrosslinked and crosslinked parts in rubber have different behaviours when interacting with bitumen. Combining the experimental findings in bitumen-rubber interactions and the knowledge of polymer dissolution, Figure 2.5 summarizes the interaction mechanisms of rubber with bitumen at different stages. The devulcanization process will break the crosslinks and make chain disentanglement happen. It should be emphasized that each interaction step does not necessarily follow the exact sequence as shown in Figure 2.5. In most instances, rubber swelling and degradation occur simultaneously because of the diversity of rubber particle size. Fine particles finish the swelling stage in a short time and start the degradation stage. Similarly, chain disentanglement, devulcanization and depolymerisation can also overlap.
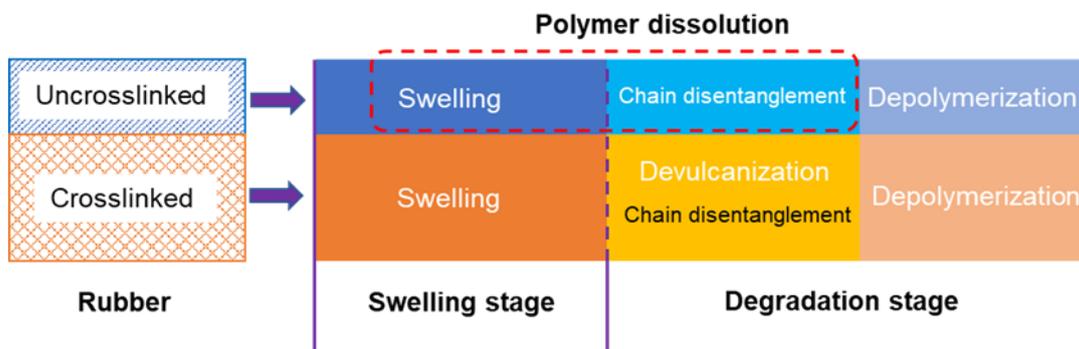
Figure 2.5 Interaction stages of rubber when mixed with bitumen.

In the following, the theoretical aspects of rubber swelling and degradation stages will be presented. As illustrated in Figure 2.5, polymer dissolution in solvents is actually a two-step process, which consists of: (a) diffusion-induced swelling of the polymer network and (b) chain disentanglement of the swollen polymer. The dissolution of a polymer in a solvent is usually a very slow process depending on the microstructure and chemical composition of a given polymer as well as the surrounding environment.

(a)   (b)   (c)
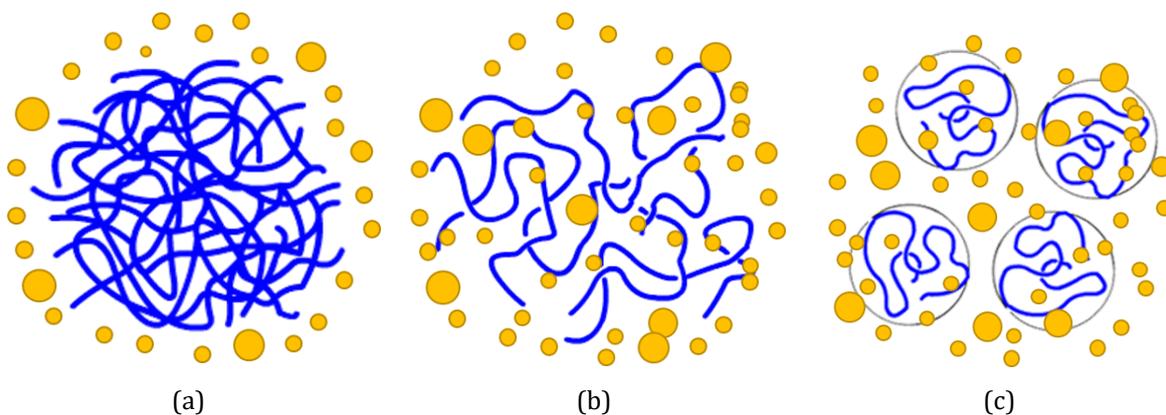
Figure 2.6 Schematic representation of the dissolution process for polymer molecules, blue lines represent polymer chains and yellow dots represent solvent molecules. (a) polymer molecules in solid state just after being added to a solvent; (b) a swollen polymeric gel; (c) solvated polymer molecules dispersed into a solution.

Figure 2.6 shows the dissolution process of an uncrosslinked polymer. Polymer molecules consist of long chains with large numbers of segments, forming tightly folded coils which are entangled to each other. When the polymer is just added into a thermodynamically miscible solvent, the coils still hold together as a solid due to the cohesive and attractive intra- and intermolecular forces, Figure 2.6a. Later on, due to polymer-solvent interactions, segments with polymer chains start to imbibe solvent molecules, increasing the volume of the polymeric network and forming a swollen polymeric gel, Figure 2.6b. The swollen gel exhibits elastic rather than plastic properties. Once all segments are solvated, the swelling reaches a critical point, beyond which the polymer chains start disentangling from the bulk. The loose/unfolded coils will slowly diffuse out of the swollen polymer gel and eventually disperse into the solution. When all the chain segments are dispersed into the solvent, the solvent molecules will fill the empty space between the loose segments, Figure 2.6c. This apparent volume occupied by the swollen polymer coil with the absorbed solvent is called hydrodynamic volume.

Therefore, there are two active mechanisms in this dissolution process as shown in Figure 2.7, i.e., solvent diffusion and chain disentanglement. When an uncrosslinked, amorphous, glassy polymer is in contact with a thermodynamically compatible solvent, the solvent will diffuse into the polymer. Due to plasticization of the polymer by the solvent, a gel-like swollen layer is formed along with two separate interfaces, one between the glassy polymer and gel layer (glassy-rubbery interface) and the other between the gel layer and the solvent (rubbery-solvent interface). As time passes, the rubbery-solvent interface moves towards the solvent while the glassy-rubbery interface moves towards the glassy part of the polymer. Eventually, the polymer is dissolved. When semicrystalline polymers are exposed to thermodynamically compatible solvents, the unfolding of the crystalline is an additional step accompanying solvent diffusion and chain disentanglement (Narasimhan 2001).
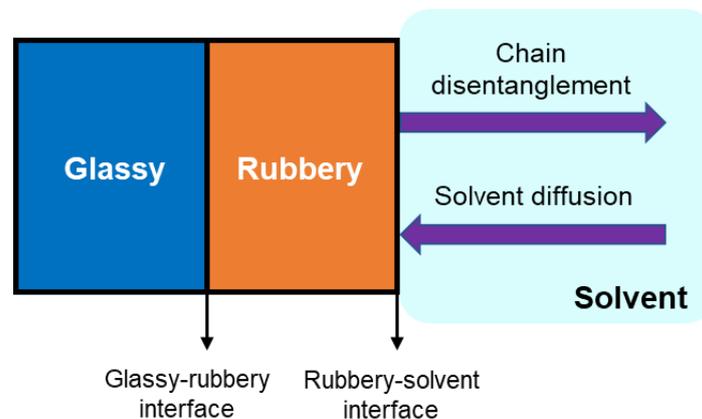
Figure 2.7 A schematic diagram of a one-dimensional solvent diffusion and polymer dissolution process adapted from (Narasimhan 2001).

To have more insights into the microstructural changes of the polymer during dissolution, Figure 2.8 displays the evolution of polymer chains from a molecular point of view.
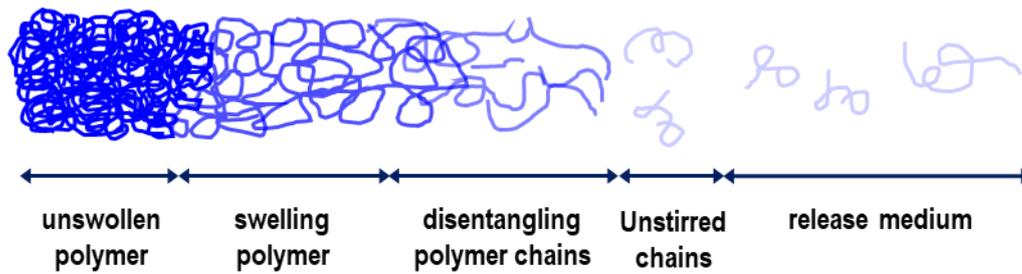
Figure 2.8 Polymer dissolution process at molecular scale.

Many researchers have proved the formation of a multilayer structure as shown in Figure 2.4 during the polymer dissolution process (Miller-Chou and Koenig 2003). The structure of the surface layer between the pure polymer and the pure solvent can be summarized as follows: the infiltration layer, the solid swollen layer, the gel layer and the liquid layer (Figure 2.9).

Figure 2.9 Schematic representation of the surface layer structure, adapted from (Miller-Chou & Koenig, 2003)

This structure classification is based on the glassy polymers. However, some of the layers may not be formed during dissolution depending on the polymer and solvent properties as well as the interaction conditions. Adjacent to the core of pure polymer is the infiltration layer. The solid swollen layer is established for the polymer-solvent system in the glassy state. When swelling equilibrium achieves, the penetrated solvent molecules start to push the polymer molecules into the solvent. During this transport process of polymer substance, chain disentanglement may happen as shown in Figure 2.7. In the gel layer, polymer chains start disentangling when the solvent concentration inside the polymer chain reaches the critical gel concentration (Peppas *et al.* 1994). At this moment, the two interfaces (polymer-gel and gel-solvent) proceed at the same velocity. As time passes, a more dilute upper layer called the liquid layer is formed to the direction of pure solvent. As the glassy-rubbery interface continues to move inward (to the direction of polymer core) in Figure 2.7, the glassy core gradually disappear. As a result, the rubbery-solvent interface keeps moving outward until the complete polymer dissolution is achieved (Vrentas and Vrentas 1998). Above is the schematic description of the polymer dissolution process. Several other models were also developed to explain the polymer dissolution behaviors: phenomenological models with diffusion equations (Tu and Ouano 1977), external mass transfer models (Lee and Peppas 1987), stress relaxation models with the reptation theory (Brochard and Degennes 1983), anomalous transport models and scaling laws (Peppas *et al.* 1994), continuum framework models (Narasimhan and Peppas 1996b).

The kinetics and thermodynamics framework of bitumen-rubber systems is discussed in the next sub-sections following the development of the various phenomena as presented in Figure 2.6.

2.4.2 Diffusion of bitumen into rubber

As mentioned above, when rubber networks are exposed to bitumen, certain fractions of the bitumen (mostly the low-molecular-weight maltenes) diffuse into and are imbibed by the polymer

network, causing its swelling. This diffusion process continues until the solvent concentrations inside and outside the polymer are equal to each other. Previous studies have shown that the Fickian model is most appropriate for describing the swelling of rubbery polymers (Papanu *et al.* 1989). The kinetics of bitumen diffusion into rubber is usually described by Fick's laws of diffusion (Artamendi and Khalid 2006, Wang *et al.* 2019a). Fick's second law predicts the evolution of bitumen concentration with time due to the progress of diffusion into rubber as:

$$\frac{\partial C}{\partial t} = \nabla \cdot D \nabla C \qquad (2.1)$$

where C is the concentration of diffusing substance; t is time; and D is the diffusion coefficient. For Fickian diffusion, it is obvious that the concentration gradient is the driving force for the diffusion process. However, for non-ideal systems including CRMB, the diffusion is often driven by the gradient of chemical potential, which can be described by the Cahn-Hilliard equation.

$$\frac{\partial \phi}{\partial t} = \nabla \cdot M \nabla \left(\frac{\partial F}{\partial \phi} \right) \qquad (2.2)$$

Where ϕ is the local polymer fraction; M is the mobility coefficient; and F is the total free energy of the system. The chemical potential is defined as $\partial F / \partial \phi$. The Cahn-Hilliard equation has a similar form to Fick's second law. In the system, the diffusion rate is positively correlated to the mobility coefficient. The Cahn-Hilliard equation is useful when considering the thermodynamics of swelling equilibrium.

There are many methods for measuring the diffusion of materials in polymers, such as the optical method, gravimetric method, vapour sorption, employing radioactive trace materials and interferometer procedures (Buckley and Berger 1962, Buckley *et al.* 1962). Because of the complexity and particularity of the combination of rubber and bitumen, the conventional gravimetric method is often used to monitor the diffusion process. Laboratory swelling tests with a rectangular rubber block have been done to obtain this parameter (Frantzis 2004, Artamendi and Khalid 2006, Feng *et al.* 2015). Following the initial linear region, it was found a clearly defined equilibrium plateau region occurred. For other geometrical rubber specimens, for instance, cylindrical specimens, the diffusion coefficient can be obtained through analytical solutions of one-, two-, three-dimensional diffusion models (Luo *et al.* 2017, Luo and Huang 2018).

2.4.3 Equilibrium swelling of rubber in bitumen

2.4.3.1 *The Flory-Rehner theory*

The classical benchmark theory for describing the swelling process in polymer gels is the Flory-Rehner theory (Quesada-Pérez *et al.* 2011). Based on this theory, the thermodynamic force of mixing (osmotic force) and the retractive force of the polymer chains (elastic force) are the two opposing forces competing to determine the swelling behaviour in gels. During swelling, each polymer network strand is stretched, and the crosslink junctions move further apart. Against the osmotic force, there is an opposite elastic force, which balances the stretching of the network and opposes its deformation. When the osmotic pressure is balanced by the elastic restraint, swelling reaches its equilibrium state (Ganji *et al.* 2010). According to the Flory-Rehner theory, the thermodynamic equilibrium of a gel is reached when the chemical potential of the solvent (designated by μ_b) is equal inside and outside the gel:

$$\mu_b^{in} = \mu_b^{out} \tag{2.3}$$

Using the concept of osmotic pressure (Π), Equation (2.3) can be rewritten in the following form:

$$\Pi = -\frac{\mu_b^{in} - \mu_b^{out}}{v_b} \tag{2.4}$$

v_b is the molar volume of bitumen. The osmotic pressure, defined as the rate of change of the total free energy of the polymer-solvent system, can be calculated using the following equation:

$$\Pi = -\frac{N_A}{v_b}\frac{\partial \Delta F}{\partial n_b} \tag{2.5}$$

where N_A is Avogadro's number; n_b is the number of bitumen molecules; ΔF is the change of Helmholtz free energy since the rubber-bitumen system is theoretically incompressible. The free energy change during the swelling process in the case of incompressible system is:

$$\Delta F_{total} = \Delta F_{mix} + \Delta F_{el} \tag{2.6}$$

where ΔF_{total} is the change of total free energy in the gel, ΔF_{mix} is the change of free energy of mixing and ΔF_{el} is the change of elastic free energy. Equilibrium swelling is achieved by minimization of the Helmholtz free energy. In the Flory-Rehner theory, the mixing free energy is formulated with the Flory-Huggins equation:

$$\Delta F_{mix} = n_b k_B T[\ln \phi_b + \chi \phi_r] \tag{2.7}$$

where k_B is the Boltzmann constant; T is the temperature; ϕ_b is the local volume fraction of solvent (bitumen); ϕ_r is the local volume fraction of rubber in a swollen state, defined by Equation (2.8); χ is the interaction parameter between the bitumen and rubber; n_b is the number of bitumen molecules.

$$\phi_r = \frac{V_0}{V} \tag{2.8}$$

Here V is the volume of the rubber gel (including the absorbed solvent within it) at a given state and V_0 is the volume of the dry rubber.

The simplest model that captures the idea of rubber elasticity is the affine network model (Flory 1950, Flory 1985), which assumes an affine deformation: the relative deformation of each network strand and the macroscopic relative deformation of the whole network are the same. The free energy required to deform a network mainly arises from the change of entropy associated to an isotropic deformation

$$\Delta F_{el} = -\frac{3}{2}v_e k_B T(\ln \alpha_s - \alpha_s{}^2 + 1) \tag{2.9}$$

where v_e is the number of effective chains in the network; α_s is the linear swelling ratio, which can be computed with the following equation by involving the molar volume of the solvent φ_b

$$\alpha_s{}^3 = \frac{V}{V_0} = (V_0 + \frac{\varphi_b n_b}{N_A})/V_0 \tag{2.10}$$

The chemical potential (Rubinstein and Colby 2003) of the bitumen in the rubber gel is defined as

$$\mu_b^{in} - \mu_b^{out} = N_A \left(\frac{\partial \Delta F_{mix}}{\partial n_b}\right)_{T,P} + N_A \left(\frac{\partial \Delta F_{el}}{\partial \alpha_s}\right)_{T,P} \left(\frac{\partial \alpha_s}{\partial n_1}\right) \tag{2.11}$$

Incorporating Equations (2.7)(2.9)(2.10) into Equation (2.11) yields

$$\mu_b^{in} - \mu_b^{out} = RT \left[\ln(1 - \phi_r) + \phi_r + \chi \phi_r{}^2 + \varphi_b \frac{v_e}{V_0}(\phi_r^{\frac{1}{3}} - \frac{1}{2}\phi_r)\right] \tag{2.12}$$

When reaching equilibrium, the chemical potential of the solvent inside and outside the swollen polymer will be equal to each other, which means the left side of Equation (2.12) will be cancelled. Rearranging Equation (2.12) gives

$$-\ln(1 - \phi_r) + \phi_r + \chi \phi_r{}^2 = \varphi_b \frac{v_e}{V_0}(\phi_r^{\frac{1}{3}} - \frac{1}{2}\phi_r) \tag{2.13}$$

The number of effective chains per unit volume can be linked with the specific volume of rubber $\bar{v}$ and the molecular weight of polymer chains between crosslinks M_c as follows

$$\frac{v_e}{V_0} = \frac{1}{\bar{v}M_c} \tag{2.14}$$

Recalling the definition of crosslink density v_x (Ganji $et\ al.$ 2010), which is a measure of crosslinked points per unit volume (mol/cm³), gives the final expression through further rearrangement

$$v_x = \frac{1}{\bar{v}M_c} = \frac{v_e}{V_0} = -\frac{\ln(1 - \phi_r) + \phi_r + \chi \phi_r{}^2}{\varphi_b(\phi_r^{\frac{1}{3}} - \frac{1}{2}\phi_r)} \tag{2.15}$$

The term $2M_c/M$ in common equation or calculating the crosslink density of polymers is eliminated due to the fact that the molecular weight of rubber (M) is much higher than M_c. It should be noted that the previous equations are derived for the crosslinked polymer system. For the polymer system with only entanglements, the number of moles of crosslinks can be replaced by the number of moles of entanglements (Papanu $et\ al.$ 1989, Narasimhan and Peppas 1996a). Then, similar calculations can be performed.

Ideally, through laboratory experiments, the swelling ratio of rubber $(q = V_0/V = 1/\phi_r)$ in certain solvents can be measured by different methods. In addition, with known values of the

Flory interaction parameter, both crosslink density and molecular weight between crosslinks can be further derived through Equation (2.15) when the solvent is determined. On the other hand, if the crosslink density of rubber and the Flory interaction parameter between rubber and bitumen are known in advance, the equilibrium swelling ratio of rubber in bitumen can be predicted.

2.4.3.2 *The Flory-Huggins parameter*

The Flory interaction parameter χ in Flory-Huggins equation for polymer solutions is of prime importance since it describes the thermodynamic state of polymer-solvent interaction in a given mixture. This parameter is used to characterize the difference of interaction energies in the mixture. If there is a net attraction between species from polymer and solvent (i.e. they like each other better than they like themselves), $\chi < 0$ and a single-phase mixture is favourable for all compositions. However, most often the situation is that a net repulsion exists between species (i.e. they like themselves more than each other) and this will oppose the mixing process. Therefore, the sign of the interaction parameter χ determines the energetic tropism for mixing, that is positive for opposing mixing, zero for ideal mixtures, and negative for promoting mixing (Rubinstein and Colby 2003).

Several methods (Liu and Shi 2008) such as vapor pressure lowering, osmometry, light scattering and inverse gas chromatography, were proposed to estimate the value of χ. However, these tests are generally time consuming and need cautious operations. Instead, with the help of solubility parameters, the interaction parameter can be rapidly estimated. The solubility parameter (δ) is a good indicator of solubility of a specific solvent. It is very useful to predict miscibility and compatibility of polymers. Liquids with similar solubility parameters will be miscible, and polymers will dissolve into solvents whose solubility parameters are close to their own (Rubinstein and Colby 2003). For non-polar, non-associating polymer-solvent system with species interacting mainly by dispersion forces, the interaction parameter χ can be estimated from the Hildebrand solubility parameters as (Hansen 2002):

$$\chi = \frac{v_1(\delta_1 - \delta_2)^2}{RT} + \beta \tag{2.16}$$

where v_1 is the molar volume of the solvent; δ_1 and δ_2 are the Hildebrand solubility parameters for the solvent and polymer respectively; R is the universal gas constant; T is the absolute temperature; β is an empirical constant. However, for complex polymer systems, the Hansen Solubility Parameters (HSP), which consider the non-polar/dispersion forces, the polar forces and hydrogen bonding forces, usually provides a better approximation. Previous studies have successfully applied the HSP to express the solubility and internal stability of bitumen (Redelius 2004). A similar equation to estimate the interaction parameter based on the HSP can be obtained (Hansen 2002)

$$\chi = \frac{v_1}{RT}\left[(\delta_{D1} - \delta_{D2})^2 + \frac{(\delta_{P1} - \delta_{P2})^2}{4} + \frac{(\delta_{H1} - \delta_{H2})^2}{4}\right] \tag{2.17}$$

where δ_D, δ_P and δ_H are respectively the dispersive, polar and hydrogen bonding components of the Hansen solubility parameters. Because polymers are not volatile, δ is often obtained through an indirect method in which polymers are mixed with a series of solvents of varying but known solubility parameters. The solubility parameter of the polymer is taken as the δ value of the

solvent which enables the maximum extent of swelling (Redelius 2000, Redelius 2004). Comparing to the average solubility parameter values, the solubility body of a material in the three-dimensional Hansen space is more realistic and useful (Zhu *et al.* 2019). Therefore, it is recommended to be used for illustrating the solubility relationship.

2.4.4 Disentanglement of rubber polymer chains

As discussed previously, polymer chains will disentangle if contacted with thermodynamically compatible solvents. Disentanglement occurs in a form of diffusional motions of chains out of the swollen polymer gel. The disentanglement of polymer chains can be described by the famous reptation model (de Gennes 1971). In the reptation model, an entangled chain diffuses along its confining tube as shown in Figure 2.10. The time needed for the chain to diffuse out of its original tube is the reptation time τ_{rep}. It is predicted to be proportional to the square of the chain size (radius of gyration) R_g divided by the reptation diffusion coefficient D_{rep}.

$$\tau_{rep} \sim \frac{R_g{}^2}{D_{rep}} \tag{2.18}$$

In the context of CRMB systems, it is important to know the rubber dissolution rate in bitumen to control the binder properties. The dissolution rate is related to the disentanglement rate r_{dis} of the polymer chain, which is taken to be proportional to the chain size divided by the reptation time. Thus,

$$r_{dis} \sim \frac{R_g}{\tau_{rep}} \sim \frac{D_{rep}}{R_g} \tag{2.19}$$

It is reported that R_g and D_{rep} can be related to polymer molecular weight and concentration (Papanu *et al.* 1989). Therefore, the disentanglement rate of rubber in bitumen can be expressed as (Papanu *et al.* 1989)

$$r_{dis} = \frac{A}{M_r{}^a \phi_r{}^b} \tag{2.20}$$

where A is an empirical constant; M_r is the molecular weight of rubber; a is related to the rubber molecular weight distribution and b is related to rubber concentration. Both a and b are larger than 1.
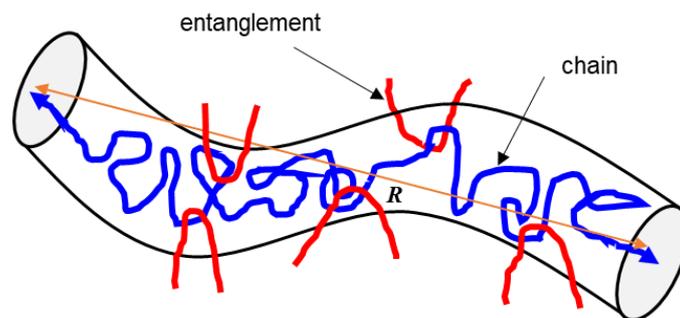
Figure 2.10 Reptation model for entangled polymer chains.

2.4.5 Chain scission of rubber network

As mentioned above, during the degradation process of rubber into bitumen, crosslinked bonds and main chain bonds will break up based on the interaction condition. For a three-dimensional crosslinked network of rubber, the chain scission reaction has three limiting cases: (a) chain scission at random; (b) cleavage of crosslinks and (c) directed scission. It was found that the soluble fraction of a network that has undergone scission can be linked to the effective number of chains in the gel fraction using a simple relationship (Horikx 1956). Specifically, the number of scissions can be measured by the soluble fraction of rubber in the degraded network. This offers an opportunity to monitor the rubber network degradation process in bitumen by measuring the dissolving fraction of rubber. The effective number of chains v_e can be determined by swelling measurements using Equation (2.15)(Flory and Rehner Jr 1944).

For the case of *chain scission at random*, the total number of crosslinks is assumed to be constant during the degradation reaction. Therefore, the following relationship in a rubber can be established.

$$1 - \frac{v_{e2}}{v_{e1}} = 1 - \frac{(1 - \sqrt{s_2})^2}{(1 - \sqrt{s_1})^2} \tag{2.21}$$

where s is the soluble fraction in the crosslinked rubber and v_e is the effective number of chains in the gel fraction (de Sousa *et al.* 2017). In the above equations as well as following equations, subscripts "1" and "2" respectively indicate the states before and after the degradation (chain scission reaction).

The soluble fraction in a polymer is given by (Charlesby 1953)

$$s = \frac{(2 + \gamma) - \sqrt{\gamma^2 + 4\gamma}}{2\gamma} \tag{2.22}$$

where γ is the crosslinking index of the whole polymer (average number of crosslinks per original chain). The crosslinking index can be calculated by

$$\gamma = \frac{v_e}{N} + 2 \tag{2.23}$$

where N is the number of primary molecules of polymer. Therefore, the number of chain scissions (n) of polymer is given by the difference of number of primary molecules after and before the degradation.

$$n = N_2 - N_1 = (v_e + 2N)\left(\frac{1}{\gamma_2} - \frac{1}{\gamma_1}\right) \tag{2.24}$$

For the case of *crosslinking scission*, no chain scission but only severance of crosslinks happens. Equation (2.21) becomes as follows

$$1 - \frac{v_{e2}}{v_{e1}} = 1 - \frac{\gamma_2(1 - \sqrt{s_2})^2}{\gamma_1(1 - \sqrt{s_1})^2} \tag{2.25}$$

Considering the difference between Equations (2.21) and(2.25), the number of scissions is equal to the number of severed crosslinks becomes

$$n = N_2 - N_1 = \frac{1}{2}N(\gamma_1 - \gamma_2) \tag{2.26}$$

For the case of *directed scission*, only those monomer units that are the nearest neighbours to a crosslink can undergo scission. Therefore, only qualitative conclusions can be drawn because of

the invalidity of the interchange of the crosslinking and scission reactions (Horikx 1956). To sum up, the number of scissions can be computed from the soluble fraction of a degraded network, as determined by the effective number of chains in the gel fraction with the help of swelling measurements.

2.5 Critical factors in practice and their theoretical bases

Similar to polymer modified bituminous binders, the interaction conditions and raw material characteristics will have a great impact on the rubber swelling and degradation process and consequently on the binder properties. A thorough understanding of these factors will guide the material selection and process optimization to obtain the desired properties from the modification.

2.5.1 Effect of interaction conditions

2.5.1.1 *Temperature*

Temperature has great influence on both bitumen and rubber as they are both temperature sensitive materials. When the temperature increases, both the mobility of bitumen molecules and rubber polymer chains increase, which enhances the diffusion process of bitumen into the rubber (Rubinstein and Colby 2003). The mobility and diffusion coefficients are highly dependent on temperature. From Equations (2.1) and (2.2), it can be found that at higher temperatures, the diffusion speed of bitumen into rubber and associated swelling rate of rubber greatly increase, which are also verified by experimental results (Green and Tolonen 1977, Artamendi and Khalid 2006, Wang *et al.* 2020a).

Table 2.4 summarizes the diffusion coefficients and equilibrium swelling data from different researchers. The mass uptake is the percentage of absorbed bitumen mass over the initial rubber mass. Theoretically, as the temperature increases, the equilibrium swelling extent of rubber decreases because the rubber network is harder to expand due to the entropy-driven retractive forces as the temperature increases (Mark 1981). However, experimental data usually show an increase in swelling with temperature, indicating other reactions which decrease the crosslink density may be occurring, i.e., chain disentanglement, devulcanization etc. (Green and Tolonen 1977). Moreover, the main conditioning parameter that influences the bitumen-rubber interaction is the temperature while interaction duration and mixing speed contribute significantly as well but with minor effects on the rubber dissolution mechanism (Ghavibazoo *et al.* 2013b).

Only when reaching certain temperatures, chemical degradation of rubber occurs. Depending on the CRM composition, chemical degradation starts at different temperatures. At an intermediate interaction temperature (e.g., 190°C), rubber dissolution in bitumen can happen with the help of high-speed mixing, which generates a more homogenous blend (Ghavibazoo *et al.* 2013b). On the other hand, a lower interaction temperature (e.g., 160°C) was not sufficient to trigger the formation of the three-dimensional network even at high mixing speeds. Also, a higher interaction temperature (e.g., 220~240 °C) led to the dramatic degradation of rubber in bitumen, hence the degradation of rheological properties of the modified blend (Ragab *et al.* 2013, Yao *et al.* 2016, Wang *et al.* 2020c).

Table 2.4 Diffusion coefficients and equilibrium mass uptake in rubber by absorbing bitumen.

Bitumen type	Temperature (°C)	Rubber type	Diffusion coefficient, $D \times 10^{-6}$ (mm²/s)	Equilibrium mass uptake (%)	Reference
100KSR	180	Car tire	0.759	75	Frantzis 2004
		Truck tire	0.764	125	
50KSR		Car tire	0.742	75	
		Truck tire	0.746	95	
100VEN		Car tire	2.243	90	
		Truck tire	3.647	150	
50VEN		Car tire	1.28	80	
		Truck tire	2.784	100	
100KSR	150	Car tire	3.80	70	Artamendi and Khalid 2006
		Truck tire	2.69	120	
	180	Car tire	5.30	75	
		Truck tire	4.15	120	
	210	Car tire	16.98	70	
		Truck tire	10.75	120	
50KSR	180	Car tire	5.30	75	
		Truck tire	4.52	95	
100VEN		Car tire	15.90	90	
		Truck tire	9.62	140	
50VEN		Car tire	8.55	80	
		Truck tire	8.04	95	
Pen 60/70	190	Natural rubber	5.96	165	Feng *et al.* 2015
Pen 70/100	160	Truck tire	2.54	115	Wang *et al.* 2020
	180		4.91	140	
	200		10.75	170	

* KSR means Kuwaiti origin; VEN means Venezuelan origin; 100 and 50 means the penetration grade.

2.5.1.2 *Time*

The interaction between bitumen and rubber is a continuous process which needs certain time to achieve desired properties. The properties of CRMB develop significantly during the early stage of interaction (e.g., the first 30 min). This coincides with the results of the diffusion process in which solvent diffuses into polymer faster at the early stage and slows down later until it reaches the plateau of diffusion curves. Through laboratory swelling tests using styrene–butadiene rubber sheets, the swelling extent increases enormously in the beginning and then reaches an equilibrium. However, as the swelling time increases, the crosslinking network of rubber is destroyed resulting in a decrease in crosslink density and an increase in the glass transition

temperature of rubber (Frantzis 2004, Artamendi and Khalid 2006, Dong *et al.* 2012). A decrease in apparent viscosity of the bitumen rubber system is noticed because of the destroyed rubber networks. Later, continuing extending the interaction time has minor effect on the physical properties of CRMB (Abdelrahman 2006).

To sum up, Figure 2.11 schematically plots the viscosity evolution curves of CRMB over time at different interaction temperatures (Abdelrahman 2006, Lo Presti and Airey 2013). At low interaction temperatures (around 160 °C), rubber swelling is dominating the interaction process, the viscosity keeps increasing until it reaches a plateau. At intermediate interaction temperatures (around 180 °C), the rubber first experiences a swelling stage and then a chemical degradation stage starts, which is reflected by the decreased viscosity. At high interaction temperatures (higher than 200 °C), rubber swelling finishes in a very short time and chemical degradation plays a dominant role during interaction. Different interaction temperatures correspond to different types of rubberized binder products, which can be determined based on the user requirements.
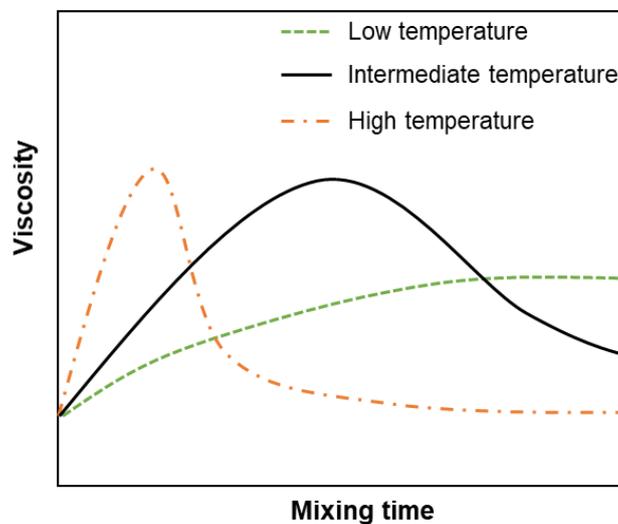
Figure 2.11 Viscosity evolution of CRMB over time at different interaction temperatures.

In addition, increasing the mixing speed has an equivalent effect as extending the mixing time. However, the effect of interaction time and mixing speed is highly dependent on the interaction temperature which has dominant effects during the processing. The other two parameters (i.e., mixing speed and time) can only facilitate the interaction process when the temperature meets the critical value (Ghavibazoo *et al.* 2013b). An ambiguous time-temperature superposition principle may exist, meaning increasing the interaction temperature can decrease the required mixing time to achieve comparable results.

2.5.1.3 *Mixer type*

The mixer type also influences the property development of CRMB. Conventionally, there are two types of mixers that exert the mechanical mixing energy during the bitumen modification process: the common blade type mixer and the high shear mixer. The mixing head varies with different application scenarios. The main difference is whether shearing energy is applied or not. Using high shear mixing can significantly reduce the rubber particle size, accelerating the interaction process. In addition, the exerted mixing energy can break the bonding between rubber particles and contribute to reducing the agglomeration (Celauro *et al.* 2012). Furthermore, carbon black and inorganic fillers attached on the rubber network are released into the bitumen under the high

shear force (Abdelrahman 2006, Attia and Abdelrahman 2009). It was reported that carbon black also tends to absorb the lightweight fraction of bitumen. The existence of carbon black in bitumen improves the anti-ageing, high-temperature performance and thermal conductivity (Cong *et al.* 2014, Wang *et al.* 2019b).

2.5.2 Effect of rubber particle characteristics

2.5.2.1 *Tire type*

The main difference between truck tires and car tires is the different proportions of natural rubber (NR), synthetic rubber (SR) and other ingredients they consist of. Truck tire rubber consists mainly of natural rubber, whereas car tire rubber consists of more synthetic rubber. From the chemical structure of different rubbers shown before, it can be found that SR with more complex network is less susceptible to degradation than NR. Also, it is easier for NR to swell in bitumen due to the relatively simple long-chain structure with less network constraints. Therefore, under the same interaction conditions, bitumen diffusion into truck-tire rubber is usually faster than into car-tire rubber and the equilibrium swelling extent of truck-tire rubber is also higher than car-tire rubber as reflected by the experimental data in Table 2.4 (Artamendi and Khalid 2006). From Equation (2.20), it can be found that polymers with higher molecular weight have a lower dissolution rate (Miller-Chou and Koenig 2003). This indicates that NR is also easier to be dissolved into hot bitumen than SR.

2.5.2.2 *Morphology and processing method*

There are two conventional methods of processing scrap tires: ambient grinding and cryogenic grinding. Ambient ground tire rubber particles usually have irregular shapes and porous appearance. In contrast, rubber particles produced through the cryogenic process are found to be more angular with smooth cracked surface. The surface area of ambient ground rubber particles is about twice larger than the cryogenic counterpart (Shen *et al.* 2009). Large specific surface area of rubber particles increases the chances of contact with bitumen, hence promoting the interaction with bitumen. The resulting faster absorption of light fractions from bitumen into rubber causes more swelling and enhances the binder properties (Billiter *et al.* 1997). Other studies also suggested that CRMB binders prepared with ambient ground crumb rubber exhibited higher viscosity and higher elasticity with higher complex modulus and lower phase angle (Shen and Amirkhanian 2007, Lee *et al.* 2008).

2.5.2.3 *Rubber particle size*

Regarding the size of crumb rubber particles, it has significant influence on its swelling kinetics and degradation into the bitumen, considering also that swelling is a result of a Fickian diffusion process. For one-dimensional diffusion, the following relationship can be derived from Equation (2.1).

$$\frac{M_t}{M_\infty} = \frac{4}{d}\sqrt{\frac{Dt}{\pi}} \tag{2.27}$$

where M_t and M_∞ represent the total mass of the diffused substance at time t and at equilibrium respectively; d is the sample thickness; and D is the diffusion coefficient. Therefore, the required interaction time for rubber with bitumen to achieve the same swelling ratio increases with the square of the particle size (Buckley and Berger 1962). Figure 2.12 shows the swelling ratio change

of different-size rubber particles (from 0.2 to 1.0 mm) from car tire rubber with time based on numerical simulation at 180 °C. Fine rubber particles require less time to react and thus swell faster and achieve the swelling equilibrium earlier than coarse rubber particles (Wang *et al.* 2019a).
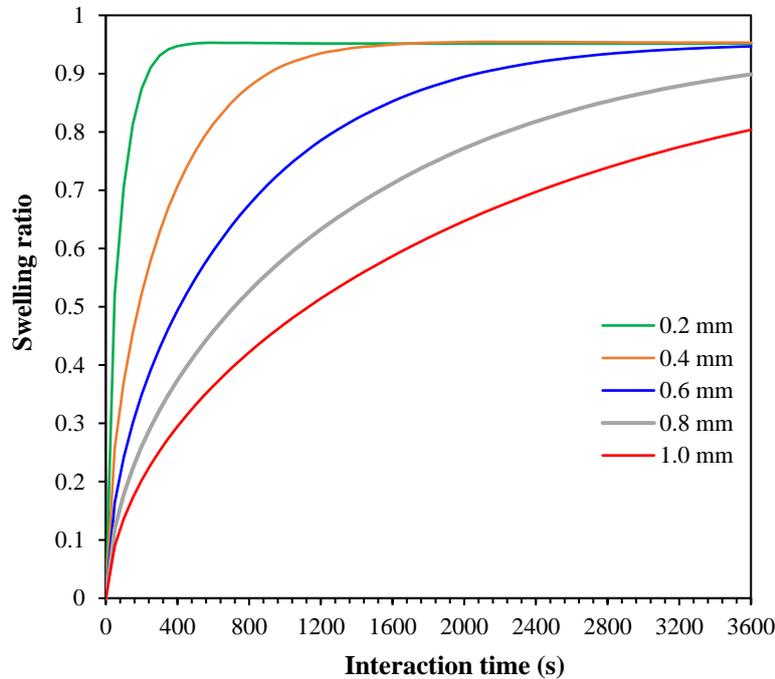
Figure 2.12 Swelling ratios of rubber particles of different sizes over the course of time.

Consequently, fine rubber particles also degrade faster, affecting the properties of the binder matrix by releasing the polymeric components. However, coarse rubber particles need more time to reach the swelling equilibrium. They have more influence on the CRMB binder properties due to their higher swelling volume. By contrast, they have less impact on the binder matrix because of their less degradation rate (Abdelrahman and Carpenter 1999). They also yield higher complex modulus/viscosity and lower phase angle values of CRMB than finer particles do under the same interaction conditions (Attia and Abdelrahman 2009, Shen *et al.* 2009). Reducing crumb rubber size can produce a more homogenous bitumen-rubber blend and improve the storage stability of binders (Ghavibazoo *et al.* 2013a). However, CRM with finer sizes significantly increases the cost because of the required additional grinding.

2.5.2.4 *Rubber particle content*

From the micromechanical theory of particulate filled composite materials, the particulate content is always of great importance to the mechanical properties of composite system. Many studies have confirmed that the rheological properties and performance-related parameters of CRMB are functions of the rubber content (Huang 2008, Lee *et al.* 2008). Unlike the common aggregate fillers which primarily have stiffening effects in bituminous binders, CRM particles also result in physiochemical interactions with bitumen which will alter both the bitumen composition and the rubber microstructure. From the multilayer structure of swollen rubber in Figure 2.9, the mechanical properties of rubber after swelling will be changed. Results show that swollen rubber is softer than dry rubber due to the absorption of bitumen and exhibits noteworthy viscoelasticity. Based on the micromechanical models, the reinforcing effect of CRM on the binders will be

enhanced with the increasing rubber content (Huang 2008, Medina and Underwood 2017, Wang *et al.* 2020b).

2.5.2.5 *Pre-treatment of CRM*

The pre-treatment of CRM particles influences the interaction efficiency between rubber and bitumen. As mentioned before, the crosslinks in rubber formed by vulcanization can significantly prevent the rubber from swelling by absorbing organic solvents. The concept of devulcanization is introduced as selective scission of crosslinks with negligible main chain scission. Therefore, CRM pre-treated with devulcanization can have a better interaction (swelling) with bitumen. Various devulcanization processes have been developed by the rubber industry, including thermo-chemical, thermo-mechanical, microwave, ultrasonic, biotechnological devulcanization (Joseph *et al.* 2016). Microwave (Ma *et al.* 2015) and ultrasonic methods (Xu *et al.* 2015) were reported to activate crumb rubber and promote the miscibility between bitumen and crumb rubber. CRMB prepared with activated crumb rubber exhibited superior storage stability and low-temperature performance. It is also common to use organic solvents to pretreat CRM to improve the miscibility (Subhy *et al.* 2015). Besides the physical treatment of CRM, chemical modification of CRMB was also achieved by adding activators or other chemicals. For instance, trans-polyoctenamer rubber (TOR) can promote the interaction between the sulfur in the rubber network and the sulfur within the asphaltenes (Liang *et al.* 2017). Polyphosphoric acid (PPA) can react with many functional groups in bitumen. It breaks the asphaltenes agglomerates and creates the possibility for better dispersion of asphaltenes in the maltenes phase, which allows for better interactions with rubber (Yadollahi and Mollahosseini 2011). This either enhances the performance of CRMB or increases the storage stability of CRMB.

2.5.3 Effect of bitumen characteristics

Bitumen from different crude oil sources usually has varying chemistry, with different SARA fractions. This will influence the compatibility with crumb rubber and, thereof the swelling of rubber. It is reported that the total solubility parameters of natural rubber and styrene-butadiene rubber (SBR) are around 16.9 $MPa^{0.5}$ and 18.1 $MPa^{0.5}$ respectively (Mark *et al.* 2013). In addition, solubility parameters for bitumens are in the range 17.2 to 18.8 $MPa^{0.5}$ (Zhu *et al.* 2019). Thus, the similarity between the solubility parameters of bitumen and natural and synthetic rubber indicates that bitumen is a swelling agent of both rubbers. Recalling the solubility parameters of different fractions of bitumen, then, theoretically, aromatics with a solubility parameter of 17-18.5 $MPa^{0.5}$ should have the highest miscibility with crumb rubber from scrap tires based on the classical "like dissolve like" compatibility principle. Therefore, in general, softer bituminous binders with lower molecular weight are more prone to diffuse into and absorbed within the rubber network (Artamendi and Khalid 2006). Various laboratory tests of preparing crumb rubber modified binders have validated the above statement. Among the same graded bitumens, the one with a higher fractions of maltenes yields a higher swelling extent of crumb rubber particles, leading to faster dissolution during the later interactions (Airey *et al.* 2004).

2.6 Summary and recommendations

The interaction between rubber and bitumen plays a very important role in controlling the properties of rubberized bituminous binders. From the viewpoint of polymer science, in the binary binder system, bitumen can be regarded as the low-molecular-weight solvent while rubber can be regarded as the polymer with high molecular weight. The bitumen-rubber interaction at

high temperatures is generally a rubber dissolution process (which consists of swelling and chain disentanglement) and a chemical degradation process. In principle, the rubber swelling process can be systematically modelled by the Flory-Rehner theory in combination with the diffusion theory. The chain disentanglement of the swollen polymer network is a subsequent process to swelling. The chemical degradation of rubber in bitumen mainly includes the chain scission reactions which are observed as devulcanization and depolymerization. Admittedly, it is of great difficulty to do quantitative analysis on the model in the context of rubber swelling in bitumen since both rubber and bitumen are very complex systems instead of pure substances. However, the fundamental knowledge in polymer-solvent interaction is still of great importance to understand the interaction process and guide the material selection and process optimization to obtain desired binder properties.

The effects of interaction conditions (temperature, time and mixing energy) and raw material characteristics (rubber type, particle size, particle content, pre-treatment, etc.) were analysed based on the proposed theoretical framework in subsection 2.4. These critical factors can fundamentally alter the bitumen-rubber interaction parameters, and consequently the binder properties. In view of the diversity of raw materials (bitumen and rubber) and varying demands of binder properties, it is difficult to draw any universal conclusion. However, the following recommendations are made in terms of specific application scenarios.

- Temperature is the dominant factor that determines the product type of rubberized binders. Different CRMB products can be produced by manipulating the interaction temperature ranges which correspond to different interaction mechanisms.
- To maximize the swelling effect of rubber in bitumen, bitumen with more maltenes (soft grade bitumen) and tire rubber with high natural rubber components should be chosen to create similarity in solubility parameters.
- Devulcanized rubber is encouraged to be used in bitumen modification to eliminate the acrid smell and to improve the mechanical property and storage stability of rubberized binders.

From the review, the following points are recommended and will be further examined in this study to enhance the understanding of this type of material and use it in a more rational way.

- The volumetric, chemical and mechanical properties of rubber in the blend during interaction should be monitored. The rubber in the blend undergoes multiple effects, including thermal aging, diffusion of bitumen, damage due to mechanical energy from mixing. It is useful to know the nature of rubber before and after interaction to control the binder properties and to predict its behavior in the long-term service.
- More dedicated laboratory tests should be done to establish a database for different bitumen-rubber systems, for instance, solubility parameters, diffusion coefficients, swelling coefficients, dissolution rates, etc.

2.7 References

Abdelrahman, M., 2006. Controlling performance of crumb rubber-modified binders through addition of polymer modifiers. *Transportation Research Record: Journal of the Transportation Research Board,* (1962), 64-70.

Abdelrahman, M.A. & Carpenter, S.H., 1999. Mechanism of the interaction of asphalt cement with crumb rubber modifier. *Transportation Research Record: Journal of the Transportation Research Board,* 1661, 106-113.

Airey, G., Rahman, M. & Collop, A.C., 2004. Crumb rubber and bitumen interaction as a function of crude source and bitumen viscosity. *Road Materials and Pavement Design,* 5 (4), 453-475.

Artamendi, I. & Khalid, H.A., 2006. Diffusion kinetics of bitumen into waste tyre rubber. *Journal of the Association of Asphalt Paving Technologists,* 75, 133-164.

Attia, M. & Abdelrahman, M., 2009. Enhancing the performance of crumb rubber-modified binders through varying the interaction conditions. *International Journal of Pavement Engineering,* 10 (6), 423-434.

Billiter, T., Davison, R., Glover, C. & Bullin, J., 1997. Production of asphalt-rubber binders by high-cure conditions. *Transportation Research Record: Journal of the Transportation Research Board,* (1586), 50-56.

Brochard, F. & Degennes, P., 1983. Kinetics of polymer dissolution. *PhysicoChemical Hydrodynamics,* 4 (4), 313-322.

Buckley, D.J. & Berger, M., 1962. The swelling of polymer systems in solvents. Ii. Mathematics of diffusion. *Journal of Polymer Science,* 56 (163), 175-188.

Buckley, D.J., Berger, M. & Poller, D., 1962. The swelling of polymer systems in solvents. I. Method for obtaining complete swelling–time curves. *Journal of Polymer Science,* 56 (163), 163-174.

Burfield, D.R. & Lim, K.L., 1983. Differential scanning calorimetry analysis of natural rubber and related polyisoprenes. Measurement of the glass transition temperature. *Macromolecules,* 16 (7), 1170-1175.

Celauro, B., Celauro, C., Lo Presti, D. & Bevilacqua, A., 2012. Definition of a laboratory optimization protocol for road bitumen improved with recycled tire rubber. *Construction and Building Materials,* 37, 562-572.

Charlesby, A., 1953. Solubility and molecular size distribution of crosslinked polystyrene. 11 (6), 513-520.

Chemistry Libretexts Library, 2017. *Bond energies* [online]. https://chem.libretexts.org/Textbook_Maps/Physical_and_Theoretical_Chemistry_Textbook_Maps/Supplemental_Modules_(Physical_and_Theoretical_Chemistry)/Chemical_Bonding/Fundamentals_of_Chemical_Bonding/Bond_Energies [Accessed Access Date 2018].

Cong, P., Xu, P. & Chen, S., 2014. Effects of carbon black on the anti aging, rheological and conductive properties of sbs/asphalt/carbon black composites. *Construction and Building Materials,* 52, 306-313.

Cui, H., Yang, J.L. & Liu, Z.Y., 1999. Thermogravimetric analysis of two chinese used tires. *Thermochimica Acta,* 333 (2), 173-175.

Daly, W.H., 2017. *Relationship between chemical makeup of binders and engineering performance.* Washington, DC, 978-0-309-39002-6.

De Gennes, P.G., 1971. Reptation of a polymer chain in the presence of fixed obstacles. *The Journal of Chemical Physics,* 55 (2), 572-579.

De Sousa, F.D.B., Scuracchio, C.H., Hu, G.-H. & Hoppe, S., 2017. Devulcanization of waste tire rubber by microwaves. *Polymer Degradation and Stability,* 138, 169-181.

Dong, D., Huang, X., Li, X. & Zhang, L., 2012. Swelling process of rubber in asphalt and its effect on the structure and properties of rubber and asphalt. *Construction and Building Materials,* 29, 316-322.

Feng, W., Minming, K., Guanlong, L., Xiaolong, Z. & Chenglie, L., 2015. Investigation of swelling and dissolution process of natural rubber in aromatic oil. *China Petroleum and Petrochemical Technology,* 17, 76-86.

Flory, P.J., 1950. Statistical mechanics of swelling of network structures. *The Journal of Chemical Physics,* 18 (1), 108-111.

Flory, P.J., 1985. Molecular theory of rubber elasticity. *Polymer Journal,* 17, 1-12.

Flory, P.J. & Rehner Jr, J., 1943. Statistical mechanics of cross-linked polymer networks ii. Swelling. *Journal of Chemical Physics,* 11, 521-526.

Flory, P.J. & Rehner Jr, J., 1944. Effect of deformation on the swelling capacity of rubber. *The Journal of Chemical Physics,* 12 (10), 412-414.

Frantzis, P., 2004. Crumb rubber-bitumen interactions: Diffusion of bitumen into rubber. *Journal of materials in civil engineering,* 16 (4), 387-390.

Ganji, F., Vasheghani-Farahani, S. & Vasheghani-Farahani, E., 2010. Theoretical description of hydrogel swelling: A review. *Iranian Polymer Journal,* 19 (5), 375-398.

Gawel, I., Stepkowski, R. & Czechowski, F., 2006. Molecular interactions between rubber and asphalt. *Industrial & Engineering Chemistry Research,* 45 (9), 3044-3049.

Ghavibazoo, A. & Abdelrahman, M., 2013. Composition analysis of crumb rubber during interaction with asphalt and effect on properties of binder. *International Journal of Pavement Engineering,* 14 (5), 517-530.

Ghavibazoo, A., Abdelrahman, M. & Ragab, M., 2013a. Effect of crumb rubber modifier dissolution on storage stability of crumb rubber-modified asphalt. *Transportation Research Record: Journal of the Transportation Research Board,* 2370, 109-115.

Ghavibazoo, A., Abdelrahman, M. & Ragab, M., 2013b. Mechanism of crumb rubber modifier dissolution into asphalt matrix and its effect on final physical properties of crumb rubber-modified binder. *Transportation Research Record: Journal of the Transportation Research Board,* (2370), 92-101.

Ghavibazoo, A., Abdelrahman, M. & Ragab, M., 2015. Evaluation of oxidization of crumb rubber–modified asphalt during short-term aging. *Transportation Research Record: Journal of the Transportation Research Board,* 2505, 84-91.

Green, E.L. & Tolonen, W.J., 1977. *The chemical and physical properties of asphalt-rubber mixtures, part i-basic material behavior.* Arizona Department of Transportation.

Hansen, C.M., 2002. *Hansen solubility parameters: A user's handbook* Boca Raton, Florida, US: CRC press.

Horikx, M., 1956. Chain scissions in a polymer network. *Journal of Polymer Science Part A: Polymer Chemistry,* 19 (93), 445-454.

Huang, S.C., 2008. Rubber concentrations on rheology of aged asphalt binders. *Journal of Materials in Civil Engineering,* 20 (3), 221-229.

Joseph, A.M., George, B., N., M.K. & Alex, R., 2016. The current status of sulphur vulcanization and devulcanization chemistry: Devulcanization. *Rubber Science,* 29 (1), 62-100.

Lee, P.I. & Peppas, N.A., 1987. Prediction of polymer dissolution in swellable controlled-release systems. *Journal of Controlled Release,* 6 (1), 207-215.

Lee, S.-J., Akisetty, C.K. & Amirkhanian, S.N., 2008. The effect of crumb rubber modifier (crm) on the performance properties of rubberized binders in hma pavements. *Construction and Building Materials,* 22 (7), 1368-1376.

Lesueur, D., 2009. The colloidal structure of bitumen: Consequences on the rheology and on the mechanisms of bitumen modification. *Adv Colloid Interface Sci,* 145 (1-2), 42-82.

Liang, M., Ren, S., Fan, W., Wang, H., Cui, W. & Zhao, P., 2017. Characterization of fume composition and rheological properties of asphalt with crumb rubber activated by microwave and tor. *Construction and Building Materials,* 154, 310-322.

Liu, Y. & Shi, B., 2008. Determination of flory interaction parameters between polyimide and organic solvents by hsp theory and igc. *Polymer Bulletin,* 61 (4), 501-509.

Lo Presti, D., 2013. Recycled tyre rubber modified bitumens for road asphalt mixtures: A literature review. *Construction and Building Materials,* 49, 863-881.

Lo Presti, D. & Airey, G., 2013. Tyre rubber-modified bitumens development: The effect of varying processing conditions. *Road Materials and Pavement Design,* 14 (4), 888-900.

Lo Presti, D., Izquierdo, M.A. & Jiménez Del Barco Carrión, A., 2018. Towards storage-stable high-content recycled tyre rubber modified bitumen. *Construction and Building Materials,* 172, 106-111.

Luo, R. & Huang, T., 2018. Development of a three-dimensional diffusion model for water vapor diffusing into asphalt mixtures. *Construction and Building Materials,* 179, 526-536.

Luo, R., Huang, T., Zhang, D. & Lytton, R.L., 2017. Water vapor diffusion in asphalt mixtures under different relative humidity differentials. *Construction and Building Materials,* 136, 126-138.

Ma, T., Zhao, Y., Huang, X. & Zhang, Y., 2015. Characteristics of desulfurized rubber asphalt and mixture. *KSCE Journal of Civil Engineering,* 20 (4), 1347-1355.

Mark, J.E., 1981. Rubber elasticity. *Journal of Chemical Education,* 58 (11), 898-903.

Mark, J.E., 2009. *The polymer data handbook,* Second Edition ed. Oxford, UK: Oxford University Press.

Mark, J.E., Erman, B. & Roland, M., 2013. *The science and technology of rubber* Waltham, Massachusetts, United States: Academic press.

Medina, J.R. & Underwood, B.S., 2017. Micromechanical shear modulus modeling of activated crumb rubber modified asphalt cements. *Construction and Building Materials,* 150, 56-65.

Miller-Chou, B.A. & Koenig, J.L., 2003. A review of polymer dissolution. *Progress in Polymer Science,* 28 (8), 1223-1270.

Narasimhan, B., 2001. Mathematical models describing polymer dissolution: Consequences for drug delivery. *Adv Drug Deliv Rev,* 48 (2-3), 195-210.

Narasimhan, B. & Peppas, N.A., 1996a. On the importance of chain reptation in models of dissolution of glassy polymers. *Macromolecules,* 29 (9), 3283-3291.

Narasimhan, B. & Peppas, N.N., 1996b. Disentanglement and reptation during dissolution of rubbery polymers. *Journal of Polymer Science: Part B: Polymer Physics,* 34, 947-961.

Papanu, J.S., Soane, D.S., Bell, A.T. & Hess, D.W., 1989. Transport models for swelling and dissolution of thin polymer-films. *Journal of Applied Polymer Science,* 38 (5), 859-885.

Peppas, N.A., Wu, J.C. & Vonmeerwall, E.D., 1994. Mathematical-modeling and experimental characterization of polymer dissolution. *Macromolecules,* 27 (20), 5626-5638.

Quesada-Pérez, M., Maroto-Centeno, J.A., Forcada, J. & Hidalgo-Alvarez, R., 2011. Gel swelling theories: The classical formalism and recent approaches. *Soft Matter,* 7 (22), 10536.

Ragab, M., Abdelrahman, M. & Ghavibazoo, A., 2013. Performance enhancement of crumb rubber-modified asphalts through control of the developed internal network structure. *Transportation Research Record: Journal of the Transportation Research Board,* 2371, 96-104.

Redelius, P., 2004. Bitumen solubility model using hansen solubility parameter. *Energy & Fuels,* 18 (4), 1087-1092.

Redelius, P. & Soenen, H., 2015. Relation between bitumen chemistry and performance. *Fuel,* 140, 34-43.

Redelius, P.G., 2000. Solubility parameters and bitumen. *Fuel,* 79 (1), 27-35.

Rubinstein, M. & Colby, R.H., 2003. *Polymer physics*: Oxford university press New York.

Shen, J. & Amirkhanian, S., 2007. The influence of crumb rubber modifier (crm) microstructures on the high temperature properties of crm binders. *International Journal of Pavement Engineering,* 6 (4), 265-271.

Shen, J., Amirkhanian, S., Xiao, F. & Tang, B., 2009. Surface area of crumb rubber modifier and its influence on high-temperature viscosity of crm binders. *International Journal of Pavement Engineering,* 10 (5), 375-381.

Shu, X. & Huang, B.S., 2014. Recycling of waste tire rubber in asphalt and portland cement concrete: An overview. *Construction and Building Materials,* 67, 217-224.

State of California Department of Transportation, 2003. *Asphalt rubber usage guide.* Sacramento, CA, USA.

Stroup-Gardiner, M., Newcomb, D.E. & Tanquist, B., 1993. Asphalt-rubber interactions. *Transportation research record,* 1417, 99.

Subhy, A., Lo Presti, D. & Airey, G., 2015. An investigation on using pre-treated tyre rubber as a replacement of synthetic polymers for bitumen modification. *Road Materials and Pavement Design,* 16, 245-264.

Tang, N., Huang, W. & Xiao, F., 2016. Chemical and rheological investigation of high-cured crumb rubber-modified asphalt. *Construction and Building Materials,* 123, 847-854.

Tu, Y. & Ouano, A.C., 1977. Model for the kinematics of polymer dissolution. *IBM Journal of Research and Development,* 21 (2), 131-142.

Vrentas, J.S. & Vrentas, C.M., 1998. Dissolution of rubbery and glassy polymers. *Journal of Polymer Science Part B-Polymer Physics,* 36 (14), 2607-2614.

Wang, H., Liu, X., Apostolidis, P., Erkens, S. & Scarpas, T., 2019a. Numerical investigation of rubber swelling in bitumen. *Construction and Building Materials,* 214, 506-515.

Wang, H., Liu, X., Apostolidis, P., Erkens, S. & Skarpas, A., 2020a. Experimental investigation of rubber swelling in bitumen. *Transportation Research Record: Journal of the Transportation Research Board,* 2674 (2), 203-212.

Wang, H., Liu, X., Apostolidis, P. & Scarpas, T., 2018. Review of warm mix rubberized asphalt concrete: Towards a sustainable paving technology. *Journal of Cleaner Production,* 177, 302-314.

Wang, H., Liu, X., Zhang, H., Apostolidis, P., Erkens, S. & Skarpas, A., 2020b. Micromechanical modelling of complex shear modulus of crumb rubber modified bitumen. *Materials & Design,* 188.

Wang, H., Liu, X., Zhang, H., Apostolidis, P., Scarpas, T. & Erkens, S., 2020c. Asphalt-rubber interaction and performance evaluation of rubberised asphalt binders containing non-foaming warm-mix additives. *Road Materials and Pavement Design,* 21 (6), 1612-1633.

Wang, H., Lu, G., Feng, S., Wen, X. & Yang, J., 2019b. Characterization of bitumen modified with pyrolytic carbon black from scrap tires. *Sustainability,* 11 (6).

Wang, S., Cheng, D. & Xiao, F., 2017a. Recent developments in the application of chemical approaches to rubberized asphalt. *Construction and Building Materials,* 131, 101-113.

Wang, T., Xiao, F., Amirkhanian, S., Huang, W. & Zheng, M., 2017b. A review on low temperature performances of rubberized asphalt materials. *Construction and Building Materials,* 145, 483-505.

Xu, M., Liu, J., Li, W. & Duan, W., 2015. Novel method to prepare activated crumb rubber used for synthesis of activated crumb rubber modified asphalt. *Journal of Materials in Civil Engineering,* 27 (5).

Yadollahi, G. & Mollahosseini, H.S., 2011. Improving the performance of crumb rubber bitumen by means of poly phosphoric acid (ppa) and vestenamer additives. *Construction and Building Materials,* 25 (7), 3108-3116.

Yao, H., Zhou, S. & Wang, S., 2016. Structural evolution of recycled tire rubber in asphalt. *Journal of Applied Polymer Science,* 133 (6).

Zanzotto, L. & Kennepohl, G., 1996. Development of rubber and asphalt binders by depolymerization and devulcanization of scrap tires in asphalt. *Transportation Research Record: Journal of the Transportation Research Board,* (1530), 51-58.

Zhu, J., Balieu, R. & Wang, H., 2019. The use of solubility parameters and free energy theory for phase behaviour of polymer-modified bitumen: A review. *Road Materials and Pavement Design*, 1-22.

3

Experimental Investigation of Rubber Swelling in Bitumen

3.1 Introduction of rubber swelling in bitumen

The use of crumb rubber modified bitumen (CRMB) has become a common practice in the asphalt paving industry for many years. Modification of bitumen with crumb rubber modifiers (CRMs) from scrap tires has been reported to improve the physical and mechanical properties of binders. Comparing to neat bitumen, CRMB has higher resistance to rutting, aging, fatigue and thermal cracking (Lo Presti 2013, Shu and Huang 2014, Wang *et al.* 2018a). These improvements are attributable to the interaction between bitumen and CRM.

Bitumen, as a refined residue from the distillation process of crude oils, is a complex mixture of thousands of different hydrocarbon molecules. Based on the differences in size and polarity, bitumen molecules can be separated into four molecular groups, saturates, aromatics, resins and asphaltenes (SARA). Bitumen is commonly accepted as a multi-disperse colloidal system, where high-molecular-weight asphaltene micelles are peptized by resins and dispersed in low-molecular-weight maltenes (saturates and aromatics) (Lesueur 2009). CRM mainly consists of natural and synthetic rubber, which are cross-linked with sulfur and reinforced with carbon black. In addition, various processing agents, such as aromatic hydrocarbons and antioxidants, are added to respectively improve its workability and prevent it from aging, (Asaro *et al.* 2018).

The frequently-referred in literature interaction during the production of CRMB is essentially the interaction between the rubber polymer and the bitumen. From the viewpoint of polymer science, the bitumen-rubber interaction can be regarded as a process in which a polymer (rubber) dissolves into a low-molecular-weight solvent (bitumen) as discussed in Section 2.3 from Chapter 2. Depending on different interaction parameters (e.g., temperature, time and mixing technique, etc.) and raw material parameters (e.g., bitumen microstructure and composition, rubber composition, morphology and particle size, etc.) (Lo Presti and Airey 2013, Ragab *et al.* 2013, Wang *et al.* 2020b), there are two mechanisms involved in the bitumen-rubber interaction process: diffusion-induced swelling of rubber network (Section 2.3.1) and chain disentanglement/scission of the swollen rubber (rubber degradation) (Section 2.3.2). Theoretically, swelling and degradation are two successive processes of the dissolution of rubber in bitumen (Wang *et al.* 2020a).

Few studies in the past have been done to quantitatively investigate the diffusion of bitumen into rubber. Frantzis (2004) measured the mass uptake of rubber in bitumen to determine the diffusion and solubility coefficients of bitumen in rubber samples (rectangles of 8 × 15 mm^2 and 1 mm thickness) from waste tires at 180 °C. Artamendi and Khalid (2006) extended this gravimetric method to different types of bitumen and rubber (sample dimensions of 15 × 10 × 1 mm^3) to investigate the diffusion kinetics. More recently, Dong *et al.* (2012) used an SBR sheet (sample dimensions of 10 × 10 × 2 mm^3) to simulate the swelling process of rubber in bitumen. Differential scanning calorimetric analysis, X-ray photoelectron spectroscopy tests, infrared spectroscopic analysis, and tensile tests were conducted to examine the physical, chemical and mechanical properties of rubber before and after swelling in rubber.

The bitumen-rubber interaction alters not only the component fractions and microstructure of bitumen but also the nature of rubber. The rubber swelling process stiffens the binder while degradation is detrimental to the mechanical properties of binder. For the conventional wet-processed CRMB at temperatures from 160 °C to 200 °C, only partial degradation occurs and, the final binder properties are dominated by the rubber swelling process (Abdelrahman and Carpenter 1999). Therefore, it is of vital importance to understand the interaction process to

guide the production of CRMB. Instead of investigating the properties of CRMB prepared at different conditions with different material combinations, this Chapter focuses on the interaction between a single rubber unit and bitumen at different conditions. It is not the intention of this study to involve many material combinations, but instead, to develop a robust methodology to determine the diffusion kinetics of bitumen into rubber and swelling properties of rubber.

3.2 Objectives of investigating rubber swelling in bitumen

This chapter aims to investigate the kinetics of bitumen diffusion into cylindrical rubber samples cut from scrap truck tires, the equilibrium swelling characteristics of rubber and the mechanical properties of rubber before and after swelling at different high temperatures. From the physical viewpoint, rubber swelling is a multiphysics phenomenon which consists of mass diffusion and volume expansion (mechanical deformation). The gravimetric method (weight gain experiments) was used to determine mass uptake parameters and the diffusion coefficient. Fourier transform infrared spectroscopy (FTIR) was employed to detect the component exchanges between rubber and solvent. The volume change of rubber during the swelling process was measured by micro X-ray computed tomography (CT) scan. Furthermore, the mechanical properties of rubber before and after swelling were tested by the Dynamic Shear Rheometer (DSR) with dedicated sample preparation procedures.

3.3 Materials and methods

3.3.1 Materials and sample preparation

Penetration grade 70/100 bitumen (Nynas) with a SARA (saturated hydrocarbons, aromatic hydrocarbons, resins, asphaltenes) fraction of 7% saturates, 51% aromatics, 22% resins and 20% asphaltenes, was used to interact with the rubber. The cylindrical rubber samples were cut from waste truck tires as shown in Figure 3.1. A uniform rubber slice of 2 mm thickness was cut from the tire tread (metal fiber free) using water jet cutting technology. Then, laser cutting was applied on the slice to obtain rubber cylinders with a diameter of 8 mm. These cylindrical rubber samples were subjected to a swelling test and a DSR test later. The rubber sample comprises of about 55% rubber polymer (natural and synthetic rubber), 25% carbon black and 20% processing agents. The processing agents mainly consist of antioxidants/antiozonants and curing additives (e.g. sulfur, zinc oxide, stearic acid, accelerator and oil etc.).
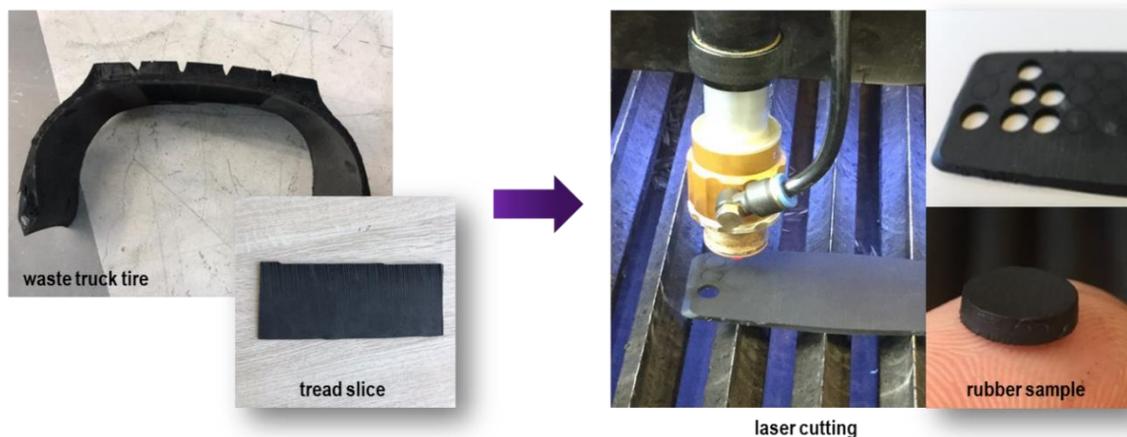
Figure 3.1 Cylindrical rubber sample (2 mm-thickness and 8 mm-diameter) preparation process.

3.3.2 Rubber swelling test

The gravimetric method (weight gain experiments) was used to determine the mass uptake parameters and the diffusion coefficient. The cylindrical rubber samples were immersed in small glass bottles containing approximately 5 g bitumen. The receptacles with lid were kept in an oven at the temperatures of 160, 180 and 200 °C, which are in the temperature range of conventional wet process. At regular time intervals (0.5, 1, 2, 3, 4, 6, 8, 18, 24, 28, 36 h) the samples were taken out of the bottles, blotted with Kimwipes (wiped dry with absorbent paper) to remove the surface-adhered excess bitumen. More frequent data collection was conducted at the early stages where bitumen diffusion is usually faster than at later stages. The rubber samples were then weighed (± 0.05 mg) on an electronic balance under closed environments. The mass uptake was obtained by difference between the initial weight and the weight after immersion in bitumen. For each temperature, three rubber replicates were used for the test.

Concurrently, another group of rubber swelling tests were performed using the same setup at the same elevated temperatures of 160, 180 and 200 °C. After swelling for different time durations (2, 6, 14, 26, 36 h), instead of taking out the rubber samples, the glass bottles containing both rubber cylinder and bitumen were scanned by a micro X-ray CT with a high resolution of 0.025 mm in all directions Figure 3.2. As a non-destructive visualizing technique, X-ray CT can distinguish the rubber part and the bitumen part in the glass bottle based on the density difference, and thereof monitor the volume change of rubber during swelling. After obtaining the 2D CT scan images, the Simpleware® software was utilized to analyze the image data and to reconstruct the 3D images of rubber samples for further volume calculation.
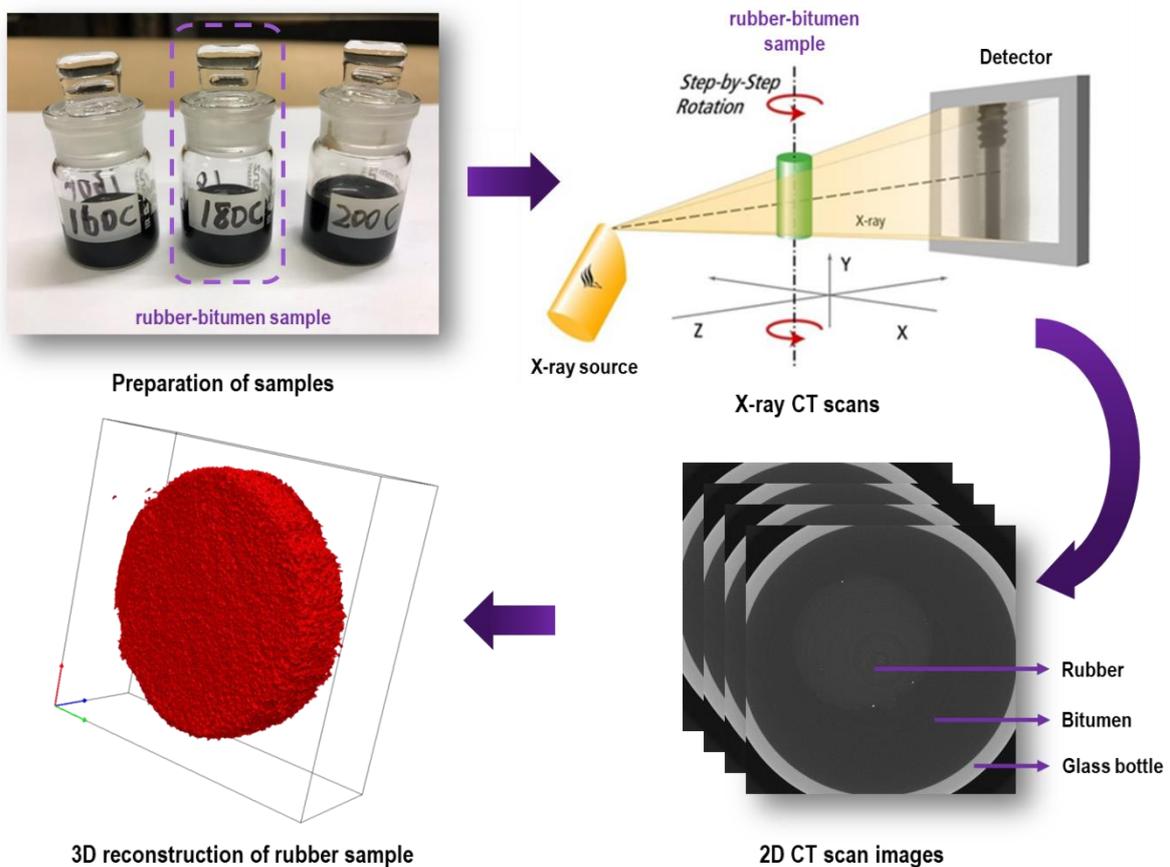
Figure 3.2 X-ray CT scan test for monitoring the rubber swelling process.

3.4 Does the rubber dissolve into bitumen? Study of rubber in naphthenic oil

Before conducting the rubber swelling test in bitumen, a question needs to be answered to ensure the results obtained from the swelling tests are the consequences of swelling—does the rubber dissolve into bitumen ? Therefore, the rubber samples were first immersed in a naphthenic oil at elevated temperatures to examine if there is dissolution of rubber taking place during the swelling process. The naphthenic oil has a Hildebrand solubility parameter of 18.5 MPa$^{0.5}$, which is closer to truck tire rubber (18.6 MPa$^{0.5}$) than most bitumen components (in the range from 17.2 to 18.8 MPa$^{0.5}$) (Artamendi and Khalid 2006, Levin and Redelius 2008, Zhu *et al.* 2019). Therefore, it is easier for rubber to dissolve into the naphthenic oil than bitumen based on the solubility theory. The naphthenic oil was collected periodically and was subjected to FTIR test to examine if new functional groups appear due to the interaction with rubber.

FTIR tests were also performed on the swollen rubbers from the rubber swelling test in bitumen. Small rubber units were cut from the core of swollen rubber samples with a special drill tool to avoid the interference of bitumen on the surface of rubber. The small rubber units were tested by FTIR to see which component of bitumen has diffused into rubber. In short, these two types of FTIR tests were performed to examine what has been released into naphthenic oil and what has diffused into rubber.

3.4.1 Fourier transform infrared spectroscopy

A Perkin Elmer Spectrum 100 FTIR spectrometer was used in the attenuated total reflectance (ATR) mode to acquire the infrared spectra for all the test samples. It was used to detect the component exchanges between rubber and solvent. The FTIR spectrum was obtained in the wavelength number range from 4,000 to 600 cm^{-1} with a scanning resolution of 4 cm^{-1} averaging twenty scans for each measurement at ambient temperatures.

3.4.2 Component exchange between rubber and solvent based on FTIR analysis

As mentioned before, the objective of immersing rubber samples into the naphthenic oil at elevated temperatures is to examine if the dissolution of rubber happens during the swelling process. The reason for choosing a naphthenic oil instead of bitumen is because its functional groups are relatively simple compared to bitumen. Besides, it is a better solvent for rubber swelling than bitumen. Therefore, it is easy to distinguish if rubber polymer molecules appear in the spectra of the collected naphthenic oil samples, Figure 3.3a. The spectrum peaks at 966 cm^{-1} and 696 cm^{-1} are often used as indicators of polybutadiene (PB) and polystyrene (PS) in rubber respectively. From Figure 3.3a, it can be seen that no rubber polymer functional groups were detected as no PB or PS peaks showed up. However, the absorption peak at 1700 cm^{-1} corresponding to the carbonyl functional group, which was not existing in the pure naphthenic oil spectrum, appeared in the reacted naphthenic oil samples. The intensity of this peak increased with higher interaction temperature and extended time. This may be attributed to the released aromatic oil and oxidation of carbon black released from rubber samples. Therefore, no rubber dissolution (or too inconspicuous to be detected) during interaction with naphthenic oil takes place in the temperature range from 160 to 200 °C.

In addition, the rubber sample retained its integrity after the interaction at a macroscale by visual inspection. It is anticipated this is the same case for the interaction of rubber with bitumen based

on the solubility theory. It may be contradictory to previous studies which claimed the dissolution of rubber particles happened during the mixing process (Ghavibazoo *et al.* 2013). In their studies, CRM dissolution was measured by considering the portion of CRM particles that passed through mesh No. 200 (smaller than 0.075 mm) as the dissolved portion. However, this portion of CRMs may be the consequence of disassociation/splitting of the big particles due to the mixing force and swelling effect (Medina and Underwood 2017). It is just a physical size-reducing process in which no dissolution happens in a chemical sense at the operational temperature. Therefore, the diffusion coefficient measured using the gravimetric method represents the accurate diffusion of bitumen components into rubber since no rubber mass loss is expected.

Figure 3.3b shows the spectra of dry rubber sample and rubber samples after swelling at different temperatures. It can be found that the absorption peaks at 1456 cm^{-1} and 1376 cm^{-1} corresponding to aliphatic components, which were not present in the dry rubber but in the bitumen, showed up in the swollen rubber samples. The two peaks close to 1456 cm^{-1} and 1376 cm^{-1} shown in the dry rubber are not related to aliphatic. This indicates that aliphatic compounds from bitumen diffused into rubber during the swelling process. Previous studies also observed the preferential absorption of compounds with linear aliphatic chains into rubber (Gawel *et al.* 2006).

(a)

(b)
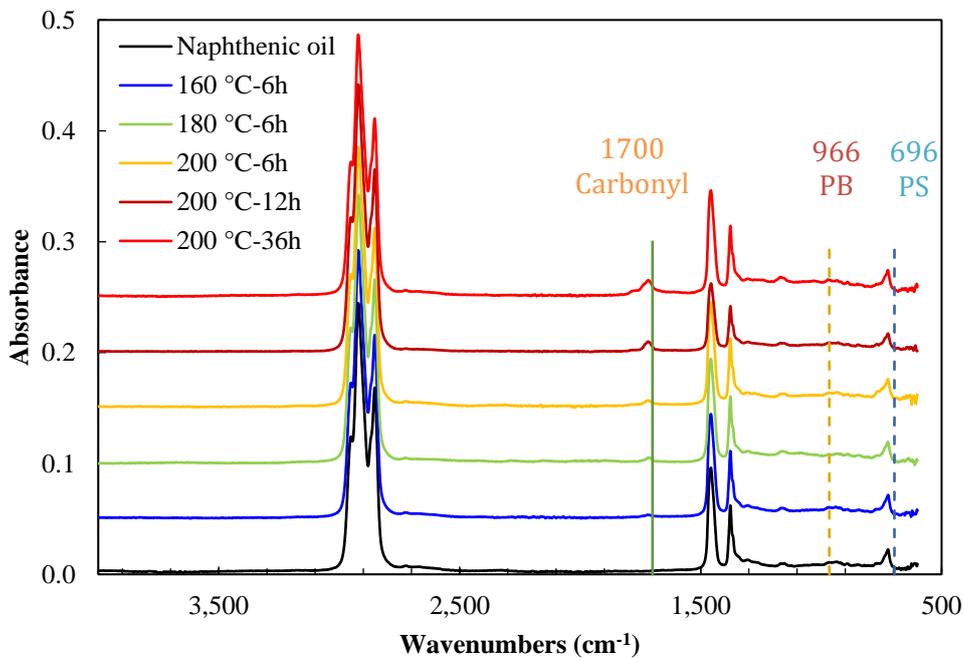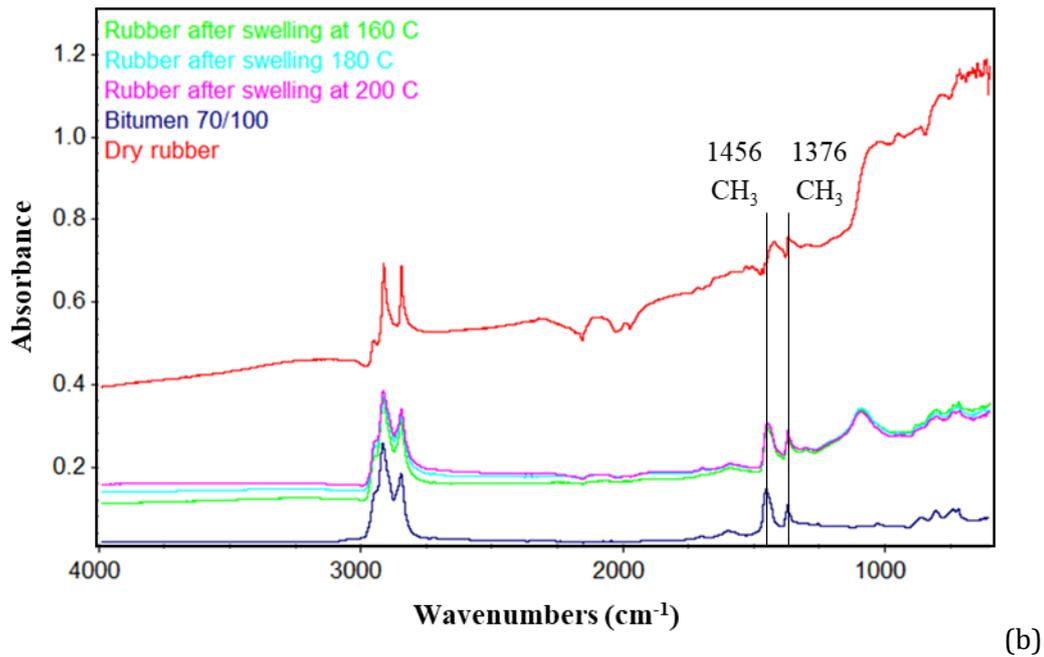
Figure 3.3 FTIR results of (a) reacted naphthenic oil samples and (b) rubber samples before and after swelling.

3.5 Rubber swelling in bitumen

A series of rubber swelling tests were performed at different temperatures to investigate the diffusion kinetics and volume change.

3.5.1 Diffusion coefficients of bitumen into rubber

In terms of physics, the swelling of rubber in bitumen is a diffusion-induced volume expansion phenomenon (Wang *et al.* 2019). The driving force of the diffusion process is the chemical potential of the external solvent (maltenes) produced from the concentration difference between rubber and bitumen. This diffusion process continues until the concentrations of light fractions inside and outside the rubber are uniform and, consequently, equilibrium swelling is reached. Fick's law of diffusion is usually used to describe the kinetics of bitumen diffusion into rubber. Considering the case of one-dimensional, bidirectional diffusion in a medium whose thickness is much smaller than the other two dimensions, as shown in Figure 3.4, the diffusing substance enters through the top and bottom plane surfaces and only a negligible amount through the edges at the end.
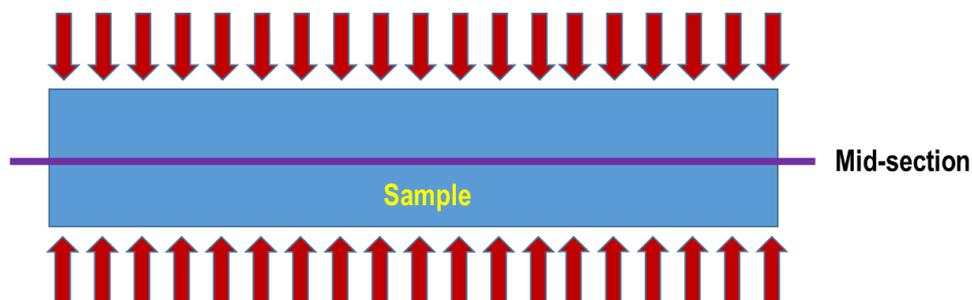
Figure 3.4 Sketch of the one-dimensional, bidirectional diffusion.

The total amount of diffusing substance into rubber at time t can be expressed as (Crank 1975, Frantzis 2004):

$$\frac{M_t - M_0}{M_0} = 4\sqrt{\frac{D}{\pi}} \cdot \frac{2\sqrt{t}}{d} \tag{3.1}$$

where M_t and M_0 are the mass of the rubber sample at immersion time t and the initial mass (g), respectively. D is the diffusion coefficient (mm^2/s). d is the sample thickness (mm). Equation (3.1) indicates that a plot of the mass uptake $(M_t - M_0)/M_0$ versus the parameter $2t^{1/2}/d$ should be initially linear. Therefore, the value of diffusion coefficient, which is assumed constant, can be calculated from the slope of the initial sorption curves experimentally. The initial linear region was found to be followed by a clearly defined equilibrium plateau region.

The bitumen uptake data collected from the sorption experiments (truck tire rubber and Pen 70/10 bitumen) at different temperatures are presented in Figure 3.5 in a plot of mass uptake versus $2t^{1/2}/d$. Each data point is an average value of three replicated samples. It can be found that the bitumen components were initially absorbed by rubber rapidly and then reach the equilibrium at elevated temperatures. The sorption curves showed a linear region followed by an equilibrium plateau region. Furthermore, bitumen uptake was faster at higher temperatures at the earlier stages as seen by the higher initial slopes of the sorption curve, which indicates a higher diffusion rate. The equilibrium mass uptake also increases as the temperature increases.
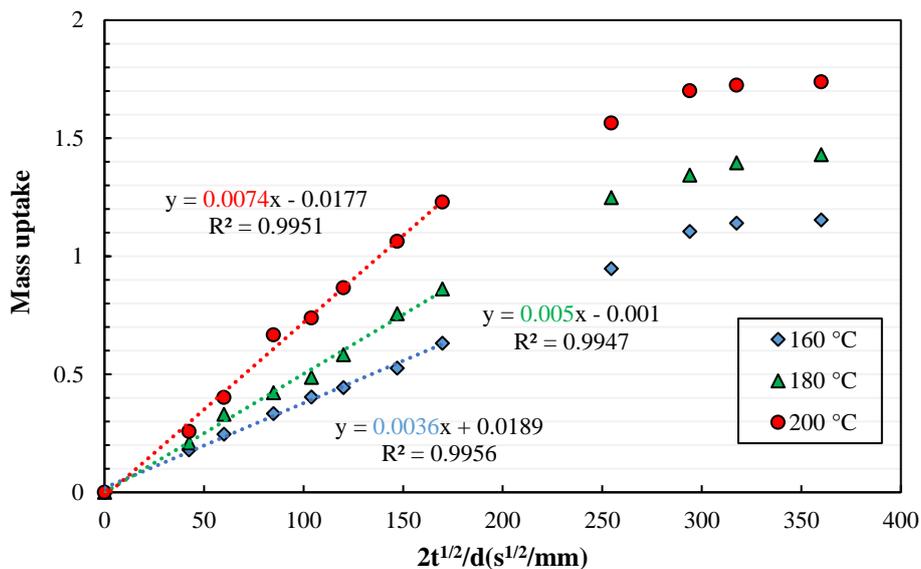
Figure 3.5 Sorption curves of bitumen into truck tire rubber.

The diffusion coefficients calculated from the initial slopes of the sorption curves and the approximate equilibrium mass uptake were summarized in Table 3.1. The diffusion coefficients determined here were considered as apparent (Artamendi and Khalid 2006) due to several reasons. First, the sample thickness was assumed as constant, which in reality the thickness increased due to swelling. Second, the diffusion coefficient was assumed as constant and independent of concentration (in other words, the surface concentration of penetrant is constant). During testing both bitumen composition and physical properties of rubber changed during the diffusion process. The light fractions of bitumen diffused into rubber preferentially at the earlier stages and the other fractions of bitumen might also diffuse into rubber at the later stages due to

changes of the internal structure of swollen rubber. Therefore, corrections to diffusion coefficients under swollen conditions were made by calculating the intrinsic diffusion coefficient D^* in Equation (3.2) (Brown *et al.* 1973).

$$D^* = \frac{D}{\phi_r^{7/3}}$$ (3.2)

where ϕ_r is the volume fraction of rubber in the swollen condition defined as Equation (2.8) in Chapter 2. The swollen rubber is essentially a polymer gel which is a mixture of solid rubber polymer and liquid bitumen components. It can be calculated based on the densities of rubber and bitumen together with the equilibrium mass uptake. The calculated equilibrium volume fraction of rubber and intrinsic diffusion coefficients were also summarized in Table 3.1.

Table 3.1 Diffusion coefficients and equilibrium mass uptake of bitumen into truck tire rubber.

Temperature (°C)	Equilibrium $(M_t - M_0)/M_0$	$D \times 10^{-6}$ (mm²/s)	ϕ	$D^* \times 10^{-6}$ (mm²/s)
160	1.15	2.54	0.465	15.15
180	1.40	4.91	0.417	37.87
200	1.70	10.75	0.370	109.12

The relationship between diffusion coefficients and temperature is shown in Figure 3.6. The temperature dependence of the diffusion coefficient can be seen to follow an Arrhenius type equation (Equation(3.3)).

$$D = D_0 e^{-\frac{E_a}{RT}}$$ (3.3)

where D_0 is a constant, E_a is the activation energy (kJ/mol), R is the universal gas constant [8.314 J/(mol·K)], T is temperature in degrees K, and D is diffusion coefficient.
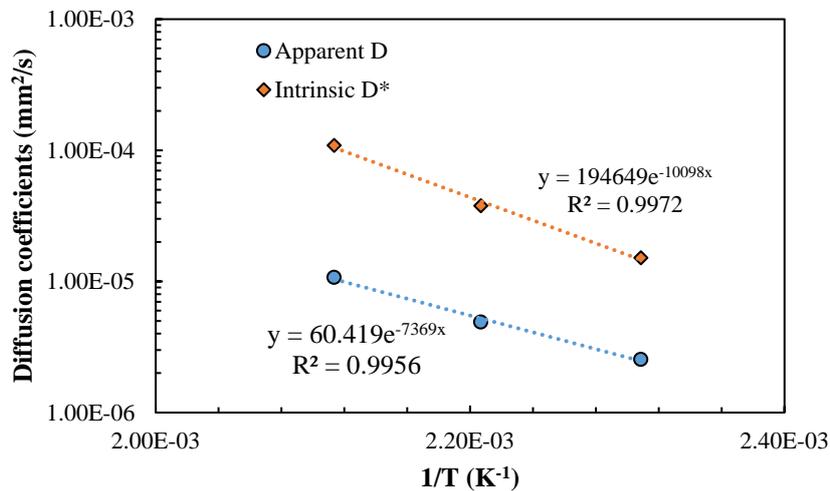
Figure 3.6 Temperature dependence of the diffusion coefficients.

As the temperature increases, both the mobility of bitumen molecules and polymer chains increase, which enhances the diffusion process of bitumen into the rubber. Greater segmental motion results in an increase in the size of free volume and subsequent increase in the diffusion coefficient (Rubinstein and Colby 2003).

3.5.2 Volume change of rubber during swelling in bitumen

X-ray CT can distinguish objects based on the difference in density and indicate them in the obtained slice images with different greyscale levels. Figure 3.7 presents the cross-sectional images of the scanned samples at different interaction conditions.
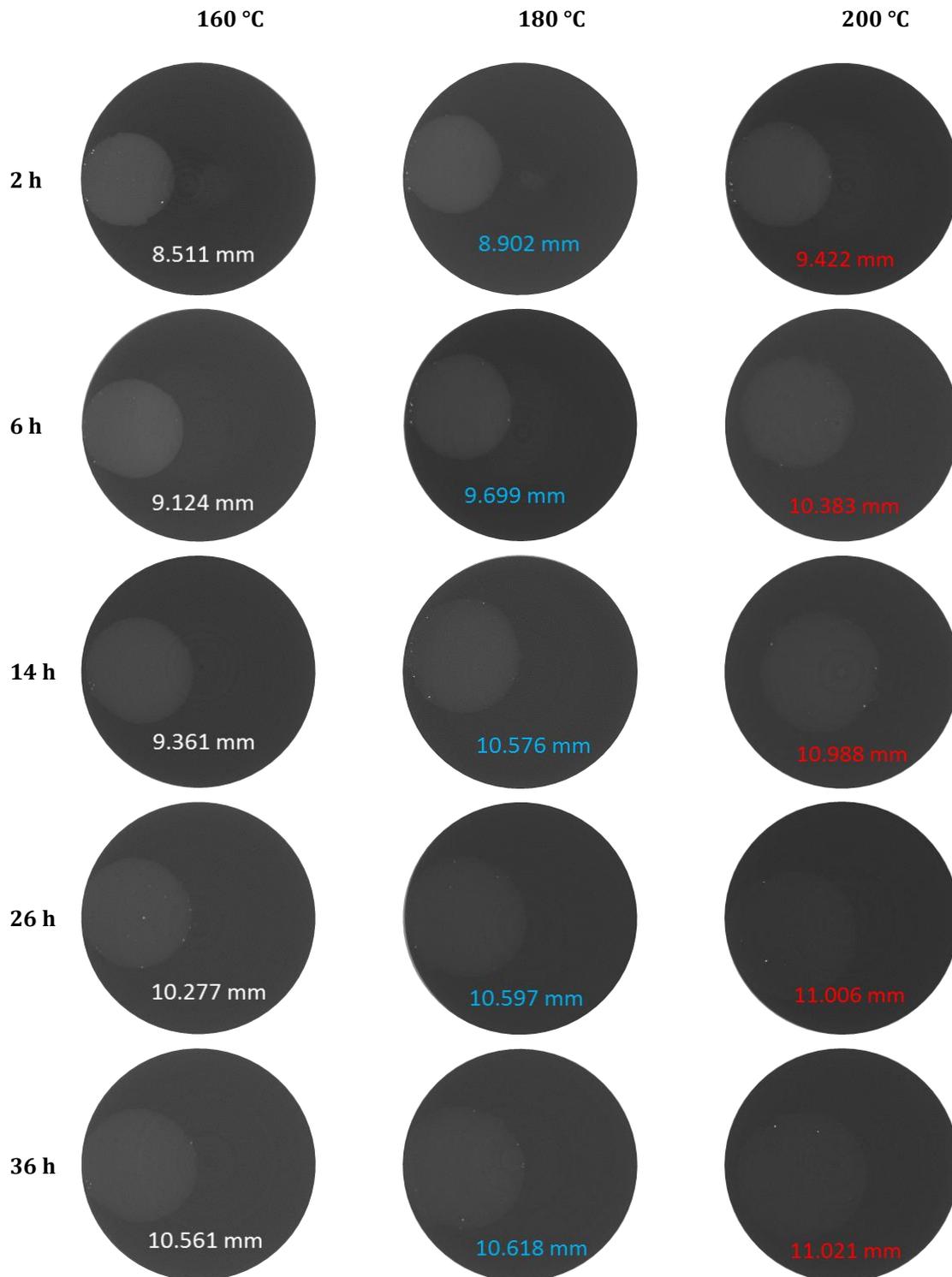
Figure 3.7 2D slice images from CT scan at different interaction temperatures and times.

The raw images were cropped to remove the glass bottle with only bitumen and rubber left. The density of bitumen is 1.03 g/cm^3 while the density of rubber is around 1.15 g/cm^3. Therefore, the light part is the rubber cylinder while the surrounding dark part is bitumen. The value shown in each image represents the diameter of the rubber circle using the measurement function in the software. Considering the diameter of the original dry rubber sample is around 8 mm, the size of rubber sample continued increasing with the increase of interaction time at different temperatures. The rubber samples swell more at higher temperatures as reflected by the larger diameter. In addition, as more bitumen diffuses into rubber, the rubber phase becomes darker and the boundary between the two phases becomes vague. Taking the image at 200 °C and 36 h as an example, it is difficult to distinguish the rubber phase and bitumen phase as the greyscale values of these two phases are already very close. It shows that the swollen rubber is saturated with bitumen components and may form a gel-like structure.

In order to quantitatively evaluate the volume change of rubber during the swelling process, the 3D images of the object were reconstructed with the 2D slice images. The volume of each swollen rubber was derived using the built-in measurement function of the software. The volumes of the rubber samples at different swelling states are summarized in Table 3.2. Rubber swells faster at the earlier stages then the expansion rate slows down. After 36 h interaction at 160 °C, rubber swelled to twice as big as the original one. The volume of rubber increased to approximately three times as the initial volume after 36 h interaction at 200 °C. Since rubber swelling is a diffusion-induced volume expansion process, it is logical that higher diffusion coefficients result in larger swelling ratios (swollen rubber volume divided by the dry rubber volume).

Table 3.2 Derived volumes of swollen rubbers through 3D reconstruction at different interaction conditions.

Time (h)	Volume (mm^3)		
	160 °C	180 °C	200 °C
0	100.5	100.5	100.5
2	116.2	129.1	177.2
6	138.4	156.3	239.5
14	157.1	190.6	287.4
26	169.2	236.5	301.3
36	197.6	247.7	304.6

3.6 Mechanical properties characterization

3.6.1 Mechanical tests by Dynamic Shear Rheometer

The mechanical properties of rubber before and after swelling were tested by a Dynamic Shear Rheometer (DSR). The unreacted (dry) cylindrical rubber sample can be directly placed between the 8 mm parallel plates of the DSR. The detailed positioning process of the dry rubber sample in the DSR device is shown in Figure 3.8.

Before the placement, a two-component adhesive, Plex 7742 and liquid Plexmon 801 (Evonik Rohm GmbH, Darmstadt, Germany), was mixed and applied on the surface of the bottom plate and the top surface of the rubber sample. Excess glue was removed from the sides. The test started after a 10 min hardening process of the adhesive to ensure a proper bonding between rubber and plates. From the technical data sheet of the adhesive, the E modulus of the cured adhesive can reach 2.1 GPa at room temperature, which is much higher than that of rubber. Therefore, the deformation of the glue is infinitesimal compared with that of rubber during the tests.

After a CT scan, the swollen rubber samples were taken out from bitumen after swelling for 36 h, which is believed to reach the swelling equilibrium at this moment based on the diffusion test. The swollen rubber samples were cleaned from bitumen by wiping with absorbent paper while hot and brushing for a few seconds with cold trichloroethylene gently. Through this process, the obtained swollen rubber sample is a gel-like material with aromatic oils inside the rubber network. Since the geometry of cylindrical rubber samples changed after swelling, a special drill tool with an inner diameter of 8 mm was used to trim the swollen sample into the desired diameter. Due to the good adhesion between the plates and swollen rubber, no glue was used. For both dry and swollen rubber samples, manual adjustment was applied on the gap between the plates until the normal force is close to zero.

1. Applying glue to lower DSR plate
2. Placing sample and applying glue to sample
3. Applying glue to sample
4. Applying glue to upper DSR plate
5. Bringing parallel plates of DSR to measuring position and removing excess of glue
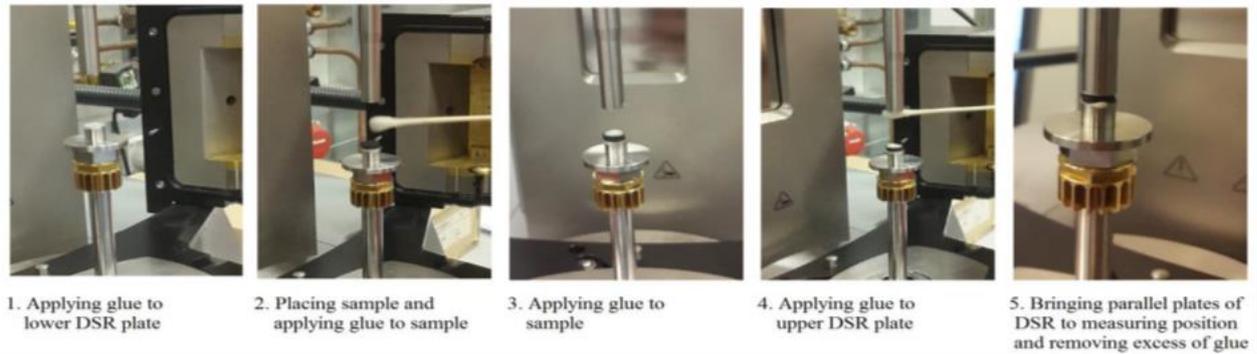
Figure 3.8 Rubber sample positioning in the DSR device.

Frequency sweep tests of rubber samples were performed from 0.1 to 100 rad/s over a temperature range of -10~130 °C with an increment of 20 °C. According to the previous study (Zegard *et al.* 2016), the measurements were carried out at a strain level of 1% under strain-controlled mode. The viscoelastic parameters (complex modulus and phase angle) of each sample were collected and analyzed.

3.6.2 Effect of swelling on the mechanical properties of rubber

From a micromechanics point of view, CRMB can be treated as a composite material in which rubber particles are included in the bitumen matrix. The change in properties of rubber after swelling has an important effect on the mechanical properties of rubber modified binders. During the rubber swelling test process, it was found the swollen rubber samples became soft and viscous due the absorption of bitumen components, forming a gel-like structure (Xu *et al.* 2012, Wang *et al.* 2020b). However, few studies have looked into the mechanical properties of this gel-like material.

To further investigate the effect of swelling on the mechanical properties of rubber, the dry and swollen rubber samples after 36 h interaction at different temperatures were tested by DSR. From the obtained data, it was found the swollen rubber is not a rheologically simple material so that common rheological models for bitumen are not suitable for it. Therefore, the master curves were established using a generalized logistic function as shown in Equation (3.4) (Rowe *et al.* 2009) and the Williams-Landel-Ferry (WLF) equation (Equation 3.5) for shift factors fitting to form smooth curves.

$$\log A = \delta + \frac{\alpha}{\left[1 + \lambda e^{(\beta + \gamma(\log \omega))}\right]^{1/\lambda}} \tag{3.4}$$

in which A is either the complex shear modulus or the phase angle. δ is the lower asymptote; α is the difference between the values of upper and lower asymptote; λ, β and γ define the shape between the asymptotes and the location of the inflection point.

$$\log \alpha_T(T) = \frac{-C_1(T - T_R)}{C_2 + (T - T_R)} \tag{3.5}$$

where C_1, C_2=empirically determined constants; T=test temperature; T_R=reference temperature; $\alpha_T(T)$=shifting factor. Based on the time-temperature superposition principle, the master curves of complex modulus and phase angle of different rubber samples at a reference temperature of 30 °C were built in Figure 3.9.
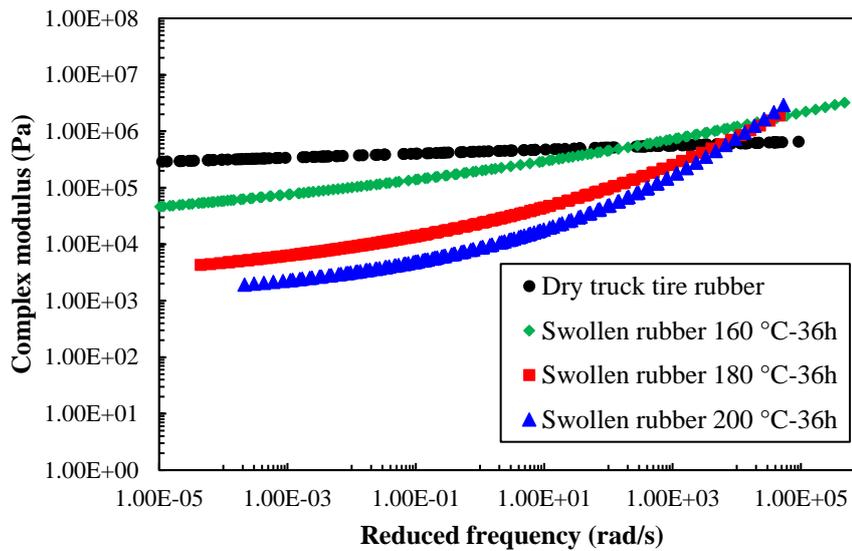
(a)
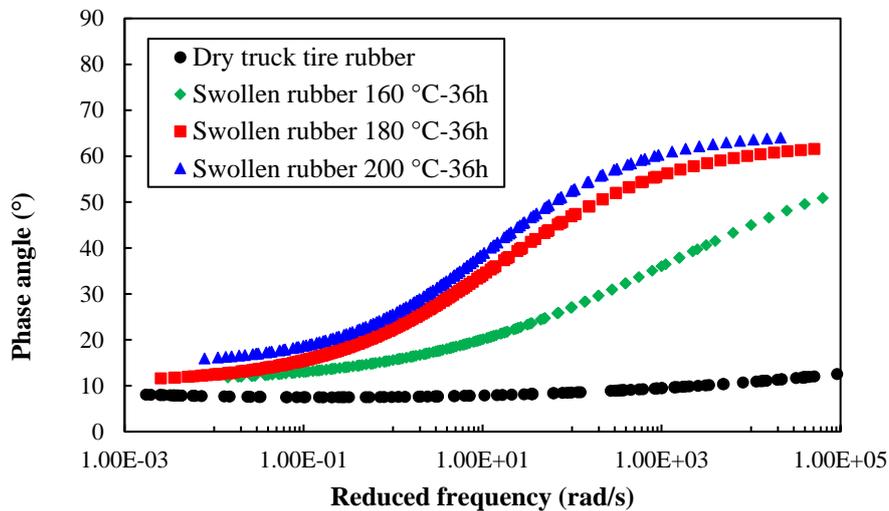
(b)

Figure 3.9 (a) Complex modulus and (b) phase angle master curves of rubber before and after swelling.

It can be seen from Figure 3.9 that at low frequencies, dry rubber exhibits an inherent but limited viscoelasticity whose complex modulus and phase angle are almost frequency independent. However, rubbers after swelling show more obvious viscoelasticity. The complex moduli of swollen rubbers were all lower than the dry rubber in the low frequency range. At high frequencies, the modulus of different samples crossed each other. Based on the existing master

curves, it can be anticipated that swollen rubber interacted at 200 °C for 36 h shows the highest modulus at very high frequencies (corresponding to very low temperatures). This is because the absorbed bitumen in the swollen rubber sample plays a more dominant role than rubber and behaves more elastic in the composite at low temperatures.

Considering the complex modulus of bitumen used in this study, at very high frequencies, is higher than that of rubber (Wang *et al.* 2018b), the swollen rubber sample containing more bitumen will exhibit higher complex moduli at very high frequencies. At the dry state, rubber polymer chains are entangled or crosslinked to each other, forming tightly folded coils, which contributes to the rubber elasticity. When the rubber polymer chain segments start to absorb bitumen molecules, the folded polymer coils start unfolding, causing the swelling and loosening of the network. Consequently, this polymer network swelling process will decrease the complex modulus at a macroscopic scale.

With the increase of interaction temperature, the modulus of swollen rubber decreases while the phase angle increases. This means the viscous component in the swollen rubber increases after the interaction at higher temperatures. It is noteworthy that the phase angles of swollen rubber samples increase with the increase of frequency, which is contradictory to the common behaviors of bitumen. This is the unique nature of rubber polymers. Actually, the phase angle of rubber usually experience an increase stage and then a decrease stage over a large frequency range (Santangelo and Roland 1998).

3.7 Preliminary investigation of the multilayer structure of swollen rubber

3.7.1 Concept of multilayer structure of swollen rubber

At the initial stage of rubber swelling, a multilayer structure of rubber will be formed with the gradual ingression of bitumen components. A schematic representation of the multilayer structure of swollen rubber is shown in Figure 3.10.
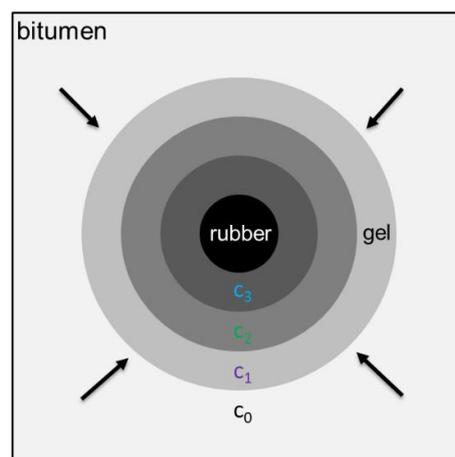
Figure 3.10 Multilayer structure of swollen rubber.

 It can be seen from Figure 3.10 that the absorbed bitumen concentration gradually changes from the outer layer to inner layer. Assuming the surrounding bitumen has a concentration of c_0, the bitumen concentration in different layers of rubber gradually decreases along the radial direction ($c_0 > c_1 > c_2 > c_3 > \cdots$), resulting in different mechanical properties of different layers. To

address the different mechanical properties of the multilayer structure, Figure 3.11 shows a potential relationship between rubber modulus and absorbed bitumen concentration.
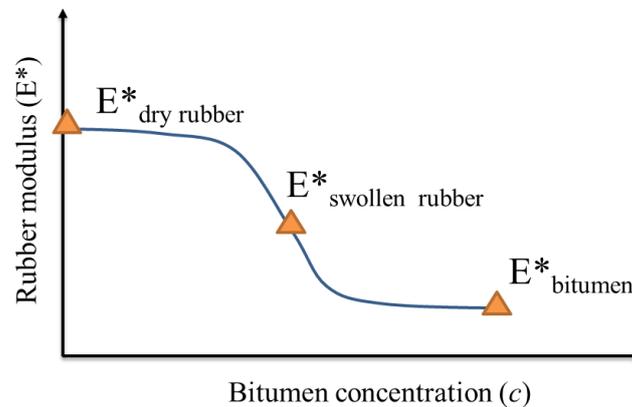
Figure 3.11 Aspired relationship between rubber modulus and absorbed bitumen concentration.

When bitumen concentration is zero, the rubber modulus is essentially the modulus of dry rubber. At the surface of rubber, where the concentration is identical to the surrounding bitumen concentration, the rubber modulus can be regarded as the same as the bitumen modulus. In between are the rubber moduli at different swelling conditions (concentrations). It should be noted that the actual variation of rubber modulus versus bitumen concentration is not necessarily as the curve shown in Figure 3.11. To more precisely determine this relationship, dedicated tests should be designed and carried out. The relationship between mechanical properties of rubber layers and diffusing bitumen concentration can enhance the understanding of the mechanism of rubber swelling and can be implemented into micromechanical models to have better predictions of binder properties.

3.7.2 Mechanical characterization of the multilayer structure of swollen rubber by nanoindentation test

3.7.2.1 *Sample preparation*

Since the swollen rubber sample is a composite of rubber and bitumen components, post-processing of samples can easily disturb the sample quality and essence, for instance, squeezing out the liquid bitumen components, distorting the rubber geometry, etc. Therefore, in-situ tests are preferable for measuring the mechanical properties of different layers of swollen rubber. Nanoindentation testing is a powerful on-site mechanical test with high accuracy for small-size samples. To prepare the rubber sample with gradient swelling for nanoindentation testing, a special sample holder was designed as shown in Figure 3.12a. The sample size is shown in Figure 3.12b. Firstly, a square rubber block with a width of 10 mm and a thickness of 2 mm was placed in the sample holder. Then, the hot bitumen was carefully poured into the right side of rubber. Excess bitumen was removed. The sample holder together with the rubber and the bitumen were horizontally put in the oven at different temperatures (160, 180, and 200 °C) for conditioning. By doing so, a one-way diffusion of bitumen into rubber was created in principle. The previous rubber samples for DSR measurements were prepared by immersing rubber samples into bitumen to prepare fully saturated rubber samples. After oven conditioning for varying times, a multilayer structure was expected to form in the rubber. The cooled samples were subjected to nanoindentation tests as illustrated in Figure 3.12c.

(a)   (b)   (c)
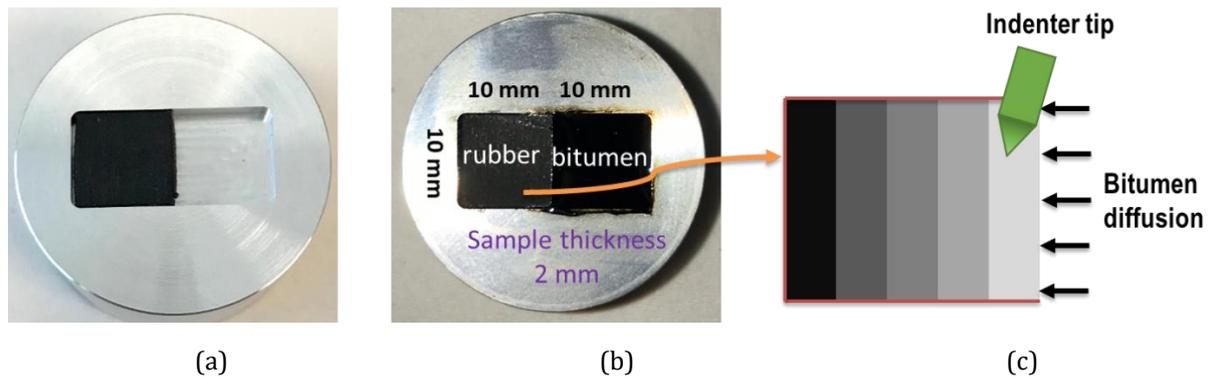
Figure 3.12 (a) Nanoindentation test sample holder (b) rubber sample and bitumen in the holder (c) Schematic diagram of multilayer rubber subjected to indentation.

3.7.2.2 *Nanoindentation test setup*

A KLA Nano Indenter G200 as shown in Figure 3.13 was used for testing the mechanical properties of rubber samples. The continuous stiffness method (CSM) was adopted to measure the complex modulus of samples. This method involves applying a small dynamic load at a certain frequency on the top of a static load while loading. The combination of dynamic and static loads offers a way to separate the in-phase and out-of-phase components of the load-displacement history (Li and Bhushan 2002). The used indenter tip is a flat-ended cylindrical punch made of diamond with a diameter of 330 μm. In view of the higher surface roughness and lower hardness of the rubber samples (compared for example to metals), a flat-ended punch was used as the tip for this test to ensure that the contact area is constant and not a function of contact depth.

As it can be seen in Figure 3.13b, the affiliated microscope was used for positioning of the measuring points. In total, 25 indentations at 25 different sites (a 5 × 5 square matrix in Figure 3.13c) were conducted on each sample to deal with data variability. The interval between these points was 500 μm to eliminate the effects of residual stresses and indenting deformations. The indenter was first brought into full contact with the test material at an approach velocity of 0.05 μm/s. A pre-test compression of 5 μm was applied after detecting the contact. Then the indenter oscillated over a frequency range from 1~45 Hz and the measuring system recorded the material responses. The harmonic oscillation amplitude was 0.05 μm. After that, the indenter was withdrawn and moved to the next test point. All the indentation tests were performed at 20 °C. After obtaining the load-displacement curves, analysis was done to calculate the complex modulus and phase angle as a function of frequency for a specific test site.

(a)   (b)   (c)
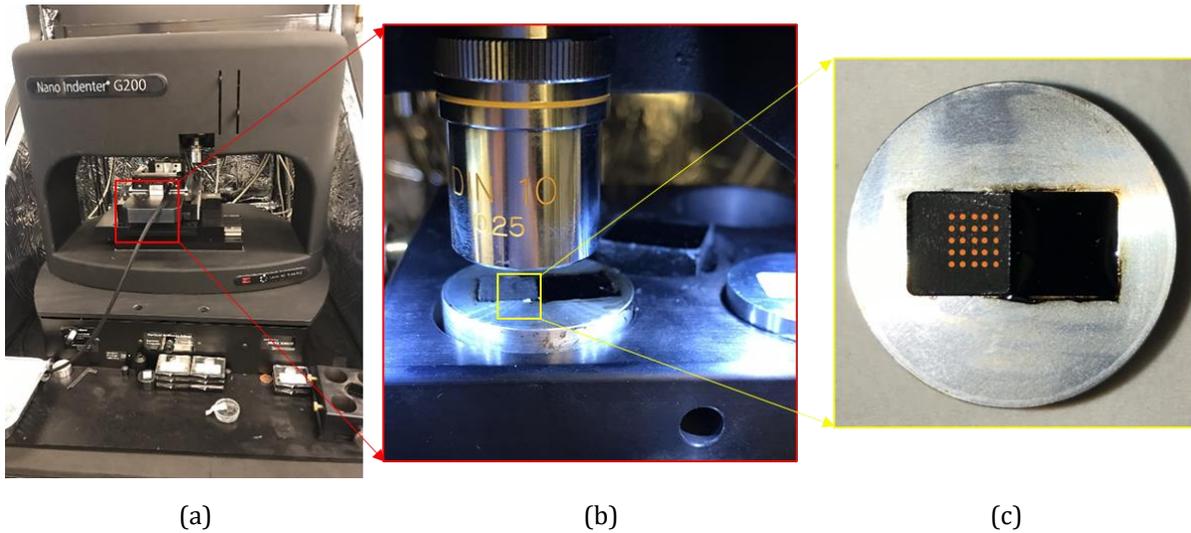
Figure 3.13 Nanoindentation test setup (a) Nano Indenter G200 (b) Operational platform (c) Sample holder and measuring points.

3.7.2.3 *Nanoindentation test results analysis*

The load applied on the sample and the displacement into the sample surface versus time during the nanoindentation tests are presented in Figure 3.14.
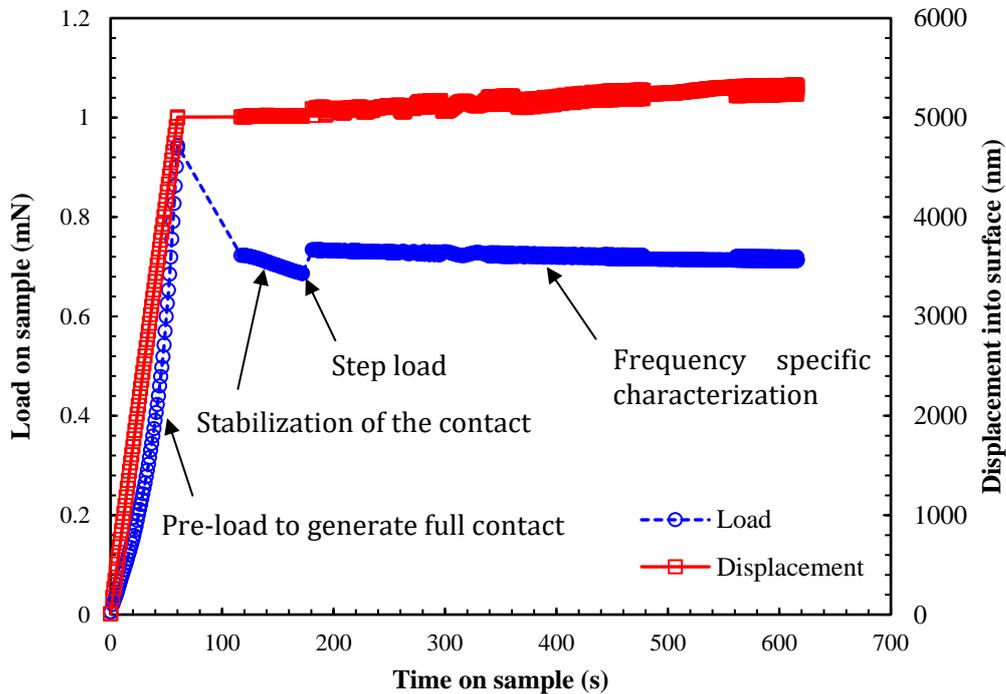
Figure 3.14 A complete indentation test to obtain the complex modulus.

Initially, a pre-load was applied to achieve a full contact between the sample surface and the flat punch face. A short stabilization period was imposed to ensure the contact to reach the equilibrium state. Then, a step-load was applied on the sample to evaluate the creep behavior. After that, frequency sweep tests starting from low frequency to high frequency were conducted.

The combined response of the instrument (oscillator) and the sample as well as the sole response of the oscillator in free space were measured in the frequency domain with a phase-lock amplifier (PLA) in the indentation system.

The material response was determined by deducting the instrument's contribution to the total measured response (Herbert *et al.* 2008) and the mechanical parameters were then calculated with the known stiffness, damping factor, and mass of the instrument. The resulted storage modulus and loss factor as a function of frequency of the dry rubber sample are presented in Figure 3.15. Each data point represents an average of 25 measurements and the error bar covers the data range with the mean value in the middle. The percent deviation is generally around 10%, which is acceptable for nanoindentation tests. Although rubber is normally treated as an elastic material, the results in Figure 3.15 clearly show the viscoelastic nature of the waste truck tire rubber. Both storage modulus and loss factor increase with frequency in the testing range.

(a)   (b)
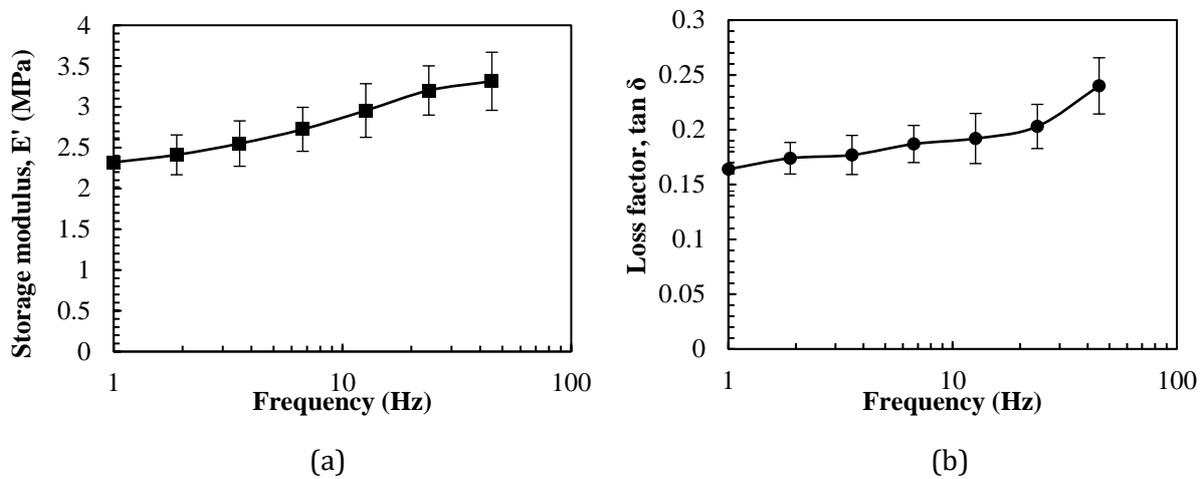
Figure 3.15 (a) Storage modulus E' and (b) loss factor tan δ versus frequency of the dry rubber sample.

To investigate how bitumen diffusion affects the mechanical properties of the rubber, nanoindentation tests were also conducted on the conditioned rubber samples, i.e., rubber samples interacted with bitumen in the oven. As shown in Figure 3.13c, the indenter tip started to indent the rubber sample surface from the position close to the right boundary (0.5 mm) to the left side. It was expected to have a lower complex modulus value at the right test site than at the left test site since the right site contains more diffused bitumen, which makes that rubber layer softer. The complex modulus data at different test positions of interacted rubber sample at room temperature are shown in Figure 3.16. The complex modulus of dry rubber sample is presented as a reference. The distance shown in the legend of Figure 3.16 represents the distance from the right boundary to the testing point. It is noted that with the exception of the complex modulus at the position of 2.5 mm, which was quite similar to the dry rubber, all the other layers of rubber exhibited higher complex moduli than the dry rubber. In addition, there is no specific trend between the complex modulus and testing positions.
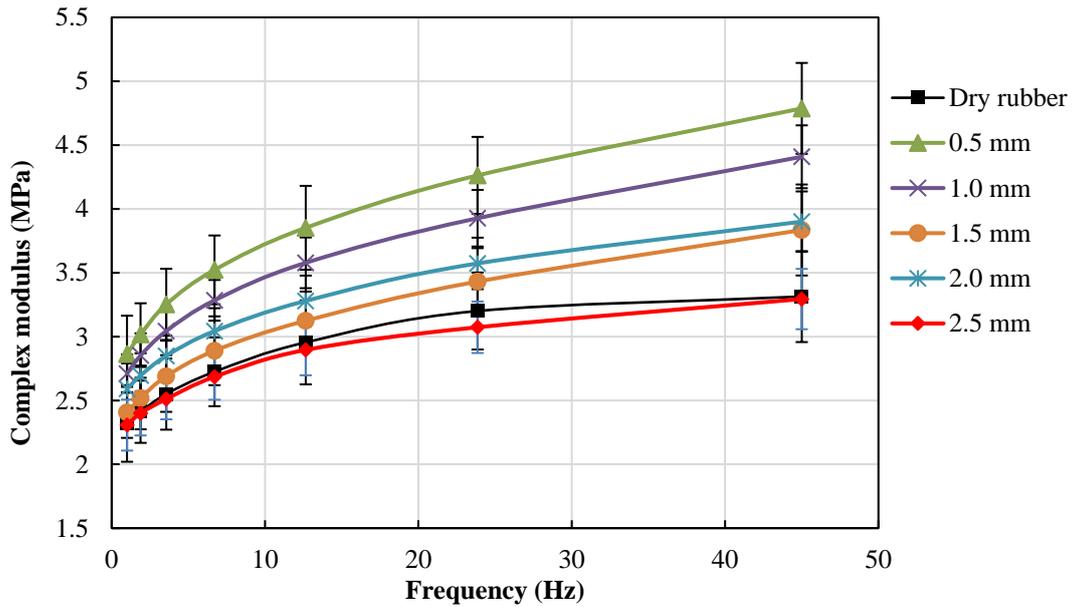
Figure 3.16 Complex modulus versus frequency at different test positions of interacted rubber sample.

The expected smaller complex moduli at the position closer to the right boundary were not observed. The results seem confusing for further analysis. The reasons for this can be mainly attributed to two aspects. Firstly, the rubber layer close to the right boundary will swell after interacting with hot bitumen, which creates surface distortion at that position. This distortion will significantly influence the nanoindentation results since nanoindentation requires a smooth and flat sample surface. Secondly, the rubber layers experienced not only the diffusion of bitumen but also oxidative aging during the conditioning in the oven (Bauer *et al.* 2007). These coupled effects of rubber aging and bitumen diffusion are illustrated in Figure 3.17. Oxidative aging normally increases the rubber modulus and reduces the elongation at break and the tensile strength (Ahagon *et al.* 1990). This explains why different rubber layers after conditioning generally have higher complex moduli than the unconditioned dry rubber sample.
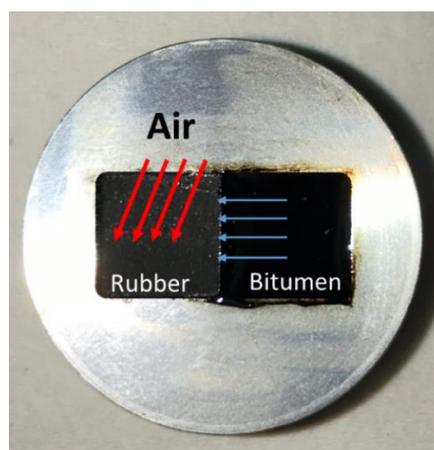
Figure 3.17 Coupled effects of rubber aging and bitumen diffusion.

The above analysis demonstrated the difficulty of investigating the multilayer structure of swollen rubber. It is difficult and impractical to attempt to experimentally separate the effects of bitumen diffusion from rubber aging. Therefore, in Chapter 7 which uses the mechanical properties of

swollen rubber as the input of micromechanical models, the properties of rubber at the equilibrium swelling state were used by considering the swollen rubber as a uniform material.

3.8 Summary

This chapter conducted various laboratory tests to investigate the swelling process of rubber from waste truck tires in bitumen. The following conclusions can be drawn:

- Through FTIR results, no rubber dissolution (or too inconspicuous to be detected) during interaction with naphthenic oil takes place in the temperature range from 160 to 200 °C. This supports that rubber does not dissolve into bitumen in the same temperature range. Aliphatic compounds from bitumen preferentially diffused into rubber during the swelling process.

- Through bitumen sorption tests, the corrected diffusion coefficients of Pen 70/100 bitumen into truck tire rubber are determined as 15.15×10^{-6}, 37.87×10^{-6} and 109.12×10^{-6} mm^2/s at 160, 180 and 200 °C, respectively. The diffusion coefficient increases with the increase of temperature in an Arrhenius fashion.

- The volume expansion of rubber during swelling was captured by the CT scan images. Rubber swells faster at the earlier stages, then the expansion rate slows down. The swelling ratio of rubber increased from 1.97 at 160 °C to 3.03 at 200 °C after 36 h interaction.

- Through DSR tests, swollen rubber becomes softer comparing to the dry rubber and exhibits obvious viscoelastic behavior. With the increase of temperature, the softening and viscous effects are more significant.

The obtained diffusion coefficients, swelling characteristics and mechanical properties can be further used as model input for both, numerical simulation of rubber swelling process and micromechanical modeling to better predict the mechanical performance of CRMB.

3.9 References

Abdelrahman, M.A. & Carpenter, S.H., 1999. Mechanism of the interaction of asphalt cement with crumb rubber modifier. *Transportation Research Record: Journal of the Transportation Research Board,* 1661, 106-113.

Ahagon, A., Kida, M. & Kaidou, H., 1990. Aging of tire parts during service. I. Types of aging in heavy-duty tires. *Rubber Chemistry and Technology,* 63 (5), 683-697.

Artamendi, I. & Khalid, H.A., 2006. Diffusion kinetics of bitumen into waste tyre rubber. *Journal of the Association of Asphalt Paving Technologists,* 75, 133-164.

Asaro, L., Gratton, M., Seghar, S. & Aït Hocine, N., 2018. Recycling of rubber wastes by devulcanization. *Resources, Conservation and Recycling,* 133, 250-262.

Bauer, D.R., Baldwin, J.M. & Ellwood, K.R., 2007. Rubber aging in tires. Part 2: Accelerated oven aging tests. *Polymer Degradation and Stability,* 92 (1), 110-117.

Brown, W., Jenkins, R. & Park, G., Year. The sorption and diffusion of small molecules in amorphous and crystalline polybutadienesed.^eds. *Journal of Polymer Science: Polymer Symposia*Wiley Online Library, 45-67.

Crank, J., 1975. *The mathematics of diffusion* Great Britain: Clarendon Press Oxford.

Dong, D., Huang, X., Li, X. & Zhang, L., 2012. Swelling process of rubber in asphalt and its effect on the structure and properties of rubber and asphalt. *Construction and Building Materials,* 29, 316-322.

Frantzis, P., 2004. Crumb rubber-bitumen interactions: Diffusion of bitumen into rubber. *Journal of materials in civil engineering,* 16 (4), 387-390.

Gawel, I., Stepkowski, R. & Czechowski, F., 2006. Molecular interactions between rubber and asphalt. *Industrial & Engineering Chemistry Research,* 45 (9), 3044-3049.

Ghavibazoo, A., Abdelrahman, M. & Ragab, M., 2013. Mechanism of crumb rubber modifier dissolution into asphalt matrix and its effect on final physical properties of crumb rubber-modified binder. *Transportation Research Record: Journal of the Transportation Research Board,* (2370), 92-101.

Herbert, E.G., Oliver, W.C. & Pharr, G.M., 2008. Nanoindentation and the dynamic characterization of viscoelastic solids. *Journal of Physics D: Applied Physics,* 41 (7).

Lesueur, D., 2009. The colloidal structure of bitumen: Consequences on the rheology and on the mechanisms of bitumen modification. *Adv Colloid Interface Sci,* 145 (1-2), 42-82.

Levin, M. & Redelius, P., 2008. Determination of three-dimensional solubility parameters and solubility spheres for naphthenic mineral oils. *Energy & Fuels,* 22 (5), 3395-3401.

Li, X.D. & Bhushan, B., 2002. A review of nanoindentation continuous stiffness measurement technique and its applications. *Materials Characterization,* 48 (1), 11-36.

Lo Presti, D., 2013. Recycled tyre rubber modified bitumens for road asphalt mixtures: A literature review. *Construction and Building Materials,* 49, 863-881.

Lo Presti, D. & Airey, G., 2013. Tyre rubber-modified bitumens development: The effect of varying processing conditions. *Road Materials and Pavement Design,* 14 (4), 888-900.

Medina, J.R. & Underwood, B.S., 2017. Micromechanical shear modulus modeling of activated crumb rubber modified asphalt cements. *Construction and Building Materials,* 150, 56-65.

Ragab, M., Abdelrahman, M. & Ghavibazoo, A., 2013. Performance enhancement of crumb rubber-modified asphalts through control of the developed internal network structure. *Transportation Research Record: Journal of the Transportation Research Board,* 2371, 96-104.

Rowe, G., Baumgardner, G. & Sharrock, M., 2009. Functional forms for master curve analysis of bituminous materials. *Advanced Testing and Characterisation of Bituminous Materials, Vols 1 and 2,* 81-+.

Rubinstein, M. & Colby, R.H., 2003. *Polymer physics*: Oxford university press New York.

Santangelo, P.G. & Roland, C.M., 1998. Temperature dependence of mechanical and dielectric relaxation incis-1,4-polyisoprene. *Macromolecules,* 31 (11), 3715-3719.

Shu, X. & Huang, B.S., 2014. Recycling of waste tire rubber in asphalt and portland cement concrete: An overview. *Construction and Building Materials,* 67, 217-224.

Wang, H., Apostolidis, P., Zhu, J., Liu, X., Skarpas, A. & Erkens, S., 2020a. The role of thermodynamics and kinetics in rubber–bitumen systems: A theoretical overview. *International Journal of Pavement Engineering*, 1-16.

Wang, H., Liu, X., Apostolidis, P., Erkens, S. & Scarpas, T., 2019. Numerical investigation of rubber swelling in bitumen. *Construction and Building Materials,* 214, 506-515.

Wang, H., Liu, X., Apostolidis, P. & Scarpas, T., 2018a. Review of warm mix rubberized asphalt concrete: Towards a sustainable paving technology. *Journal of Cleaner Production,* 177, 302-314.

Wang, H., Liu, X., Apostolidis, P. & Scarpas, T., 2018b. Rheological behavior and its chemical interpretation of crumb rubber modified asphalt containing warm-mix additives. *Transportation Research Record: Journal of the Transportation Research Board,* 2672 (28), 337-348.

Wang, H., Liu, X., Zhang, H., Apostolidis, P., Scarpas, T. & Erkens, S., 2020b. Asphalt-rubber interaction and performance evaluation of rubberised asphalt binders containing non-foaming warm-mix additives. *Road Materials and Pavement Design,* 21 (6), 1612-1633.

Xu, B., Di, X. & Mckenna, G.B., 2012. Swelling behavior of cross-linked rubber: Explanation of the elusive peak in the swelling activity parameter (dilational modulus). *Macromolecules,* 45 (5), 2402-2410.

Zegard, A., Helmand, F., Tang, T., Anupam, K. & Scarpas, A., 2016. Rheological properties of tire rubber using dynamic shear rheometer for fem tire-pavement interaction studies. *8th*

International Conference on Maintenance and Rehabilitation of Pavements. Singapore: Research Publishing Services, 535-544.

Zhu, J., Balieu, R. & Wang, H., 2019. The use of solubility parameters and free energy theory for phase behaviour of polymer-modified bitumen: A review. *Road Materials and Pavement Design*, 1-22.

4

Numerical Investigation of Rubber Swelling in Bitumen

Part of this chapter contains published material from "Wang, H., Liu, X., Apostolidis, P., Erkens, S. & Scarpas, T., 2019. Numerical investigation of rubber swelling in bitumen. Construction and Building Materials, 214, 506-515."

4.1 Introduction of rubber swelling in bitumen

As pointed out in Section 2.3 of Chapter 2, there are two mechanisms involved in the bitumen-rubber interaction process: diffusion-induced swelling of rubber network and chain disentanglement/scission of the swollen rubber (rubber degradation). Figure 2.4 has illustrated the different stages of bitumen-rubber interactions with increasing time at elevated temperatures, i.e., *initial configuration, swelling phase, post-swelling and beginning of degradation, degradation and complete dissolution*. However, at the traditional mixing temperatures of wet-processed rubberized binders (around 180°C), only partial degradation occurs, and the final binder properties are dominated by the rubber swelling process (Abdelrahman and Carpenter 1999).

In general, rubber swelling has three effects on the properties of bitumen: (a) changing the component proportions due to absorption of maltenes; (b) changing the microstructure of bitumen; (c) stiffening the binder due to the inclusions of CRM particles with increased volume. Therefore, it is of vital importance to understand the swelling behavior of rubber to control the property development of CRMB. It was shown that the bitumen-rubber interactions and their effects on the final binder properties depend on the raw material parameters (e.g., bitumen characteristics, CRM type, morphology, particle size and dosage) and interaction conditions (e.g., mixing temperature, time and rate, energy type of the mechanical mixing exerted) (Airey *et al.* 2004, Abdelrahman 2006, Shen and Amirkhanian 2007).

Extensive laboratory tests have investigated the influence of these factors on the swelling behavior of rubber and the properties of CRMB. Particularly, several dedicated studies were carried out to investigate the swelling behavior of individual rubber block or sheet in hot bitumen (Frantzis 2004, Artamendi and Khalid 2006, Dong *et al.* 2012, Feng *et al.* 2015). However, these laboratory tests are always time and cost consuming. In addition, the findings from the laboratory tests are highly dependent on the combinations of materials and processing methods, which are lack of universality. Based on their findings, it is generally assumed that the swelling of CRM in bitumen is a diffusion induced process with volume expansion. A numerical approach through a simplified system can provide a convenient way to quickly identify the parameters that affect the swelling process and hence can be used to perform a preliminary evaluation before the experimental tests.

4.2 Objectives

In order to acquire a better understanding of the swelling behavior of rubber in bitumen, this chapter aims to develop a modeling methodology capable of simulating the rubber swelling process in bitumen. The mass diffusion and volume expansion phenomena of the rubber are incorporated in a multi-physics tool to predict rubber swelling in bitumen. The model is calibrated with data generated from previous studies proving the reliability of the tool to evaluate the various influential factors on the design of rubberized bituminous materials with the desired properties and subsequently performance.

4.3 Multiphysics modeling of the rubber swelling behavior in bitumen

From the physical viewpoint, rubber swelling is a multiphysics phenomenon which consists of mass diffusion and volume expansion (mechanical deformation) (Wang *et al.* 2018). Numerical modeling of rubber swelling will provide new insights into the mechanical processes taking place.

This section presents the theory of mass diffusion and large deformations based on the balance equations driving the solvent diffusion and the force equilibrium and the constitutive equations for rubber particles.

4.3.1 Mass diffusion

As reported by many studies, it is the maltenes in bitumen that diffuse into the rubber network due to the similar solubility parameters between aromatics and rubber (Artamendi and Khalid 2006). As shown in Figure 4.1, the driving force of the diffusion process is the concentration gradient of the external solvent (maltenes) between rubber and bitumen (Frantzis 2004).
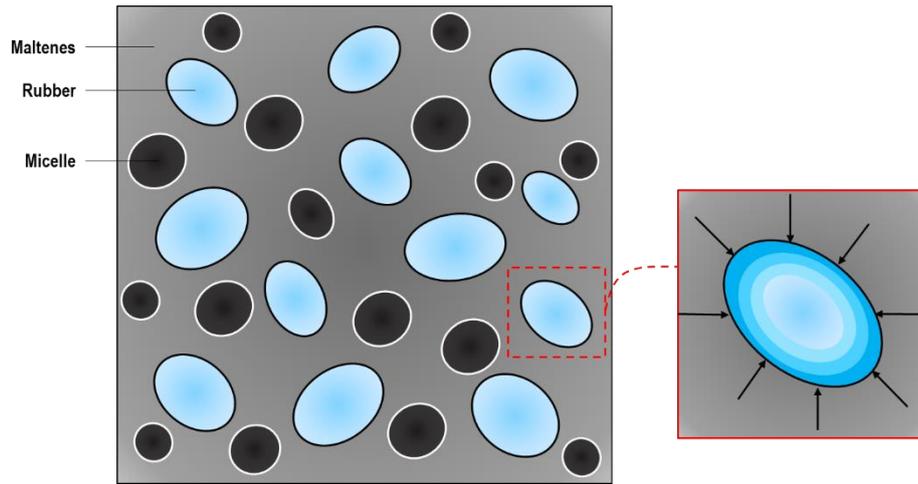
Figure 4.1 Schematic representation of maltenes diffusion into rubber.

This diffusion process continues until the concentrations of light fractions inside and outside the rubber are uniform and, consequently, equilibrium swelling is reached. Fick's law of diffusion is usually used to describe the kinetics of bitumen diffusion into rubber. Fick's first law postulates that the diffusive flux goes from domains of high concentration to domains of low concentration, with a magnitude that is proportional to the concentration gradient measured normal to the domain boundary:

$$\boldsymbol{J} = -D\nabla C \tag{4.1}$$

where $\boldsymbol{J}$ is the diffusion flux vector; D is the diffusion coefficient, C is the concentration; ∇ is the gradient operator. Fick's second law predicts how diffusion causes the concentration to change with time given as

$$\frac{\partial C}{\partial t} = D\nabla^2 C \tag{4.2}$$

where t is time; other parameters are the same as Equation (4.1). The flux vector is associated with the mass balance equation above and imposed at the boundary conditions of the rubber domain.

4.3.2 Volume expansion

The volume expansion of rubber can be treated as a large deformation problem. The rubber particle is considered as a homogenized continuum body. In principle, the equations that govern the mechanics of rubber particles during swelling include balance equations, kinematic equations

and constitutive equations (Scarpas 2004). The equilibrium equation of the system is given by Newton's second law $\sum F = ma$. Considering both force and area are represented in the material configuration, the equation of motion can be written as

$$\nabla \cdot \mathbf{FS} + \mathbf{F_v} = 0 \tag{4.3}$$

where $\mathbf{F}$ is the deformation gradient tensor; $\mathbf{S}$ is the second Piola-Kirchhoff stress; $\mathbf{F_v}$ is the volume force vector. The deformation gradient tensor $\mathbf{F}$ is defined in terms of displacement gradient as:

$$\mathbf{F} = \nabla \mathbf{u} + \mathbf{I} \tag{4.4}$$

where $\mathbf{u}$ is the displacement; $\mathbf{I}$ is the identity tensor. In a geometrically nonlinear analysis, the stress should be interpreted as the second Piola-Kirchhoff stress in general. The Lagrange-Green strain tensor $\mathbf{E}$ is related to the displacements by:

$$\mathbf{E} = \frac{1}{2}(\mathbf{F^T F} - \mathbf{I}) = \frac{1}{2}[\nabla \mathbf{u} + (\nabla \mathbf{u})^{\mathbf{T}} + (\nabla \mathbf{u})^{\mathbf{T}} \nabla \mathbf{u}] \tag{4.5}$$

To include the notion of material inelastic deformation into a large deformation framework, the following multiplicative decomposition of the total deformation gradient tensor $\mathbf{F}$ is proposed:

$$\mathbf{F} = \mathbf{F_{el} F_{inel}} \tag{4.6}$$

where $\mathbf{F_{el}}$ is the undamaged elastic deformation tensor; $\mathbf{F_{inel}}$ is the inelastic deformation tensor. Then, the undamaged elastic deformation gradient can be written as:

$$\mathbf{F_{el}} = \mathbf{F F_{inel}^{-1}} \tag{4.7}$$

In this study, the initial strain was considered as zero and the inelastic strain refers only to the swelling strain. The elastic Lagrange-Green strain tensor is computed as:

$$\mathbf{E_{el}} = \frac{1}{2}\left(\mathbf{F_{el}}^{\mathbf{T}} \mathbf{F_{el}} - \mathbf{I}\right) \tag{4.8}$$

The constitutive equation for a linear elastic material relates the stress tensor to the elastic strain tensor.

$$\boldsymbol{\sigma} = \mathbf{C} : \mathbf{E_{el}} \tag{4.9}$$

Here, the Cauchy stress tensor $\boldsymbol{\sigma}$ and strain tensor $\mathbf{E_{el}}$ are second-order tensor, while the constitutive elasticity tensor $\mathbf{C}$ is a fourth-order tensor. With the relationship between Cauchy stress and second Piola-Kirchhoff stress,

$$\boldsymbol{\sigma} = J^{-1} \mathbf{FSF^T} \tag{4.10}$$

where J is the determinant of deformation tensor, the constitutive equation for the elastic rubber can be written as:

$$\mathbf{S} = J_{in} \mathbf{F_{inel}^{-T}} (\mathbf{C} : \mathbf{E_{el}}) \mathbf{F_{inel}^{-1}} \tag{4.11}$$

4.3.3 Multiphysics coupling

Rubber swelling creates an inelastic strain that is proportional to the difference between the concentration and the strain-free reference concentration (Pyo *et al.* 2016):

$$\boldsymbol{\varepsilon}_s = \boldsymbol{\beta}_s c_{\text{diff}} \tag{4.12}$$

where $\boldsymbol{\varepsilon}_s$ is the inelastic strain caused by swelling; c_{diff} is the concentration difference; $\boldsymbol{\beta}_s$ is the coefficient of swelling which is a second-order tensor that can be defined as either isotropic, diagonal, or symmetric. In this case, the coefficient of swelling is isotropic, so only uniform volumetric expansion is taken into account. Since the swelling strain is assumed to be the only contribution to the inelastic strain in this case

$$\mathbf{F}_{\text{inel}} = J_s{}^{1/3}\mathbf{I} \tag{4.13}$$

Then, on the basis of Equation (4.7), the total deformation gradient tensor $\mathbf{F}$ is scaled by the swelling stretch to form the elastic deformation gradient tensor $\mathbf{F}_{\text{el}}$:

$$\mathbf{F}_{\text{el}} = \mathbf{F}J_s{}^{-1/3} \tag{4.14}$$

where J_s is the swelling ratio (volumetric expansion ratio) or the determinant of inelastic deformation tensor, and it relates to swelling strain as:

$$J_s = (1 + \varepsilon_s)^3 = (1 + \beta_s c_{\text{diff}})^3 \tag{4.15}$$

As the swelling process consists of mass diffusion and volume expansion, it induces a coupling between concentration and mechanics. In general, the maltenes concentration within the rubber is unknown and has to be computed with a preceding simulation with known material parameters. Therefore, the concentration is calculated first in a time-dependent study in the mass transport domain and, then, the structural domains are computed in a stationary study based on the results obtained from the transport domain. This sequential approach will significantly reduce the computation time compared to a single solution including all physical interfaces.

4.4 Finite element model

4.4.1 Model definitions

The coupled diffusion-expansion model described in the previous section was implemented in the finite element software COMSOL Multiphysics. The numerical simulations were performed on a square two-dimensional domain of 1.0×1.0 mm meshed with triangular elements. This domain represented the typical microscopic image of CRMB considering the real sizes of rubber particles in this study. To simplify the model, the rubber particle was assumed to be a homogenous isotropic sphere embedded in the bitumen matrix. The complete geometry and mesh of a single rubber particle are shown in Figure 4.2a. The diameter of the single rubber particle was set as 0.3 mm. In terms of the boundary conditions (Figure 4.2b), the left and bottom sides of the domain were set as symmetric in which the two boundaries are free in the plane and fixed in the out-of-plane direction. The right and top sides of the domain were set as free in terms of displacement and no influx imposed. The free boundary conditions of right and top were set to demonstrate the volume expansion visually by the movement of the bitumen matrix.

(a)   (b)
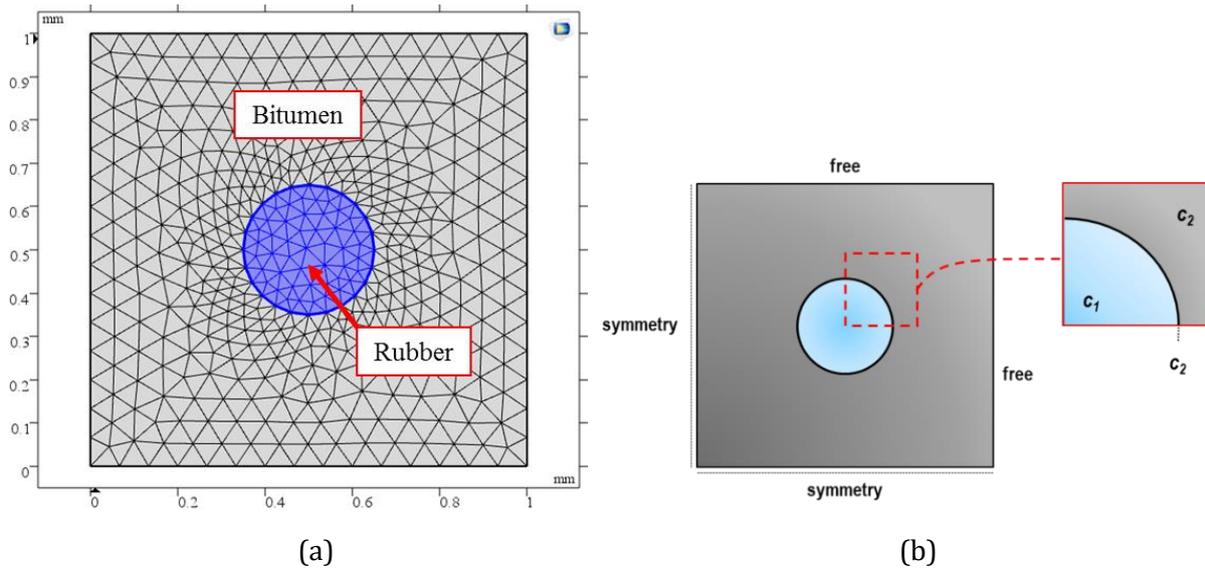
Figure 4.2 (a) Geometry and mesh of the modelling domain: single rubber particle; (b) Schematic of boundary conditions.

4.4.2 Input parameters for modelling

The model input parameters as shown in Table 4.1 were determined and collected from both literature and the current research. To investigate the effects of various factors (e.g. bitumen composition, CRM type, size and shape, interaction temperature and time) on the swelling behavior, five types of bitumen, car tire rubber and truck tire rubber were employed to interact at different temperatures. The simulated cases (1-8) in this study were based on the research conducted by Artamendi and Khalid (2006) and the simulated cases (9-11) were based on the results from Chapter 3.

Based on the laboratory tests, the related parameters, such as equilibrium concentration, diffusion coefficient and swelling coefficient, were calculated. The swelling coefficient was calculated by dividing the swelling strain by the concentration difference in Equation (4.12). In this case, the concentration difference is the equilibrium concentration in the swollen rubber since the initial concentration was zero. The equilibrium concentration is the bitumen fractions in the swollen rubber at the equilibrium state. By defining different values for the material property parameters, the simulation cases listed in Table 4.1 were numerically implemented in the model. At high temperatures, the densities of both bitumen and rubber decrease. The density of bitumen was set as 0.93 g/cm^3 at high temperatures (Hunter *et al.* 2015). The rubber particle was set to have a density of 1 g/cm^3, a Young's modulus of 8 MPa, and a Poisson's ratio of 0.45 (Mark 2009). Based on the experimental results in Table 4.1, it was found that both swelling coefficients and diffusion coefficients are highly temperature dependent.

Table 4.1 Material parameters used in the simulation.

Case	Bitumen type	SARA fractions (%)	Temperature (°C)	Rubber source	Equilibrium concentration (kg/m³)	Diffusion coefficient, D (m²/s)	Swelling coefficient, β_s (m³/kg)
1	100KSR	S=7.1 A=57.6 R=19.1 A=16.2	180	Car tire	399.4	1.96×10⁻¹¹	4.85×10⁻⁴
2				Truck tire	523.9	2.61×10⁻¹¹	5.73×10⁻⁴
3	50KSR	S=8.0 A=48.0 R=22.0 A=22.0	180	Car tire	415.2	1.96×10⁻¹¹	4.95×10⁻⁴
4				Truck tire	469.9	2.15×10⁻¹¹	5.30×10⁻⁴
5	100VEN	S=9.7 A=49.8 R=23.5 A=17.0	180	Car tire	457.4	7.11×10⁻¹¹	5.22×10⁻⁴
6				Truck tire	558.8	7.42×10⁻¹¹	6.06×10⁻⁴
7	50VEN	S=8.0 A=51.4 R=19.7 A=20.9	180	Car tire	430.1	3.37×10⁻¹¹	5.03×10⁻⁴
8				Truck tire	469.9	3.82×10⁻¹¹	5.30×10⁻⁴
9	Pen 70/100 Nynas	S=7.0 A=45.0 R=22.0 A=20.0	160	Truck tire	579.0	1.52×10⁻¹¹	4.37×10⁻⁴
10			180		628.1	3.79×10⁻¹¹	5.58×10⁻⁴
11			200		674.6	10.91×10⁻¹¹	6.63×10⁻⁴

4.4.3 Model validation

4.4.3.1 *Comparison of mass uptake curves*

Model validation is concerned with quantifying the accuracy of the model by comparing numerical solutions to experimental data. To validate the developed swelling model, the simulation of rubber swelling in 100KSR bitumen at 180 °C (case 1 and 2) were taken as an example and the simulation results were compared with the experimental data (Artamendi and Khalid 2006). The mass uptake during the diffusion process was automatically calculated by the FE model.

The analytical solution of Fick's laws for one-dimensional diffusion in a medium bounded by two parallel planes is given by

$$\frac{M_t}{M_\infty} = 1 - \sum_{n=0}^{\infty} \frac{8}{(2n+1)^2 \pi^2} \exp\left\{-D(2n+1)^2 \frac{\pi^2 t}{d^2}\right\} \tag{4.16}$$

The corresponding solution useful for small times used to fit the experimental results is (Crank 1975).

$$\frac{M_t}{M_\infty} = \frac{4}{d}\sqrt{\frac{Dt}{\pi}} \tag{4.17}$$

where M_t and M_∞ are the masses of the diffusing substance absorbed at time t and at equilibrium respectively; t is the immersion time (s) for the rubber in bitumen and d is the rubber sample thickness (mm). This equation indicates a linear relationship between initial weight gain ($M_t/M_\infty < 0.6$) and the square root of time.
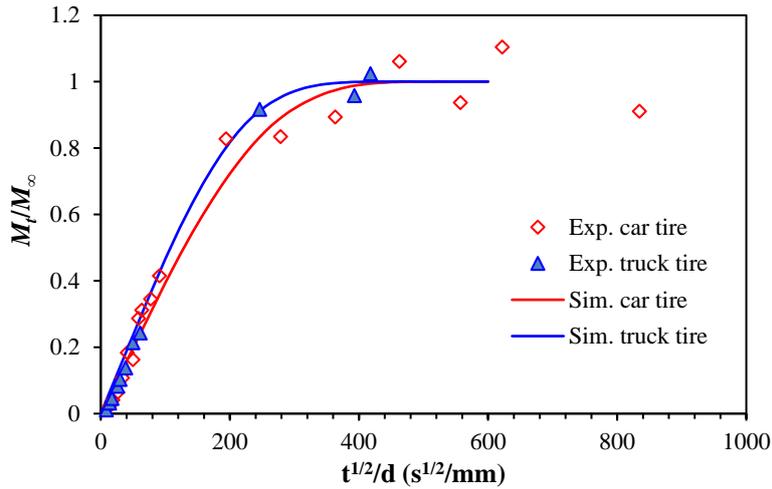
Figure 4.3 Bitumen absorption into rubber at 180 °C during the swelling process.

Figure 4.3 shows the variation in M_t/M_∞ with $t^{1/2}/d$ for the absorption of 100KSR bitumen into the truck and car tire rubber at 180 °C. Both experimental and numerical data in Figure 4.3 verify the linear regions in the early stages of diffusion for both types of rubber. It can be seen from Figure 4.3 the numerical data correlates well with the experimental data. In addition, truck-tire rubber reaches the equilibrium earlier than car-tire rubber does. This finding is consistent with the experimental results and is because truck-tire rubber contains more natural rubber than car tire rubber. Natural rubber swells faster than the synthetic rubber in bitumen.
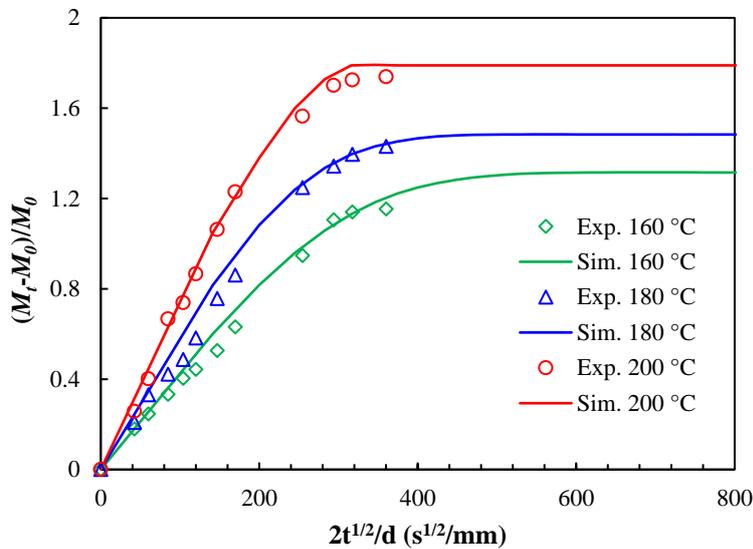
Figure 4.4 Bitumen (Pen 70/100 Nynas) absorption into truck-tire rubber at different temperatures during the swelling process.

Alternatively, the sorption curves of bitumen (Pen 70/100 Nynas) into truck-tire rubber at different temperatures are shown in Figure 4.4. A plot of the mass uptake $(M_t - M_0)/M_0$ versus the parameter $2t^{1/2}/d$ was used to be consistent with the experimental data presented in Chapter 3. It can be seen from Figure 4.5 that correlations between the experimental data and data from numerical simulations are good. Furthermore, diffusion of bitumen into rubber occurs faster at

higher temperatures, resulting in the sorption curve reaching the equilibrium state at an earlier stage.

4.4.3.2 Calculation of swelling ratio

Figure 4.5a presents the total displacement contour of rubber particle in bitumen when equilibrium swelling reaches for Case 1 and 2 simulations. The maximum displacements for two cases were also annotated in the figure. It can be found that car-tire rubber produces less swelling than truck-tire rubber under the same condition. Truck-tire rubber contains more natural rubber components, which are more prone to swell in bitumen due to the high chain flexibility of simple long-chain structures with less network constraints comparing to the synthetic rubber in car-tire rubber. It is noteworthy that, due to the swelling of rubber in bitumen, the bitumen matrix was squeezed out of the original boundary. In addition, the swelling of rubber is not uniform due to the constraints of the surrounding bitumen.

(a)

(b)
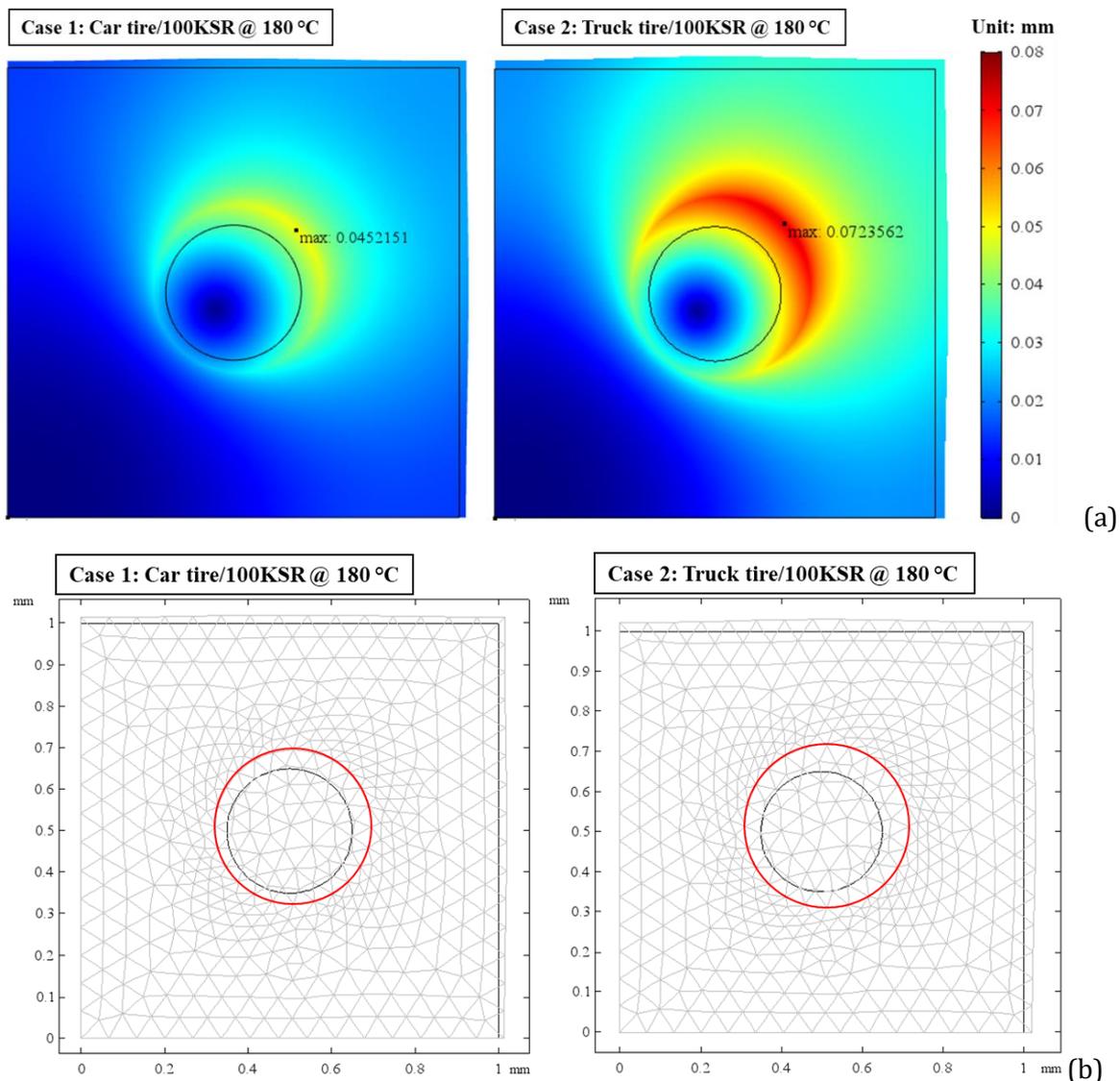
Figure 4.5 Simulation results for Case 1 and 2: (a) total displacement of rubber particle in bitumen at the equilibrium swelling state; (b) deformed mesh of the model at the equilibrium swelling state.

To calculate the volume change (area change in 2D model) of rubber during swelling, deformed geometries were generated as shown in Figure 4.5b. The black circle represents the original

rubber particle while the red one represents the swollen rubber particle. The area of swollen rubber particle was calculated using the surface integral based on the deformed geometry. The volume change of rubber particles during the swelling process was illustrated in terms of swelling ratio in Figure 4.6. The swelling ratio was defined as the area increase divided by the original area of rubber particle. It can be seen from Figure 4.6 that swelling of rubber happens faster at the earlier stage of interaction, which is consistent with the diffusion process. With the increase of interaction time, car-tire and truck-tire rubber sequentially reached the swelling equilibrium at 1150 s and 900 s, respectively. The equilibrium times from simulation are close to the experimental counterparts, 1014 s and 762 s. As expected, truck-tire rubber has a larger equilibrium swelling ratio in bitumen than car-tire rubber. For the case of 100KSR bitumen at 180 °C, the equilibrium swelling extent for car-tire and truck-tire rubber was 0.49 and 0.79, respectively.
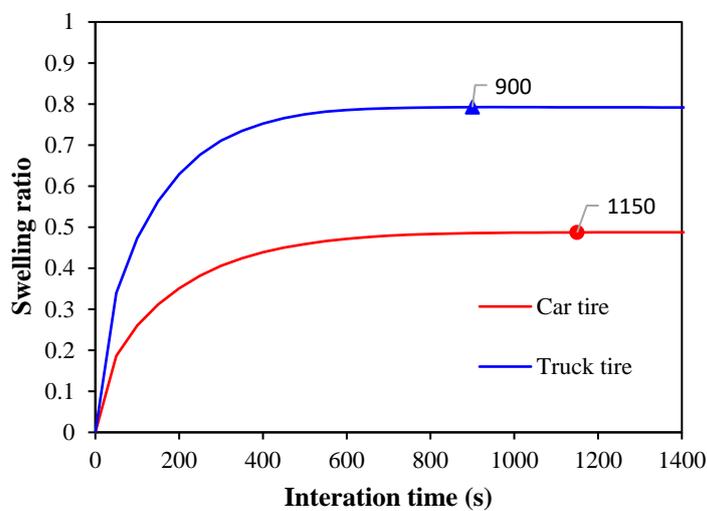
Figure 4.6 Volume change of rubber particles during swelling for simulation Case 1 and 2.

4.5 Parametric analysis for factors affecting rubber swelling

4.5.1 Effect of temperature on swelling

The simulation results for Case 9-11 were summarized in Figure 4.7 in terms of variation in swelling ratio with interaction time. It is clear that with the increase of interaction temperature, swelling of rubber particles in bitumen takes place faster. The higher the interaction temperature, the shorter time rubber particles need to reach the equilibrium. This is because of the increased diffusion coefficients at elevated temperatures which stems from the greater segmental motion of polymer chains. Since rubber swelling in bitumen is a diffusion-induced phenomenon, it is logical that higher temperatures also result in higher equilibrium swelling ratios of rubber. The simulation results exactly correspond to the experimental data in Chapter 3. Some studies also found that as the temperature increases, the rate of swelling increases and the swelling extent decreases (Abdelrahman and Carpenter 1999). This contradictory result maybe stems from the partial dissolution of rubber into bitumen at elevated temperatures. The measured mass uptake and hence swelling ratio was smaller than expected due to the loss of the sample integrity.
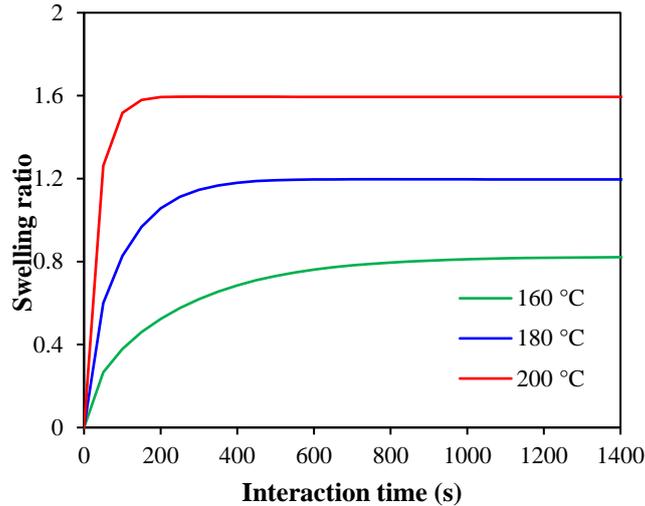
Figure 4.7 Truck-tire rubber swelling in bitumen (Pen 70/100 Nynas) at different temperatures.

4.5.2 Effect of bitumen composition on swelling

The different crude oil sources and diverse fuel processing technologies produce various chemistry of bitumen, specifically with various SARA fractions, and consequently influence the compatibility with CRM and the rubber swelling development in bitumen. The simulation results for demonstrating the effect of bitumen composition on swelling were summarized in Figure 4.8 in terms of variation in swelling ratio with interaction time.

(a)   (b)
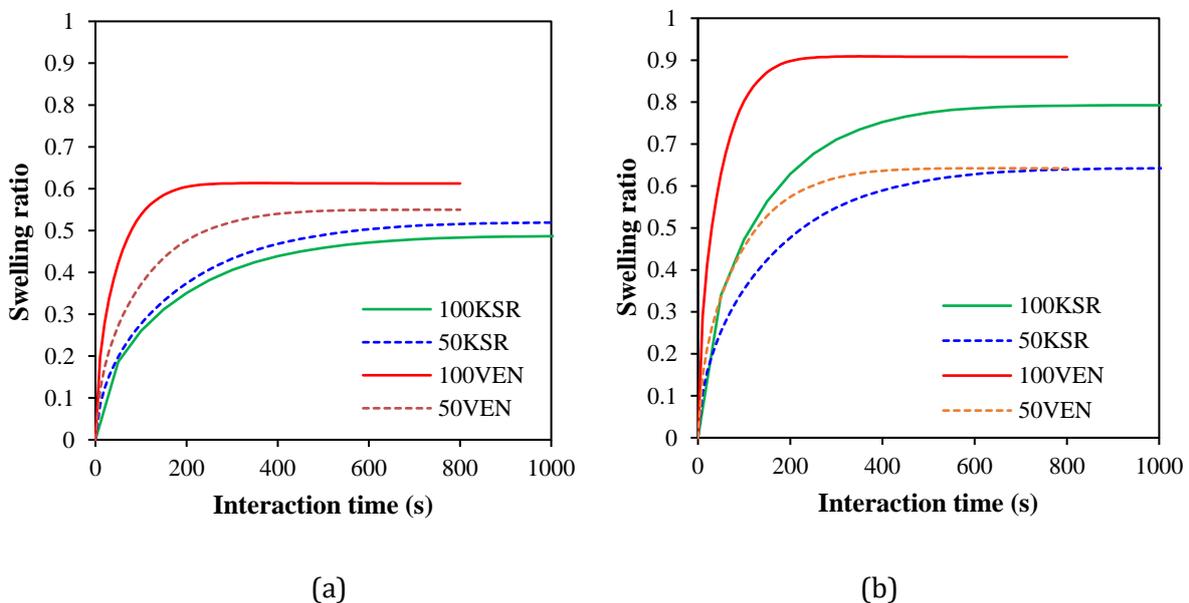
Figure 4.8 Rubber swelling in different bitumens at 180 °C: (a) car tire, (b) truck tire.

It can be seen from Figure 4.8 that even in the same grade bitumen from different origins, rubber particles swell differently. For the same grade bitumen, both car-tire and truck-tire rubber particles seems to be more prone to swell in the Venezuelan bitumen than the Kuwaiti. In addition, within each bitumen type, rubber can swell faster and more in the high penetration grade bitumen, which correspond to the bitumen with higher maltenes content and lower asphaltene

content. This is because the aromatic fractions (maltenes) of bitumen have similar solubility parameters with rubber and therefore better compatibility (Lesueur 2009). Asphaltenes have high molecular weight and are not likely to diffuse into the rubber network and make it swell.

4.5.3 Effect of rubber particle shape on swelling

Previous studies have reported that the rubber particle shape also has an impact on the bitumen-rubber interaction and hence the binder property (Shen *et al.* 2009). To investigate the particle shape effects on the swelling process of rubber in bitumen, several different particle shapes, including triangle, square, pentagon, octagon, ellipse and circle, were implemented for the rubber in the numerical model. To eliminate the size effect, all the particles with different shapes have a consistent area (size). The material parameters from Case 1 were used for the simulation. Figure 4.9 presents the simulation results of the swelling of rubber particles with different shapes. The effects of particle shape on the concentration after 200 s diffusion were in Figure 4.9a. It can be seen that the particle shape mainly has impacts on the edge and periphery of the particle. Figure 4.9b demonstrates the different swelling curves of rubber particles with different shapes. In general, with the increase of side of the polygon, the equilibrium swelling ratios are closer to that of a circular particle. Rubber particle with a circular shape yields the highest equilibrium swelling ratio followed by the elliptical particle. It is also noteworthy that the elliptical particle has the largest swelling rate at the early stages. The above findings coincide with the practical experience that rubber particles with irregular shapes have a faster swelling rate but a relatively smaller equilibrium swelling ratio (Shen and Amirkhanian 2007).

(a)

(b)

Figure 4.9 Rubber particles of varying shapes swelling in bitumen at 180 °C (a) concentration at t=1200 s; (b) variation in swelling ratio with time.

4.5.4 Effect of rubber particle size on swelling

In order to directly visualize the effect of rubber particle size on swelling, another finite element model consisting of five rubber particles with varying radiuses (0.2, 0.4, 0.6, 0.8, 1.0 mm) was also developed as shown in Figure 4.10a. The boundary conditions (Figure 4.10b) were set as fixed boundaries in the structural domain to simulate the real mixing scenario by considering the constraints from the vessel. The interparticle effect (interference) on the rubber swelling can also be demonstrated by this case. The initial solvent concentration within the rubber was set as zero, which is the strain-free reference concentration. The periphery boundaries of the rubber particle contacted directly to the bitumen were set to have the same concentration as the surrounding bitumen matrix. The swelling process of different-size rubber particles in different types of bitumen at various interaction conditions were simulated based on the proposed coupled diffusion-expansion model.

(a)   (b)
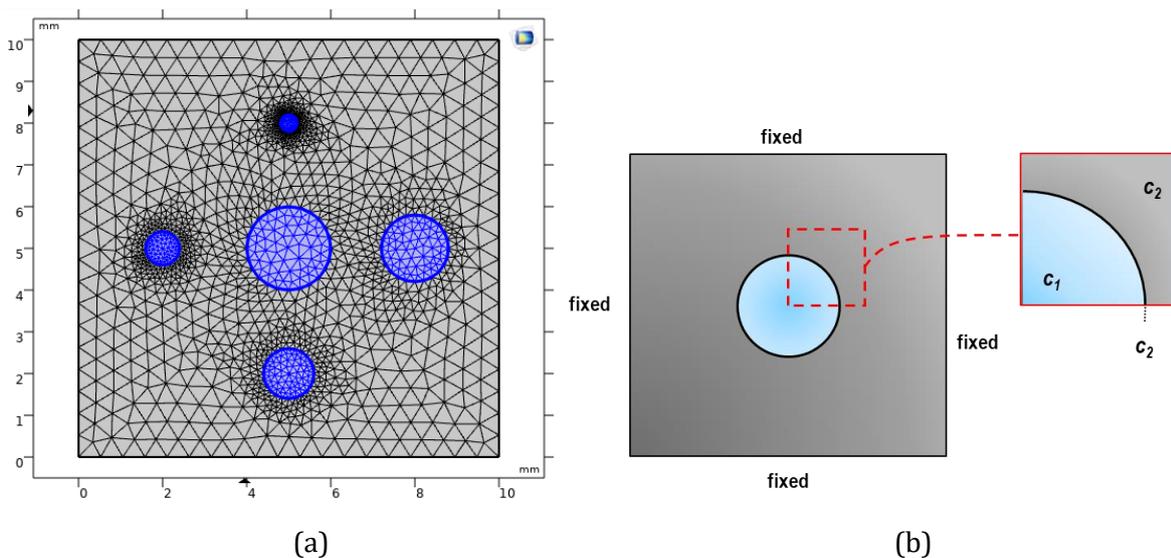
Figure 4.10 (a) Geometry and mesh of the modelling domain: multiple rubber particles of varying sizes; (b) Schematic of boundary conditions.

The input material parameters for Case 10 were applied for this specific simulation. Figure 4.11 presents the simulation results of swelling of rubber particles with different sizes.

(a)   (b)

(c)
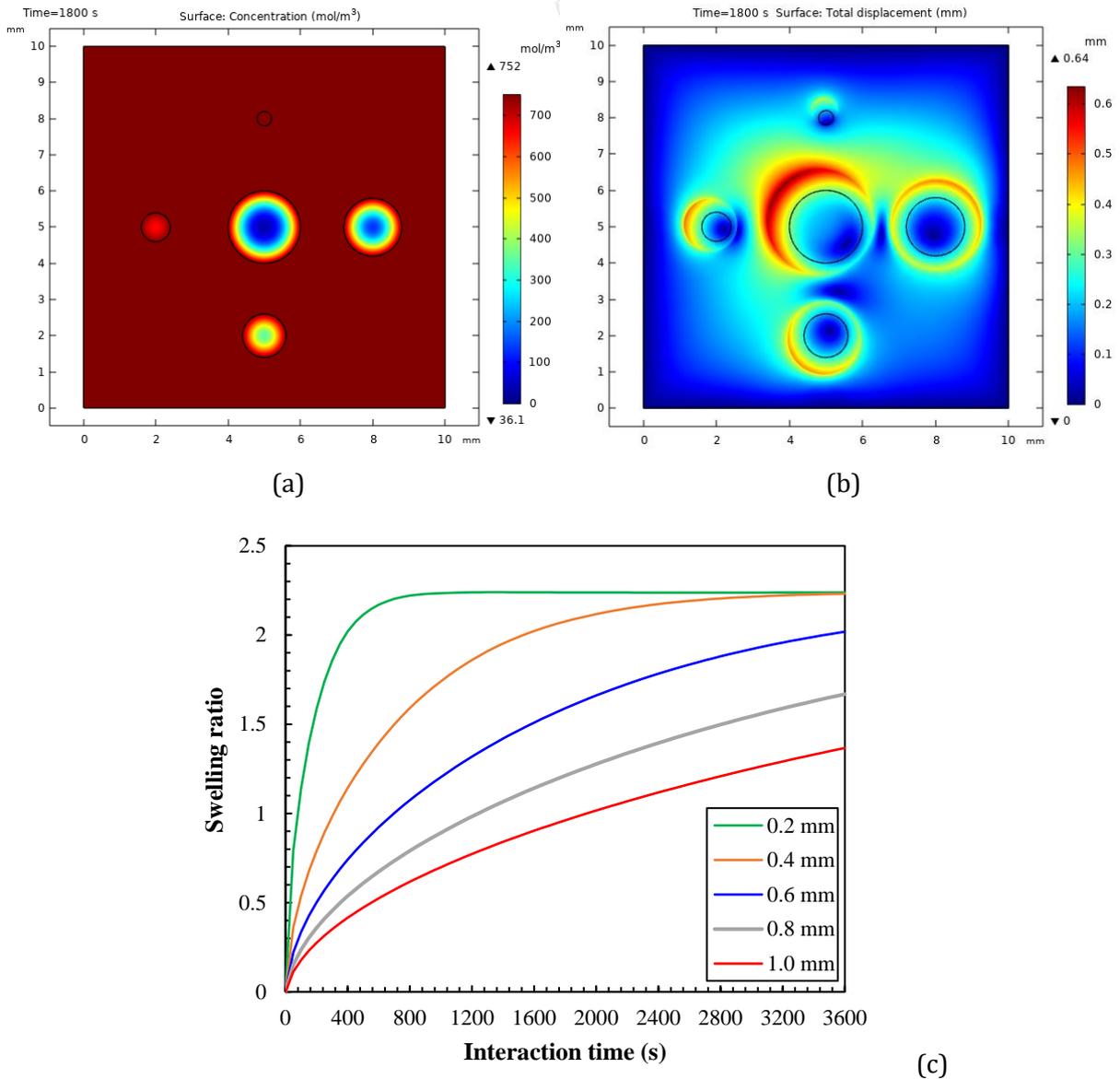
Figure 4.11 Rubber particles of varying sizes swelling in bitumen at 180 °C: (a) concentration at t=1800 s; (b) total displacement of rubber particles at t=1800 s; (c) variation in swelling ratio with time.

It can be seen from Figure 4.11a that small rubber particles (with a radius of 0.2 mm) are fully saturated with maltenes at t=1800 s while other particles still have a concentration gradient along the direction from outer to inner. The particle size has an impact on the time-dependent diffusion process and further affects the swelling behavior of rubber. It is understandable that large rubber particles have larger volume changes after the same interaction time as shown in Figure 4.11b. However, small rubber particles swell faster and reach the equilibrium swelling at an earlier stage than big particles do as shown in Figure 4.11c. The asymmetric displacement of a certain rubber particle is due to the interference effect from neighbor particles, which creates extra forces on the rubber particles. Since the input material parameters for the rubber particles are identical, it is predictable that rubber particles with varying sizes will have the same swelling ratio when equilibrium swelling reaches. The only difference is that big rubber particles need a longer time

to reach the equilibrium. This is also can be explained by Equation (4.17) that if considering swelling as a Fickian diffusion process, the required interaction time to achieve the same swelling ratio increases with the square of the particle size.

4.5.5 Effect of rubber particle concentration on swelling

In the real mixing process of bitumen and rubber, the effect of rubber particle concentration on swelling cannot be ignored. To address this issue, two aspects were considered. Firstly, the configuration of rubber particles was considered by varying the particle distance as shown in Figure 4.12a. Secondly, different numbers of rubber particles were simulated as shown in Figure 4.12b comparing with Figure 4.10a. To simplify the issue, the distance between surrounding particles and the center particle is set to be equal.

(a)   (b)
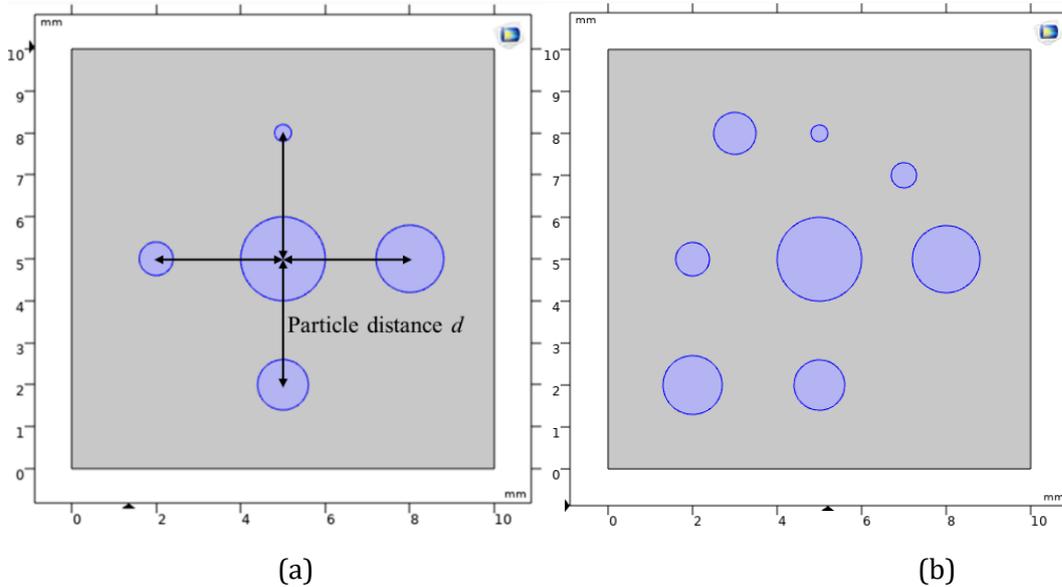
Figure 4.12 Addressing the effect of rubber particle concentration on swelling through (a) varying particle distance; (b) varying particle numbers.

The input material parameters for Case 10 were applied for this specific simulation. Figure 4.13 presents the deformed meshes of simulated models in two scenarios of different particle distances. From Figure 4.13a, when the particle distance is relatively large (d=3 mm), all the particles finished the swelling process more or less centering the original position. However, when condensing the particle distance to 2 mm in Figure 4.13b, the positions of different particles were changed significantly after swelling. This is because of the pushed forces exerted by the neighbor particles. It can be seen the swollen particles have already contacted each other. Because these particles are impenetrable solids, they were pushed away from the original positions due to the expansion forces. What is of particular interest is whether these different arrangements of rubber particles (either distance or number) will affect the swelling ratio of rubber. To answer this question, the simulations of particle distance effect was extended to other cases, d=2, 2.5, 3, and 3.5 mm.

(a)   (b)
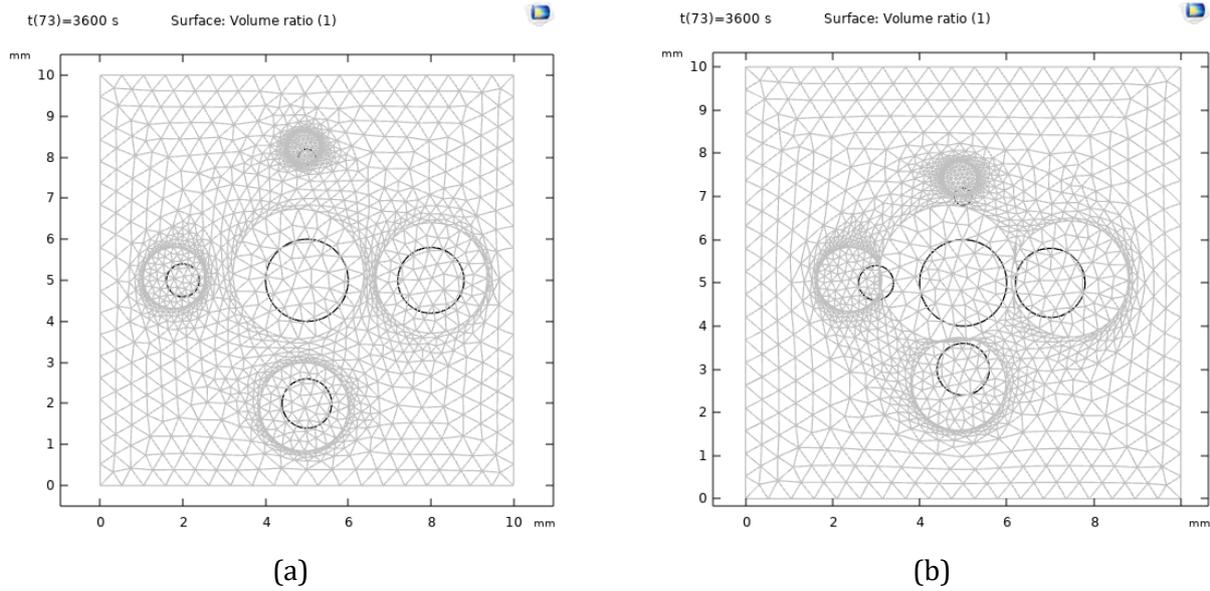
Figure 4.13 Deformed mesh of the FE model (a) particle distance *d*=3 mm; (b) particle distance *d*=2 mm.

Taking the centre particle as an example since it has the interference of all the surrounding particles, the swelling ratio of the centre particle with a radius of 1 mm was plotted with the change of time in Figure 4.14. The particle distance may have effects the positions of particles but have almost no effects on the swelling ratio. The reason for this phenomenon is that bitumen matrix has a very small modulus at high temperatures and hence has very limited constraints on the expansion of rubber particles. Because of the low resistance imposed by bitumen, rubber particles can be easily pushed to other positions.
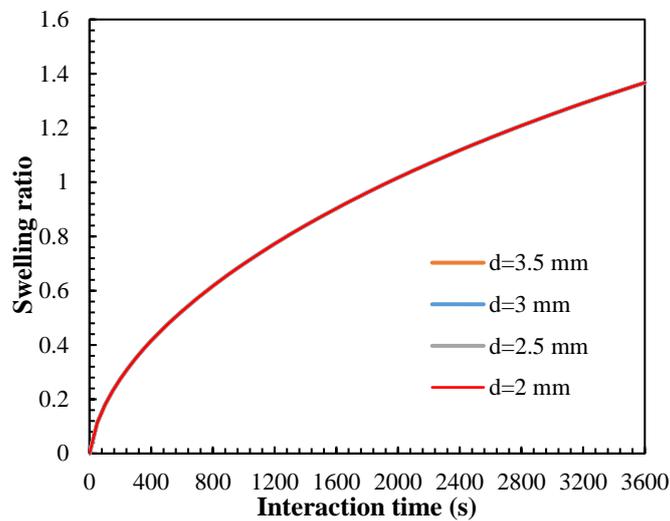
Figure 4.14 Variation in the swelling ratio of rubber particle with a radius of 1 mm.

Figure 4.15 also shows the deformed mesh of the model with eight rubber particles. The original five particles in Figure 4.15 have almost the same swelling patterns as that in Figure 4.13a.
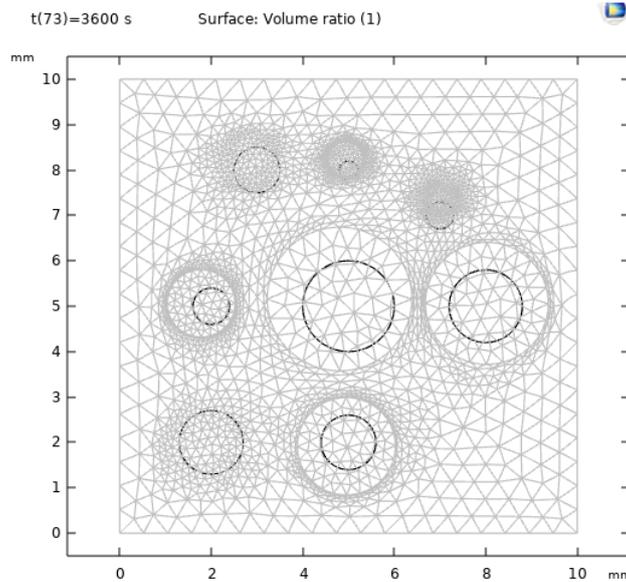
Figure 4.15 Deformed mesh of the FE model with eight rubber particles.

The simulation results of swelling ratio in two scenarios (particle number *n*=5 and 8) are compared in Figure 4.16. The number of particles seems have no effects on the rubber swelling ratio. Similar reasons as the effect of particle distance can be used to explain this phenomenon. The prerequisite to make this occur is that there is enough bitumen for rubber to swell, which is the case in this study where the bitumen concentration is set as constant. It was proved in the laboratory that when the rubber concentration is lower to a certain value (around 25%), there are sufficient bitumen (light fractions) to allow absorption to occur (Airey *et al.* 2004). Rubber concentration of 25% is normally the upper limit when preparing CRMB binders.
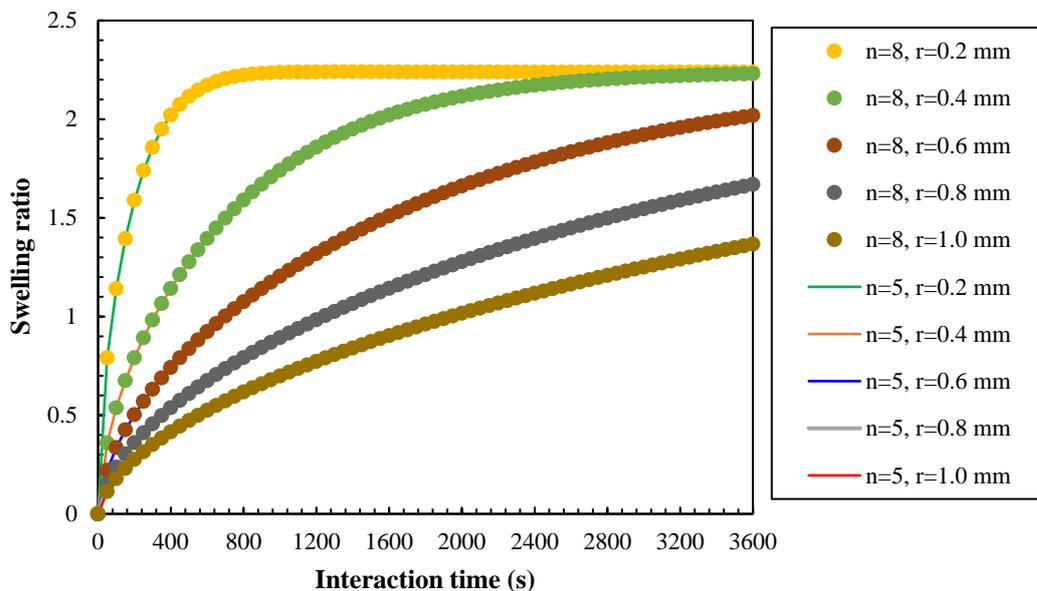
Figure 4.16 Evolution of swelling ratios of different size rubber particles in two scenarios.

4.5.6 Potential application

The inclusion of CRMs in bitumen stiffens the binder. Such a modified bitumen is similar to particulate filled polymer matrix composites. Comparing to the rigid mineral filler in asphalt mastics, the stiffening or reinforcement mechanisms of CRMs in bitumen may include volume-filling reinforcement, physiochemical reinforcement and particle-interaction reinforcement (Buttlar *et al.* 1999, Putman and Amirkhanian 2010). The effective viscoelastic behavior of CRMB can be predicted by particulate composite micromechanical models addressing the above reinforcement mechanisms. The micromechanical models are generally based on the mechanical properties and volume fractions of individual constituents (Yin *et al.* 2008). The importance of estimating the swelling of CRMs in bitumen is that if known, then it may be possible to use suitable micromechanical models with some level of accuracy to estimate the viscoelastic properties of CRMB. With the predicted properties of CRMB, it might be possible to optimize the design and process of bitumen-rubber blends and to set quality control limits to ensure a well-performing mixture.

4.6 Summary

With the aim of predicting the swelling behavior of rubber in bitumen, this chapter presented a coupled diffusion-expansion model to address the multiphysics of swelling which consists of mass diffusion and volume expansion. In this model, a one-way coupling was introduced between concentration and mechanics. Firstly, the mass concentration is calculated in a time-dependent study in the mass transport domain, and then the structural domains are computed in a stationary study based on the results got from transport domain. Based on the numerical simulation results, the following conclusions can be drawn:

- There is a good correlation between the simulation results and the previously reported experimental results. The developed model can effectively predict the swelling behavior of rubber in bitumen.

- Under the same condition, truck-tire rubber can absorb more bitumen and cause more swelling than car-tire rubber.

- Temperature is a crucial factor affecting the swelling process. With the increase of temperature, the diffusion coefficient increases and the equilibrium swelling time decreases.

- In general, high penetration grade bitumen with higher aromatic fractions is more compatible with rubber and therefore increases the swelling extent of rubber.

- Under the same condition, small rubber particles swell faster and reach the equilibrium swelling at an earlier stage than large rubber particles.

- Rubber particle concentration seems have no effects on the swelling in this simulation.

The developed multiphysics model creates an opportunity to apply the estimated swelling behaviors of rubber into the suitable micromechanical models for further property predictions of CRMB, see Chapter 7. Further dedicated experimental studies are recommended to be conducted to establish a database of the material properties of various rubbers and bitumens to serve as the input parameters in the developed model.

4.7 References

Abdelrahman, M., 2006. Controlling performance of crumb rubber-modified binders through addition of polymer modifiers. *Transportation Research Record: Journal of the Transportation Research Board,* (1962), 64-70.

Abdelrahman, M.A. & Carpenter, S.H., 1999. Mechanism of the interaction of asphalt cement with crumb rubber modifier. *Transportation Research Record: Journal of the Transportation Research Board,* 1661, 106-113.

Airey, G., Rahman, M. & Collop, A.C., 2004. Crumb rubber and bitumen interaction as a function of crude source and bitumen viscosity. *Road Materials and Pavement Design,* 5 (4), 453-475.

Artamendi, I. & Khalid, H.A., 2006. Diffusion kinetics of bitumen into waste tyre rubber. *Journal of the Association of Asphalt Paving Technologists,* 75, 133-164.

Buttlar, W., Bozkurt, D., Al-Khateeb, G. & Waldhoff, A., 1999. Understanding asphalt mastic behavior through micromechanics. *Transportation Research Record: Journal of the Transportation Research Board,* (1681), 157-169.

Crank, J., 1975. *The mathematics of diffusion* Great Britain: Clarendon Press Oxford.

Dong, D., Huang, X., Li, X. & Zhang, L., 2012. Swelling process of rubber in asphalt and its effect on the structure and properties of rubber and asphalt. *Construction and Building Materials,* 29, 316-322.

Feng, W., Minming, K., Guanlong, L., Xiaolong, Z. & Chenglie, L., 2015. Investigation of swelling and dissolution process of natural rubber in aromatic oil. *China Petroleum and Petrochemical Technology,* 17, 76-86.

Frantzis, P., 2004. Crumb rubber-bitumen interactions: Diffusion of bitumen into rubber. *Journal of materials in civil engineering,* 16 (4), 387-390.

Hunter, R.N., Self, A. & Read, J., 2015. *The shell bitumen handbook*: ICE Publishing.

Lesueur, D., 2009. The colloidal structure of bitumen: Consequences on the rheology and on the mechanisms of bitumen modification. *Adv Colloid Interface Sci,* 145 (1-2), 42-82.

Mark, J.E., 2009. *The polymer data handbook,* Second Edition ed. Oxford, UK: Oxford University Press.

Putman, B.J. & Amirkhanian, S.N., 2010. Characterization of the interaction effect of crumb rubber modified binders using hp-gpc. *Journal of Materials in Civil Engineering,* 22 (2), 153-159.

Pyo, J.B., Lee, T.I., Kim, C., Kim, M.S. & Kim, T.S., 2016. Prediction of time-dependent swelling of flexible polymer substrates using hygro-mechanical finite element simulations. *Soft Matter,* 12 (18), 4135-41.

Scarpas, A., 2004. *A mechanics based computational platform for pavement engineering*. Delft University of Technology.

Shen, J. & Amirkhanian, S., 2007. The influence of crumb rubber modifier (crm) microstructures on the high temperature properties of crm binders. *International Journal of Pavement Engineering,* 6 (4), 265-271.

Shen, J., Amirkhanian, S., Xiao, F. & Tang, B., 2009. Influence of surface area and size of crumb rubber on high temperature properties of crumb rubber modified binders. *Construction and Building Materials,* 23 (1), 304-310.

Wang, H., Apostolidis, P., Liu, X. & Scarpas, T., 2018. Modeling of rubber swelling in bituminous binders. *Advances in Materials and Pavement Prediction: Papers from the International Conference on Advances in Materials and Pavement Performance Prediction (AM3P 2018).* Doha, Qatar: CRC Press, 181.

Yin, H.M., Buttlar, W.G., Paulino, G.H. & Benedetto, H.D., 2008. Assessment of existing micro-mechanical models for asphalt mastics considering viscoelastic effects. *Road Materials and Pavement Design,* 9 (1), 31-57.

5

CRMB preparation and property characterization

5.1 Optimization of bitumen-rubber mixing conditions

5.1.1 Materials

5.1.1.1 *Base bitumen*

Base bitumen of 70/100 penetration grade provided by Nynas (Stockholm, Sweden) was selected as the base bitumen because this grade of bitumen is commonly used in the Netherlands. The specification of the base bitumen is shown in Table 5.1 according to EN 12591. The SARA (saturated hydrocarbons, aromatic hydrocarbons, resins, asphaltenes) analysis of base bitumen was done by Iatroscan TLC-FID (Bechenheim, Germany). The four-component proportions are 7% for saturates, 51% for aromatics, 22% for resins, and 20% for asphaltenes, respectively.

Table 5.1 Specifications of Nynas 70/100.

	Test Description	**Unit**	**Value**
Consistency at intermediate service temperature	Penetration at 25 °C	mm/10	80
Consistency at elevated service temperature	Softening Point	°C	46
Resistance to hardening at 163°C	Change in mass	%	0.72
	Retained penetration	%	52
	Softening point after hardening	°C	51
Technical characteristic	Density at 25 °C	g/cm^3	1.027
	Kinematic viscosity at 135 °C	mm^2/s	265
	Solubility	%	>99.0

5.1.1.2 *Crumb rubber modifier*

Crumb rubber produced from the ambient grinding process of scrap truck tyre was utilized as a bitumen modifier in this study as shown in Figure 5.1.

Figure 5.1 Appearance of crumb rubber with particle sizes ranging from 0~0.71 mm.

The CRM particle size range from 0 to 0.71 mm. The basic properties, composition and particle gradation of CRM are shown in Table 5.2. The processing agents mainly consist of antioxidants/antiozonants and curing additives (e.g., sulfur, zinc oxide, stearic acid, accelerator and oil etc.). The morphology and elemental composition of CRM were analyzed by Environment Scanning Electron Microscopy (ESEM) with an energy dispersive X-ray spectroscopy (EDX) in Figure 5.2 (Wang *et al.* 2020). The EDX spectrum was presented as a plot of X-ray counts versus energy (keV). The energy peaks corresponding to the various elements in the sample are also shown. It should be noted that elements lighter than the atomic number of Na cannot be detected. It can be found rubber particles ground from the ambient process have an irregular shape and multiaperture structure. Rubber particles also contain different types of chemical compounds (e.g., oxide, zinc, iron and silicon, etc.).

Table 5.2 Basic properties and particle size distribution of CRM.

Properties		**Description or value**	
Source		Scrap truck tires	
Colour		Black	
Morphology		Porous	
Specific gravity (g/cm^3)		1.15	
Decomposition temperature (°C)		~200	
Chemical composition	Total rubber (natural and synthetic)	55	
	Carbon Black (%)	25	
	Processing agents (%)	20	
Gradation	Sieves (mm)	Passing (%)	Retained (%)
	0.710	100	0
	0.500	93	7
	0.355	63	30
	0.180	21	42
	0.125	9	12
	0.063	2	7
	pan	-	2
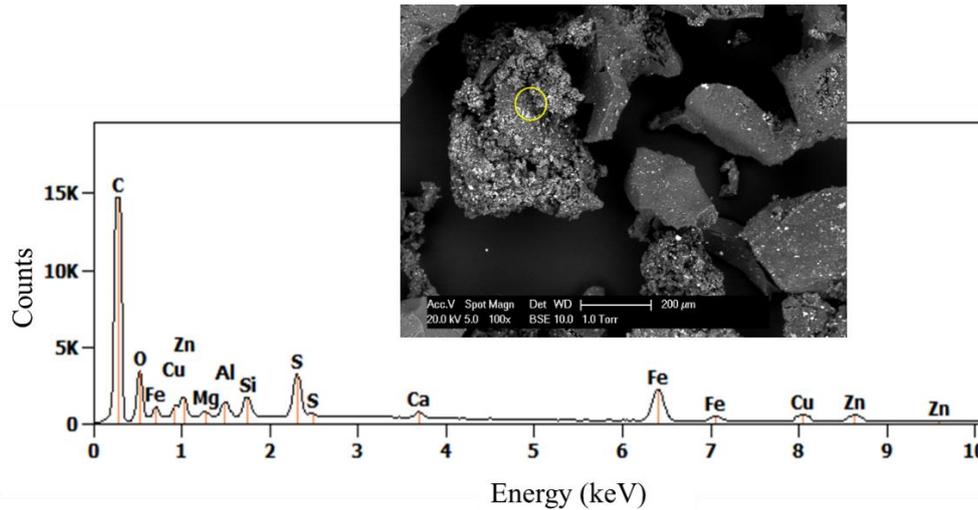
Figure 5.2 Morphology and elemental compositions of CRM processed by ambient grinding.

5.1.2 Bitumen-rubber mixing program

From the results of previous chapters on rubber swelling in bitumen, it is known temperature and time are two critical factors affecting the bitumen-rubber interaction process. For given base bitumen and CRM, the interactions of bitumen and rubber are functions of mixing temperatures, time and rate. Since the mixing rate has a similar effect as the mixing time (Ghavibazoo *et al.* 2013), only two interaction variables (temperature and time) were considered in this study to determine the optimized mixing procedure to produce desirable CRMB binders. The dosage of CRM was set as 22% by weight of base bitumen based on previous studies (Huang 2008, Wang *et al.* 2018b). The selection of CRM dosage of 22% was inspired by the specification of typical asphalt rubber used in California, where it is specified to include 22 to 28 percent CRM by mass of the base bitumen (State of California Department of Transportation 2003). Manual stirring for 5 min was applied to pre-distribute CRM in the base bitumen, then the blend was mixed using a Silverson high shear mixer (Figure 5.3) with a square hole screen at 6000 rpm with different combinations of temperature and time. Three interaction temperature levels were chosen: 160 °C, 180 °C, and 200 °C. At each temperature, different mixing time, 30 min, 60 min, 90 min were applied for the CRMB blends. During the laboratory mixing process, the mixing head (square hole) was immersed into the hot bitumen to avoid vortex which may involve the potential oxidative aging. Binder samples prepared at different conditions were subjected to different tests later to determine the optimal mixing condition.
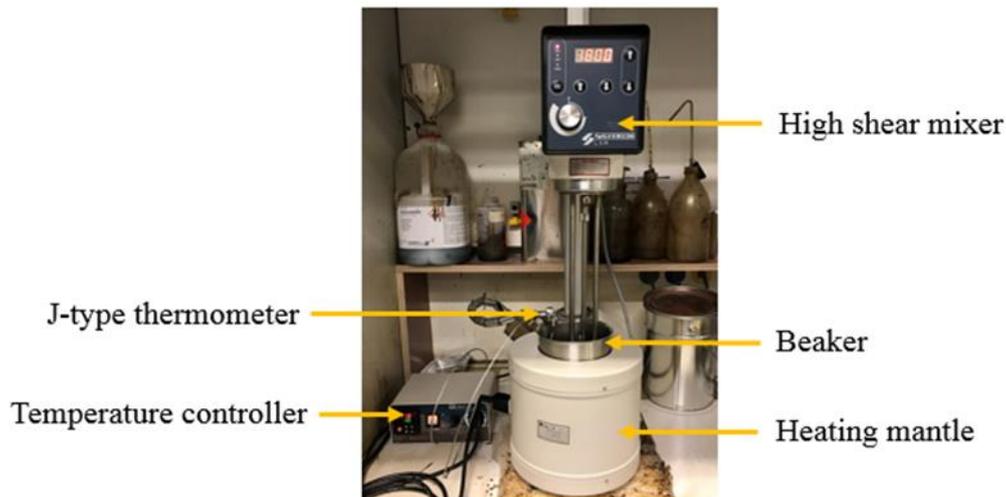
Figure 5.3 Laboratory equipment used to prepare CRMB binders.

5.1.3 Rheological and chemical characterization

5.1.3.1 *Multiple Stress Creep and Recovery (MSCR) Test*

The MSCR test was conducted using a DSR with parallel plates at two stress levels (0.1 kPa and 3.2 kPa) at 64 °C according to AASHTO T350-14. The test protocol includes a creep load of 1 s duration followed by 9 s recovery at zero loads in each cycle. Ten creep and recovery cycles were tested at each stress level. The non-recoverable creep compliance (J_{nr}) and percent recovery (R) were calculated to characterize the stress dependence and elastic response of asphalt binders. Before the creep and recovery test, a certain number of cycles for conditioning were applied to reach a steady state.

From the previous MSCR test results of various modified asphalt binders, it was known that MSCR test method is sensitive to the microstructure of the polymer modified binders (D'Angelo and Dongré 2009). It is anticipated that MSCR test can be also utilized to characterize the microstructural changes of CRMB binders at various interaction conditions. In this study, test samples for MSCR were prepared and moulded immediately after the interactions to avoid reheating the solidified CRMB binders, which may cause potential interactions within the binders and therefore produce confounded results. Three replicates were prepared for each sample.

Figure 5.4 shows a typical plot of the first creep and recovery cycle at 3.2 kPa. For brevity, only the results of CRMB binders prepared with 30-min mixing were shown. The effects of interaction on the creep and recovery behaviours of CRMB binders are clearly identified by the distinct stress-strain responses. To see the whole strain response at the stress level of 0.1 kPa and 3.2 kPa,
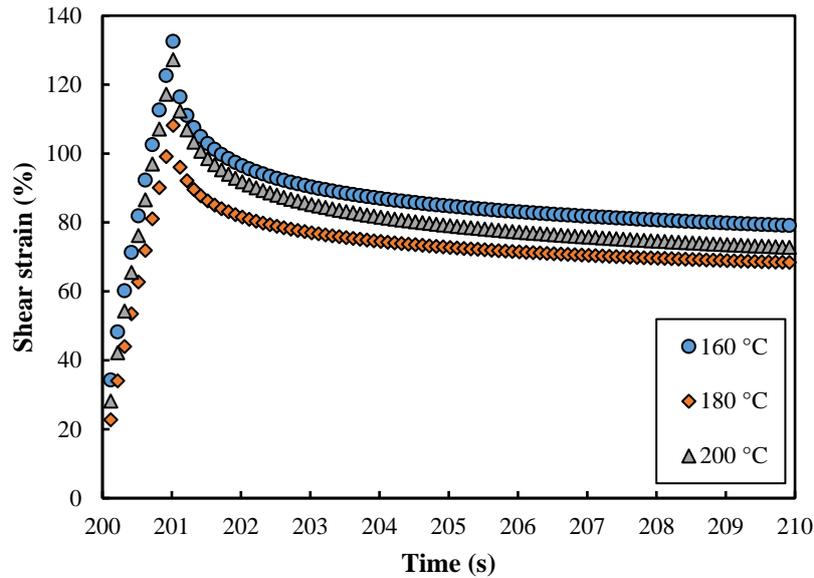
Figure 5.4 Creep and recovery cycle at 3.2 kPa for CRMB binders prepared at different temperatures.

Figure 5.5 summarizes the whole MSCR response curves for different CRMB binders. The first 100 s was the conditioning cycles, which are not shown in the graph. It can be seen that CRMB prepared at 180 °C-30 min showed the least shear deformation after the entire creep-recovery cycles while CRMB prepared at 200 °C-90 min showed the highest shear deformation. The strain response curves of other CRMB binders were in between the above two cases. The reason for the different responses was explained as follows.
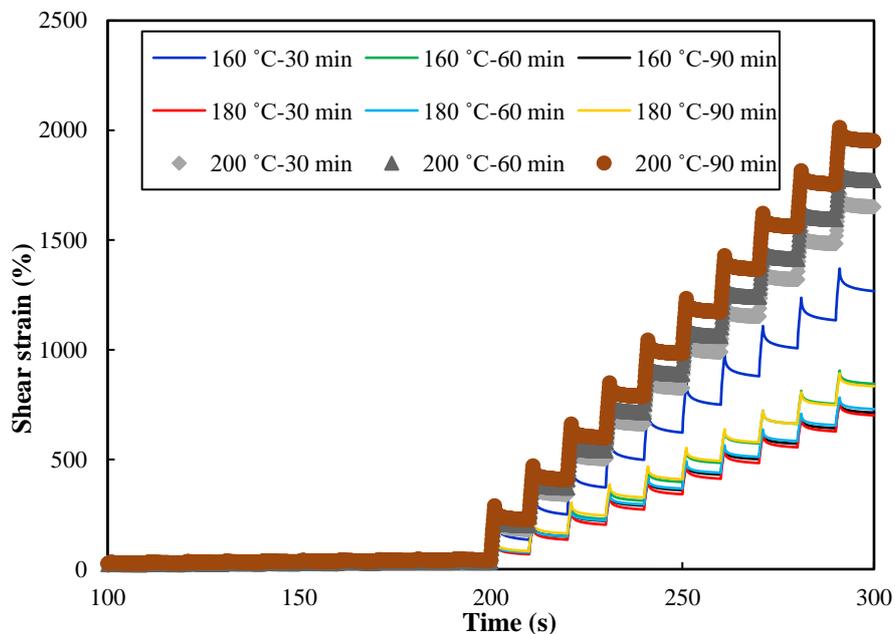
Figure 5.5 MSCR response curves of CRMB binders prepared at different conditions.

Specifically, the non-recoverable compliance J_{nr} and percent recovery R of CRMB binders with different interaction combinations at 3.2 kPa are illustrated in Figure 5.6.
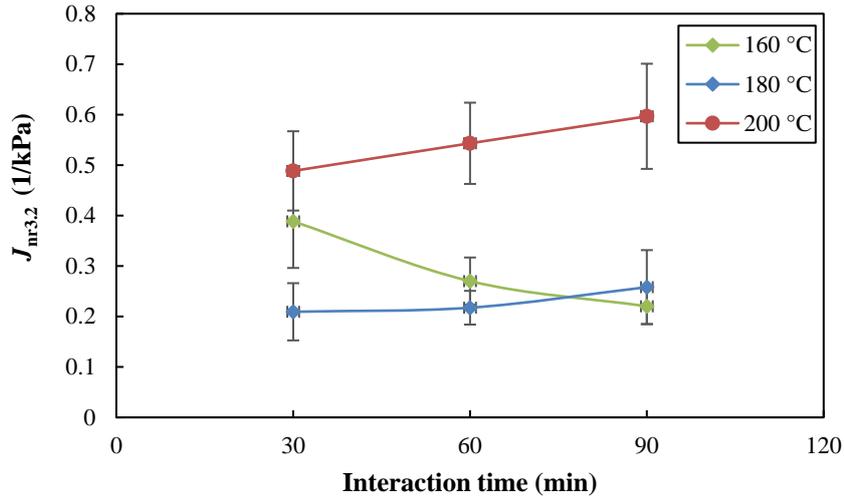
(a)
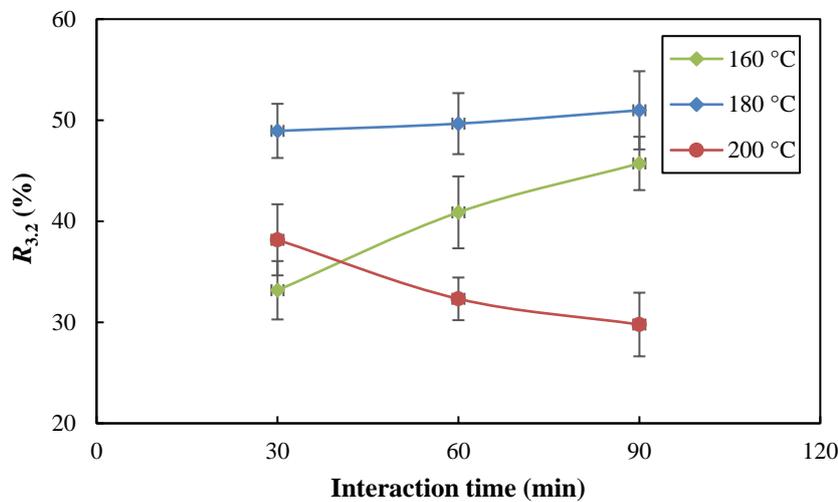
(b)

Figure 5.6 MSCR test results as a function of interaction temperature and time: (a) Non-recoverable creep compliance and (b) percentage of recovery.

In general, both $J_{nr3.2}$ and $R_{3.2}$ show different trends with the increasing interaction temperatures, which implies that there may be different interaction mechanisms that occurred during the mixing process. At a relatively low temperature of 160 °C, swelling of rubber particles continuously happened over the entire interaction period as illustrated by the continual decrease in compliance value. Rubber particles were swollen by absorption of the aromatic oils from the bitumen matrix to form a gel-like structure. The change in rubber particle volumes and the formation of gel structures in the binder reduces the distance between swollen rubber particles, and therefore stiffening the composite material. At the intermediate temperature of 180 °C, both $J_{nr3.2}$ and $R_{3.2}$ only had limited changes. The flat curves showed the CRMB binder interacted at 180 °C reached a certain equilibrium. Based on the previous research (Abdelrahman 2006), it was known that at this temperature level, swelling happened faster than at 160 °C. Since CRMA binders prepared at 180 °C for 30 min exhibited similar $J_{nr3.2}$ as the one prepared at 160 °C for 90 min, it is possible that swelling reached the same level at 180 °C for 30 min as at 160 °C for 90 min. After 30-min interaction at 180 °C, a small amount of the swollen rubber particles might start depolymerization, releasing some polymeric components to the bitumen matrix. At the high temperature of 200 °C,

rubber particles reached the swelling equilibrium in a very short time (Artamendi and Khalid 2006). Generally, swelling of elastomeric polymers (rubber) in organic solvents (aromatic oils) is a diffusion process (Buckley and Berger 1962). As the temperature increases, the diffusion coefficient also increases, which accelerates the swelling process. Noticing from Table 5.2 that the decomposition temperature of CRM is around 200 °C, the significant increase of J_{nr} and decrease of percent recovery at 200 °C were mainly due to the depolymerization and/or devulcanization of rubber. The degradation of rubber particles at high temperature destructed the polymer network and cross-linking structure, resulting in a less elastic response.

Alternatively, the $J_{nr3.2}$ and $R_{3.2}$ values for different CRMB binders are plotted in Figure 5.7. The red line in Figure 5.7 showing the relationship between $J_{nr3.2}$ and $R_{3.2}$ is recommend by the AASHTO M332 standard for verifying the presence of polymer (Salim *et al.* 2019). Data that is plotted on or above the curve is considered to have a significant elastic response for the associated value of $J_{nr3.2}$, indicating the binder has been modified by polymers. Even though this criterion curve is not universal, it is still useful to compare the properties of CRMB prepared at different conditions. As shown in Figure 5.7, only binders prepared at proper conditions can be considered as polymer modified bitumen. Binders prepared at 160 °C for 30 or 60 min and at 200 °C for 60 or 90 min cannot meet the requirements of modification. Binders prepared at 180 °C all pass the modification criterion. It is therefore reasonable to choose a mixing temperature at 180 °C.
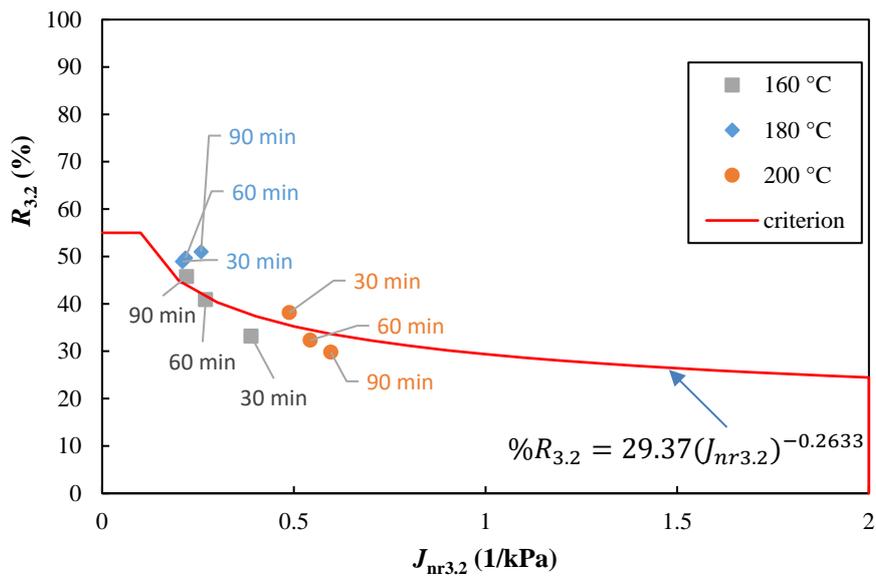
Figure 5.7 Positions of CRMB binders in the $J_{nr3.2}$ versus $R_{3.2}$ space.

5.1.3.2 *Fourier transform infrared (FTIR) spectroscopy*

The above analysis clearly shows the dominant effect of temperature on the swelling and degradation process of rubber particles. To verify the above speculations on bitumen-rubber interaction process at different temperatures, FTIR tests were done on CRMB binders to further reveal the interaction mechanism. A Perkin Elmer Spectrum 100 FTIR spectrometer (PerkinElmer, Wellesley, Massachusetts) was used in the attenuated total reflectance (ATR) mode to acquire the infrared spectra for all the bitumen samples. The wavelength of the reflected beam is characteristic of each element and indicates the presence of specific chemical functional groups. Sample preparation is simple for the ATR technique. A small sample of the material was taken

using a spatula and placed on the top of the ATR crystal. The FTIR spectrum was obtained in the wavelength number range from 4,000 to 600 cm^{-1} with a scanning resolution of 4 cm^{-1} averaging twenty scans for each measurement at ambient temperatures.

Figure 5.8 FTIR spectra of base bitumen and CRMB binders prepared at different temperatures.

The FTIR spectra of base bitumen 70/100 and CRMB binders prepared at different temperatures with a mixing time of 30 min are shown in Figure 5.8. The polybutadiene (PB) peak at 965 cm^{-1} indicating the =C-H in phase out-of-plane bending of trans-1,4-butadiene is usually used to indicate the presence of butadiene copolymers in polymer modified bitumen. From Figure 5.8, no PB peaks are observed in base bitumen 70/100 and CRMB binders prepared at 160 and 180 °C. Only when the mixing temperature increases to 200 °C, the resulted CRMB shows an obvious PB peak. The presence of butadiene copolymers in CRMB is mainly because of the chemical degradation of rubber particles, which release polymeric components into the bitumen matrix. Therefore, the FTIR results imply that at temperatures of 160 and 180 °C, the interaction between bitumen and rubber is mainly a swelling phenomenon. When increasing the mixing temperature to 200 °C, the swollen rubber particles start to devulcanize or/and depolymerize. The FTIR results correlate well with the findings from MSCR results.

5.1.3.3 *Optimal bitumen-rubber mixing condition*

Figure 5.9 illustrates the different stages of asphalt-rubber interactions with increasing interaction temperatures. Initially, at low temperatures, swelling of rubber particles continuously happens at a low speed to form a gel-like material (Condition 1). With the increase of temperature, rubber particles swell fast and reach the swelling equilibrium quickly (Condition 2). At this stage, only limited degradation of rubber particles happens. When the temperature reaches a certain elevated level, degradation of swollen rubber particles happens drastically (Condition 3).

Rheological and chemical characterization on CRMB binders prepared at different conditions show consistent findings. Based on the above analysis, mixing bitumen and rubber at 180 °C for 30 min was chosen as the optimized bitumen-rubber interaction procedure, which produces

CRMB binders with a lower J_{nr} and a higher percent recovery. In addition, from a practical viewpoint, the bitumen-rubber interaction process is more stable at 180 °C with the increase of interaction time, which makes it easy for CRMB product quality assurance/control in plants.
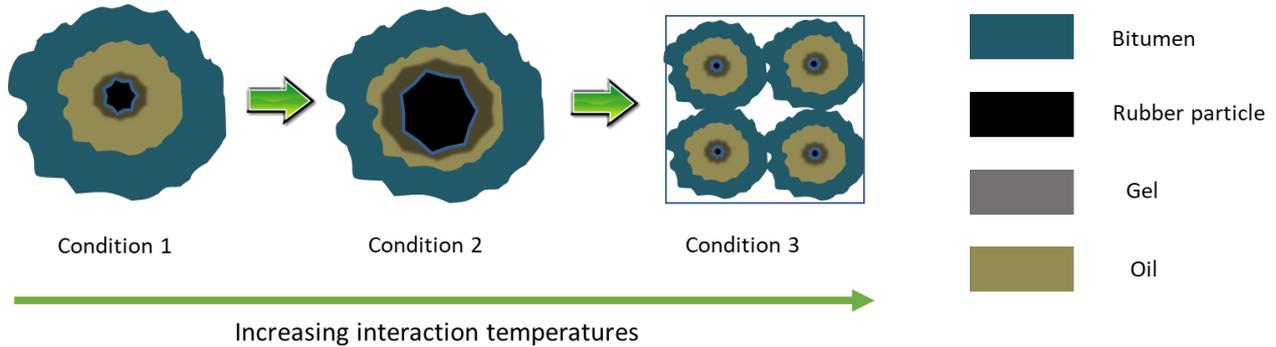
Figure 5.9 Schematic diagram of bitumen-rubber interaction at different conditions.

5.2 Preparation of binders with warm-mix additives

5.2.1 Warm-mix additives

Warm mix asphalt (WMA) technologies are developed to lower the production and construction temperatures of asphalt mixtures. The widely used classification categorizes WMA technologies into three main types (Rubio *et al.* 2012): foaming processes (subdivided into water-containing and water-based processes); addition of organic (wax-based) additives; and addition of chemical additives. Previous studies have successfully incorporated non-foaming WMA additives into rubberized bituminous materials (Wang *et al.* 2018c). In this study, two types of commercial warm-mix additives were used: wax-based additive (designated as W) and chemical-based additive (designated as C). The physical and chemical properties of the two WMA additives are shown in Table 5.3. Additive W is a synthetic hard wax free of sulphur and other impurities. The additive can be completely soluble in bitumen at temperatures above 115 °C. It starts to crystallize at a temperature lower than 90 °C and forms a lattice structure (Jamshidi *et al.* 2013). Additive C at ambient conditions is a liquid cocktail of chemical products, such as surfactants, polymers, anti-stripping agents, etc. Based on the technical data sheet, the additive can be directly injected into the bitumen. The product is very compatible with hot bitumen and will not require high shear blending. It is unnecessary to heat the product before use. If heating is desired, the heating temperature should not exceed 60 °C. Based on the manufacturers' recommendation, the dosages of wax-based W and chemical-based C were 2.0% and 0.6% for both base bitumen and CRMB binders.

Table 5.3 Physical and chemical properties of the used non-foaming WMA additives.

Properties	Wax-based additive W	Chemical-based additive C
Physical state	Prills (5-mm diameter)	Liquid
Colour	Greyish-white	Dark amber
Odour	No	Amine-like
Bulk density (g/cm³)	0.622	0.99
Solubility in water	Insoluble	Partially soluble

Boiling point (°C)	N/A	150-170
Melting point (°C)	105-115	N/A
Appearance		

5.2.2 Preparation procedure

From the product descriptions, both WMA additives can be added to bitumen to significantly reduce viscosity and reduce the working temperatures by 20~30 °C. For the base bitumen, both additives were manually blended with hot bitumen at 140 °C for 10 minutes. For the CRMB, both additives at room temperatures were added into the hot CRMB which was at 160 °C due to its higher viscosity and manually mixed for 10 minutes. Considering the viscosity-reduction effect of warm-mix additives, one question emerges: Is it possible to add warm-mix additives to bitumen prior to mixing with rubber to prepare CRMB at lower mixing temperatures (warm blended) without compromising the rheological properties comparing to the hot blended CRMB (at 180 °C)? The earlier incorporation of warm-mix additives may reduce the required mixing temperature for CRMB and hence save more energy (Leng *et al.* 2017, Yu *et al.* 2017). However, as described in the technical data sheet of chemical-based additive C, it is not recommended to reheat the product higher than 60 °C because of its volatile components. The additive may lose its viscosity-reduction effect when heating the binder again for mixture production. In contrast, wax-based additive can keep its effectiveness even being heated several times under certain temperatures. Therefore, to investigate the effect of preparation procedure on the rheological properties of CRMB containing wax-based additives, the following procedures were used:

- Hot-produced CRMB. Bitumen and rubber were first mixed at 180 °C for 30 min to prepare CRMB. Then wax-based additive was added to the prepared CRMB at 160 °C and manually blended for 10 min.
- Warm-produced CRMB. Bitumen, rubber and wax-based additive were blended and mixed at 160 °C for 30 min.

The binders prepared by the above methods were designated as H-CRMB and W-CRMB, respectively. To have a further understanding of the interaction mechanism among the components (i.e., bitumen, rubber and wax-based additive), the liquid phases of H-CRMB and W-CRMB were extracted by removing the insoluble CRM particles from the bitumen matrix. In this regard, the required amount of freshly prepared CRMB binders were drained through a mesh sieve (0.063 mm) in the oven at 165 °C for 20 min (Wang *et al.* 2018a). To allow for a fast and uniform filtration, the heated CRMB samples were manually flattened on the mesh before the drainage. The residual (drained) binders designated as H-CRMB-LP and W-CRMB-LP were collected on an aluminum pan. The extracted liquid phase was stored in the refrigerator immediately to prevent any unwanted aging or reaction.

5.2.3 Rheological and thermal characterization

5.2.3.1 *MSCR test*

MSCR tests were conducted on CRMB and liquid phase binders to compare their rheological properties. MSCR tests were performed at 64 °C according to the procedure described before. The test results are summarized in Table 5.4. It can be seen that the $J_{nr3.2}$ of W-CRMB is slightly lower than that of H-CRMB, indicating higher resistance to permanent deformation. In addition, W-CRMB has a higher elastic recovery than H-CRMB at 3.2 kPa, which implies that different polymer networks and rubber structures may exist within the binder. To further investigate the effect of wax-based additive on the bitumen-rubber interaction process, the liquid phases of these two CRMB binders were also compared in Table 5.4. The liquid phase of hot-produced CRMB (H-CRMB-LP) has a very small $J_{nr3.2}$. Two reasons contribute to this result. First, the light fractions of bitumen were absorbed by rubber particles and therefore, the liquid phase became stiffer because of a large proportion of asphaltenes. Second, the wax-based additives can be completely dissolved into bitumen. The wax-based additives remained in the liquid phase after extraction and stiffen the binder. Similar explanations are also applicable to the small $J_{nr3.2}$ value of W-CRMB-LP. However, its $J_{nr3.2}$ is larger than that of H-CRMB-LP. Previous studies have demonstrated that reducing the bitumen viscosity has a similar effect on rubber swelling as increasing the interaction temperature (Artamendi and Khalid 2006). It was actually shown in Figure 5.16 in Section 5.3 that the viscosity of neat bitumen at 180°C is very close the viscosity of neat bitumen with wax-based additive at 160°C. If assuming similar bitumen-rubber interactions occurred for both H-CRMB and W-CRMB, the reason for the difference in the non-recoverable compliance is because of the different wax contents in each liquid phase (Yu *et al.* 2016).

Table 5.4 MSCR test results of CRMB and liquid phase binders.

Binder type	Average *R* (%)		Average *J_nr* (1/kPa)	
	0.1 kPa	3.2 kPa	0.1 kPa	3.2 kPa
H-CRMB	91.76	42.25	0.0176	0.2024
W-CRMB	96.59	45.83	0.0033	0.1856
H-CRMB-LP	56.57	38.08	0.0605	0.1011
W-CRMB-LP	36.56	27.26	0.1046	0.1654

5.2.3.2 *Frequency sweep test*

Frequency sweep tests of CRMB and liquid phase binder samples were carried out with a parallel-plate geometry (25 mm diameter and 1 mm gap) from 0.1 to 100 rad/s at temperatures of 10, 30, 50 and 70 °C. Before the frequency sweep tests, strain amplitude sweep tests were conducted to identify the linear viscoelastic (LVE) range of different binders and thus to ensure the frequency sweep tests were undertaken within the binder's LVE region of response. The LVE limit was defined as the point where complex modulus has decreased to 95% of its initial value (Airey *et al.* 2002). Based on the LVE limits, all the measurements were carried out at a strain level of 0.1% under strain-controlled mode.

In the present study, a modified Christensen-Anderson-Marasteanu (CAM) model (Equations (5.1) and (5.2)) was used to develop complex modulus and phase angle master curves for binders based on the frequency sweep test results (Bahia *et al.* 2001).

$$G^* = \frac{G_g^*}{[1 + (f_c/f_r)^k]^{m/k}}$$ (5.1)

where $G_g^* = G^*$ (f→∞), glass complex modulus; f_c = crossover frequency at which the elastic component is approximately equal to the viscous component; f_r = reduced frequency, a function of both temperature and strain; and k, m = shape parameters, dimensionless.

$$\delta = 90I - \frac{90I - \delta_m}{\left\{1 + \left[\frac{log(f_d/f_r)}{R_d}\right]^2\right\}^{m_d/2}}$$ (5.2)

where δ_m = phase-angle constant at f_d, the value at the inflexion for binders; f_r = reduced frequency; f_d = location parameter with dimensions of frequency, at which δ_m occurs; R_d, m_d = shape parameters; and for binders, $I=0$ if $f > f_d$, $I=1$ if $f \leq f_d$. The Williams-Landel-Ferry (WLF) equation (Equation (5.3)) was used to obtain the shift factors.

$$\log \alpha_T(T) = \frac{-C_1(T - T_R)}{C_2 + (T - T_R)}$$ (5.3)

where C_1, C_2 = empirically determined constants; T = test temperature; T_R = reference temperature; $\alpha_T(T)$ = shifting factor.

The complex modulus and phase angle master curves of H-CRMB and W-CRMB at a reference temperature of 30 °C are shown in Figure 5.10.
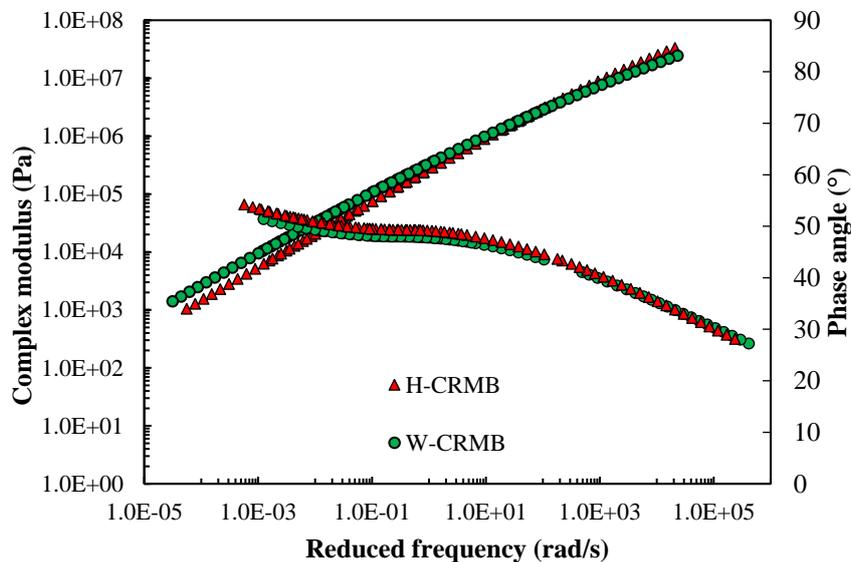
Figure 5.10 Complex modulus and phase angle master curves of H-CRMB and W-CRMB.

It can be found that the complex modulus and phase angle curves of these two binders are close to each other. The plateaus indicate the presence of rubber networks within the binder. The peculiar feature of phase angle plateau at intermediate frequencies was also observed. W-CRMB is slightly stiffer (higher modulus) and more elastic (lower phase angle) than H-CRMB. In general, the mixing procedure does not significantly influence the bitumen-rubber interaction and hence the binder's linear viscoelasticity. As stated earlier, the existence of wax-based additive may affect

the interaction between bitumen and rubber. In this regard, the viscoelastic master curves of liquid phases of H-CRMB and W-CRMB are compared in Figure 5.11.
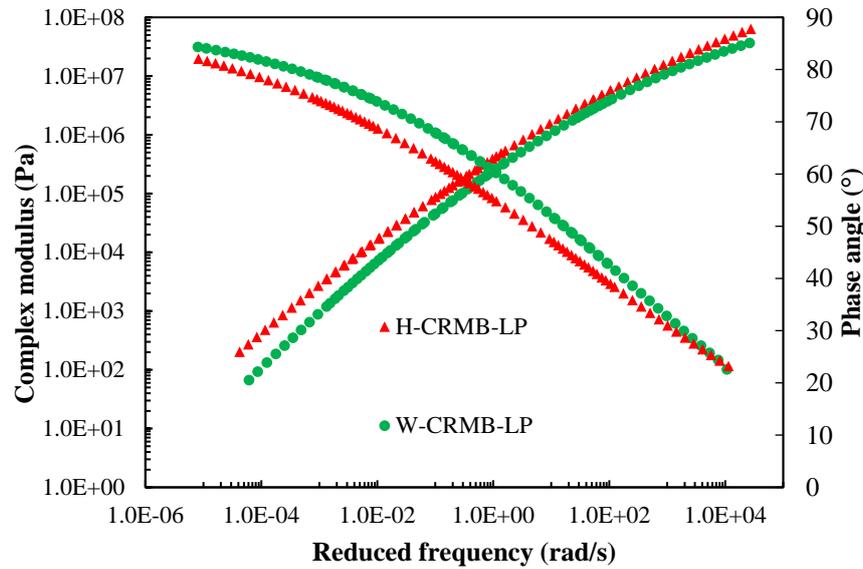
Figure 5.11 Complex modulus and phase angle master curves of the liquid phases of H-CRMB and W-CRMB.

It is obvious that W-CRMB-LP is softer (lower modulus) and more viscous (higher phase angle) than H-CRMB-LP. Since rubber particles were removed from the liquid phase, their contributions to binder viscoelasticity were assumed to be neglected. Again, if assuming similar bitumen-rubber interactions occurred for both H-CRMB and W-CRMB, the difference in rheological properties of these two liquid phases may stem from the wax-based additives. It is reported from previous studies (Wang *et al.* 2018d) that the addition of wax into bitumen can improve the viscoelastic response by increasing the modulus and decreasing the phase angle. Therefore, it is speculated that H-CRMB-LP may have a higher wax content than W-CRMB-LP. This speculation will be further investigated by the Differential Scanning Calorimetry (DSC) test on the liquid phases.

5.2.3.3 *Differential Scanning Calorimetry test*

To verify the assumption that the higher $J_{nr3.2}$ and lower complex modulus of binder W-CRMB-LP comparing to H-CRMB-LP is because of the less wax content in the liquid phase of the binder, DSC tests were performed on the liquid phases to determine the wax content. Previous studies have demonstrated the applicability and validity of using DSC to determine the wax content in crude oils, residues and bitumens (Chen *et al.* 2004, Lu *et al.* 2008). As described before, wax-based additive W is a synthetic microcrystalline wax which will show a melting peak during the heating process and a crystallization peak during cooling process in a DSC test (Jamshidi *et al.* 2013). Figure 5.12 shows a DSC curve of a typical waxy bitumen having a melting peak temperature of 103.7 °C during a heating process. The melting enthalpy, which is the area underneath the melting peak, is of particular interest because it reflects the total thermal effect of the precipitated wax in the sample. With a known value of melting enthalpy for wax, the wax content in the sample can be estimated using Equation (5.4) (Soenen *et al.* 2013):

$$c_{wax} = \frac{\Delta H_{bitumen}}{\Delta H_{wax}}$$

(5.4)

where c_{wax} is the wax content; $\Delta H_{bitumen}$ is the melting enthalpy of the bitumen sample; ΔH_{wax} is the melting enthalpy of wax, which is chosen as 121 J/g for natural wax and 250 J/g for synthetic wax.
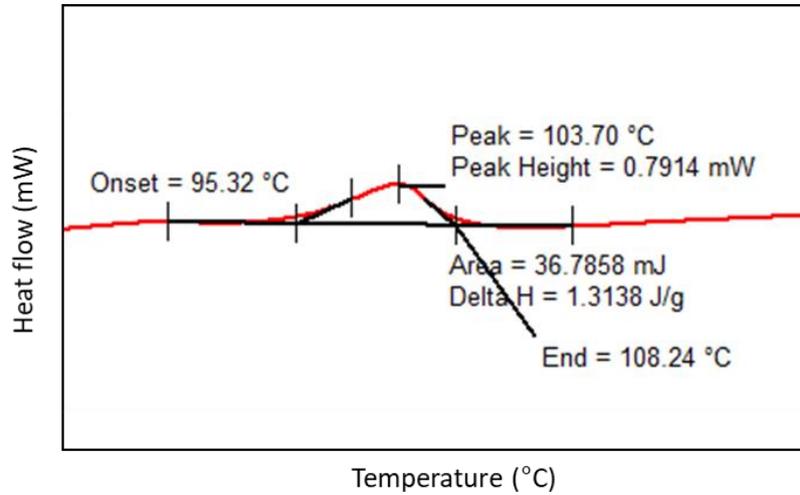
Figure 5.12 DSC curve of bitumen showing melting peak.

To perform the DSC tests, approximately 15 mg of bitumen sample is placed in a DSC cup. The cup is sealed with a lid using a special tool to ensure proper contact between the sample and the bottom surface. The cup containing testing materials was placed in the apparatus and conditioned at 25 °C for 5 minutes. Then the temperature was decreased from 25 °C to -60 °C. The measurement started after the isothermal conditioning at -60 °C for 5 minutes, with temperature ramping from -60 to 140 °C at a rate of 20 °C /min (Soenen *et al.* 2013). The heat flows of test samples were monitored and compared to those of the reference sample (an empty aluminum pan) for further derivations. It is reported the reproducibility on the enthalpies from heating scans is generally better than those from cooling scans. For each binder, three replicates were tested.
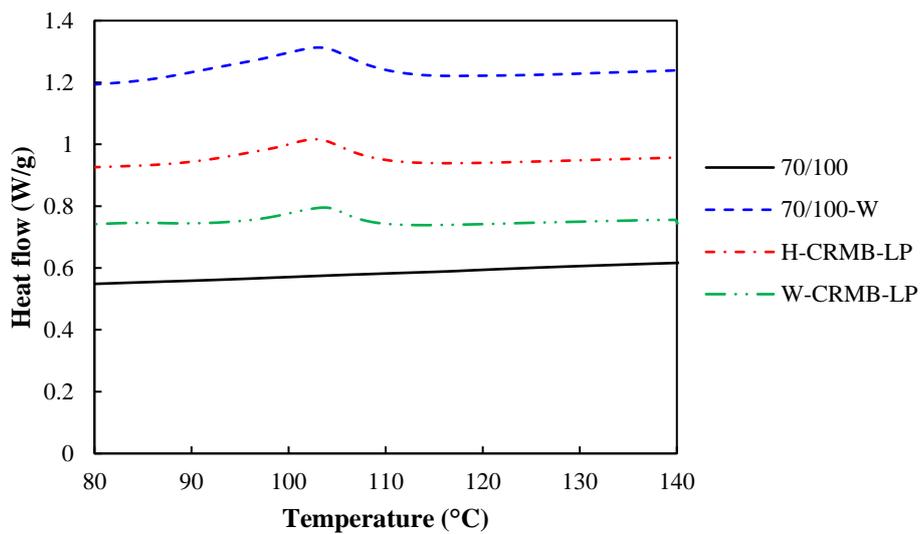
Figure 5.13 DSC curves of different binders.

For comparison, Figure 5.13 shows the DSC curves of neat bitumen 70/100, neat bitumen with wax-based additive 70/100-W, liquid phases of both H-CRMB and W-CRMB during the heating scan. For clarity, only curves close to the melting region are shown. It is clear that neat bitumen shows no melting signal, which means it is wax free. For the other three binders, they all show a melting peak because of the addition of wax-based additives. The melting peak temperatures of three binders are around 104 °C. However, the respective melting enthalpy is different from each other. The average melting enthalpies for 70/100-W, H-CRMB-LP and W-CRMB-LP are 4.27 J/g, 4.01 J/g and 2.34 J/g respectively. According to Equation (5.4), melting enthalpy of 250 J/g for synthetic wax was used to estimate the wax content of each binder and the results are summarized in Figure 5.14. The estimated wax content of 70/100-W is 1.71 %, which is close to the dosage of additive W. The estimated wax content of H-CRMB-LP is lower than that of 70/100-W, which is probably because some additives were remained on/in the rubber particles after the extraction process. W-CRMB-LP shows the lowest wax content of 0.94 %, indicating a large portion of the wax-based additives penetrated into rubber particles (Yu *et al.* 2016).
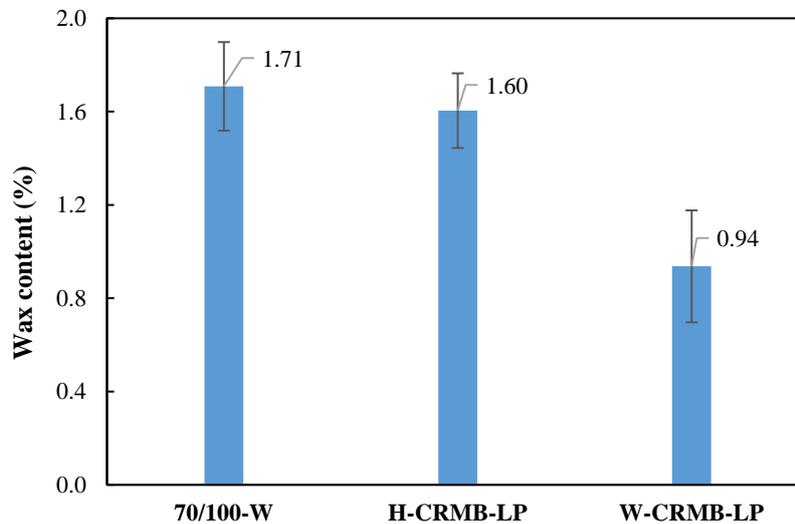
Figure 5.14 Wax content determined by DSC method.

5.2.4 Recommended preparation procedure of CRMB containing warm-mix additives

Warm-mix additives (wax-based) were incorporated in CRMB using different procedures. The influence of preparation procedure on CRMB containing warm-mix additives was investigated from both rheological and thermal characteristics in the previous subsection. In general, warm-produced CRMB (mixing bitumen, rubber and additives together at a lower temperature) slightly improved the rheological properties by increasing the modulus and elasticity compared to hot-produced CRMB. However, it was found that a significant proportion of wax-based additives penetrated rubber particles for the warm-produced CRMB procedure. This may cause workability issues when producing asphalt mixtures with W-CRMB. Based on Leng *et al.* (2017), asphalt mixtures prepared with H-CRMB can achieve the desired mixture density with less compaction efforts than W-CRMB does, which indicates a better workability. This is mainly because the absorbed wax-additives in rubber particles cannot effectively reduce the binder viscosity and function as a lubricator to improve the workability. From this perspective, although warm-produced CRMB may save energies compared to hot-produced CRMB, it is not recommended to replace the traditional hot-produced CRMB procedure with warm-produced method because of

the compromised workability. Therefore, for consistency, both types of warm-mix additives were added to prepared CRMB using the hot-produced method for the current study.

5.3 Rheological behavior and its chemical interpretation of CRMB

5.3.1 Binder sample preparation

After determining the binder preparation procedure, to further investigate the effects of CRM content and warm-mix additive on the rheological and chemical properties of bitumen, the following nine binders as shown in Table 5.5 were prepared.

Table 5.5 Description of prepared binders.

Binder ID	Description
70/100	Base bitumen
70/100-W	Base bitumen with 2 wt% wax-based additive
70/100-C	Base bitumen with 0.6 wt% chemical-based additive
CRMB-5	CRM content of 5% by weight of base bitumen
CRMB-10	CRM content of 10% by weight of base bitumen
CRMB-15	CRM content of 15% by weight of base bitumen
CRMB-22	CRM content of 22% by weight of base bitumen
CRMB-22-W	CRMB-22 with 2 wt% wax-based additive
CRMB-22-C	CRMB-22 with 0.6 wt% chemical-based additive

Four CRM contents including 5%, 10%, 15% and 22% by mass of base bitumen were used. As determined in the previous section, all CRMB binders were prepared by mixing CRMs and base bitumen using a Silverson high shear mixer at 180°C with a shearing speed of 6000 rpm for 30 min. Also as indicated in the previous section, warm-mix additives were incorporated into either base bitumen or prepared CRMB by manually blending for 10 minutes. All the binders at fresh state were subjected to frequency sweep tests to obtain the rheological parameters (complex shear modulus, phase angle and complex viscosity) using a DSR.

It can be seen in Table 5.5 that warm-mix additives were only added to CRMB with a high rubber content (i.e., CRMB-22). This is because CRMB-22 exhibited extremely high viscosities, which will significantly influence its pumpability, mixability and workability if not reduced. To examine the effect of rubber content and warm-mix additives on the viscosity of binder, the Brookfield viscometer was used to measure the rotational viscosities of different binders at a constant rotational speed of 20 rpm using the #27 cylindrical spindle. Viscosity tests were conducted at various temperatures, 110, 135, 160, 177 and 190°C, which cover the temperature range of production, transport, and construction (Zhang *et al.* 2015). Figure 5.15 shows the rotational viscosities of CRMB binders at various temperatures. It is obvious that binder viscosity decreases with the increase of testing temperature. With the increase of rubber content, the binder viscosity increases dramatically. Even at 190°C, the rotational viscosity of CRMB-22 has exceeded 4000 mPa·s. Excessively high viscosities of CRMB will impede its application in asphalt production and construction. Based on the recommended specification for rubberized bitumen in California (State

of California Department of Transportation 2003), the apparent viscosity of CRMB at 190°C should be in the range of 1500-4000 mPa·s to ensure the proper plant production. CRMB binders with rubber contents lower than 15% have acceptable viscosities. Therefore, warm-mix additives need to be incorporated into CRMB-22 to reduce the viscosity.
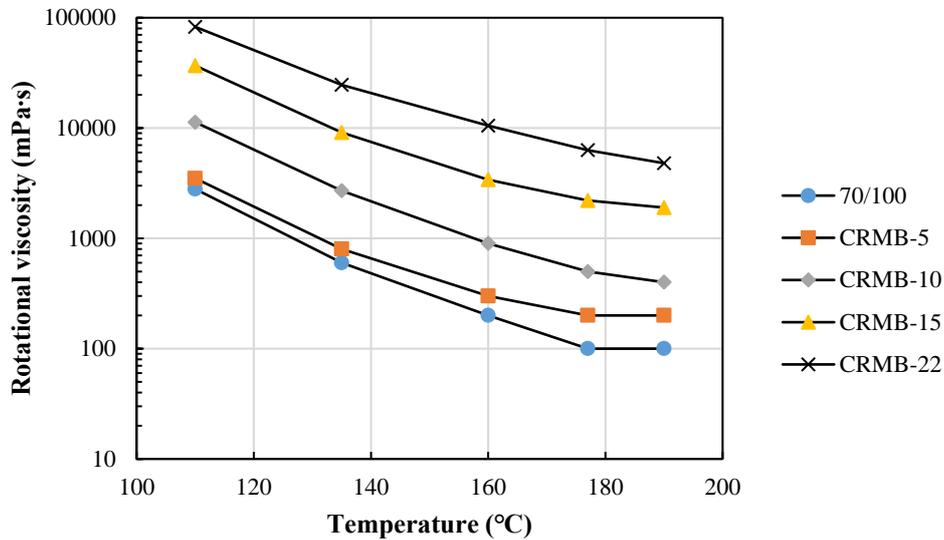
Figure 5.15 Rotational viscosities of CRMB binders with different rubber contents.

Figure 5.16 shows the effect of warm-mix additives on the viscosity of CRMB binders. For comparison, additives were also added to neat bitumen. As expected, both additives effectively reduce the viscosity of both neat bitumen and CRMB. Particularly, the viscosity of CRMB-22 has reduced to lower than 4000 mPa·s at 190 °C, which satisfies the specifications for rubberized bitumen as proposed by Caltrans. Therefore, for the rest of the study, warm-mix additives were only added to CRMB-22 and neat bitumen for comparison reason.
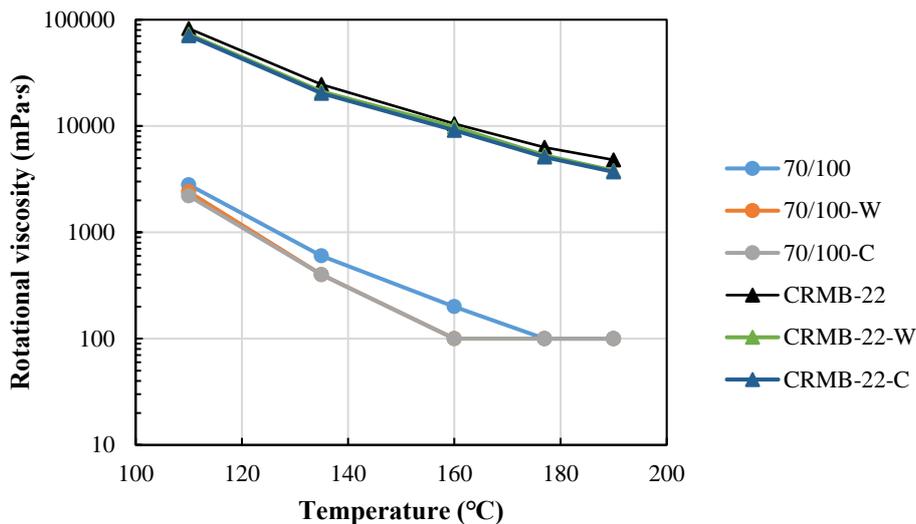
Figure 5.16 Rotational viscosities of binders with warm-mix additives.

5.3.2 Chemical interpretation from rheology

Bitumen is commonly accepted as a multi-disperse colloidal system, where high molecular weight asphaltene micelles are peptized by resins in low molecular weight maltenes, with rheological behavior resembling that of a low-molecular-weight polymer (Lesueur 2009). The chemical composition and microstructure of asphalt binder has a significant effect on the material rheological properties and hence its performance as a road paving binder. A large amount of research has been done to link the chemical nature of bitumen with physical behavior, and thus to explain the mechanical performance. Typically, the microstructure and composition of bitumen can be determined through classical chemical characterization techniques, such as atomic force microscopy (AFM) to obtain surface topography, gel permeation chromatography (GPC) to obtain molecular weight distribution, thermogravimetric analysis (TGA) for thermal analysis, Fourier transform infrared (FTIR) spectroscopy to identify functional groups, etc. (Zofka *et al.* 2013) However, these chemical characterization methods need exclusive instruments, special training and complex sample preparation. More importantly, due to the chemo-physical complexity of certain bitumen products (modified or emulsified), it is not suitable to use all the above techniques for every case (Zanzotto *et al.* 1999, Themeli *et al.* 2015). Recently, a few attempts were made to obtain the molecular weight distribution (MWD) and activation energy (E_a) for flow of bitumen through rheological tests (Jamshidi *et al.* 2015, Themeli *et al.* 2015).

5.3.2.1 *Relationship between rheology and flow activation energy*

Viscosity, defined as a measure of resistance to deformation or flow, is one of the most important properties of bituminous binders used as paving materials. Profound knowledge of the viscosity of these binders at manufacturing and construction temperatures (generally above 135 °C) provides vital information about their pumpability, mixability and workability (Wang *et al.* 2012, Wang *et al.* 2016). The viscosity of bitumen should be controlled within a certain range to facilitate its application in production and construction as well as to guarantee the bitumen grade (Sybilski 1993). Generally, bituminous binders can exhibit Newtonian or non-Newtonian behaviors under different conditions. Unmodified bituminous binders usually exhibit Newtonian behavior at relatively elevated temperatures (generally above the softening point) or at very low shear rates. However, considering the large service temperature range of these binders or short loading times, their viscosity is not always an absolute value at intermediate and low temperatures. Rather, it varies with the applied shear rate and shear stress. That is why it is an apparent value which needs a well-defined temperature, shear rate and shear stress. For the majority of highly modified bituminous binders, they exhibit obvious non-Newtonian behaviors due to the interaction between the bitumen and the modifier (Zoorob *et al.* 2012). Apart from the difference among the viscometers and rheometers, the non-Newtonian behavior of some binders (e.g., polymer modified bitumen) is a main reason for the observed measurement difficulties and this subsequently leads to issues in the interpretation and comparison of interlaboratory test results (Sybilski 1996). Therefore, it is necessary to investigate the non-Newtonian behaviors of highly modified bituminous binders and propose universal parameters (e.g., zero shear viscosity) (Anderson *et al.* 2002) that are independent of applied shear loading instead of merely comparing the apparent viscosity values.

The concept of flow activation energy of bitumen describes the minimum energy barrier which bitumen molecules must overcome for flow to occur (Salomon and Zhai 2002). It can be used to differentiate bitumen and characterize the thermal susceptibility of bitumen (Haider *et al.* 2011).

The temperature dependence of the viscosity of bitumen can be described by an Arrhenius equation (Equation (5.5)).

$$\eta^* = Ae^{E_a/RT} \qquad\qquad (5.5)$$

where A is a pre-exponential parameter, R is the universal gas constant [8.314 J/(mol·K)], E_a is the activation energy (kJ/mol), T is the temperature in degrees K, and η^* is the complex viscosity at zero or low shear rate (Pa·s). The activation energy can be calculated based on known paired data of temperature and zero-shear or low-shear viscosity (García-Morales *et al.* 2004). Since zero shear viscosity (ZSV) is a theoretical concept and is impossible to measure the absolute value directly, various models were developed to extrapolate the ZSV value (Biro *et al.* 2009). However, it was reported that highly modified bituminous binders exhibit extreme high viscosity gradients at low frequencies, resulting in unrealistically high ZSV values using model predictions (De Visscher and Vanelstraete 2004). Alternatively, the concept of low shear viscosity (LSV) was introduced to overcome this issue (Morea *et al.* 2010). It was also found in this study that CRMB binders and wax-based additive modified binders yielded unpractical ZSV values. Therefore, the low shear viscosity at 0.01 rad/s was used as a replacement to calculate the activation energy. In addition, the E_a values can also be obtained through fitting shift factors using Arrhenius equation during the process of constructing master curves (Partal *et al.* 1999). Others reported similar E_a values using shift factor-based Arrhenius equation as viscosity-based Arrhenius equation did (Ait-Kadi *et al.* 1996, Partal *et al.* 1999). This is mainly because different rheological parameters are interrelated.

5.3.2.2 *Relationship between rheology and molecular weight distribution*

It is well known that bitumen is composed of low (aromatic oils), medium (resins), and high (asphaltenes) molecular weight constituents and the incorporation of new additives (e.g., polymers and chemical surfactants) into base asphalt will inevitably change the proportions of these components. Consequently, the MWD alters due to the various interactions. Since MWD is associated with the internal structure as well as the structure-sensitive properties (e.g., rheological properties) of bituminous binders, comparing the MWDs of base and modified binders is a useful method to evaluate the chemo-physical interactions between base bitumens and additives. It is known that the linear viscoelastic parameters of polymer solutions and melts, as well as bitumen are strong functions of molecular weight. Zanzotto et al. (Zanzotto *et al.* 1996) inverted the fractional model of complex modulus to generate the MWD of regular and modified bitumen and compared with the MWDs obtained by GPC test. It was found that the MWDs calculated from rheological data are in good agreement with the corresponding GPC data. In subsequent research, Zanzotto et al. (Zanzotto *et al.* 1999) found the phase angle is more sensitive to the high molecular weight components (associates) than the complex modulus. It is noticeable that solvents used to dilute bitumen in GPC test potentially change the microstructure of bitumen, resulting in an erroneous representation of the MWDs of the undiluted bitumen. On the other hand, in case of materials containing insoluble components (e.g. rubber) in common solvents, the use of the chromatographic method is not feasible. Considering the above two limitations of GPC test for bituminous materials, in terms of CRMB binders containing WMA chemicals, deducing MWDs from linear viscoelastic parameters seems a more promising alternative.

Before deriving the MWDs from the linear viscoelastic properties, two important definitions should be known, namely differential molecular weight distribution (DMWD) and cumulative molecular weight distribution (CMWD). DMWD is a molecular weight distribution function (or a probability density function) of molecular weight. CMWD is an integral of DMWD from zero to a

specified molecular weight. The relationship between DMWD and CMWD can be described using molecular weight as follows:

$$w(M) = \frac{d\, f_c(M)}{d \log M} \qquad (5.6)$$

or

$$f_c(M) = \int_{-\infty}^{\log M'} w(M) d \log M \qquad (5.7)$$

where M = molecular weight; $w(M)$ = molecular weight distribution function or probability density function, it represents the relative amount of different molecular weights; $f_c(M)$ = the cumulative weight fractions of molecules from zero up to a specified molecular weight (M'). Based on the double reptation mixing rule (Tsenoglou 1991), the phase angle can be related to the MWD through the following relationship:

$$\delta(\omega) = \int_0^{\infty} w(M') c(M', \omega) dM' \qquad (5.8)$$

where $\delta(\omega)$ = phase angle as a function of angular frequency; $w(M')$ = weight distribution function; $c(M', \omega)$ = monodisperse phase angle of a relaxation unit. With the assumption that the monodisperse phase angle is proportional to the Heaviside step function H:

$$c(M', \omega) \sim 1 - H(M' - M) \qquad (5.9)$$

Equation (5.9) explains that at a given frequency, if the specified molecular weight (M') is smaller than the corresponding molecular weight (M), it will relax and make no contributions to viscoelastic phase angle (Tuminello 1986). A simple power law was used to relate the molecular weight domain to the frequency domain (ω= crossover frequency):

$$M = \kappa \omega^{-\alpha} \qquad (5.10)$$

The calibrated values for constants in Equation (5.10) based on test data were $\log \kappa = 2.544$, $\alpha = 0.06768$ at reference temperature of 0 °C (Zanzotto *et al.* 1999). Substituting Equations (5.9) and (5.10) into Equation (5.8), the following relationship can be obtained for normalized molecular weight:

$$\delta(x) \sim \int_0^{M = \kappa 10^{-\alpha x}} w(M') dM' \qquad (5.11)$$

where $x = \log \omega$. Comparing Equations (5.7) and (5.11), it can be found that both cumulative weight fractions and phase angle are functions of molecular weight and there exists a link between cumulative weight fractions and phase angle in logarithmic scale. Since phase angle is also a function of frequency, if the power-law relationship between molecular weight and frequency is known, then the phase angle can be plotted as a function of molecular weight. Considering the constraint and boundary conditions of the cumulative weight fractions:

when $M \to 0$, $\delta(M) = 0$, $f_c(M) = 0$;
when $M \to \infty$, $\delta(M) = 90°$, $f_c(M) = 1$.

Thus, the relationship between cumulative weight fractions and phase angle can be written as:

$$f_c(M) = \frac{1}{90} \delta(M) \qquad (5.12)$$

Therefore, with the phase angle master curve and the calibration of Equation (5.10), the molecular weight distribution can be obtained through Equations (5.6) and (5.12). Based on the above

derivations, one should note that rheological properties actually depend on the apparent MWDs that include the associations of various molecular weight constituents rather than on the MWDs of an individual molecule. Therefore, the MW obtained in this study means the apparent MWs of different molecular associations. Figure 5.17 summarizes the flow diagram of the steps and representative graphs involved in the conversion of linear viscoelastic data into an MWD, which is called the phase angle inversion method in this study.
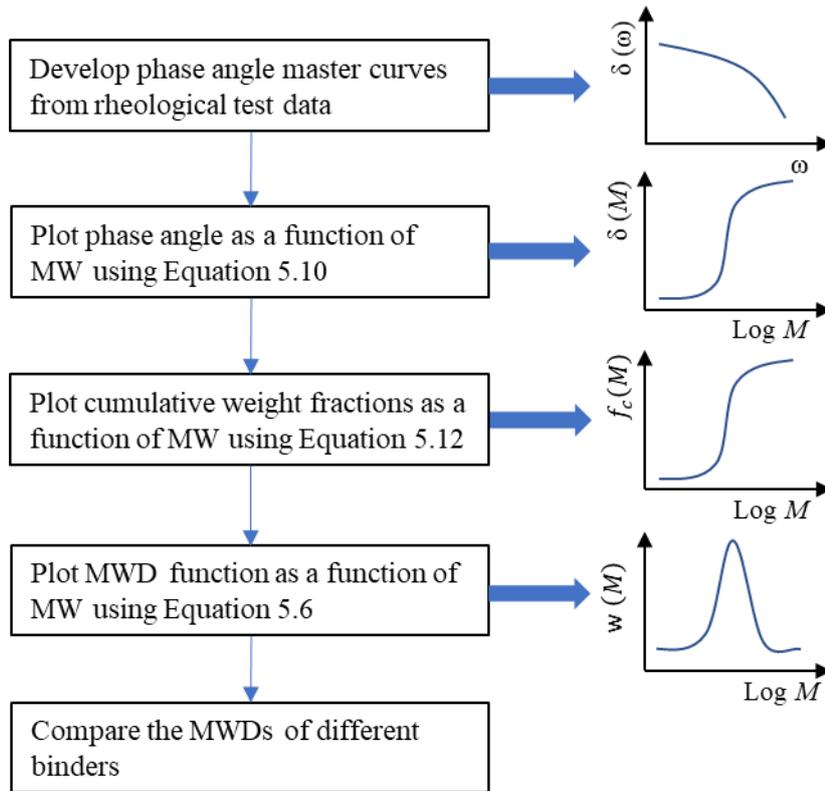
Figure 5.17 Flow chart of converting phase angle data to MWD data.

5.3.3 Complex viscosity

5.3.3.1 *Influence of temperature and shear rate on complex viscosity*

Figure 5.18 plotted the complex viscosities of different binders as a function of shear rate (angular frequency) at 10 °C and 70 °C respectively. Viscosities at various combinations of temperature and frequency showed similar trends, therefore, they are omitted here.

(a)

(b)
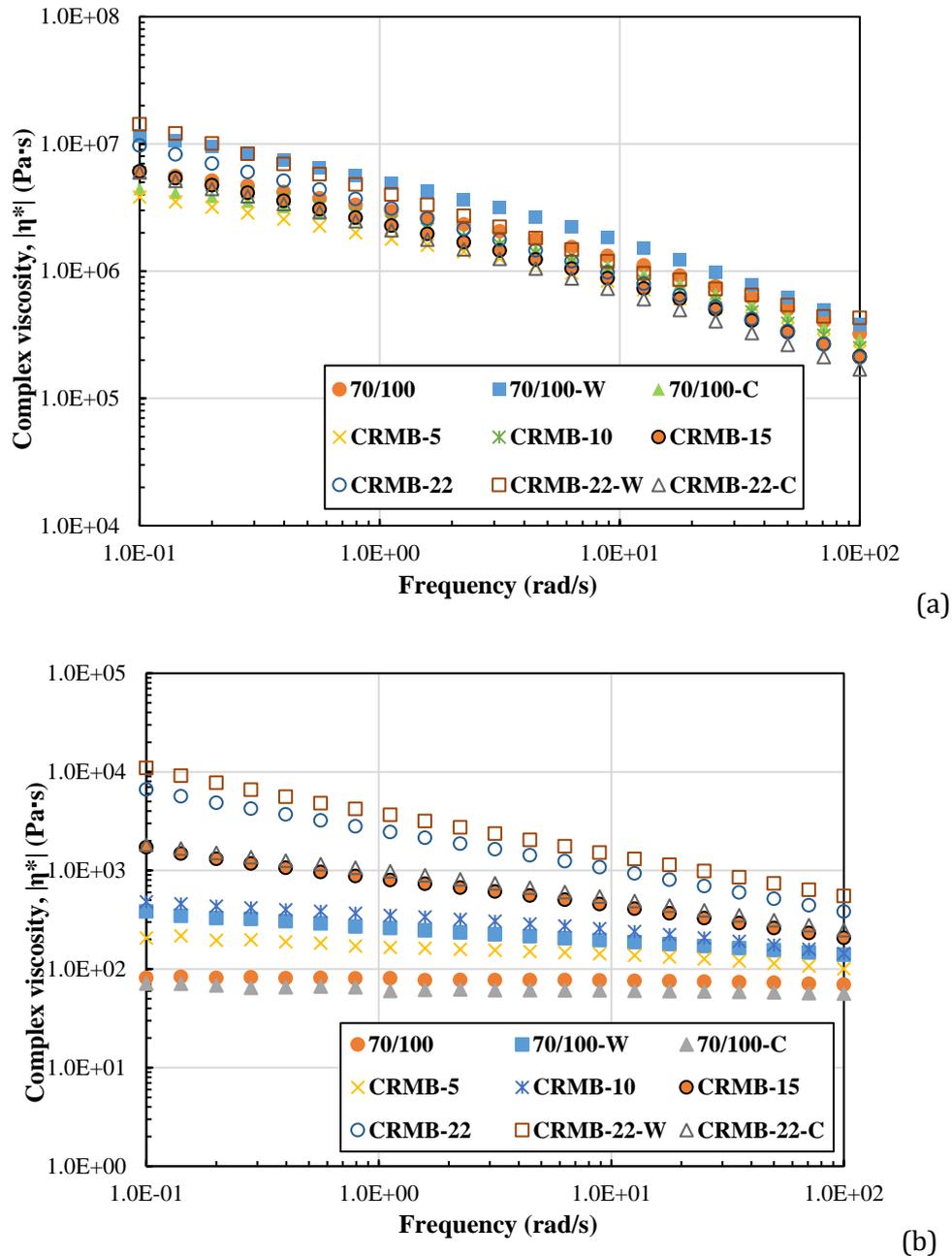
Figure 5.18 Complex viscosity of different binders as a function of frequency at (a) 10 °C and (b) 70 °C.

It can be clearly seen that the viscosity is temperature and shear rate (frequency) dependent, which decreases as the temperature and/or frequency increases. Figure 5.18a shows that all binders exhibit non-Newtonian behaviors at 10 °C whose viscosities decrease as the increase of shear rate. Figure 5.18b shows at 70 °C, base bitumen 70/100 with and without additive C both behave like Newtonian fluids, whose viscosities are almost independent of shear rates. In contrast, 70/100-W and all CRMB based binders exhibit non-Newtonian behaviors as the viscosities increase significantly as the shear rate decreases, which is categorized as the shear-thinning behavior. In addition, it is notable from Figure 5.18a that although the viscosity of CRMB-22 is higher than that of base bitumen at lower shear rates, it becomes lower when the shear rate reaches 100 rad/s. This is due to the more evident shear-thinning behavior of CRMB, whose mechanism will be explored in the following subsections.

In terms of warm-mix additives, the addition of chemical-based additive decreased the viscosity of both base and CRMB binders at a certain shear rate. However, wax-based additive increases the viscosities of both base and CRMB binders significantly, which seems contradictory to the viscosity-reduction effect of wax-based additive W at high construction temperatures (Jamshidi *et al.* 2013). It should be noted that additive W is a synthetic wax with high molecular hydrocarbon chains, and its melting point is around 100 °C. Therefore, when tested at 70 °C, additive W in binders will crystallize to form a lattice structure and hence stiffen the binders. Beyond its melting point, the wax liquefies and can be fully miscible in the binder, which significantly reduces the binder viscosity. This phase transition characteristic of additive W also explains the improved deformation resistance of binders containing W at service temperatures.

5.3.3.2 *Shear-thinning behaviors*

The previous subsection has shown the shear-thinning behaviors of different bituminous binders at certain temperatures. The occurrence of shear-thinning in non-Newtonian fluids can be attributed to the changes in particle/molecular orientations and/or alignment in the direction of flow. Specifically, there are three types of mechanisms as shown in Figure 5.19 can explain the complex shear-thinning behaviors of the unmodified and modified binders (Barnes *et al.* 1989).
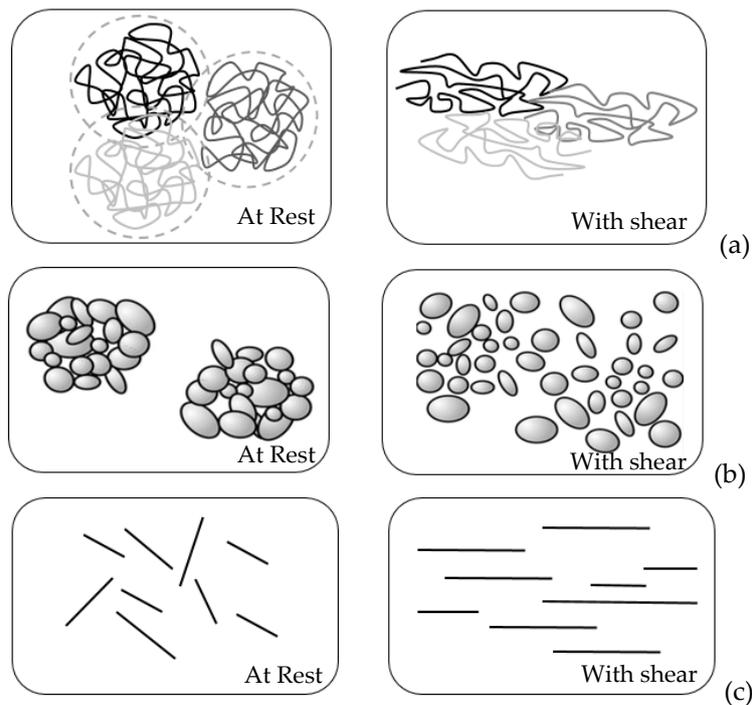
Figure 5.19 Schematic representation of shear-thinning mechanisms (a) polymer solutions/melts; (b) suspensions; (c) dispersions, adapted from (Barnes *et al.* 1989).

For polymer solutions or melts, polymer entanglements or coils are formed in the polymer network at rest. When the polymer solution/melts are subjected to shear loading, the entanglements or coils will unfold and align with the applied shear force, which in turn makes the polymer network easy to deform as shown in Figure 5.19a. For suspensions, solid particles in the liquid are prone to agglomerate at rest. With the applied shear loading, agglomerates tend to break up and disseminate into the matrix as shown in Figure 5.19b. For colloidal dispersions, when particles are introduced into a liquid at rest, they are randomly oriented to reach a thermodynamic equilibrium state (disordered state). With the applied shear force, particles will

try to align themselves to the shear direction as shown in Figure 5.19c. In all cases, materials in a disordered state at rest will shift to an orientationally ordered state with applied shear, which corresponds to a shift from high viscosity to low viscosity. This means shear-thinning behavior is an entropy-decreasing process (Angelico *et al.* 2003, Angelico *et al.* 2010). Bitumen is commonly recognized as a multi-disperse colloidal system, where high molecular weight asphaltene micelles are peptized by resins in low molecular weight maltenes. For base bitumen, the asphaltene can be regarded as particles that are randomly oriented in the maltenes and have the tendency to aggregate at rest. When the bitumen is subjected to shear loading at certain temperatures, the asphaltenes which contribute mainly to the viscosity will tend to an orientationally ordered state in the maltenes. Therefore, shear-thinning happens. A similar explanation that regards wax as solid particles can be applied for the shear-thinning behavior of wax-modified bitumen. In terms of CRMB, the potential polymer entangled/crosslinked network formed in the bitumen microstructure due to the rubber–bitumen interaction will unfold and stretch itself to adjust with the applied shear forces. The other two types of shear-thinning mechanism may also exist in CRMB. For the rest bituminous binders, a combination of these three types of mechanism will be capable to explain the shear-thinning behavior.

5.3.4 From rheology to flow activation energy

Figure 5.20 presents the plot of logarithmic viscosity as the ordinate and reciprocal temperature as the abscissa. The E_a values can be calculated based on the slope of ln (η^*)-1/T curves with known *R*-value according to Equation (5.5) and are summarized in Table 5.6. As can be seen from Table 5.6, CRM modification leads to a decrease in the activation energy of base bitumen.
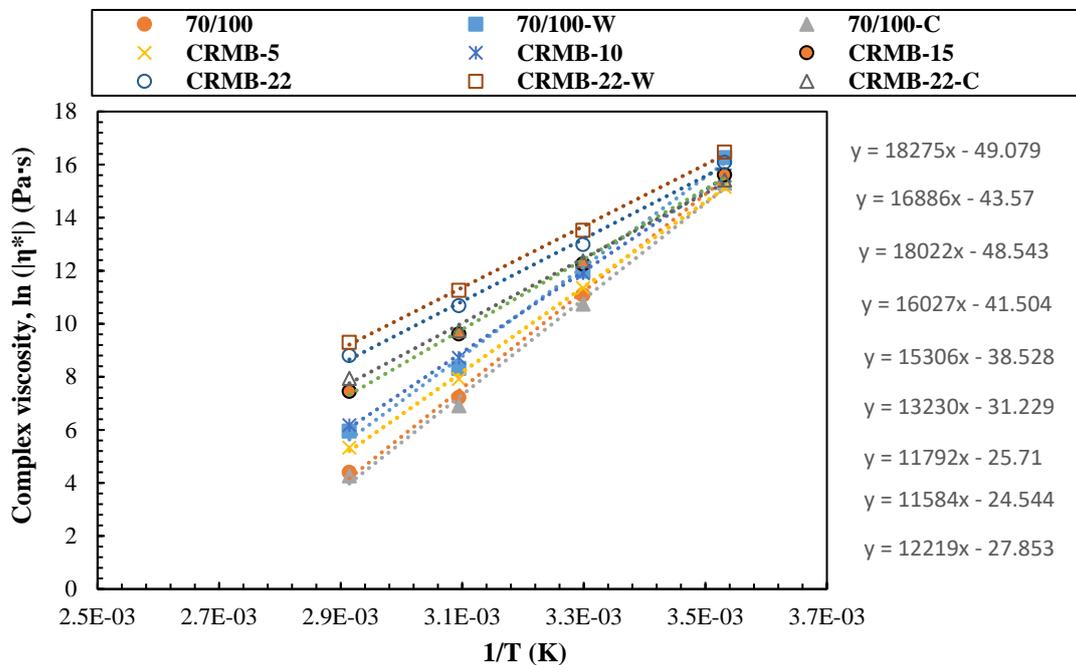
Figure 5.20 Temperature dependence of low-shear viscosity and calculation of activation energy.

Table 5.6 Activation energy value for different binders.

Binder type	70/100	70/100-W	70/100-C	CRMB-5	CRMB-10	CRMB-15	CRMB-22	CRMB-22-W	CRMB-22-C
Activation energy E_a **(kJ/mol)**	151.9	140.4	149.8	133.2	127.3	110.0	98.0	96.3	101.6

The higher CRM content, the lower activation energy of binder can be achieved as shown in Figure 5.21. This implies that CRM modification results in microstructural changes in the bitumen which significantly affect its rheological behavior. Chemical-based additive C had insignificant effects on the activation energies of both base asphalt and CRMB, while wax-based additive W consistently decreased the activation energies. Activation energy can be used as an indicator for characterizing the thermal susceptibility of bituminous binders. Binders with lower activation energy were found to be less susceptible to the temperature changes (Ait-Kadi *et al.* 1996, Salomon and Zhai 2002, Haider *et al.* 2011). It should be emphasized that bitumen with higher E_a values do not necessarily mean it has higher viscosities. The calculated activation energy is highly dependent on the testing temperatures at which the material can be in different physical states. Jamshidi *et al.* (2015) found E_a values of bitumen blends at different phases (liquid, semiliquid or solid) have opposite variation laws. Therefore, base bitumen, which has lower viscosity and higher activation energy, is more vulnerable to temperature change in the testing temperature range. From this point of view, the incorporation of CRM or additive W into base binders can improve the thermal susceptibility and deformation resistance within the service temperature range, which coincides with the results of this study and previous research findings (Attia and Abdelrahman 2009, Jamshidi *et al.* 2013).
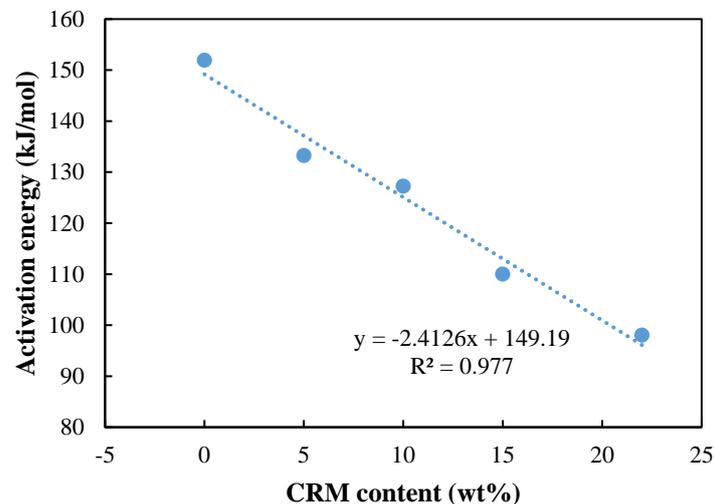
Figure 5.21 Activation energy of CRMB with different CRM contents.

5.3.5 Complex modulus and phase angle

5.3.5.1 *Black diagram*

A black diagram is a graph plotting complex shear modulus (G^*) versus phase angle (δ) obtained from frequency sweep tests. This type of representation of test data eliminates the frequency and

temperature and allows to compare the viscoelastic response of bituminous materials without manipulating the raw data through time-temperature superposition principle. Generally, a black diagram is a useful tool in identifying possible discrepancies in test data, in verifying time-temperature equivalence and thermo-rheological simplicity (Airey 2002) of test samples, and in identifying different types of bitumen.

(a)

(b)
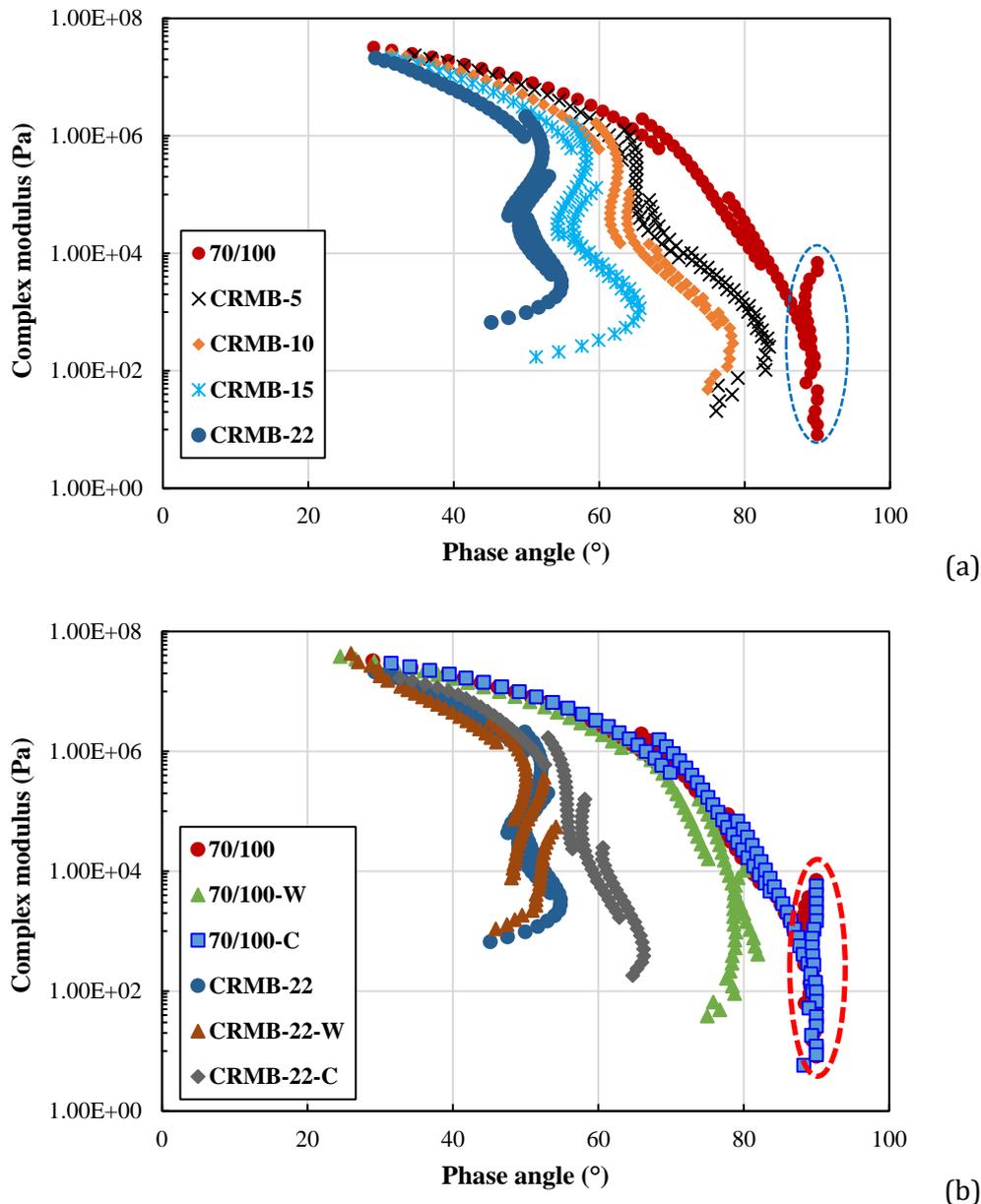
Figure 5.22 Black diagram of (a) CRMB binders and (b) binders with warm-mix additives.

Figure 5.22 shows the representation of dynamic data in black space. It can be clearly seen that the circled data of 70/100 and 70/100-C is out of line compared with the rest of the data. This unconformity indicates either instrument compliance errors or sample integrity loss at the particular temperatures and frequencies. After checking the broad raw data (e.g., shear strain, shear stress, torque), it was found that the circled data were measured at 70 °C and the torques corresponding to the circled data were as small as 0.0004 mN·m, which almost reach the minimum torque value of the DSR instrument. This means the sample at this temperature may become fluid

and cannot provide sufficient resistance to the instrument. Therefore, it is not suitable to perform the frequency sweep test on fresh neat bitumen samples at 70 °C in the current study. Therefore, these erroneous data were omitted before generating an accurate master curve. Except for the limited erroneous data, all the dynamic data produced smooth curves with slight scattering, indicating the bituminous binders can be considered as thermo-rheologically simple materials. Compared to base bitumen and 70/100-C, the addition of CRM or additive W to the base bitumen results in a shifting of the rheological data towards lower phase angle (left), which means these binders show more elastic behaviors. This could be due to the polymer network of CRM and the crystalline structure of W formed within the bitumen matrix. The higher CRM content, the more shift of the data to the left can be observed. Since different binders show different curve patterns in black space, the black diagram can also be used to differentiate materials. Unlike base bitumen and 70/100-C, the black diagrams of all CRMB based binders show an inverse and distorted "W" pattern which is typically found in rubberized asphalt binders (Celauro *et al.* 2012). The single modification by additive W changes the curve in black space into an inverse "C" pattern which is similar to that of SBS modified binder (Airey 2002). At the phase angle of around 78 °, there is evidence of phase transition of wax existing in the 70/100-W binder.

5.3.5.2 *Master curves of complex modulus and phase angle*

Master curves are developed from the measured linear viscoelastic data using time-temperature superposition principle at a reference temperature. In the present study, a modified CAM model (Bahia *et al.* 2001) and WLF equation for shift factors fitting were used to develop complex modulus and phase angle master curves. The master curves of complex modulus and phase angle at a reference temperature of 30 °C are shown in Figure 5.23. Similar effects of CRM and warm-mix additives on the rheological properties of bitumen were observed as previous analysis. From Figure 5.23a, at low frequencies (corresponding to high temperatures), CRMB binder is stiffer than neat bitumen and more elastic, while at high frequencies (corresponding to low temperatures), CRMB binder is softer than neat bitumen. It is noteworthy that phase angles of all the binders merged together when approaching the high-frequency range. This because at high frequencies (low temperatures), bitumen plays a dominant role in contributing to the viscous effect of the binder. The stiffening or softening extent is intensified as the CRM content increases. The phase angle master curves of all CRMB binders show the characteristic plateau in the intermediate frequency domain. This unique feature represents the presence of polymer (rubber) network in the bitumen. From Figure 5.23b, the addition of additive W resulted in marked reductions in phase angle and increases in complex modulus for both base bitumen and CRMB-22. The addition of additive C had insignificant effects on the viscoelastic properties of base bitumen. However, the addition of additive C evidently decreased the complex modulus and increased the phase angle of CRMB-22 due to the softening effect of the unique chemicals, which may be beneficial to the low-temperature performance. To sum up, the CRM and additive W enhanced the stiffness and elasticity of base bitumen, which is derived from the physical crosslinking of molecules into the three-dimensional network and the unique crystalline lattice structure at the service temperature range, respectively.

Furthermore, the phase angle master curves are less uniform than complex modulus master curves. Measurements of phase angle are more sensitive to the chemical structure change and thus the modification of bitumen than complex modulus does. This finding has driven the work of linking phase angle to the chemical characteristics of bituminous materials.

(a)

(b)
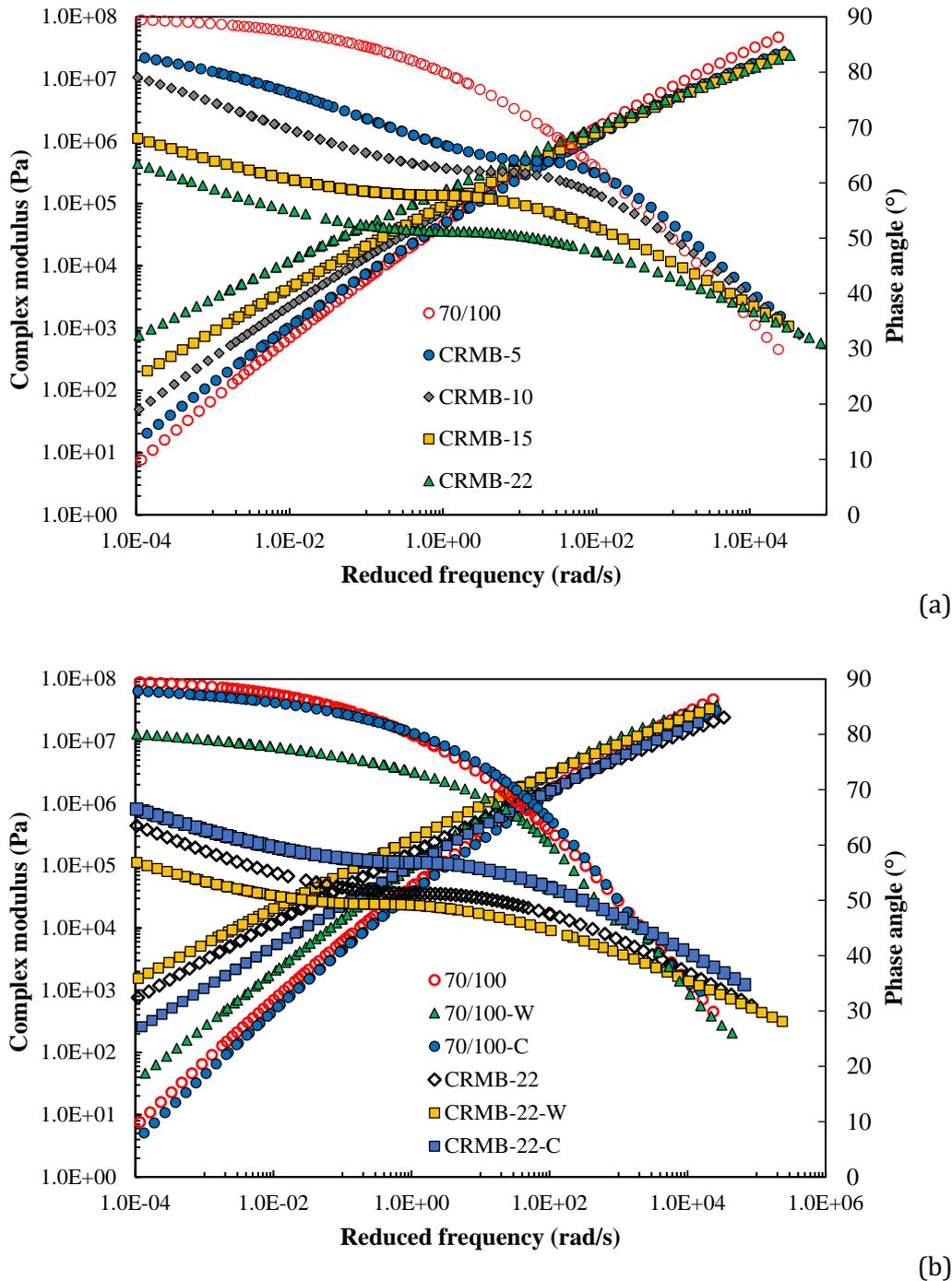
Figure 5.23 Complex modulus and phase angle master curves of (a) CRMB with different CRM contents; (b) binders with warm-mix additives.

5.3.6 From rheology to molecular weight distribution

After obtaining the CMWD curve ($f_c(M)$ versus $\log M$), the DMWD curve ($w(M)$ versus M is determined by numerical differentiation according to Equation (5.6) with the help of mathematical tool to guarantee convergence. The DMWD curves of different binders are presented in Figure 5.24. In general, Figure 5.24 clearly shows the internal structural changes of modified binders. From Figure 5.24a, the phase angle inversion method gives a similar number-

average molecular weight of around 800 Da for base bitumen as reported in the literature using GPC test (Domin *et al.* 1999, Zanzotto *et al.* 1999, Themeli *et al.* 2015).

This comparable result verifies the robustness of the inversion method. Comparing the MWDs of base bitumen and CRMB, it can be found that the unimodal MWD of base bitumen changed to bimodal MWD due to the interactions of CRM. In addition, the molecular population shifts to the position of heavier MW. This MWD change provides evidence that the internal structure of base bitumen was altered due to the addition of CRM. The large crosslinking molecules of rubber and the potential released polymer components from rubber make contributions to the increase the average molecular weight of base bitumen. With the increase of CRM content, the MWD shifts to the direction of larger molecular weight. This is understandable because larger molecules from rubber take an increasing proportion within the binder.

In terms of the effect of warm-mix additives, both additives changed the unimodal nature of MWD of base bitumen as shown in Figure 5.24b. It seems the MWD of base bitumen was not affected significantly by additive C. The addition of W into base bitumen shifted the molecular weight to the heavier direction. It is known that additive W is a kind of microcrystalline wax with high molecular weight hydrocarbons in the range $C_{40}\sim C_{120}$. Besides the molecular population of average MW ($\approx$900 Da), a new molecular population of average MW ($\approx$1200 Da) came up due to the modification of W. For CRMB-22, both warm-mix additives (W and C) did not change the bimodal nature of MWD of CRMB-22 in Figure 5.24c. The addition of both additives seems to not affect the first molecular population of MW of around 1000 Da. However, the second molecular population of MW of around 2600 Da was shifted to the position of higher MW. In addition, both additives decreased the relative amounts of molecular weights corresponding to the peak distribution.

In principle, the valley between two peaks of the MWDs should be smooth for real cases. The appearance of the sharpness in this case is mainly due to the inherent limitations of the phase angle master curve model and numerical differentiation error. Based on the above analysis, it can be concluded that the phase-angle inversion method has sufficient sensitivity to distinguish the structural changes of different binders and give comparable molecular weight distributions. However, the accuracy of this inverse method relies on the calibration Equation (5.10) and phase angle master curve. More works need to be done regarding these two aspects (i.e., improving the smoothness of molecular weight distribution curve and the correlation accuracy reflected by the calibration equation) to interpret the real molecular structure of bituminous materials.

(a)

(b)

(c)
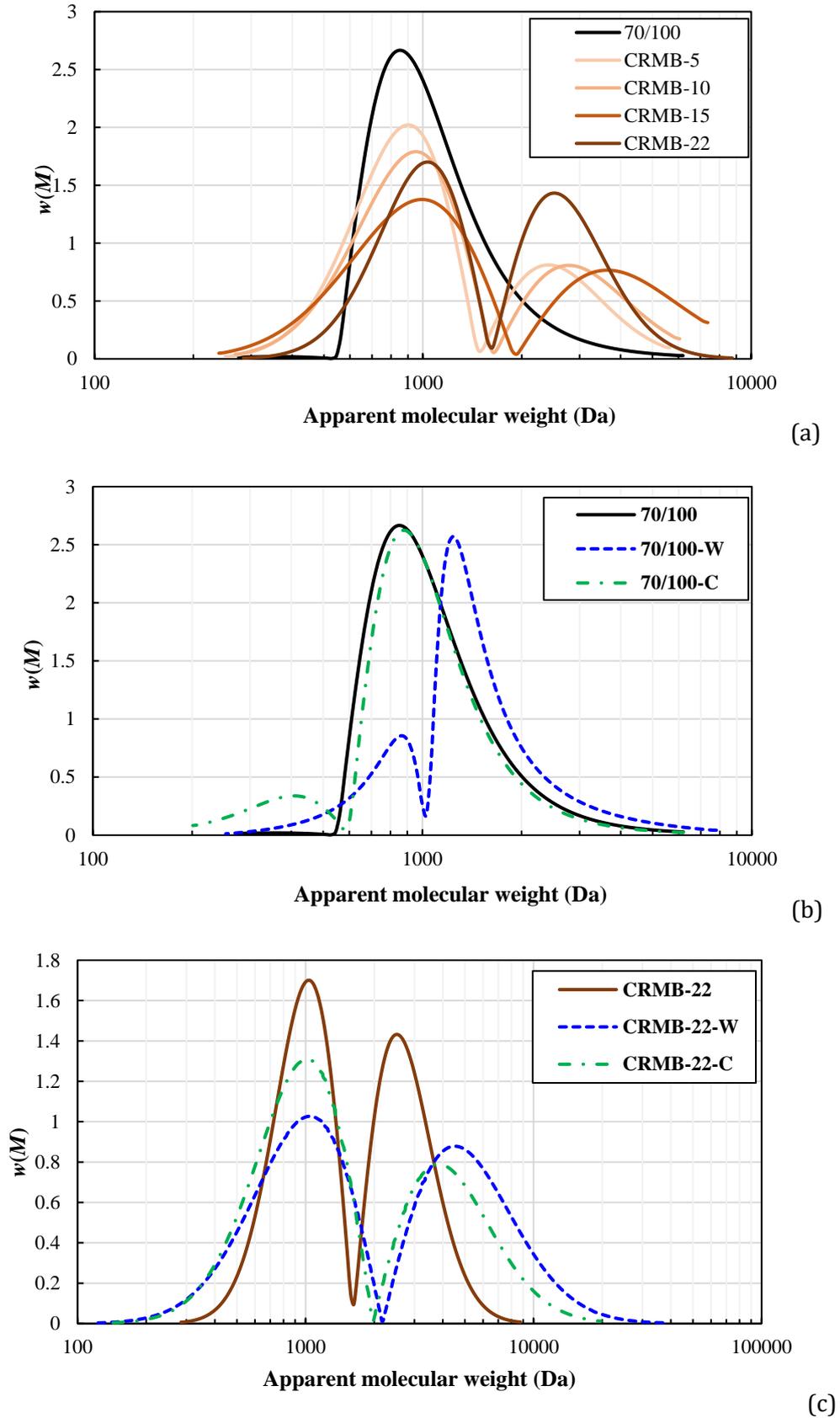
Figure 5.24 Molecular weight distributions of (a) CRMB with different CRM contents; (b) base bitumen with warm-mix additives; (c) CRMB with warm-mix additives.

5.4 Summary

This chapter first investigated the bitumen-rubber interaction at various mixing combinations of temperature and time. Rheological and chemical characterization on CRMB binders prepared at different conditions was carried out to determine the optimized interaction condition. Warm-mix additives (wax-based) were incorporated in CRMB using different procedures. The influence of preparation procedure on CRMB containing warm-mix additives was investigated from both rheological and thermal characteristics. Results show that the bitumen-rubber interaction is highly mixing temperature and time-dependent. With the increase of interaction temperature, the swelling and degradation of rubber particles successively occurred. The optimum bitumen-rubber interaction condition was determined at the mixing temperature of 180°C for 30 min, which produces CRMB binders with a lower J_{nr} and a higher percent recovery. In terms of the incorporation of warm-mix additives, both types of warm-mix additives were added to the prepared CRMB using the hot-mix method for the current study.

In the second part of this chapter, the rheological behaviour and its chemical interpretation from the perspective of activation energy and molecular weight distribution were investigated. Frequency sweep tests were done at various temperatures. CRMB and binders with wax additives show apparent shear-thinning behaviours at certain temperatures. The incorporation of CRM into base bitumen dramatically increases the complex viscosity. It also improves the rheological properties of base bitumen with enhanced stiffness and elasticity provided by the cross-linking polymer network. Wax-based additive increases the complex viscosity and complex modulus, and decreases the phase angle of bitumen due to the stiffening effect of the unique microcrystalline lattice structure at service temperatures. The chemical type of the additive has an insignificant effect on the rheological properties at the in-service temperatures. Binders modified by either CRM or wax-based additive have decreased flow activation energies, indicating lower thermal susceptibility. The higher CRM content, the lower activation energy of binder can be achieved. The phase-angle inversion method provides adequate and comparable molecular weight distributions, and this simply implemented method offers new perspectives in the interpretation of rheological data to monitor the change in the molecular structure of bitumen. Both CRM and the wax-based additive increased the average molecular weight of bitumen. The chemical-based additive had an insignificant effect on the molecular weight distribution of bitumen.

5.5 References

Abdelrahman, M., 2006. Controlling performance of crumb rubber-modified binders through addition of polymer modifiers. *Transportation Research Record: Journal of the Transportation Research Board,* (1962), 64-70.

Airey, G.D., 2002. Use of black diagrams to identify inconsistencies in rheological data. *Road Materials and Pavement Design,* 3 (4), 403-424.

Airey, G.D., Rahimzadeh, B. & Collop, A.C., 2002. Linear viscoelastic limits of bituminous binders. *Journal of the Association of Asphalt Paving Technologists,* 71, 89-115.

Ait-Kadi, A., Brahimi, B. & Bousmina, M., 1996. Polymer blends for enhanced asphalt binders. *Polymer Engineering & Science,* 36 (12), 1724-1733.

Anderson, D., Le Hir, Y., Planche, J.-P., Martin, D. & Shenoy, A., 2002. Zero shear viscosity of asphalt binders. *Transportation Research Record: Journal of the Transportation Research Board,* (1810), 54-62.

Angelico, R., Burgemeister, D., Ceglie, A., Olsson, U., Palazzo, G. & Schmidt, C., 2003. Deuterium nmr study of slow relaxation dynamics in a polymer-like micelles system after flow-induced orientation. *Journal of Physical Chemistry B,* 107 (38), 10325-10328.

Angelico, R., Rossi, C.O., Ambrosone, L., Palazzo, G., Mortensen, K. & Olsson, U., 2010. Ordering fluctuations in a shear-banding wormlike micellar system. *Phys Chem Chem Phys,* 12 (31), 8856-62.

Artamendi, I. & Khalid, H.A., 2006. Diffusion kinetics of bitumen into waste tyre rubber. *Journal of the Association of Asphalt Paving Technologists,* 75, 133-164.

Attia, M. & Abdelrahman, M., 2009. Enhancing the performance of crumb rubber-modified binders through varying the interaction conditions. *International Journal of Pavement Engineering,* 10 (6), 423-434.

Bahia, H.U., Hanson, D.I., Zeng, M., Zhai, H., Khatri, M.A. & Anderson, R.M., 2001. *Characterization of modified asphalt binders in superpave mix design.* Washington D.C.: Board, T.R.

Barnes, H.A., Hutton, J.F. & Walters, K., 1989. *An introduction to rheology*: Elsevier.

Biro, S., Gandhi, T. & Amirkhanian, S., 2009. Determination of zero shear viscosity of warm asphalt binders. *Construction and Building Materials,* 23 (5), 2080-2086.

Buckley, D.J. & Berger, M., 1962. The swelling of polymer systems in solvents. Ii. Mathematics of diffusion. *Journal of Polymer Science,* 56 (163), 175-188.

Celauro, B., Celauro, C., Lo Presti, D. & Bevilacqua, A., 2012. Definition of a laboratory optimization protocol for road bitumen improved with recycled tire rubber. *Construction and Building Materials,* 37, 562-572.

Chen, J., Zhang, J. & Li, H., 2004. Determining the wax content of crude oils by using differential scanning calorimetry. *Thermochimica Acta,* 410 (1-2), 23-26.

D'angelo, J. & Dongré, R., 2009. Practical use of multiple stress creep and recovery test. *Transportation Research Record: Journal of the Transportation Research Board,* 2126, 73-82.

De Visscher, J. & Vanelstraete, A., 2004. Practical test methods for measuring the zero shear viscosity of bituminous binders. *Materials and Structures,* 37 (5), 360-364.

Domin, M., Herod, A., Kandiyoti, R., Larsen, J.W., Lazaro, M., Li, S. & Rahimi, P., 1999. A comparative study of bitumen molecular-weight distributions. *Energy & Fuels,* 13 (3), 552-557.

García-Morales, M., Partal, P., Navarro, F.J., MartíNez-Boza, F., Gallegos, C., González, N., González, O. & Muñoz, M.E., 2004. Viscous properties and microstructure of recycled eva modified bitumen. *Fuel,* 83 (1), 31-38.

Ghavibazoo, A., Abdelrahman, M. & Ragab, M., 2013. Mechanism of crumb rubber modifier dissolution into asphalt matrix and its effect on final physical properties of crumb rubber-modified binder. *Transportation Research Record: Journal of the Transportation Research Board,* (2370), 92-101.

Haider, S.W., Mirza, M.W., Thottempudi, A.K., Bari, J. & Baladi, G.Y., Year. Characterizing temperature susceptibility of asphalt binders using activation energy for flowed.^eds. *Transportation and Development Institute Congress 2011: Integrated Transportation and Development for a Better Tomorrow*, 493-503.

Huang, S.C., 2008. Rubber concentrations on rheology of aged asphalt binders. *Journal of Materials in Civil Engineering,* 20 (3), 221-229.

Jamshidi, A., Hamzah, M.O., Shahadan, Z. & Yahaya, A.S., 2015. Evaluation of the rheological properties and activation energy of virgin and recovered asphalt binder blends. *Journal of Materials in Civil Engineering,* 27 (3).

Jamshidi, A., Hamzah, M.O. & You, Z., 2013. Performance of warm mix asphalt containing sasobit®: State-of-the-art. *Construction and Building Materials,* 38, 530-553.

Leng, Z., Yu, H., Zhang, Z. & Tan, Z., 2017. Optimizing the mixing procedure of warm asphalt rubber with wax-based additives through mechanism investigation and performance characterization. *Construction and Building Materials,* 144, 291-299.

Lesueur, D., 2009. The colloidal structure of bitumen: Consequences on the rheology and on the mechanisms of bitumen modification. *Adv Colloid Interface Sci,* 145 (1-2), 42-82.

Lu, X., Kalman, B. & Redelius, P., 2008. A new test method for determination of wax content in crude oils, residues and bitumens. *Fuel,* 87 (8-9), 1543-1551.

Morea, F., Agnusdei, J.O. & Zerbino, R., 2010. The use of asphalt low shear viscosity to predict permanent deformation performance of asphalt concrete. *Materials and Structures,* 44 (7), 1241-1248.

Partal, P., Martınez-Boza, F., Conde, B. & Gallegos, C., 1999. Rheological characterisation of synthetic binders and unmodified bitumens. *Fuel,* 78 (1), 1-10.

Rubio, M.C., Martínez, G., Baena, L. & Moreno, F., 2012. Warm mix asphalt: An overview. *Journal of Cleaner Production,* 24, 76-84.

Salim, R., Gundla, A., Underwood, B.S. & Kaloush, K.E., 2019. Effect of mscr percent recovery on performance of polymer modified asphalt mixtures. *Transportation Research Record: Journal of the Transportation Research Board*.

Salomon, D. & Zhai, H., 2002. Ranking asphalt binders by activation energy for flow. *Journal of Applied Asphalt Binder Technology,* 2 (2), 52-60.

Soenen, H., Besamusca, J., Fischer, H.R., Poulikakos, L.D., Planche, J.-P., Das, P.K., Kringos, N., Grenfell, J.R.A., Lu, X. & Chailleux, E., 2013. Laboratory investigation of bitumen based on round robin dsc and afm tests. *Materials and Structures,* 47 (7), 1205-1220.

State of California Department of Transportation, 2003. *Asphalt rubber usage guide.* Sacramento, CA, USA.

Sybilski, D., 1993. Non-newtonian viscosity of polymer-modified bitumens. *Materials and Structures,* 26 (1), 15-23.

Sybilski, D., 1996. Zero-shear viscosity of bituminous binder and its relation to bituminous mixture's rutting resistance. *Transportation Research Record: Journal of the Transportation Research Board,* (1535), 15-21.

Themeli, A., Chailleux, E., Farcas, F., Chazallon, C. & Migault, B., 2015. Molecular weight distribution of asphaltic paving binders from phase-angle measurements. *Road Materials and Pavement Design,* 16 (sup1), 228-244.

Tsenoglou, C., 1991. Molecular weight polydispersity effects on the viscoelasticity of entangled linear polymers. *Macromolecules,* 24 (8), 1762-1767.

Tuminello, W.H., 1986. Molecular weight and molecular weight distribution from dynamic measurements of polymer melts. *Polymer Engineering & Science,* 26 (19), 1339-1347.

Wang, D., Li, D., Yan, J., Leng, Z., Wu, Y., Yu, J. & Yu, H., 2018a. Rheological and chemical characteristic of warm asphalt rubber binders and their liquid phases. *Construction and Building Materials,* 193, 547-556.

Wang, H., Liu, X., Apostolidis, P. & Scarpas, T., 2018b. Non-newtonian behaviors of crumb rubber-modified bituminous binders. *Applied Sciences,* 8 (10), 1760.

Wang, H., Liu, X., Apostolidis, P. & Scarpas, T., 2018c. Review of warm mix rubberized asphalt concrete: Towards a sustainable paving technology. *Journal of Cleaner Production,* 177, 302-314.

Wang, H., Liu, X., Apostolidis, P. & Scarpas, T., 2018d. Rheological behavior and its chemical interpretation of crumb rubber modified asphalt containing warm-mix additives. *Transportation Research Record: Journal of the Transportation Research Board,* 2672 (28), 337-348.

Wang, H., Liu, X., Zhang, H., Apostolidis, P., Scarpas, T. & Erkens, S., 2020. Asphalt-rubber interaction and performance evaluation of rubberised asphalt binders containing non-foaming warm-mix additives. *Road Materials and Pavement Design,* 21 (6), 1612-1633.

Wang, H., Yang, J. & Gong, M., 2016. Rheological characterization of asphalt binders and mixtures modified with carbon nanotubes. *8th RILEM International Symposium on Testing and Characterization of Sustainable and Innovative Bituminous Materials.* Springer, 141-150.

Wang, H., You, Z., Mills-Beale, J. & Hao, P., 2012. Laboratory evaluation on high temperature viscosity and low temperature stiffness of asphalt binder with high percent scrap tire rubber. *Construction and Building Materials,* 26 (1), 583-590.

Yu, H., Leng, Z. & Gao, Z., 2016. Thermal analysis on the component interaction of asphalt binders modified with crumb rubber and warm mix additives. *Construction and Building Materials,* 125, 168-174.

Yu, H., Leng, Z., Zhou, Z., Shih, K., Xiao, F. & Gao, Z., 2017. Optimization of preparation procedure of liquid warm mix additive modified asphalt rubber. *Journal of Cleaner Production,* 141, 336-345.

Zanzotto, L., Stastna, J. & Ho, K., 1996. Characterization of regular and modified bitumens via their complex modulus. *Journal of applied polymer science,* 59 (12), 1897-1905.

Zanzotto, L., Stastna, J. & Ho, S., 1999. Molecular weight distribution of regular asphalts from dynamic material functions. *Materials and Structures,* 32 (3), 224-229.

Zhang, J.P., Yang, F.H., Pei, J.Z., Xu, S.C. & An, F.W., 2015. Viscosity-temperature characteristics of warm mix asphalt binder with sasobit (r). *Construction and Building Materials,* 78, 34-39.

Zofka, A., Chrysochoou, M., Yut, I., Johnston, C., Shaw, M., Sun, S.-P., Mahoney, J., Farquharson, S. & Donahue, M., 2013. *Evaluating applications of field spectroscopy devices to fingerprint commonly used construction materials.* Washington, D.C.

Zoorob, S.E., Castro-Gomes, J.P. & Pereira Oliveira, L.A., 2012. Assessing low shear viscosity as the new bitumen softening point test. *Construction and Building Materials,* 27 (1), 357-367.

6

Binder Performance Characterization of CRMB containing Warm-mix Additives

6.1 New performance-related test methods for binders

Permanent deformation, fatigue cracking and thermal cracking are three primary forms of distress that are highly correlated to high, intermediate and low-temperature range in asphalt pavements. Extensive research has shown that the mechanical characteristics of the asphalt binder-mastic phase have predominant effects on the final performance of asphalt mixture (Bahia *et al.* 2001a). The effective and accurate characterization of binder performance is of great importance from the point view of its potential applications (Hajj and Bhasin 2017): (a) as a tool for binder grading and design specification; (b) as a screening/ranking tool to examine the influence of modifiers and additives; (c) to obtain fundamental material properties of binders, which can be used as model inputs to predict the mechanical behaviors of asphalt mixture. Current performance related binder specifications were primarily developed for unmodified binders and were based on linear viscoelastic properties of the material. For example, the rutting resistance of bitumen in Superpave is evaluated by the so-called rutting parameter ($G^*/\sin \delta$) obtained at high temperatures. Correspondingly, the fatigue resistance of bitumen is addressed by the fatigue parameter ($G^* \cdot \sin \delta$) measured at intermediate temperatures. However, it has been proven that the two complex modulus-phase angle based parameters of bitumen obtained by Dynamic Shear Rheometer (DSR) have poor correlations with the mixture/pavement performance, especially for modified binders which often demonstrate superior damage resistance (Bahia *et al.* 2001a). Therefore, a number of new testing methods have been proposed in recent years for damage characterization of binders considering the non-linear viscoelasticity. Among them, multiple stress creep recovery (MSCR) test and linear amplitude sweep (LAS) test of bituminous binders were found to be more successful in correlating with mixture performance and have been proposed to provide efficient test and analysis methods for measuring the high-temperature rutting resistance and intermediate-temperature fatigue resistance, respectively (D'Angelo and Dongré 2009, Masad *et al.* 2009, Hintz *et al.* 2011, Hintz and Bahia 2013a). In terms of the low-temperature performance test, a recently developed frequency sweep (FS) test at low temperatures using a 4-mm DSR (4-mm diameter parallel plates) was proposed as an alternative with a number of advantages to the bending beam rheometer (BBR) (FHWA 2017). Therefore, in principle, binder properties in the whole temperature range can be characterized by using only one DSR instrument with different accessories (4-, 8- and 25-mm diameter plates) as shown in Figure 6.1. The choice of the parallel plate size is generally dependent on the testing temperatures. This unified DSR method is believed to be a technical breakthrough allowing improvement in the ability to provide performance-related specifications for road paving materials. Since rutting is primarily critical during the early in-service period of pavements, high-temperature performance tests were conducted on the short-term aged samples. By contrast, thermal and fatigue cracking mainly occurs at late in-service period, hence intermediate- and low-temperature performance tests were conducted on the long-term aged samples. The aging simulation methods are discussed and determined in subchapter 6.5 and also in (Wang *et al.* 2020c).
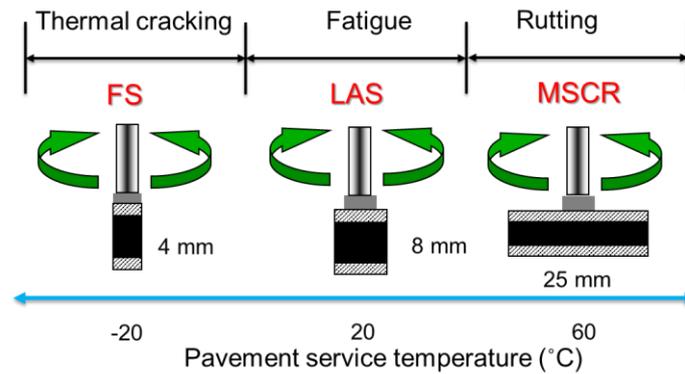
Figure 6.1 Unified DSR method for binder performance characterization from low to high temperatures.

6.2 High-temperature performance

6.2.1 Binder characterization for rutting

Under repeated traffic loadings, it is believed the accumulated strain in bituminous binder is mainly responsible for the rutting of asphalt pavements. Different methods and criteria have been developed to characterize the propensity of a binder to permanent deformation under periodic loading. The Superpave performance grading (PG) system uses the viscoelastic parameter (G*/sin δ) measured from DSR at a frequency of 10 rad/s as the rutting parameter at high temperatures. The rutting parameter obtained in the linear viscoelastic range can estimate the total dissipated energy during a loading cycle, which is believed to be related to rutting. To minimize rutting, the energy dissipated per loading cycle should be minimized. Hence in a stress-controlled test, the rutting parameter G*/sin δ should be maximized for binders at both fresh and short-term aged states (Anderson and Kennedy 1993). However, many studies have demonstrated the inadequacy of G*/sin δ in correlating with mixture rutting resistance, especially for polymer modified binders (Bahia *et al.* 2001b). Attempts have been made to replace this inaccurate rutting parameter.

Sybilski (1994) proposed the concept of the zero-shear viscosity (ZSV) at 60 °C to characterize binder's rutting resistance. Good correlations between ZSV of binders and rutting performance of mixtures were observed. However, other researchers found that highly polymer-modified binders, which behave as viscoelastic solids, exhibit extreme high viscosity gradients at low frequencies, resulting in unrealistically high ZSV values using model predictions (De Visscher and Vanelstraete 2004). Alternatively, the concept of low shear viscosity (LSV) was introduced to overcome this issue (Morea *et al.* 2010).

Since the rutting parameter was obtained using small cyclic reversible loadings, the contribution of binder damage accumulation was not considered. To address this, Bahia *et al.* (2001a) proposed the repeated creep recovery (RCR) test using DSR to simulate the intermittent nature of traffic loading during the NCHRP 9-10 project. The RCR test is capable of separating the dissipated energy between permanent deformation and delay elasticity. A new parameter G_v derived from the four-element Burger's model was introduced to characterize the binder's resistance to permanent deformation. Considering the significant stress dependency of polymer modified binders and different loading stress conditions, D'Angelo *et al.* (2007) improved the RCR by introducing a multiple stress creep and recovery (MSCR) test. MSCR is an easy-to-use and performance related test for both unmodified and modified binders. The nonrecoverable creep compliance (J_{nr}) and the percentage of recovery were calculated to characterize the stress

dependence and elastic response of bituminous binders. Parameters from MSCR tests have been proven to have a much better correlation to mixture rutting performance than the existing Superpave binder criteria (D'Angelo 2009).

6.2.2 Experimental methods

The MSCR test was conducted using a DSR with 25-mm parallel plates at two stress levels (0.1 kPa and 3.2 kPa) at 64 °C according to AASHTO T350-14. The predetermined temperature was stabilized within +/- 0.1 °C tolerance for 10 minutes. The chosen two stress levels can characterize both linear and nonlinear responses of binders. The test protocol includes a creep load of 1 s duration followed by 9 s recovery at zero loads in each cycle as shown in Figure 6.2. Ten creep and recovery cycles were tested at each stress level. The non-recoverable creep compliance (J_{nr}) and percent recovery (R) were calculated to characterize the stress dependence and elastic response of asphalt binders. The non-recoverable creep compliance is defined as the residual/permanent strain in a specimen after a creep and recovery cycle divided by the applied stress. The percent recovery is defined as the ratio of the recoverable strain to the peak/instantaneous strain, expressed as a percentage. The stress sensitivity of the binders (J_{nrdiff}) is evaluated by the percent difference in non-recoverable creep compliance between two different stress levels as shown in Equation (6.1). Before the creep and recovery test, a certain number of cycles for conditioning were applied to reach the steady state. Since rutting is primarily critical during the earlier in-service period of pavements at high-temperature conditions, MSCR tests were conducted on the short-term aged binder samples to simulate the aging after road constructions.

$$J_{nrdiff} = \frac{J_{nr,3.2} - J_{nr,0.1}}{J_{nr,0.1}} \times 100 \qquad (6.1)$$
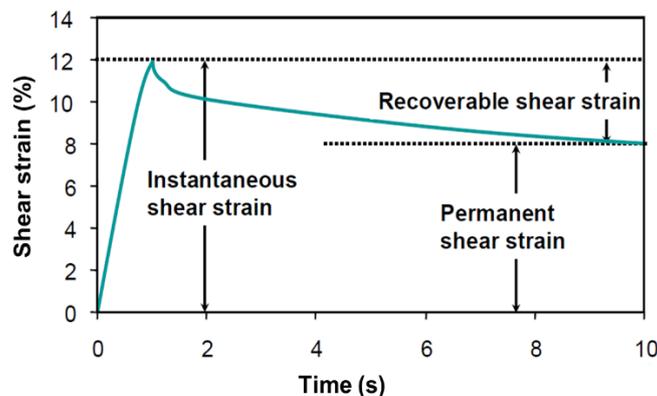
Figure 6.2 Schematic representation of shear strain evolution in the creep and recovery cycle.

6.2.3 MSCR results and discussion

Table 6.1 summarizes the MSCR test results of both base bitumen and CRMB with warm-mix additives. It is clear that the J_{nr} values of bitumen at both stress levels significantly decreased as the rubber content increased, indicating an improved rutting resistance of CRMB. In addition, CRMB binders had a considerably higher ability to recover (R) than the unmodified bitumen 70/100 at both stress levels. The lower J_{nr} and higher percent recovery of CRMB comparing to neat bitumen resulted from the superior polymer network established by the bitumen-rubber interaction.

In terms of warm-mix additives, the addition of wax-based additive to both neat bitumen and CRMB-22 decreased the J_{nr} value but did not significantly change the percent recovery. The improvement of resistance to permanent deformation stems from the microcrystalline structure of wax-based additive at the temperature below its melting point. The lattice structure formed by uniformly distributed wax particles at service temperature stiffened the binder. The chemical-based additive generally had insignificant effects on the MSCR results of neat bitumen. By contrast, the chemical-based additive seemed to make CRMB-22 a bit softer and slightly decreased the percent recovery.

Table 6.1 Summary of MSCR results of different binders at the short-term aged state.

Binder type	J_{nr} (1/kPa)		J_{nrdiff} (%)	$J_{nrslope}$ (%)	R (%)		Traffic level
	0.1 kPa	3.2 kPa			0.1 kPa	3.2 kPa	
70/100	3.489	3.938	12.87	14.48	1.55	0.00	S
70/100-W	0.602	2.478	311.63	60.52	45.78	0.18	S
70/100-C	3.323	3.778	13.69	14.68	1.52	0.00	S
CRMB-5	1.336	1.780	33.23	14.33	22.35	3.73	H
CRMB-10	0.466	0.914	96.14	14.45	48.12	15.47	V
CRMB-15	0.142	0.413	192.86	8.71	76.32	32.45	E
CRMB-22	0.022	0.182	727.27	5.16	91.44	41.66	E
CRMB-22-W	0.019	0.176	826.32	5.06	93.42	45.69	E
CRMB-22-C	0.046	0.292	534.78	7.94	86.57	35.26	E

The J_{nrdiff} parameter, defined as the difference of J_{nr} at different stress levels, is intended to evaluate the stress sensitivity of binders and is imposed an upper limit of 75%. It can be seen from Table 6.1 that all CRMB binders except CRMB-5 and 70/100-W exceeded the maximum allowable J_{nrdiff} value. However, the low J_{nr} values of these binders prove adequate resistance to permanent deformation at high service temperatures. It seems the J_{nrdiff} parameter lacks universality to characterize the stress sensitivity of highly modified binders. It unfairly penalizes binders with low J_{nr} values. Other research also confirmed this statement and recommended not evaluating the J_{nrdiff} parameter for accreditation purposes. Alternatively, the most recent specification AASHTO M 332-19 addresses the concern by removing the J_{nrdiff} requirement for binders having a $J_{nr3.2}$ value of 0.5 kPa^{-1} or lower at the selected test temperature. In this context, an alternate parameter $J_{nrslope}$ defined as the change in J_{nr} for an incremental change in applied stress τ, was proposed in Equation (6.2) (Stempihar *et al.* 2018).

$$J_{nrslope} = \frac{dJ_{nr}}{d\tau} = \frac{J_{nr3.2} - J_{nr0.1}}{\tau_{3.2} - \tau_{0.1}} \times 100 \qquad (6.2)$$

From Table 6.1, it can be seen all binders meet the requirement of stress sensitivity (lower than 75%) using the $J_{nrslope}$ parameter, which can be considered a more appropriate representation of stress sensitivity. In addition, CRMB binders exhibited superior stress insensitivity as expected using the new parameter. The acceptable non-recoverable creep compliance at 3.2 kPa and percent differences for varying levels of traffic as specified in AASHTO MP 19-10 are given in Table 6.2. Using the alternate parameter $J_{nrslope}$, the traffic level each binder can reach at the

temperature of 64 °C was also shown in Table 6.1. Base bitumen with and without warm-mix additives are suitable for pavements with standard traffic conditions. With the increase of rubber content, CRMB can be used for heavier traffic conditions.

Table 6.2 Binder grading requirements from AASHTO MP 19.

Traffic level	ESALs and traffic speed	$J_{nr3.2}$	J_{nrdiff} (%)
Standard, S	<10 million *and* standard traffic loading (>70 km/h)	≤4.0	<75
Heavy, H	10-30 million *or* slow traffic loading (20-70 km/h)	≤2.0	<75
Very Heavy, V	>30 million *or* standing traffic loading (<20 km/h)	≤1.0	<75
Extremely Heavy, E	>30 million *and* standing traffic loading (>70 km/h)	≤0.5	<75

6.3 Low-temperature performance

6.3.1 Binder characterization for thermal cracking

Thermal cracking is the primary distress in asphalt pavements operating in cold climates. With the decrease of temperature, significant tensile stresses will develop in the asphalt layer and ultimately lead to the initiation and propagation of cracks. As cracks mainly occur in the binder or mastic phase, it is vital to select appropriate binders in mix design which meet the requirements of low-temperature performance for binders (Hajj *et al.* 2019). Many methods have been proposed to evaluate the low-temperature properties of binders, such as the Fraass breaking point test and low-temperature ductility test. However, these traditional tests cannot accurately predict the temperature at which the thermal cracking occurs (Wang *et al.* 2017). The inadequacy is more significant when using these tests for the assessment of polymer modified binders (Isacsson and Lu 1995).

The current Superpave PG system utilizes the bending beam rheometer (BBR) test to determine the low-temperature PG of binders. Two parameters obtained from the BBR test, namely creep stiffness and *m*-value (relaxation rate), were used to determine the critical cracking temperature by applying two threshold limits on them. The low-temperature PG of the binder is ruled as the higher of below two criteria: the temperature above which the maximum creep stiffness should not exceed 300 MPa and the temperature above which the minimum *m*-value should not be less than 0.3. The creep stiffness is directly related to the thermal stress that can build up in the bituminous material when temperature drops. Meanwhile, the *m*-value shows the ability to retain the viscoelasticity and relaxing the accumulated thermal stress.

Standard BBR testing requires a relatively large amount of materials (15 g for each beam sample) which may be inconvenient and difficult when assessing binders recovered from reclaimed asphalt pavement (RAP) or emulsion residues. To overcome this limitation, previous researchers have explored the potential of using a DSR with parallel plates of 4 mm in diameter (4-mm DSR) as an alternative to the BBR (Sui *et al.* 2011, Farrar *et al.* 2015, Lu *et al.* 2017, Oshone 2018, Wang *et al.* 2019a). Besides the primary advantage of requiring a small amount of binder, 4-mm DSR is a simple and more precise method than BBR when measuring low-temperature rheology to determine thermal stress build-up (Farrar *et al.* 2013). It was also reported 4-mm DSR has good repeatability and good consistency among data collected from different DSR plate sizes (Sui *et al.* 2010, Hajj *et al.* 2019). 4-mm DSR is believed to be a major technological breakthrough allowing

improvement in our ability to provide low-temperature performance-related specifications for bituminous materials.

6.3.2 Objectives and approach

The main objective of this subchapter is to characterize the low-temperature rheology and performance of binders using 4-mm DSR. Frequency sweep tests using 4-mm DSR were performed on long-term aged binders. The dynamic data from DSR were interconverted to BBR related relaxation parameters to further determine the low-temperature PG of binders. The effects of CRM content and warm-mix additives on the fatigue performance of binders were also investigated.

6.3.3 4-mm DSR test methods

With 4-mm parallel plates, frequency sweeps from 1 to 100 rad/s were performed at low temperatures from -30 to 10 °C with a step of 10 °C. It was reported that DSR measurements at low temperatures may generate errors in the values of dynamic data due to instrument compliance. It is generally recommended to use small-diameter plates with a high gap between the plates in the low temperature range to reduce the instrument compliance error (Schroter *et al.* 2006). In the current study, a gap of 3 mm between the plates was used with the 4-mm parallel plate geometry, which was validated and recommended by Braunschweig Pavement Engineering Centre (ISBS) at Technical University of Braunschweig (Wang *et al.* 2019a). Besides, automatic real-time compliance corrections were done using the pre-input machine compliance for the 4-mm parallel plates on the measuring system. To accommodate the specimen on such a small plate, a specifically designed butterfly silicone mold was manufactured to prepare and install the binder specimen on the DSR plates. The detailed sample preparation steps can be found in (Wang *et al.* 2019a). When chamber temperature drops to -30 °C, the resulting shrinkage of the binder could potentially cause its debonding from the top plate. To ensure good adhesion between the sample and plates, the normal force was set automatically zero during cooling phase. For each type of binder, at least two replicates were tested to obtain reliable experimental results.

6.3.4 Correlation between DSR measured data and BBR parameters

While BBR is a flexural test in the time domain, DSR measures the shear properties of the binder in the time/frequency domain. Therefore, frequency sweep measurements from DSR must be mathematically manipulated to be comparable to those from BBR. Previous studies have developed methods to convert DSR data into the parameters related to BBR tests (i.e., interconversion from dynamic frequency sweep to shear stress relaxation). The corresponding grading criteria for binders determine the low-temperature PG using 4-mm DSR were also proposed. Table 6.3 summarizes the methods and corresponding criteria for grading binders when using 4-mm DSR.

Table 6.3 Methods and criteria for low-temperature grading binders using 4-mm DSR

Reference	Conversion methods	Creep stiffness grading criterion	*m*-value grading criterion
Sui et al. 2011	Generalized Maxwell model or Ninomiya and Ferry approximation method	$G(t)$ <180 MPa at t=7200 s at actual PG temperature	m>0.26 from $G(t)$ at t=7200 s at actual PG temperature

Farrar et al. 2015	Christensen approximation method	$G(t)$<143 MPa at t=60 s at PG temperature + 10 °C	m>0.28 from $G(t)$ at t=60 s at PG temperature + 10 °C
Lu et al. 2017	Empirical equation (6.8)	$S(t)$<143 MPa at t=60 s at PG temperature + 10 °C	m>0.28 at $\omega = 2/\pi t$ at PG temperature + 10 °C
Oshone 2018	Empirical equation (6.10)	NA	NA
Hajj et al. 2019	Ninomiya and Ferry approximation method	$S(t)$<300 MPa at t=60 s at PG temperature + 10 °C	m>0.30 from $S(t)$ at t=60 s at PG temperature + 10 °C

Regarding the methods of interconversion from dynamic frequency sweep to shear stress relaxation, both exact conversion methods based on linear viscoelastic theory and approximate conversion methods were used as mentioned in Table 6.3. The exact interconversion using generalized Maxwell model relates the shear relaxation modulus $G(t)$ in time domain to the storage and loss modulus in the frequency domain ($G'(\omega)$ and $G''(\omega)$) by the following equations.

$$G(t) = \sum_{i=1}^{n} g_i e^{-t/\lambda_i} \tag{6.3}$$

$$G'(\omega) = \sum_{i=1}^{n} g_i \frac{\omega^2 {\lambda_i}^2}{1 + \omega^2 {\lambda_i}^2} \tag{6.4}$$

$$G''(\omega) = \sum_{i=1}^{n} g_i \frac{\omega \lambda_i}{1 + \omega^2 {\lambda_i}^2} \tag{6.5}$$

Where g_i and λ_i define the discrete relaxation spectrum and represent the stiffness and relaxation time of the ith Maxwell component. ω is the angular loading frequency from DSR tests. By fitting the dynamic frequency sweep data to Equations (6.4) and (6.5), the shear relaxation modulus in time domain can be obtained by Equation (6.3).

The shear stress relaxation modulus can also be converted from frequency sweep data by using the empirical conversion methods. The approximation method proposed by (Ninomiya and Ferry 1959) is given in Equation (6.6).

$$G(t) = G'(\omega) - 0.4G''(0.4\omega) + 0.014G''(10\omega)|_{\omega=2/\pi t} \tag{6.6}$$

Alternatively, Christensen further simplified the approximate expression as

$$G(t) \approx G'(\omega)|_{\omega=2/\pi t} \tag{6.7}$$

After obtaining the relaxation modulus curve in the time domain, the m-value is determined as the relaxation rate at the time of interest. Lu *et al.* (2017) utilized an approximate model originally proposed by (Anderson *et al.* 1994) to correlate BBR creep stiffness with modulus from DSR. This model requires only the complex modulus and phase angle for the interconversion as shown in Equation (6.8). The m-value was also empirically approximated as Equation (6.9) at the temperature and frequency of interest.

$$S(t) = \frac{3G^*(\omega)}{1 + 0.2\sin(2\delta)} \tag{6.8}$$

$$m = \delta/90 \tag{6.9}$$

Similarly, Oshone (2018) proposed empirical equations to determine creep stiffness and *m*-value as shown in Equations (6.10) and (6.11).

$$S(t) = 1.28G^*(\omega) + 19.2 \qquad (6.10)$$

$$m = 0.008\delta + 1 \qquad (6.11)$$

Equations (6.8) and (6.10) are linear functions derived based on empirical correlations between DSR and BBR testing. Besides the interconversion process from the frequency domain to time domain, Hajj et al. (2019) also converted the shear response of binders to the uniaxial response using the following equation.

$$S(t) = G(t)(1 + 2v) \qquad (6.12)$$

where v is the Poisson's ratio of the binder. A constant Poisson's ratio of binder was assumed as 0.35, which was believed to be more reasonable at low temperatures (Benedetto *et al.* 2007). By doing so, original grading criteria for BBR can be directly applied to the DSR derived parameters. It was reported that the exact interconversion method and approximate conversion method give almost identical stress relaxation curve (Sui *et al.* 2011). For simplicity, the empirical conversion method as shown in Equation (6.6) was used in this study.

6.3.5 Low-temperature rheology and performance grading

6.3.5.1 *Black diagram*

The raw dynamic data of different binders from 4-mm DSR frequency sweep tests were compared in the black diagrams (Figure 6.3). As pointed in Chapter 5, a black diagram is a useful tool to analyse the rheological data. It can identify possible discrepancies in test data, verify time-temperature equivalence and thermo-rheological simplicity of test samples, and compare different types of bitumen. It can be seen from Figure 6.3 that there are no obvious discontinuities or sudden change in the slope of the curves. The smooth curves indicate that 4-mm DSR with the current test configurations can generate reliable rheological data. The test samples are also confirmed as thermo-rheologically simple. Unlike the black diagrams in the high-temperature range in Figure 5.20, the curves of binders in the black space in the low-temperature range do not show any symbolic patterns. Although bitumen with the addition of CRM becomes more elastic as reflected by the shift of rheological data towards lower phase angle (left), the change in the elastic behavior is not as significant as shown in Figure 5.20. This is because at low temperatures, the bitumen matrix plays a more dominant role than rubber particles in determining the rheological properties of CRMB. With the same phase angle value, CRMB binders exhibit lower complex moduli compared to unmodified bitumen. This implies that CRMB may possess better low-temperature performance than unmodified bitumen, which will be discussed in the following subsections.

(a)

(b)
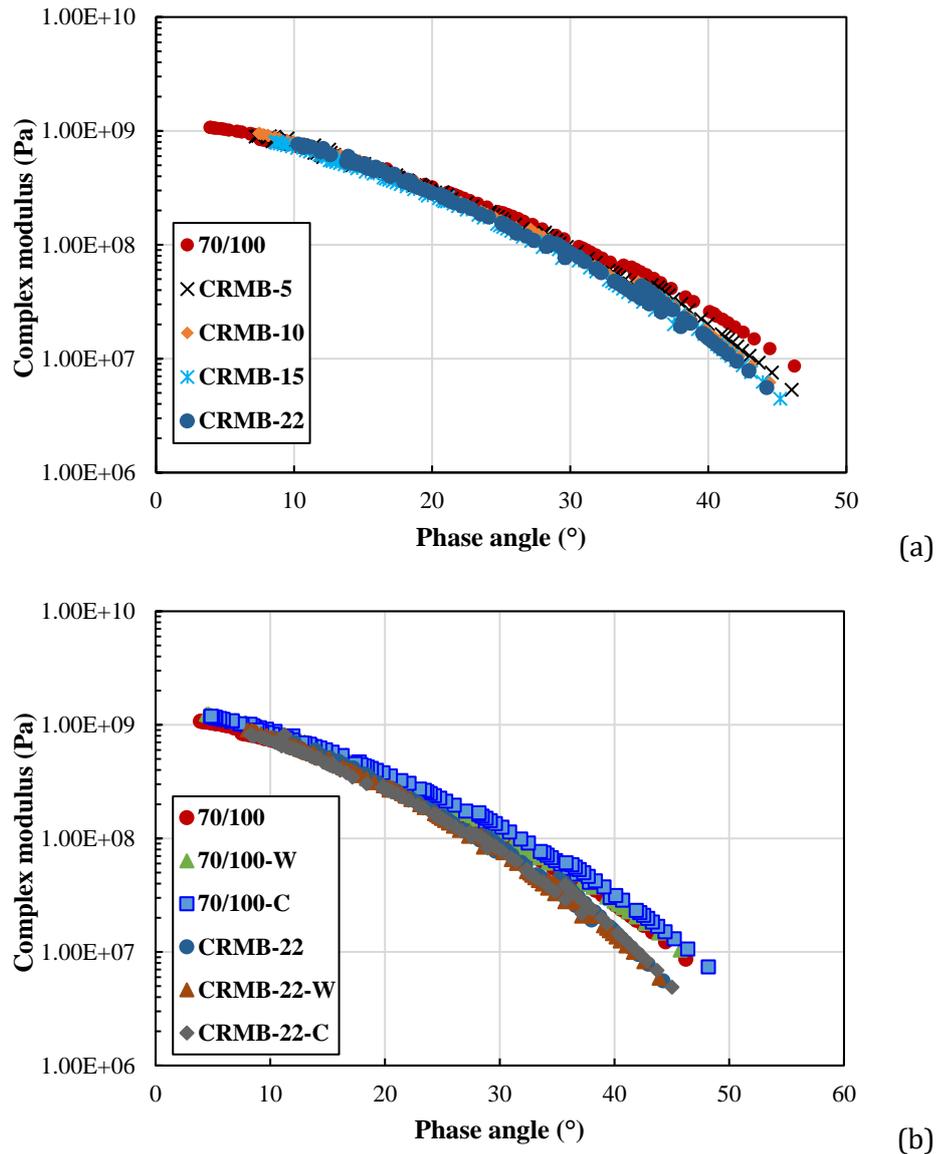
Figure 6.3 Black diagram of (a) CRMB binders and (b) binders with warm-mix additives.

6.3.5.2 *Analysis methods for interpreting 4-mm DSR data*

As discussed earlier, there are two main transformations required to obtain BBR parameters from the DSR data: i) converting dynamic data from the frequency domain to the time domain; and ii) converting shear response to flexural response. Then, the critical cracking temperatures for low-temperature PG can be determined by the BBR criteria, i.e., $S(t)$=300 MPa and m=0.30 at t=60 s at PG temperature + 10 °C. To demonstrate the calculation process, the neat bitumen of 70/100 was taken as an example.

- Step 1. The CAM model was used to generate the complex modulus and phase angle master curves at a reference temperature using the frequency sweep data (Figure 6.4)
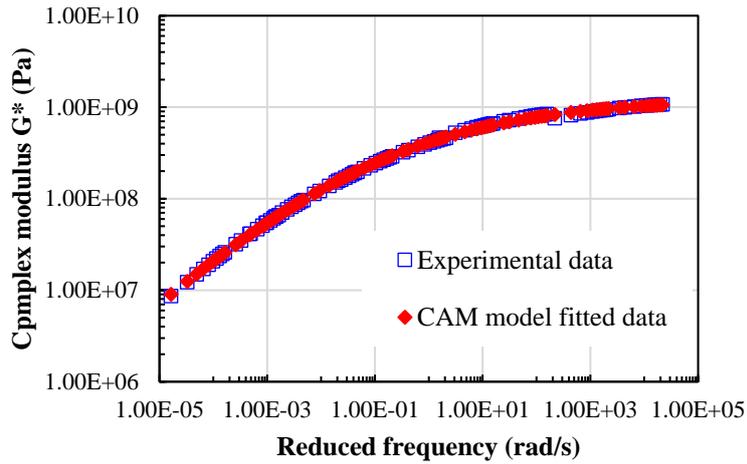
(a)
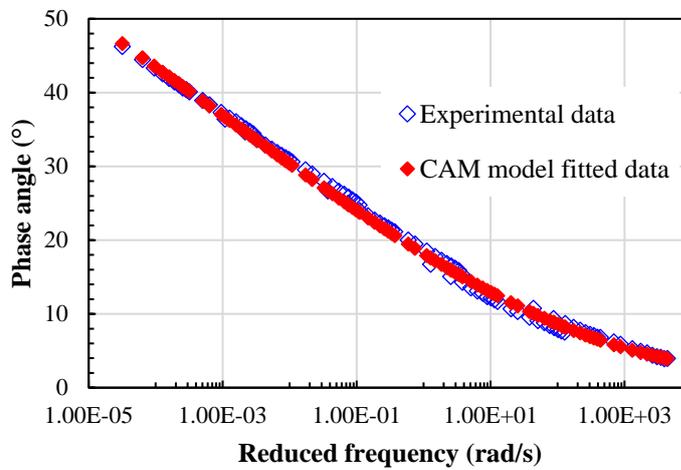
(b)

Figure 6.4 (a) Complex modulus and (b) phase angle master curves of neat bitumen 70/100 at a reference temperature of -18 °C.

- Step 2. The shear stress relaxation modulus curve in time domain was converted using the approximation method as given in Equation (6.6). The master curves of storage modulus and loss modulus were derived by the following relationships.

$$G'(\omega) = |G^*| \sin \delta, \text{ and } G''(\omega) = |G^*| \cos \delta \tag{6.13}$$

- Step 3. Convert the shear relaxation modulus to flexural creep stiffness using Equation (6.12) as shown in Figure 6.5.
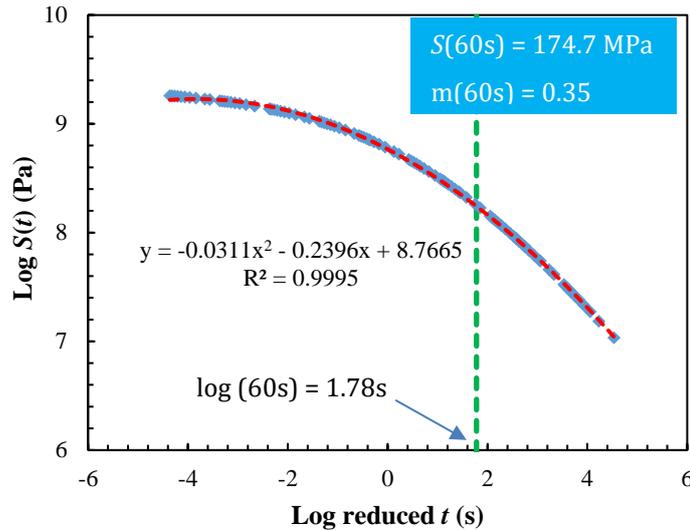
Figure 6.5 Master curve of creep stiffness at a reference temperature of -18 °C.

- Step 4. Determine the value of $S(t)$ and m-value at t= 60 s through the creep stiffness master curve. The m-value was determined by taking the first derivative after obtaining the trendline equation. The calculated values of S and m are shown in Figure 6.5.
- Step 5. Calculate the critical cracking temperatures by interpolation. Steps 1-4 at a different reference temperature were repeated. The selected reference temperatures should bracket specified values of S and m. The critical cracking temperatures were thus determined by interpolating between passing and failing temperatures based on the limiting values of S and m (see Equations (6.14) and (6.15)).

$$T_{c,S} = T_1 + \frac{(T_1 - T_2)(\log 300 - \log S_1)}{\log S_1 - \log S_2} - 10 \qquad (6.14)$$

$$T_{c,m} = T_1 + \frac{(T_1 - T_2)(0.3 - m_1)}{m_1 - m_2} - 10 \qquad (6.15)$$

where $T_{c,S}$ and $T_{c,m}$ are the critical temperatures or true grade controlled by the creep stiffness and m-value respectively. T_1 is the temperature at which S or m passes the criterion while T_2 is the temperature at which S or m fails the criterion. S_1 and S_2 are the creep stiffness (MPa) at T_1 and T_2. m_1 and m_2 are the creep rate at T_1 and T_2.

6.3.5.3 *Critical cracking temperature*

Using the above calculation process, the derived values of S and m from 4-mm DSR test results at different temperatures are summarized in Table 6.4. Generally, binders with lower creep stiffness and higher creep rate have better resistance to low-temperature cracking. The values of S and m shaded by grey colour in Table 6.4 are the data that bracket the specifications and are used to calculate the critical cracking temperatures (Equations (6.14) and (6.15)).

Table 6.4 Creep stiffness and *m*-value derived from 4-mm DSR test results.

Binder type	-18 °C		-24 °C		-30 °C		-36 °C		Low PG
	S (MPa)	*m*	*S* (MPa)	*m*	*S* (MPa)	*m*	*S* (MPa)	*m*	(°C)
70/100	174.7	0.35	402.4	0.28	785.2	0.20	1112.4	0.16	-28
70/100-W	216.1	0.33	625.9	0.24	1283.8	0.15	1453.9	0.13	-28
70/100-C	161.7	0.37	466.0	0.28	1092.8	0.17	1394.4	0.13	-28
CRMB-5	107.1	0.38	253.2	0.31	524.7	0.24	797.2	0.19	-34
CRMB-10	92.0	0.39	223.9	0.32	469.6	0.25	723.8	0.20	-34
CRMB-15	70.9	0.40	163.2	0.33	333.6	0.27	595.7	0.21	-34
CRMB-22	56.0	0.42	124.9	0.36	252.3	0.30	453.9	0.24	-40
CRMB-22-W	66.1	0.42	156.9	0.35	277.4	0.29	459.2	0.23	-34
CRMB-22-C	61.2	0.43	134.1	0.37	237.7	0.31	443.9	0.26	-40

It can be seen from Table 6.4 that there are no consistent trends for the change in creep stiffness and creep rate of different binders at different temperatures. At the temperatures that bracket the specifications (shaded data), the addition of wax-based additive to neat bitumen increases the creep stiffness and decreases the creep rate. This is possibly due to the crystallization of wax in the binders at low temperatures which has a stiffening effect. In contrast, the addition of chemical-based additive made the base bitumen softer by decreasing its stiffness and increasing the creep rate. The polymers and anti-stripping agents in the chemical additive may be responsible for the improvement of cracking resistance. Similar effects of warm-mix additive were found on CRMB. In short, the wax-based additive has adverse effects on the low-temperature performance of binders while chemical-based additive can improve the low-temperature performance. Comparing the neat bitumen with CRMB binders, the modification with CRM decreases the stiffness and increases the creep rate at low temperatures because of the presence of elastic CRM particles in the bitumen matrix. With the increase of CRM content, the improvement of low-temperature performance is more prominent. As pointed out in Chapter 3, at low temperatures, the modulus of swollen rubber particles is lower than the bitumen matrix. This explains why CRMB has a smaller creep stiffness and a higher creep rate than the neat bitumen at low temperatures. The above findings are consistent with previous studies using BBR tests to characterise the low-temperature performance of binders (Akisetty *et al.* 2010).

The low PGs of different binders based on the current PG specifications are also shown in Table 6.4. The addition of warm-mix additives does not change the low-temperature PG of neat bitumen as -28 °C. The modification by CRM further decreases the low-temperature PG. When increasing the CRM content to 22%, the low PG of CRMB is improved to -40 °C compared to other CRMBs with lower CRM contents which have a low PG of -34 °C. The wax-based additive degrades the low PG of CRMB by one level while CRMB-22 with the chemical-based additive remains the same.

Since the current PG grading system adopts an increment of 6 °C, binders having the same PG may have slightly different performance at a certain temperature. Therefore, the critical temperatures (true continuous grade) of different binders for low-temperature PG calculated using Equations (6.14) and (6.15) are summarized in Figure 6.6.
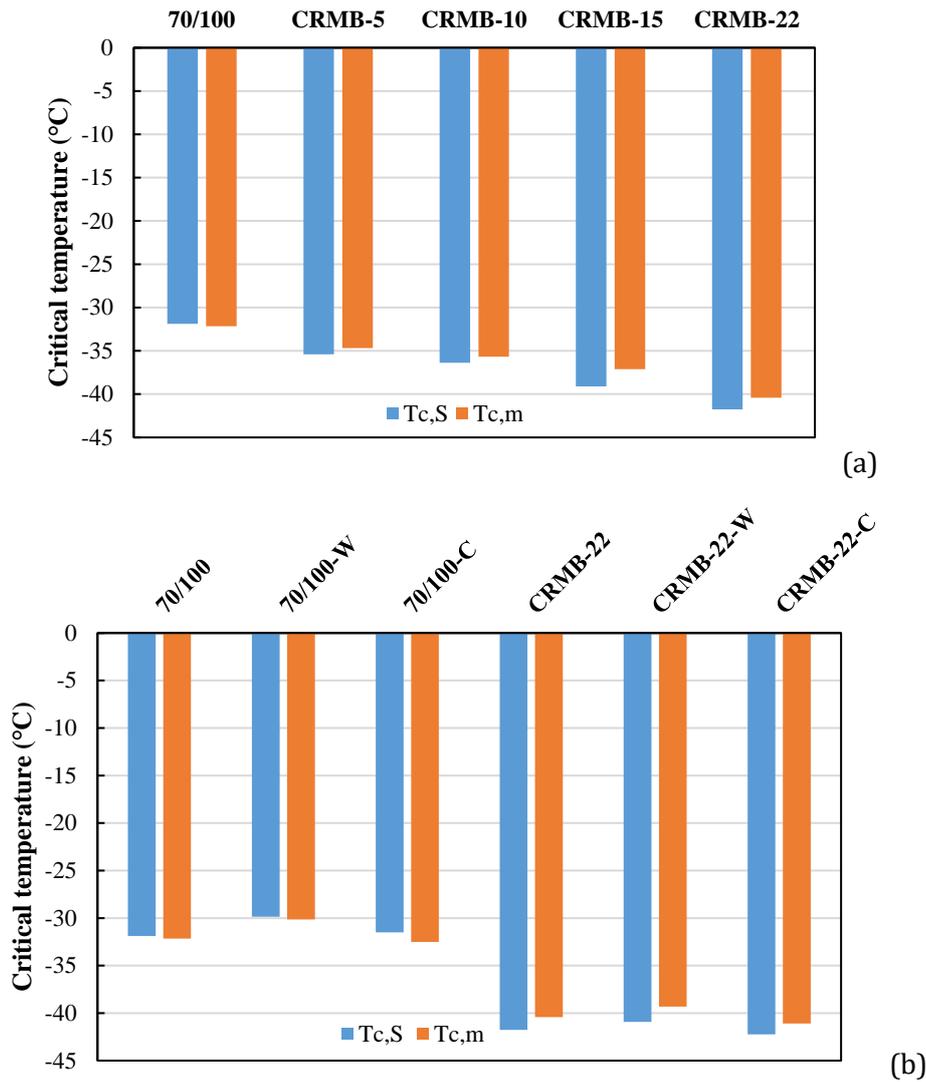
Figure 6.6 Critical cracking temperatures determined by creep stiffness and *m*-value for different binders (a) CRMB binders and (b) binders with warm-mix additives.

It can be seen from Figure 6.6a that both $T_{c,S}$ and $T_{c,m}$ of CRMB gradually decrease as the increase of CRM content, indicating a lower low-temperature PG. In terms of the effect of warm-mix additives in Figure 6.6b, the addition of wax-based additive increases the critical temperatures of both neat and CRM modified binders while chemical-based additive slightly decreases the critical temperature. In addition, it is noteworthy that the $T_{c,S}$ of 70/100 based binder (with/without warm-mix additives) is higher than the corresponding $T_{c,m}$. By contrast, CRMB based binder has the opposite situation in which its $T_{c,S}$ is lower than $T_{c,m}$. This implies that the low-temperature PG of 70/100 based binders are creep stiffness controlled while CRMB binders are *m*-value controlled. Creep stiffness does not present a complete picture of binder cracking tendency at low temperatures. This is because bitumen is a viscoelastic material, which is able to relax applied stresses. In other words, if given sufficient time, bitumen will shed the built-up stresses when applying a load or changing the temperature condition. This ability to relax stresses of bituminous binders is defined as creep rate or *m*-value in the BBR test. From the different controlling mechanisms, to further improve the low-temperature performance of binders, different strategies

should be used for neat bitumen and CRMB. For neat bitumen, emphasizes should be put on decreasing the creep stiffness while for CRMB, efforts should be done in increasing the creep rate.

6.3.6 Summary

This subchapter investigated the low-temperature rheology and performance of binders using 4-mm DSR. Frequency sweep tests using 4-mm DSR were performed on long-term aged binders. The dynamic data from DSR were interconverted to BBR related relaxation parameters (creep stiffness and creep rate) to further determine the low-temperature PG of binders. The effects of CRM content and warm-mix additives on the thermal cracking performance of binders were also investigated. The following conclusions can be drawn:

- The obtained relaxation parameters from DSR tests can be used to determine the low-temperature PG by directly applying the BBR criterion. Two transformations were done in this process, namely converting complex modulus and phase angle master curves from the frequency domain to the shear relaxation modulus in the time domain, and converting shear response to flexural response by assuming a constant Poisson's ratio.
- The wax-based additive has adverse effects on the low-temperature performance of binders while chemical-based additive can improve the low-temperature performance. Comparing the neat bitumen with CRMB binders, the modification with CRM decreases the stiffness and increases the creep rate at low temperatures. With the increase of CRM content, the improvement of low-temperature performance is more prominent.
- In terms of the critical cracking temperature, the low-temperature PG of 70/100 based binders are creep stiffness controlled while CRMB binders are *m*-value controlled. CRM modification changes the controlling mechanism of low-temperature performance.

6.4 Fatigue performance at intermediate temperatures

6.4.1 Fatigue characterization of binders using DSR

The current Superpave performance grading (PG) specifications utilize the so-called fatigue parameter ($G^* \cdot \sin \delta$) to evaluate the binder's resistance to fatigue cracking. It is based on linear viscoelastic (LVE) properties of the RTFOT and PAV aged binder obtained from dynamic shear rheometer (DSR) at a frequency of 10 rad/s (Anderson and Kennedy 1993). Since this parameter is an indicator of dissipated energy of a material due to incremental damage propagation, it should be minimized for bitumen to ensure a good resistance to fatigue cracking. The value of the parameter $G^* \cdot \sin \delta$ of a long-term aged bitumen at intermediate temperatures should not exceed 5000 kPa. A major drawback of this fatigue parameter is that it cannot really account for real damage since it is determined within the LVE range of the binder where the nonlinear response is not captured (Bahia *et al.* 1999). Previous studies have shown that the parameter $G^* \cdot \sin \delta$ of binders has a low correlation with the fatigue performance of asphalt mixture and pavement. This is more evident for modified binders (Bahia *et al.* 2001b). Recently, another rheological parameter $G^* \cdot (\cos \delta)^2 / \sin \delta$ also based on the LVE properties from the DSR testing was proposed (Rowe *et al.* 2014). This parameter is called the Glover-Rowe (G-R) parameter, which can be calculated from frequency sweep test results at 15 °C and 0.005 rad/s. The G-R parameter was found to show a very strong correlation with binder ductility and can be used as an index for quantifying binder cracking resistance. A higher value of this parameter indicates increased brittleness or decreased ductility of binders (Anderson *et al.* 2011). A damage zone has been proposed for the G-R parameter plot in the black space. The lower limit of the damage zone is 180 kPa corresponding

to damage onset, while the high limit is 450 kPa corresponding to significant pavement cracking. While the G-R parameter correlates well with the cracking resistance of pavements with unmodified asphalt mixtures, whether it is still valid for polymer modified binders needs further research. In addition to the uncertainty of both fatigue parameters and G-R parameter for characterizing the fatigue resistance of modified binders, these two parameters have the following limitations: (1) both parameters are based on a single point measurement at one temperature and one frequency. Therefore, they provide no insights into the fatigue damage evolution and the effects of temperature and loading rates. (2) both parameters only consider the material response within the LVE range. Binders may experience much higher strain levels in the real pavement structure. In summary, these two parameters cannot account for the effect of the magnitude of traffic loading and link fatigue life to strain/stress levels.

To address the limitations of the above parameters, different test approaches and analysis methods were introduced to improve the fatigue characterization of binders. One of the introduced tests based on the same DSR measurement system to study the fatigue properties of binder is the time sweep (TS) test. Strain-controlled or stress-controlled repeated cyclic loading is applied on the binder specimen in the TS test at a fixed frequency and temperature (Bahia *et al.* 2001a). The number of load cycles to failure at a prescribed stress or strain amplitude is usually used as an index to quantify the fatigue performance of the binder. Different fatigue failure definitions, e.g., stiffness reduction or physical failure, peak in phase angle, peak in $S \times N$ (stiffness times loading cycles), dissipated energy concept, etc., are proposed for fatigue analysis (Anderson *et al.* 2001, Wang *et al.* 2016). Particularly, the dissipated energy (DE) parameters (Bonnetti *et al.* 2002) have been widely used to identify the fatigue failure point to determine the binder fatigue life. It was reported that TS test results can be effectively related to field performance under fatigue (Delgadillo and Bahia 2005). The obvious shortcomings of TS include the uncertainty of instability flow which interferes the fatigue analysis and the long testing time. Under this circumstance, the linear amplitude sweep (LAS) test was developed to accelerate the binder fatigue process. This test procedure also involves cyclic loading on a binder specimen at a constant temperature and frequency with the DSR, but with an increasing strain amplitude in a stepwise manner. Simplified viscoelastic continuum damage (S-VECD) theory was used for LAS test results analysis and prediction of binder fatigue life at any strain amplitude of interest. Similar to the TS test, the fatigue failure point needs to be clearly defined to allow for the prediction of fatigue life. The proposed thresholds of fatigue failure in the LAS test includes 35% reduction in so-called material integrity (as represented by $G^* \cdot \sin \delta$), peak in phase angle, peak in shear stress, and peak of $C \times N$ (material integrity times loading cycles) (Cao and Wang 2018). More recently, pseudo-strain energy (PSE) based failure definition and criterion have been developed and implemented into the S-VECD modelling to predict the binder fatigue life (Wang *et al.* 2015). It was found that the binder fatigue life predicted from LAS test results showed a promising correlation with the measured crack length in actual asphalt pavements of the Long-Term Pavement Preservation (LTPP) program (Hintz *et al.* 2011). Since the LAS test uses the same parallel-plate configuration with the DSR as the TS test, it also inherits similar drawbacks of the TS test, such as non-uniform shear stress distribution and instability flow at the edge (Hintz and Bahia 2013b). This study attempts to characterize the fatigue performance of long-term aged CRMB with warm-mix additives using the above fatigue test methods with the DSR equipment. Different indicators of binder fatigue performance from different methods will be compared.

The objectives of this subchapter are: (1) to compare the fatigue performance indicators from different fatigue test methods; (2) to investigate the effect of CRM content and warm-mix additives on the fatigue performance of binders.

6.4.2 Experimental design

As described above, in total nine different binders are prepared. All the fresh binder samples were first short-term aged and then subjected to the pressure aging vessel (PAV) test in a pressurized environment (2.1±0.1 MPa) at an elevated temperature of 100 °C for 20 hours. Different DSR tests were conducted on these long-term aged binder samples to compare their fatigue performance.

6.4.2.1 *Frequency sweep test*

The rheological parameters (mainly complex shear modulus and phase angle) of different binders were measured with a DSR (Anton Paar). Frequency sweep (FS) tests were performed using the 25-mm parallel plate geometry with a 1-mm gap from 0.1 to 100 rad/s at temperatures of 10, 20, 30, 40 and 50 °C following the standard test procedure. All FS tests were conducted at a constant strain level of 0.1% to ensure the LVE response of binders. The Superpave fatigue parameter $G^* \cdot \sin \delta$ and G-R parameter were extracted from the master curves established based on FS test results. Rheological parameters in the undamaged condition can also be obtained through FS tests.

6.4.2.2 *Time sweep and linear amplitude sweep test*

Both TS and LAS tests were carried out using the 8-mm parallel-plate and 2-mm gap configuration. Two replicates were tested for each testing scenario. As mentioned in previous studies, adhesive failure and unstable flow may occur during the fatigue test process under either low or high temperatures (Safaei and Castorena 2016). To measure "true" fatigue of the binder, the testing temperature for both TS and LAS tests were chosen at 20 °C, which produced the cohesive cracking with limited flow. The testing frequency was chosen as 10 Hz. Strain-controlled TS tests were conducted at strain levels of 2.5% and 5% which are able to obtain the rheological parameters in damaged condition. For the LAS test, the strain is increased linearly from 0.1 to 30% over the course of 3,100 cycles of loading for a total test time of 310 seconds. Peak shear strain and stress, along with complex shear modulus and phase angle are recorded every 1 second (10 cycles of loading).

6.4.3 Analysis method

6.4.3.1 *Dissipated energy-based modelling of TS test*

Figure 6.7 shows the three main damage stages during the fatigue damage evolution of binders (Bonnetti *et al.* 2002). In the first stage, the dissipated energy (DE) for each cycle is constant and no damage occurs. In the second stage, the material integrity of binders is deteriorated gradually and crack initiates. In the crack propagation stage, a rapid change of material response is observed, and damage is accumulated more aggressively until complete failure is reached.

Figure 6.7 Fatigue damage evolution of binders.

The two transition points separating the three damage stages can be defined using the cumulative dissipated energy ratio (DER) concept as shown in Equation (6.16).

$$\text{DER}_n = \frac{\sum_{i=1}^{n} W_i}{W_n} \tag{6.16}$$

where W_i is the DE in a given cycle, which can be calculated using the stress and strain amplitudes in the ith cycle, $\tau_{0,i}$ and $\gamma_{0,i}$ with Equation (6.17). W_n is the dissipated energy in the nth cycle.

$$W_i = \pi \tau_{0,i} \gamma_{0,i} \sin(\delta_i) \tag{6.17}$$

The DER of each cycle is calculated using Equation (6.16) and plot against the cycles of loading to monitor the fatigue evolution. For a strain-controlled TS test, the material deteriorates as the test progresses resulting in lower stress levels to maintain the constant strain amplitude. Therefore, with the increase of number of load cycles in a strain-controlled test, the DE in each cycle decreases while the DER steadily increases. For a stress-controlled TS test, a larger strain level will be observed in the specimen with the deterioration of material. In contrary to the stress-controlled TS test, there is no clear failure point for the strain-controlled test. A parameter referred as N_{p20} is proposed as a failure criterion. It is defined as the number of load cycles at which the DER deviates from the equality line by 20%. The parameter N_p in the plot corresponds to the intersection of two asymptotes. The relationship between fatigue life and the initial DE is described by a traditional power function (Equation (6.18)) (Bonnetti *et al.* 2002).

$$N_{p20} = K_2 \left(\frac{1}{W_i}\right)^{K_1} \tag{6.18}$$

where K_1 and K_2 are the fitting parameters related to the energy input of binder and testing temperature (Delgadillo and Bahia 2005). Figure 6.8 summarizes the evolution of the DER and the determination of N_{p20} in a strain-controlled TS test. Conceptually, the fatigue life of the binder defined as N_{p20} previously is represented by the cycles of loading required to undergo the crack initiation without reaching the crack propagation.
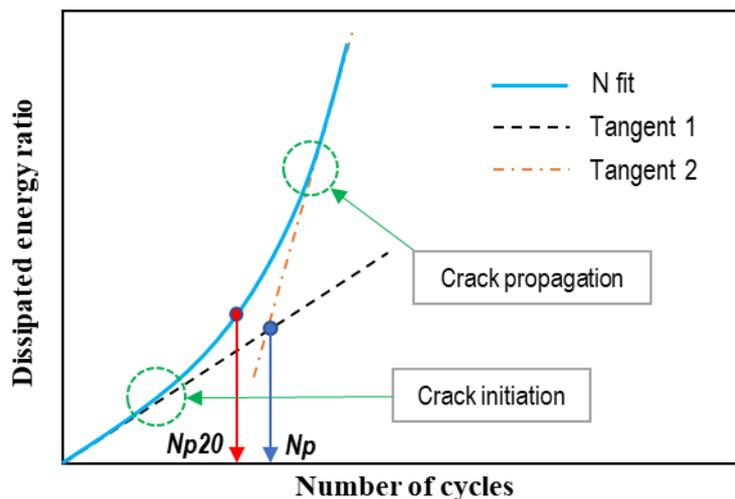
Figure 6.8 Variation in the DER for a strain-controlled TS test.

6.4.3.2 *Simplified viscoelastic continuum damage (S-VECD) modelling of LAS test*

The LAS test results are interpreted using the S-VECD theory. An integrated S-VECD fatigue characterization framework is made up of three material functions, namely LVE property, damage

characteristic curve, and fatigue failure criterion (Underwood *et al.* 2012). To quantify the damage in the VECD modelling, an internal state variable S is introduced based on Schapery's work potential theory (Schapery 1991) and can be derived from the damage evolution law:

$$\frac{dS}{dt} = \left(-\frac{\partial W^R}{\partial S}\right)^{\alpha} \tag{6.19}$$

where α is a material-dependent constant that represents the rate of damage accumulation; t is time; W^R is the pseudo-strain energy density. The power uses the macrocracking phenomenon to relate to linear viscoelastic time dependence (Underwood *et al.* 2010). For asphalt mixtures, the material parameter α is defined as $1/m + 1$, where m is the maximum slope of the relaxation modulus master curve in the log space. For asphalt binders, α is defined as $1/m$, where m is the steady-state slope of the dynamic shear modulus master curve in the log space, which is equivalent to the m parameter of the CAM model (Equation (5.1)) (Safaei *et al.* 2014). Pseudo-strain energy (PSE) is defined as (Wang and Richard Kim 2017):

$$W^R = \frac{1}{2}C(S)(\gamma^R)^2 \tag{6.20}$$

The C is the pseudo stiffness to quantify the material integrity as defined in Equation (6.21).

$$C(S) = \frac{\tau_p}{\gamma^R} \tag{6.21}$$

where τ_p is the peak stress in a given cycle; γ^R is the pseudo strain amplitude in a given cycle which can be defined as in Equation (6.22).

$$\gamma^R = \frac{1}{G_R}\left(\gamma_p \cdot |G^*|_{LVE}\right) \tag{6.22}$$

where G_R is an arbitrary reference modulus; γ_p is the strain amplitude in a given cycle; $|G^*|_{LVE}$ is the LVE dynamic shear modulus at the fatigue testing temperature and frequency. Combining the above equations, the damage at any time t (damage characteristic curve) can be derived in terms of material integrity as:

$$S(t) = \sum_{i=1}^{N}\left[\frac{1}{2}(\gamma^R)^2(C_{i-1} - C_i)\right]^{\frac{\alpha}{\alpha+1}} \cdot (t_i - t_{i-1})^{\frac{1}{1+\alpha}} \tag{6.23}$$

Where N is the cycles of loading and i refers to the cycle number. Since the relationship between $C(S)$ and S is independent of loading history, the S-VECD model is capable of back-calculating fatigue life under any loading condition of interest (e.g., strain level). To allow for fatigue life predictions, a power law model is fitted to the damage characteristic curve (Equation (6.24)) (Hintz *et al.* 2011).

$$C(S) = 1 - C_1 \cdot S^{C_2} \tag{6.24}$$

where C_1 and C_2 are model fitting parameters. Combining the above equations, the relationship between fatigue life N_f and strain amplitude γ_p can be derived as (Wang *et al.* 2015):

$$N_f = \frac{f \cdot 2^{\alpha} \cdot S_f^{1-\alpha C_2+\alpha}}{(1 - \alpha C_2 + \alpha)(C_1 C_2)^{\alpha}\left(\gamma_p \cdot |G^*|_{LVE}\right)^{2\alpha}} \tag{6.25}$$

where S_f is the damage at failure point; f is the loading frequency.

6.4.4 Superpave fatigue parameter and G-R parameter

Complex shear moduli and phase angles of different binders at various temperatures and frequencies were obtained from the frequency sweep tests. The values of the Superpave fatigue parameter and G-R parameter were calculated for different binders and shown in Figure 6.9 and Figure 6.10, respectively.
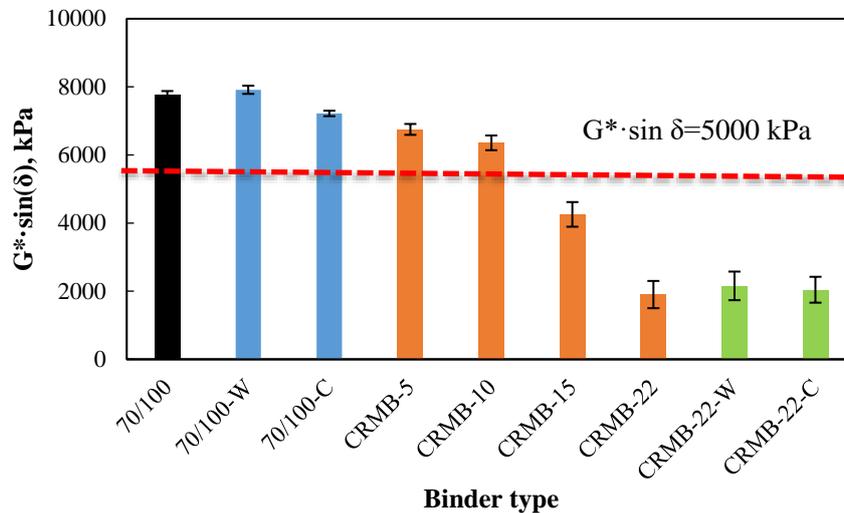
Figure 6.9 Superpave fatigue parameters of different binders (temperature=20 °C, frequency=10 rad/s).

A lower value of $G^* \cdot \sin \delta$ is preferred to ensure better fatigue performance based on the Superpave specification. It can be seen from Figure 6.9 that two types of warm-mix additives have different effects on the fatigue parameter of both neat bitumen and CRMB. Wax-based additive is detrimental to the fatigue resistance of the binder while the chemical-based additive improves fatigue resistance. It is obvious that CRMB binders possess higher fatigue resistance than neat bitumen. With the increase of CRM content, the G*·sin δ decreases, indicating an increase in binder elasticity and fatigue resistance at intermediate temperatures. However, only CRMB binders with a CRM content higher than 10% in this study meet the G*·sin δ requirement of not exceeding 5000 kPa at the PAV-aged condition and this particular temperature.
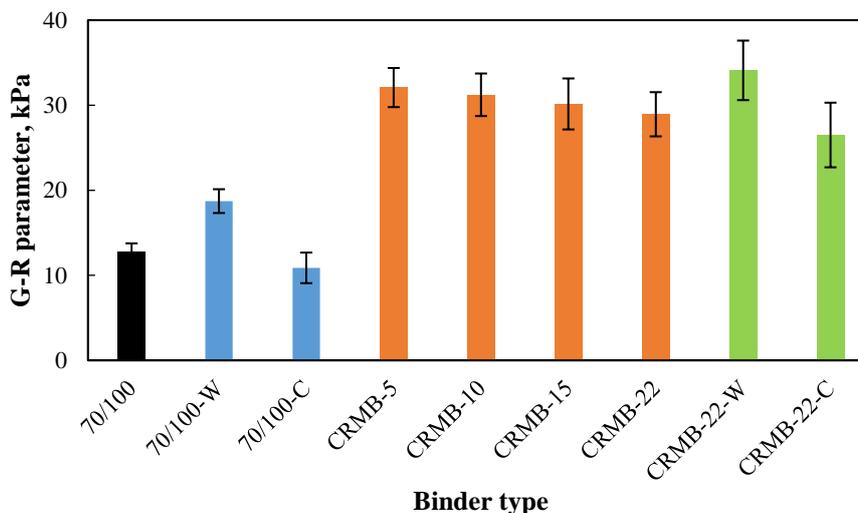
Figure 6.10 G-R parameters of different binders (temperature=15 °C, frequency=0.005 rad/s).

In terms of the G-R parameter in Figure 6.10, similar to the results of the fatigue parameter, warm-mix additives have opposite effects on the binder. The addition of wax-based additive makes the binder more brittle (higher stiffness/lower phase angle) while chemical-based additive has a softening effect on the binder. However, the modification with CRM increases the value of the G-R parameter of the binder, indicating a more brittle behavior. With the increase of CRM content, the ductility of the binder slightly increases as reflected by the decreased G-R parameter. If considering a G-R parameter value of 180 kPa as the point of damage onset, all the binders tested are still at the undamaged condition.

Based on the above results, the Superpave fatigue parameter and G-R parameter provide inconsistent findings on the fatigue performance of the binder. As mentioned before, both parameters are based on the point values of complex shear modulus and phase angle at a certain temperature and frequency under a low strain loading condition. Therefore, fatigue damage evolutions of a binder under large-strain nonlinear range cannot be captured. TS tests and LAS tests were further conducted to investigate the fatigue performance of different binders.

6.4.5 Time sweep test

6.4.5.1 *DER curve*

The TS test was designed to quantify the binder fatigue resistance by monitoring the deterioration of the material integrity (usually modulus) under repeated loading. Figure 6.11 presents a typical material response during the strain-controlled TS test of the neat bitumen 70/100. The other binders also showed similar trends thereof omitted here. It is obvious that the complex modulus of the binder deteriorates faster at the high strain level of 5% than 2.5%, resulting in a shorter fatigue life. The simplest fatigue failure definition for TS tests is the point corresponding to the 50% loss in stiffness. The red dashed line in Figure 6.11 represents the approximate 50% reduction of the initial complex modulus of the neat bitumen. The corresponding loading cycles of the two crossover points are the fatigue life values at the two strain levels. However, this fatigue failure definition has been criticized since it is arbitrary and lacks theoretical verification (Wang *et al.* 2016). Dissipated energy-based parameters were proposed to be more fundamentally related to fatigue failure. The DER approach was adopted to evaluate the fatigue property of binders and derive the fatigue law based on the TS results.
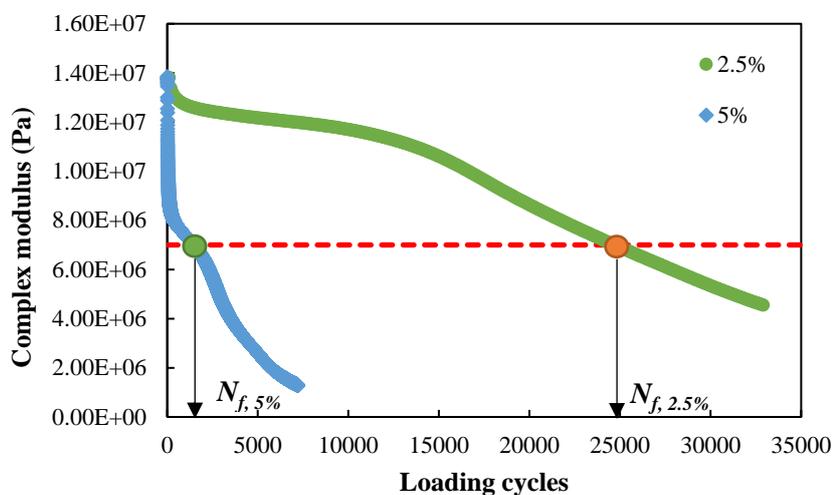
Figure 6.11 Complex modulus evolution of neat bitumen 70/100 in the strain-controlled TS fatigue tests.

Figure 6.12 shows the DER curves of different binders with the progress of loading cycles at the strain level of 2.5%. At the initial stage, all the binders display a linear increase of DER values with the increase of loading cycles. This stage is believed to be the no-damage stage as the dissipated energy contributes completely to the viscoelastic damping without any damage. As the cyclic loading progresses, the trend line of DER versus number of cycles deviates from the initial linear slope. The deviation point is regarded as the crack initiation point. After more damage cumulated as the testing carries on, the DER value will increase more rapidly, and the crack propagation point will be reached. In terms of the modification of CRM, it can be seen from Figure 6.12a that CRMB binders show a wide range of results. Compared to the neat bitumen, a delayed crack initiation can be observed for the CRMB binders from Figure 6.12a. For neat bitumen and CRMB binders with relatively low CRM content, the slopes of the DER curves increase rapidly. The slope deviation from linearity was less pronounced for the CRMB-15 and CRMB-22 binders, indicating significant improvement in fatigue resistance. With regard to warm-mix additives, it seems that the wax-based additive causes earlier crack initiation compared to the neat bitumen while the addition of chemical-based additive delays the crack initiation as shown in Figure 6.12b. However, the DER curves are overlapping at the later stage. Therefore, the exact fatigue life of each binder needs to be further determined by modeling the test results. In contrast with the results for the neat bitumen, both types of warm-mix additives improve the fatigue resistance of CRMB-22 as shown in Figure 6.12c.
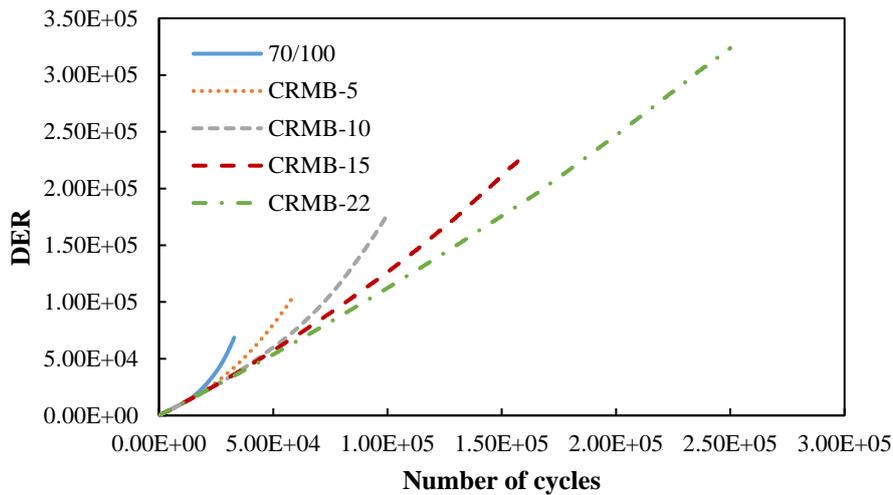
(a)
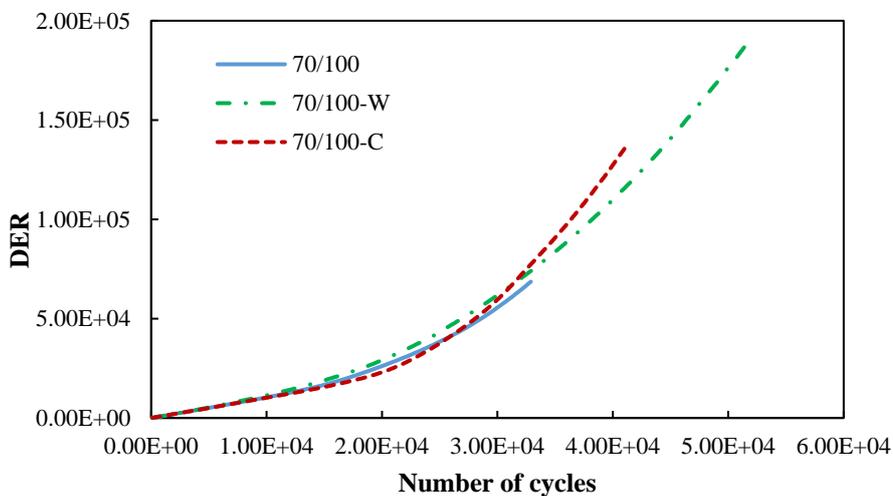
(b)
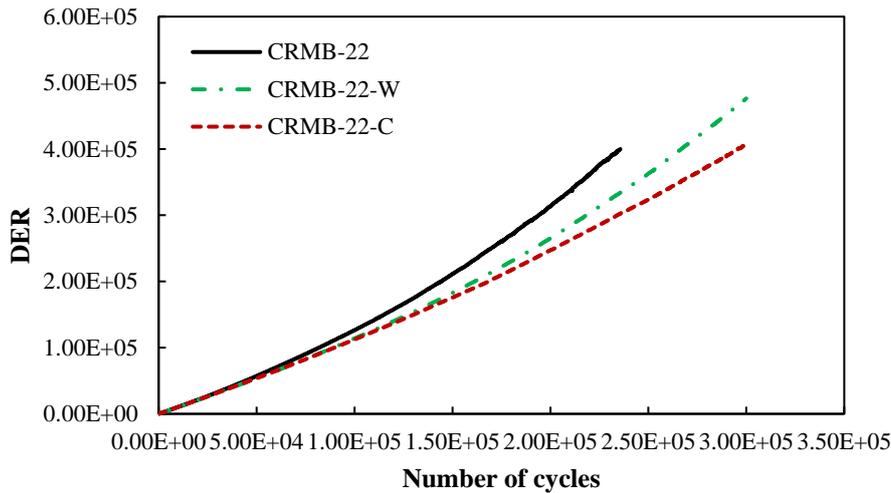
(c)

Figure 6.12 Plots of DER versus number of load cycles from strain-controlled TS tests at a strain level of 2.5%: (a) CRMB with different CRM contents; (b) base bitumen with warm-mix additives; (c) CRMB with warm-mix additives.

6.4.5.2 *Determination of fatigue life*

To determine the binder fatigue life N_{p20}, the following model was used to fit the curve of DER versus number of load cycles (Bonnetti *et al.* 2002).

$$N = N_c + b_1(R - R_c) + T(b_2 - b_1)\ln\{1 + e^{[(R-R_c)/T]}\} \qquad (6.26)$$

where R represents DER; N_c and R_c are the model fitting parameters, representing the number of load cycles and dissipated energy ratio respectively; b_1 and b_2 are respectively the slopes of the lower asymptote and upper asymptote of the curve of N versus R; and T is the shape parameter. The solver function in Microsoft Excel was adopted to compute the values of the model parameters using the least-square method.
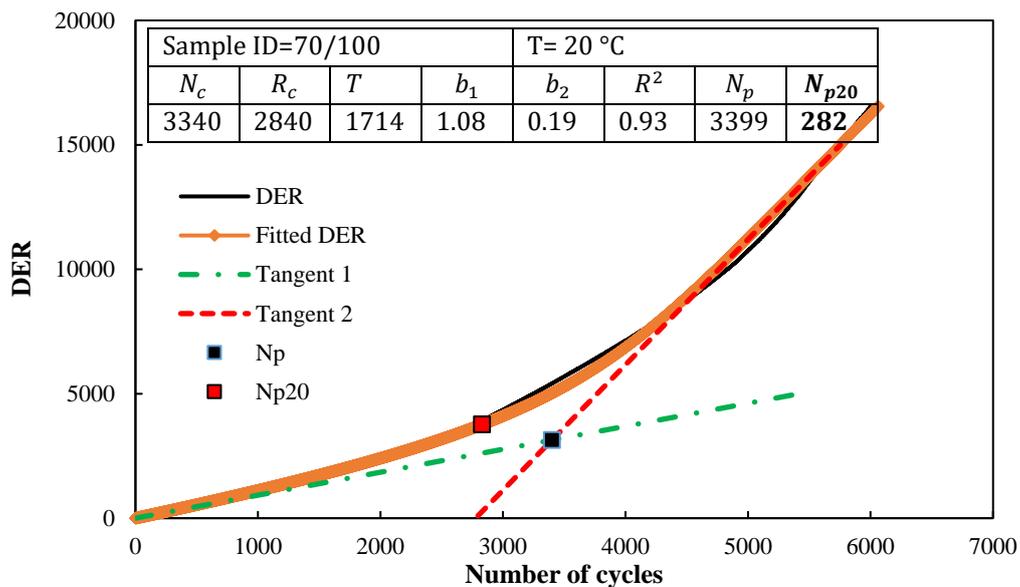
Figure 6.13 Modeling of the relationship between DER and number of cycles of neat bitumen at the strain level of 5%.

Figure 6.13 shows an example of the calculation of the fatigue life N_{p20} of the neat bitumen. Similar procedures were applied to the other binders. For neat bitumen 70/100, the fatigue life N_{p20} at a strain level of 5% is 2829 as summarized in Figure 6.13. To obtain the fatigue relationship in Equation (6.18), at least two levels of energy input need to be applied. This was achieved by conducting the TS tests at two different strain levels, respectively 2.5% and 5%. The determined fatigue life N_{p20} and fatigue model parameters W_i, K_1 and K_2 of all the tested binders are summarized in Table 6.5.

It can be seen from Table 6.5 that the initial energy input W_0 has a negative correlation with the fatigue life N_{p20}. Samples with a higher initial energy level have a shorter fatigue life. Measured fatigue life and related model parameters of different binders summarized in Table 6.5 verified the effects of modifiers on the fatigue performance of base bitumen found from the DER evolution curves. The modification effect on the fatigue properties of base bitumen depends on the modifier's peculiar characteristics and the interaction between the modifier and bitumen. The addition of wax-based additive decreases the (strain controlled) fatigue life of the base bitumen. The wax components form a crystallized structure at 20 °C within the bitumen matrix, which makes the binder stiffer, resulting in higher stresses at a certain strain level, and vulnerable to fatigue damage. The chemical-based additive improves the fatigue resistance of the base bitumen due to the softening effect. The CRM modification significantly prolongs the fatigue life of the base bitumen. The resistance to fatigue damage improves with higher CRM content in the strain-controlled test. Rubber particles are swollen by absorbing aromatic oils from the bitumen during the preparation stage. The interaction between CRM and bitumen results in a three-dimensional polymer network, which prevents or delays the formation of microcracks under fatigue loading. Unlike for the neat bitumen, both additives contribute to the improvement of the fatigue performance of CRMB-22 binder. A possible explanation could be that the additives promote the interactions between bitumen and CRM (Yu *et al.* 2016).

Table 6.5 Fatigue life and model parameters from strain-controlled TS tests (20 °C, 10 Hz).

Sample code	Strain level	W_0 (Pa)	N_{p20}	K_1	K_2
70/100	2.5	2.05E+04	*1.90E+04*	4.57E+17	1.74E-03
	5.0	2.18E+04	2.83E+03		
70/100-W	2.5	2.29E+04	*1.26E+04*	1.86E+07	3.18E-04
	5.0	2.88E+04	1.96E+03		
70/100-C	2.5	2.12E+04	*2.17E+04*	3.36E+12	9.35E-04
	5.0	2.34E+04	3.07E+03		
CRMB-5	2.5	1.35E+04	*3.43E+04*	5.55E+21	2.93E-03
	5.0	1.43E+04	3.93E+03		
CRMB-10	2.5	1.16E+04	*5.18E+04*	3.17E+10	1.15E-03
	5.0	1.36E+04	5.35E+03		
CRMB-15	2.5	8.93E+03	*8.63E+04*	2.05E+08	8.70E-04
	5.0	1.15E+04	9.25E+03		
CRMB-22	2.5	6.54E+03	*1.15E+05*	1.72E+08	1.12E-03
	5.0	8.51E+03	1.27E+04		
CRMB-22-W	2.5	4.57E+03	*1.45E+05*	7.17E+06	8.54E-04
	5.0	7.12E+03	1.64E+04		
CRMB-22-C	2.5	3.26E+03	*1.81E+05*	3.86E+06	9.38E-04
	5.0	5.63E+03	1.96E+04		

6.4.6 LAS test

6.4.6.1 *Linear viscoelastic complex modulus master curves*

To obtain the material properties of the binder in the undamaged state, FS tests were performed. Figure 6.14 shows the complex shear modulus $|G^*|_{LVE}$ master curves of different binders at the reference temperature of 20 °C.
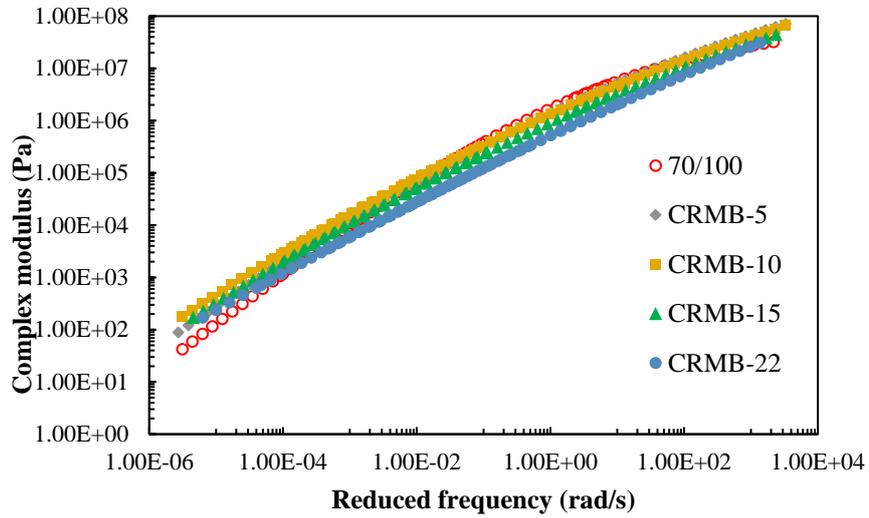
(a)
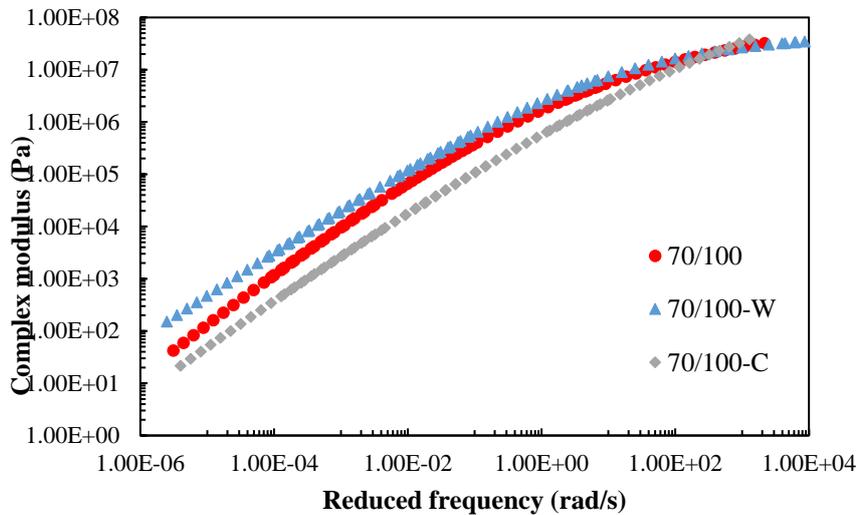
(b)
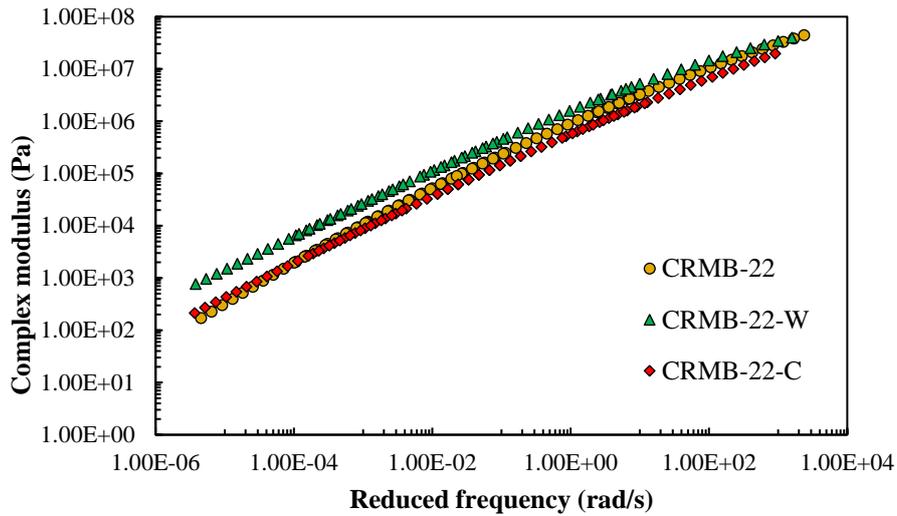
(c)

Figure 6.14 Complex shear modulus master curves of binders at 20 °C: (a) CRMB with different CRM contents; (b) base bitumen with warm-mix additives; (c) CRMB with warm-mix additives.

In general, CRMB binders have a higher complex shear modulus than neat bitumen in the low-frequency range, while they have a lower complex shear modulus than the neat bitumen in the high-frequency range at the fatigue testing temperature of 20 °C. This can be explained by the nature of rubber which behaves as an elastic material with a modulus higher than bitumen at high temperatures and lower than bitumen at lower temperatures. It can be seen from Figure 6.14a that CRMB-22 has the lowest complex modulus at a frequency of around 62.8 rad/s (10 Hz). With respect to warm-mix additives, the wax-based additive has a consistent stiffening effect on both neat bitumen and CRMB binder, while the chemical-based additive decreases the complex modulus of both neat bitumen and CRMB binder. The reason for this has been explained before by the nature of the additives.

6.4.6.2 *Stress-strain response of different binders*

LAS tests were carried out to evaluate the fatigue damage tolerance of binders and were further analyzed using the S-VECD model. The apparent shear stress-strain curves of different binders from LAS test results are plotted in Figure 6.15.
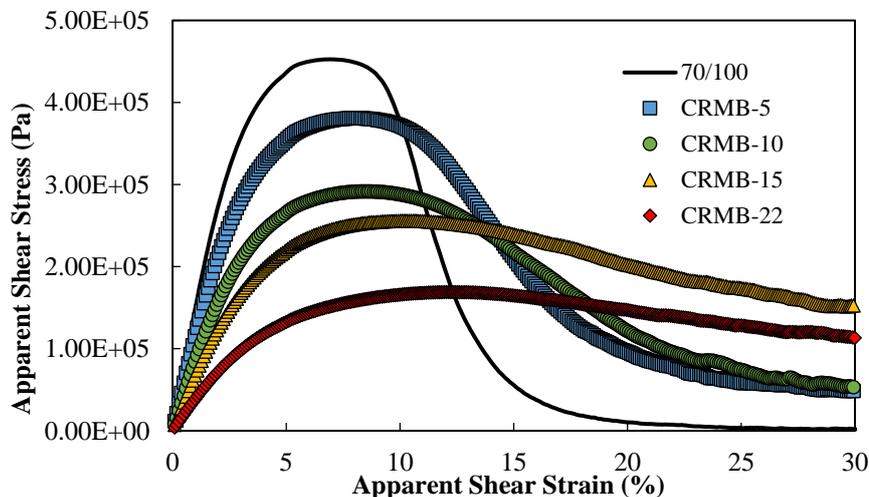
(a)
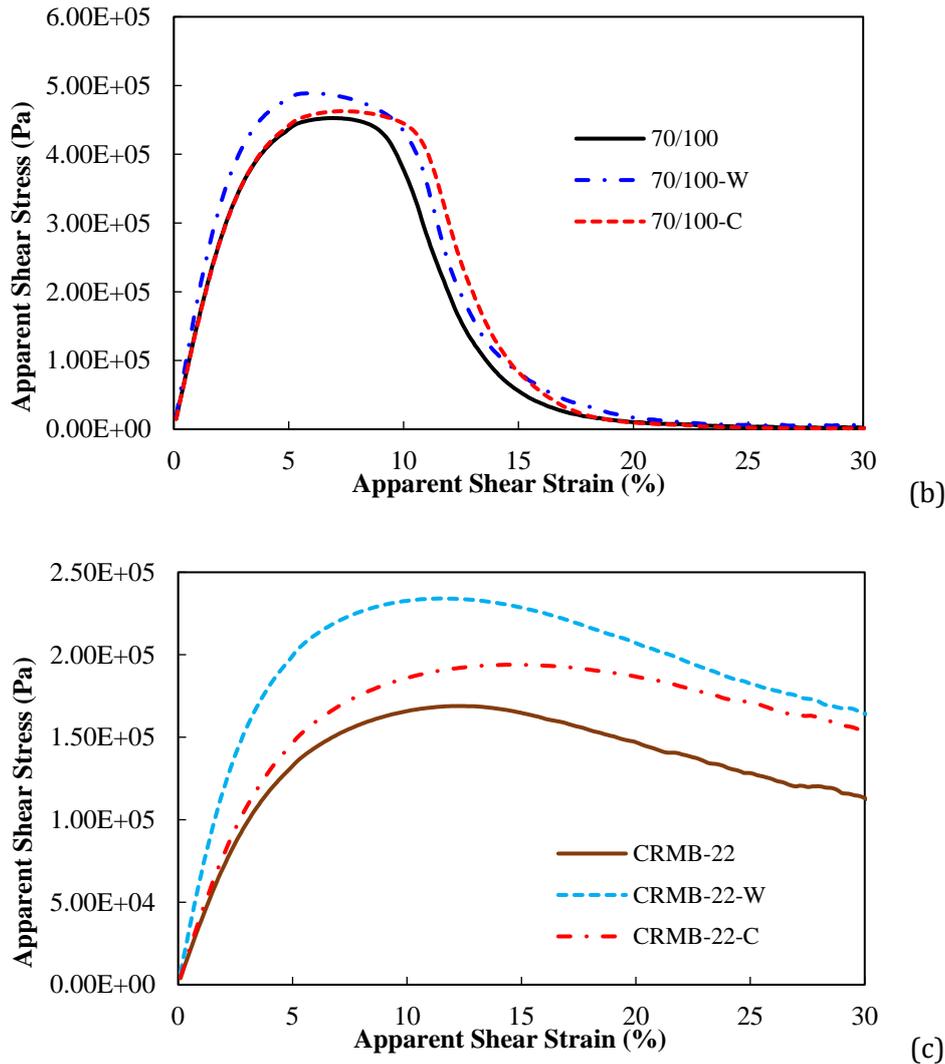
Figure 6.15 Apparent stress versus apparent strain from LAS tests (strain rate=0.1%/s): (a) CRMB with different CRM contents; (b) base bitumen with warm-mix additives; (c) CRMB with warm-mix additives.

In the initial stage, the shear stress increases linearly with the increase of loading strain. Further increasing the strain amplitude slows down the increase of the shear stress. This is the moment where binders enter the nonlinear regions. Binders reach the peak shear stress at different strain amplitudes. After the peak, the shear stress continuously decreases when further increasing the strain level, indicating significant damage has been induced in the material. It can be seen from Figure 6.15a that CRMB binders with a higher CRM content reach the stress peak at a larger strain amplitude. This indicates that CRMB binders with higher CRM contents exhibit higher damage resistance to shear loading under certain stress levels (e.g., lower than the peak stress level of CRMB-22). The addition of warm mix additives to neat bitumen changes the strain level at which the peak stress occurs. When reaching the peak shear stress, the corresponding strain for 70/100 is smaller than for 70/100-C, while larger than for 70/100-W. Both additives increase the value of the peak shear stress and the corresponding strain for CRMB-22.

6.4.6.3 *Damage characteristic curves*

The stress-strain curves of different binders were further analyzed with the S-VECD model. The damage characteristic curves (C versus S in Equation (6.24)) of different binders are shown in Figure 6.16.

(a)

(b)

(c)
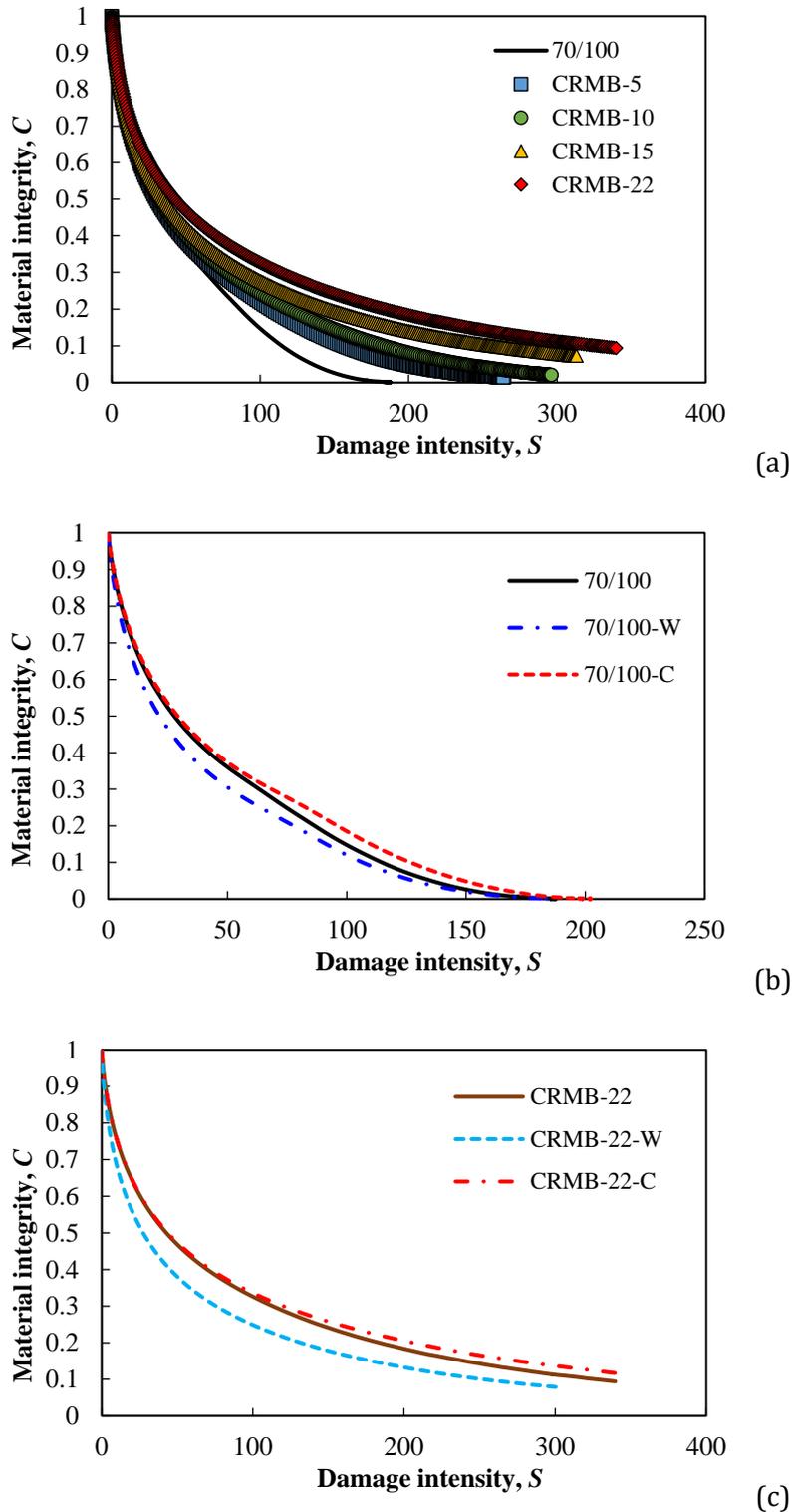
Figure 6.16 Damage characteristic curves of different binders: (a) CRMB with different CRM contents; (b) base bitumen with warm-mix additives; (c) CRMB with warm-mix additives.

Different binders show different damage evolution trends related to the resistance to fatigue damage. By fitting the damage characteristic curves using Equation (6.24), the material integrity of the binder can be determined at any damage intensity of interest. Taking Figure 6.16a as an example, at a particular damage intensity, CRMB binders with higher CRM content display higher material integrity, indicating a better fatigue performance. From Figure 6.16a and b, the addition of warm-mix additives influences the damage evolution of both neat and CRMB binders in a similar way. However, the damage characteristic curves cannot tell the whole story about the binder fatigue performance. As mentioned before, the S-VECD fatigue characterization includes three material functions, namely the linear viscoelastic properties, damage evolution characteristics and failure criterion. It is inadequate to determine the final fatigue performance merely based on one or two material properties.

6.4.7 Fatigue performance prediction

Fatigue failure point needs to be clearly defined to accurately predict the binder fatigue performance. In addition, a failure criterion needs to be proposed to enable the prediction when the fatigue failure occurs under loading conditions (of interest) that are different from the testing loading conditions.

The proposed definitions of fatigue failure in the LAS test include peak in shear stress, peak in phase angle, peak of $C \times N$ (material integrity times loading cycles), and maximum stored pseudo-strain energy (PSE). It was reported and also found in this study that the variation in phase angle during LAS test in the failure region is minimal, especially for the modified binders. This makes the identification of a fatigue failure point difficult in some cases. In addition, the peak of $C \times N$ defined failure point is always overlapped with the peak stress defined point because $C \times N$ is mathematically relying only on the peak shear stress for a given LAS test condition. Furthermore, the implementation of the failure criterion based on PSE variables requires conducting several LAS tests with different rates of strain amplitude increase (Wang *et al.* 2015). Therefore, for practical and efficient reasons, the current LAS analysis protocol with peak shear stress as the failure point was still used for the fatigue characterization. The damage intensity at the failure point S_f is further calculated as

$$S_f = \left(\frac{1 - C_f}{C_1} \right)^{1/C_2} \tag{6.27}$$

where C_f is the C value at failure, corresponding to the C value when reaching the peak stress in this case. Through a combination of Equations (6.25) and (6.27), the fatigue criterion which describes the relationship between fatigue life N_f and strain amplitude γ_p can be derived as

$$N_f = A\left(\gamma_p\right)^B \tag{6.28}$$

where A is the model parameter defined in Equation (6.29) with $B = -2\alpha$.

$$A = \frac{f \cdot 2^\alpha \cdot S_f{}^k}{k(C_1 C_2)^\alpha (|G^*|_{LVE})^{2\alpha}} \tag{6.29}$$

where $k = 1 - \alpha C_2 + \alpha$; f is the loading frequency.

With the determined LVE property, damage characteristic curve and fatigue failure criterion, the values of fatigue life and model parameters from LAS tests for different binders are determined (Table 6.6). Specifically, fatigue life at two strain levels 2.5% and 5% was predicted. It can be found that CRM modification significantly increases binder fatigue life. Warm-mix additives affect the

fatigue life of the base bitumen differently compared to CRMB binder. Both additives improve the fatigue performance of CRMB binder. A possible explanation could be that warm-mix additives enhance the interaction between bitumen and CRM, which makes the binder more resistant to fatigue damage. However, wax-based additive significantly decreases the fatigue life of the base bitumen.

Table 6.6 Fatigue life and model parameters from LAS tests.

Sample code	*Parameter A*	*Parameter B*	N_f (@2.5%)	N_f (@5%)
70/100	1.576E+05	-3.285	7.77E+03	7.97E+02
70/100-W	1.464E+05	-3.555	5.63E+03	4.79E+02
70/100-C	2.005E+05	-3.240	1.03E+04	1.09E+03
CRMB-5	5.093E+05	-3.485	2.09E+04	1.87E+03
CRMB-10	6.361E+05	-3.664	2.22E+04	1.75E+03
CRMB-15	1.627E+06	-3.468	6.78E+04	6.12E+03
CRMB-22	1.991E+06	-3.302	9.66E+04	9.80E+03
CRMB-22-W	3.681E+06	-3.631	1.32E+05	1.07E+04
CRMB-22-C	3.843E+06	-3.344	1.80E+05	1.77E+04

6.4.8 Fatigue cracking in binders under dynamic shear loading

Above results have demonstrated that CRM and warm-mix additives affect the fatigue resistance of binders in different ways. This is due to the different microstructural compositions of binders and their viscoelastic characteristics. Figure 6.17 shows the formation of fatigue cracks in the binder sample under dynamic shear loading by using a DSR device. Because of the non-uniform shear stress distribution within the circular binder sample under the applied torque (Figure 6.17a), circumferential hairline cracks initiate at the periphery of the sample and then propagate towards the center of the sample. Figure 6.17b shows a typical cracking morphology of the binder sample on the parallel plate with an annular crack zone and a circular uncrack zone, which is adapted from (Zhang and Gao 2019). A small area in the crack zone was selected as the representative area element to analyze how the microstructures of different binders influence the crack formation. For binders modified with CRM, Figure 6.17c shows a swollen rubber particle embedded in the bitumen matrix with a multilayer structure due to the sequential diffusion process of bitumen into rubber (Wang *et al.* 2019b). The formed gel-like layers have transitional mechanical properties from bitumen to rubber, which means the mechanical property of the outer layer of the swollen rubber resembles the surrounding bitumen. In addition, previous studies have shown that the swollen rubber is softer than bitumen at the intermediate temperature of 20 °C (Wang *et al.* 2020b). When the fatigue cracks initiated in the stiff bitumen phase start to propagate, they will encounter the swollen rubber particle. Due to the resemblance between bitumen and the outer layer of the rubber, microcracks will propagate into the rubber. However, because of the polymer network inside the rubber gel, the crack propagation will be delayed. At a larger scale, swollen rubber particles will form a three-dimensional network which can reinforce the binder to have a higher resistance to cracking. This is the reason why CRMB binders have better fatigue performance than neat bitumen. In terms of the neat bitumen modified with wax-based additive, the wax will crystallize at the testing temperature of 20 °C and become very stiff. Stress concentration may occur at the interface between bitumen and wax. When the microcracks meet the wax structure, instead of propagating into the structure, they can only develop into other directions within the bitumen (Figure 6.17d), which accelerates the crack formation process.

Therefore, binder 70/100-W has a lower cracking resistance than the neat bitumen. With respect to the neat bitumen modified with chemical-based additive, the softening effect is believed to be the main reason for improved fatigue resistance. As for the CRMB-22 with wax-based additive, the enhanced interaction between rubber and bitumen due to the existence of wax could be a possible explanation for the improved fatigue performance (Yu *et al.* 2016).
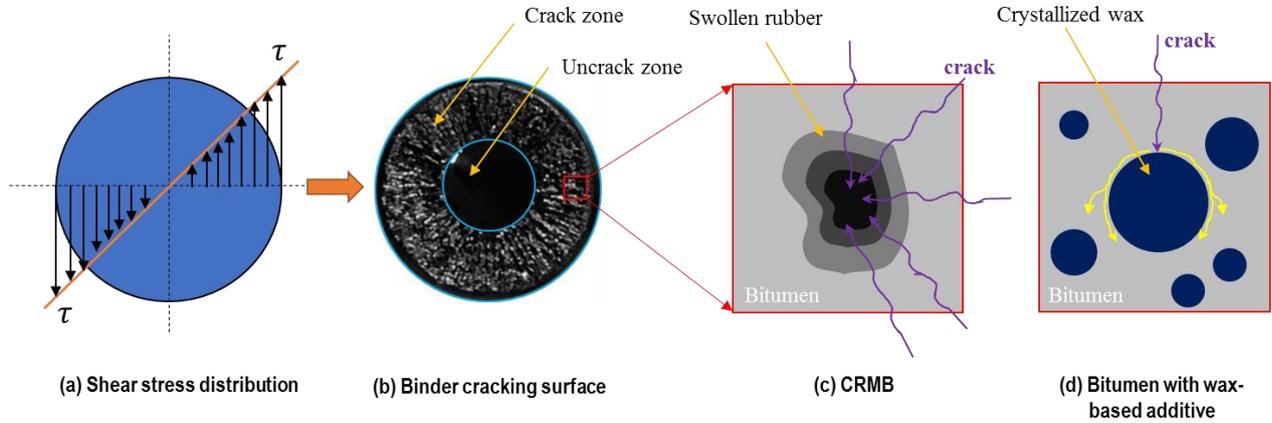
Figure 6.17 Fatigue cracking in binders under dynamic shear loading.

6.4.9 Comparison of binder fatigue parameters

An important objective of this study was to compare the fatigue performance indicators from different fatigue test methods. Figure 6.18 compares the TS measured fatigue life and LAS predicted fatigue life for different binders. There is a good correlation between these two fatigue life values at both strain levels. Generally, for each studied binder, the TS measured fatigue life is longer than the LAS predicted fatigue life at both strain levels. Apparently, this difference in fatigue life of the two methods is related to the different loading mode and rate which affect the fatigue damage accumulation of the binders.
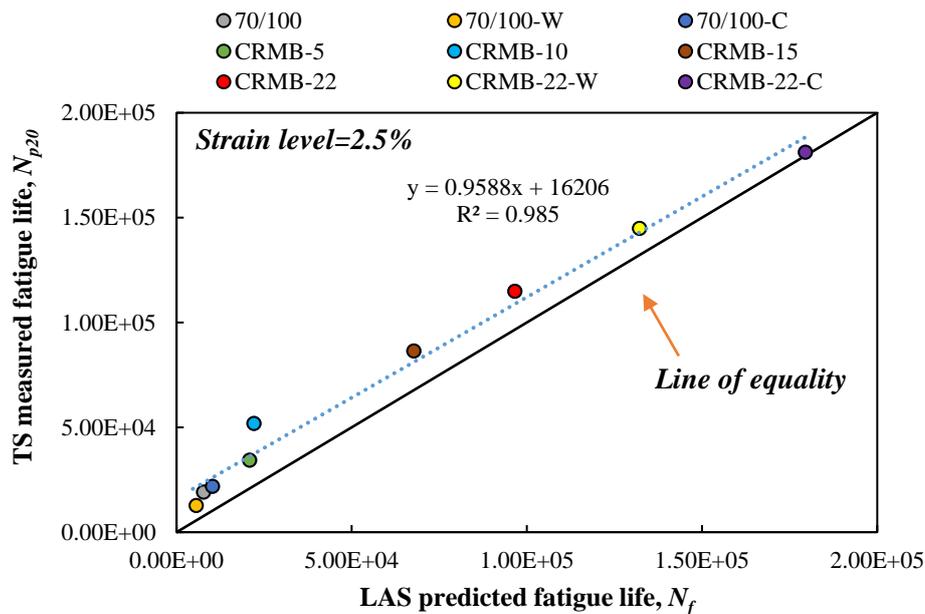
(a)
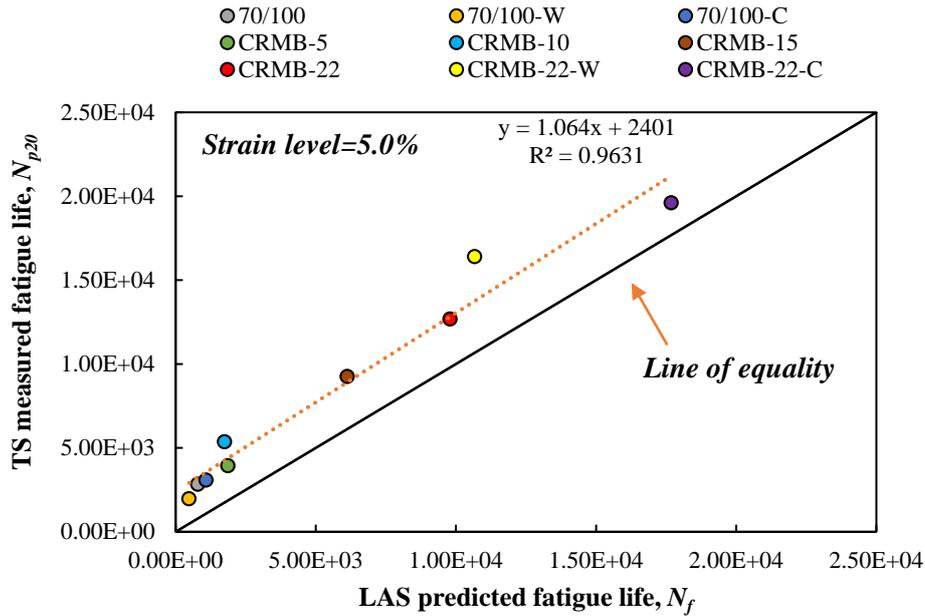
(b)

Figure 6.18 Comparison between TS measured fatigue life and LAS predicted fatigue life: (a) at the strain level of 2.5%; (b) at the strain level of 5.0%.

Table 6.7 summarizes the values of the Superpave fatigue parameter, G-R parameter and fatigue life at the strain level of 2.5% from both TS and LAS tests. The relative ranking of fatigue performance of different binders is also given. A value from 1 to 9 represents the best to worst with respect to fatigue performance.

Table 6.7 Binder fatigue performance rankings based on different parameters.

Sample code	G*·sin δ		G-R parameter		N_f (@2.5%) from		N_f (@2.5%) from LAS	
	Value (kPa)	Rank	Value (kPa)	Rank	Value	Rank	Value	Rank
70/100	7777	8	12.76	2	1.90E+04	8	7.77E+03	8
70/100-W	7913	9	18.73	3	1.26E+04	9	5.63E+03	9
70/100-C	7219	7	10.87	1	2.17E+04	7	1.03E+04	7
CRMB-5	6751	6	32.08	8	3.43E+04	6	2.09E+04	6
CRMB-10	6356	5	31.23	7	5.18E+04	5	2.22E+04	5
CRMB-15	4256	4	30.15	6	8.63E+04	4	6.78E+04	4
CRMB-22	1901	1	28.94	5	1.15E+05	3	9.66E+04	3
CRMB-22-W	2156	3	34.12	9	1.45E+05	2	1.32E+05	2
CRMB-22-C	2043	2	26.58	4	1.81E+05	1	1.80E+05	1

It can be found that TS and LAS tests give the same ranking for the fatigue performance of the different binders. The Superpave fatigue parameter ranks the fatigue performance of binders in a similar sequence as TS and LAS tests except for the CRMB-22 with warm-mix additives. However, the ranking of fatigue performance from the G-R parameter is confusing and unreasonable. This is probably because the G-R parameter is a non-load associated parameter and was determined at 15 °C which is different from the fatigue testing temperature. Since TS test results of binders have been proven to have a good correlation with the mixture fatigue performance, they can be taken as the benchmark for characterizing binder fatigue performance. Based on that, the above

findings confirm that the LAS test can be used as a good surrogate for the fatigue performance characterization of CRMB-type binders at intermediate temperatures. The Superpave fatigue parameter fails to characterize the fatigue performance when the binder is incorporated with CRM and warm-mix additives. The G-R parameter is not suitable for characterizing the fatigue damage resistance of binders.

6.4.10 Summary

In this subchapter the fatigue performance of long-term aged CRMB containing warm-mix additives was investigated using different fatigue test methods. FS tests were performed to obtain the Superpave fatigue parameter and the G-R parameter, as well as the linear viscoelastic properties of binders which serve as the parameters under undamaged conditions. TS test results were analyzed using the DER concept to determine the binder fatigue life. S-VECD theory was applied in modelling the LAS test results to predict the binder fatigue life. The following conclusions can be drawn based on the test results:

- In terms of the comparison between different fatigue characterization methods, LAS test results correlate well with TS (strain-controlled) test results. Both test methods give the same ranking of fatigue life for different binders. The LAS test can be used as an alternative for the TS test to characterize the fatigue performance of CRMB-type binders at intermediate temperatures. The Superpave fatigue parameter performs well, but partly "fails" to characterize the fatigue performance for CRMB with warm-mix additives. The G-R parameter does not seem to be suitable for characterizing the fatigue damage resistance of binders.

- With respect to the effects of CRM modification and warm-mix additives, CRMB binders exhibit superior fatigue performance than the neat bitumen. With the increase of CRM content, the improvement of fatigue life is more significant. The wax-based additive adversely influences the fatigue performance of the neat bitumen while the chemical-based additive improves it. Both additives are beneficial for CRMB-22 with regards to the increase of fatigue damage resistance.

6.5 Aging of CRMB

6.5.1 Introduction

Bitumen, as a refined residue from the distillation process of crude oils, is composed of an extremely large number of different organic molecules, which makes it susceptible to the changes of environmental conditions (Apostolidis *et al.* 2017). The aging of bitumen affects nearly all critical aspects of asphalt paving materials, which makes aging a fundamentally important factor that influences the performance and durability of asphalt pavements. Aging of bitumen takes place in two stages, short-term aging during the mixing, transport and paving process, and long-term aging during the in-service period of asphalt pavement in the field (Hofko and Hospodka 2016). Short-term aging of bitumen is primarily associated with the loss of volatile components and fast oxidation at high temperatures while long-term aging is more related to progressive oxidation, steric hardening and ultraviolet radiation (Airey 2003). Among all, oxidation is regarded as the most important and best-understood aging process of bitumen.

Oxidative aging changes both chemical composition and physical properties of bitumen. Based on the polarity, bitumen can be separated into four fractions: saturates, aromatics, resins and

asphaltenes, of which asphaltenes are the most polar. Each fraction is a continuum of molecules with varying molecular sizes, aromatic contents and polarity (Lesueur 2009). More reactive molecules with high polarity are more susceptible to oxygen. The types of oxidation products, mainly sulfoxides and ketones are consistently the same for bitumen from different sources (Lu and Isacsson 2002). Therefore, the corresponding carbonyl and sulfoxide functional groups (Petersen and Glaser 2011), as characterized by infrared spectroscopy, have long been used to indicate the aging level of bitumen. During aging, the reaction of bitumen and atmospheric oxygen leads to the transformations of its generic fractions to more polar components, and increases in the number of large molecules, molecular weight and polydispersity. Specifically, part of the aromatic fraction of bitumen transforms into the resins, which in turn transforms into asphaltenes. On the other hand, the concentration of saturates does not change significantly due to their low reactivity (Lu and Isacsson 2002, Lesueur 2009). The changes of bitumen chemistry after aging significantly influence the physical and rheological characteristics of bitumen. Aging causes stiffening of bitumen with reduced molecular flow, which can be verified by the increase in viscosity and complex modulus and decrease in phase angle (Tarsi *et al.* 2018, Jing *et al.* 2019). The stiffening effect increases the permanent deformation resistance, but reduces the relaxation capacity under environmental and traffic loadings resulting in performance deterioration of asphalt pavements (Rahbar-Rastegar *et al.* 2018, Wang *et al.* 2020e).

Crumb rubber modification of bitumen has become common practice in the asphalt paving industry due to its improved physical properties and environmental benefits (Wang *et al.* 2018). For crumb rubber modified bitumen (CRMB), aging is also an inevitable process and plays a critical role in determining the in-service performance of the rubberized pavement. However, compared to neat bitumen, the aging mechanism for CRMB is much more complex because of the interaction between crumb rubber modifier (CRM) and bitumen and the unique chemical compositions of CRM. Two parallel reactions were reported during the aging process of CRMB: the aging of the bitumen phase and the degradation of included rubber particles (Liang *et al.* 2017). During the preparation of a bitumen-rubber blend, crumb rubber particles absorb the low-molecular-weight fractions of bitumen (part of the maltenes) because of the thermodynamic compatibility and swell up to several times their original sizes at elevated temperatures. When subjected to more severe interaction conditions (i.e., higher temperatures and extended time), the dissolution of rubber into bitumen takes place (Abdelrahman and Carpenter 1999, Wang *et al.* 2019b). The bitumen-rubber interaction changes not only the component fractions and microstructure of bitumen but also the nature of CRM. The absorption of maltenes and swelling of CRM particles together contributes to the stiffening of CRMB binder (Wang *et al.* 2020f). This change also definitely influences the aging mechanisms and reaction kinetics of CRMB. Moreover, the unique and complex compositions of CRM affect the ageing process of bitumen individually. CRM generally consists of rubber polymer, carbon black and various processing agents which include antioxidants/antiozonants and curing additives (sulfur, zinc oxide, stearic acid, accelerator and oil etc.). Previous studies have shown that CRM particles can release their components into bitumen in different ways given the different interaction conditions (Gawel *et al.* 2006, Ghavibazoo and Abdelrahman 2013). The component exchange between bitumen and CRM alters the aging process and physical properties of CRMB binder. The released polymeric chains from the rubber network function as retardants in bitumen during aging. They can hinder the penetration of oxygen molecules into the bitumen and reduce the oxidation rate of the bitumen phase itself. Besides, from the mechanical point of view, polymer degradation from chain scission during aging, which is detrimental to the mechanical properties of the binder, partly offset the age

hardening of bitumen components (Cortizo *et al.* 2004). It was also reported that the addition of carbon black into bitumen increases its aging resistance (Wang *et al.* 2019c). Antioxidants, which are added to protect rubber particles from oxidation, can also retard the reactive groups of bitumen and protect them against the attack of oxygen (Ouyang *et al.* 2006). In summary, the crumb rubber modification of bitumen significantly increases the complexity of aging mechanism and is expected to improve the aging resistance of bitumen.

6.5.2 Objective and approach

This subchapter aims to investigate the effects of laboratory short-term and long-term aging on the chemistry and rheology of crumb rubber modified bitumen. Fourier transform infrared spectroscopy (FTIR) and dynamic shear rheometer (DSR) were employed to detect possible changes in the chemical composition and rheological properties of binders at different aging states. FTIR was used to characterize the changes of chemical functional groups of the binder. Both frequency sweep tests and multiple stress creep and recovery tests were performed to obtain the rheological parameters of the binder in the linear viscoelastic and nonlinear viscoelastic regions. First, an alternative short-term aging procedure (oven aging) was proposed for CRMB due to the problems with the traditional aging method (i.e., rolling thin film oven test). Then, the effect of CRM concentrations on the aging performance of bitumen was examined.

6.5.3 Materials and methods

6.5.3.1 *Aging procedure*

- Standard aging procedure

Currently, the most commonly used laboratory aging methods for simulating the short-term (plant, transport and construction) aging and long-term (in-service) aging of bitumen are the rolling thin film oven (RTFO) test (ASTM D2872) and the pressure aging vessel (PAV) test (ASTM D6521), respectively (Erkens *et al.* 2016). In the RTFO aging procedure, 35 grams of bitumen sample is poured into a specifically designed glass bottle which is later placed in a circular carriage in a strictly specified oven. The conditioning temperature of the oven is maintained at 163 °C for 85 minutes. During the aging process, the bottles containing bitumen samples are rotated to allow binders to fully and uniformly coat the bottles to create a film thickness of about 1.25 mm. In addition, fresh and hot air is periodically injected into the bottles to intensify the binder aging process. In the PAV aging procedure, 50 grams of previously RTFO aged bitumen samples are collected and poured into a 140-mm diameter pan to create a film thickness of approximate 3.2 mm. The prepared samples are further aged in a pressurized environment (2.1±0.1 MPa) at an elevated temperature of 100 °C for 20 hours.

- Alternative short-term aging procedure

While the RTFO aging procedure works well for unmodified binders, it encounters problems with modified binders, especially highly viscous binders (e.g., some polymer modified bitumen and the CRMB in this study). Because of their high viscosity at the fixed temperature of 163 °C, these modified binders do not flow properly inside the bottles to fully coat the bottle and may even roll out of the bottles (Bahia *et al.* 1998). In addition, highly viscous CRMB is difficult to scrape out of the RTFO bottle after the aging process. Given these issues, an alternative thin film oven aging method was proposed in an attempt to reach a similar aging level as the standard RTFO test.

The modified oven aging procedure is based on the thin-film oven test (ASTM D1754) where the hot bitumen is placed in 140-mm diameter pans on a shelf in an oven maintained at 163 °C for specific durations. However, the differences include (a) the static shelf is used instead of a rotating shelf; (b) the weight of hot bitumen is adjusted to be only 20 grams, so the binder film thickness is approximately the same as the one in the RTFO test (~1.25 mm). Thus, the unknown factor making the modified oven aging comparable to the standard RTFO aging is the test duration. In this study, the base bitumen (Pen 70/100) was taken as the reference material since the RTFO tests were initially designed based on unmodified bitumen (Airey 2003). Bitumen Pen 70/100 samples were subjected to the modified oven aging procedure for 1 h, 2 h, 3 h and 4 h to simulate the short-term aging. After that, both modified oven-aged and RTFO-aged samples were compared by performing the FTIR and DSR tests (frequency sweep and MSCR) to determine which oven aging duration can give a comparable short-term aging effect as the standard RTFO aging procedure. Based on the results, the modified oven aging procedure was adopted to perform the short-term aging of CRMB binders. By treating the neat and CRMB binders under the same aging condition, the influence of CRM modification on the aging characteristics of binders can be compared. For the long-term aging procedure, the standard PAV test was applied to all short-term aged binders.

6.5.3.2 *Fourier transform infrared spectroscopy*

A Perkin Elmer Spectrum 100 FTIR spectrometer (PerkinElmer, Wellesley, Massachusetts) was used in the attenuated total reflectance (ATR) mode to acquire the infrared spectra for all the bitumen samples. The wavelength of the reflected beam is characteristic of each element and indicates the presence of specific chemical functional groups. Sample preparation is simple for the ATR technique. A small sample of the material was taken using a spatula and placed on the top of the ATR crystal. The FTIR spectrum was obtained in the wavelength number range from 4,000 to 600 cm^{-1} with a scanning resolution of 4 cm^{-1} averaging twenty scans for each measurement at ambient temperatures. For each type of material, five trials were performed at each aging condition for analysis. Quantitative analysis of the obtained spectra was carried out to identify the changes of functional groups of bitumen at different aging states.

The oxidation process can alter the chemical compositions of the bitumen by bonding bitumen molecular groups with atmospheric oxygen. Carbonyl compounds and sulfoxides are commonly formed during the chemical transformations caused by oxidative aging. Therefore, to quantitatively analyze the changes of specific functional groups due to the aging effects, the peak areas under the specific band were measured from valley to valley at specifically selected wavenumbers of the obtained spectrum (Lamontagne *et al.* 2001).Two aging related indices, the carbonyl index ($I_{C=O}$) and sulfoxide index ($I_{S=O}$) are defined as Equations (6.30) and (6.31). In addition, the aliphaticity index (I_{Al}) and aromaticity index (I_{Ar}) were also calculated to monitor the evolution of chemical constituents of binder during aging (Tarsi *et al.* 2018).

$$I_{C=O} = \frac{A_{1700}}{\sum A} \tag{6.30}$$

$$I_{S=O} = \frac{A_{1030}}{\sum A} \tag{6.31}$$

$$I_{Al} = \frac{A_{1376} + A_{1460}}{\sum A} \tag{6.32}$$

$$I_{Ar} = \frac{A_{1600}}{\sum A} \tag{6.33}$$

$$\sum A = A_{(2953,2862)} + A_{1700} + A_{1600} + A_{1460} + A_{1376} + A_{1030} + A_{864} + A_{814} + A_{743} + A_{724} \tag{6.34}$$

where A represents the peak area under specific waveband and $\sum A$ is the sum of the total considered peak areas.

6.5.4 Determination of the oven aging duration

Figure 6.19 shows the master curves of complex modulus and phase angle of the neat bitumen at different short-term aging conditions. The reference temperature for the master curves was chosen as 30 °C. For the oven aged bitumen, the complex modulus increases while the phase angle decreases with the extension of aging time. The increased age hardening effect of bitumen was also observed in terms of the MSCR results in Table 6.8. Both frequency sweep and MSCR test results pointed out that bitumen aged in the oven at 163 °C for 2 hours has similar rheological properties as the bitumen aged in the RTFOT. Therefore, based on the rheological parameters, the 2-hour static oven aging is comparable to the standard RTFO ageing and can be used as an alternative to RTFOT for simulating short-term aging.
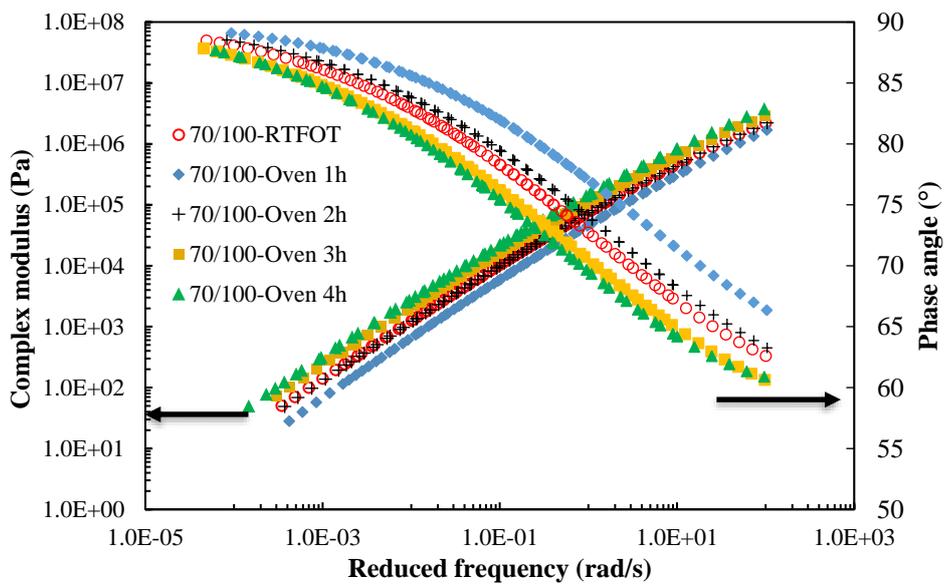
Figure 6.19 Complex modulus and phase angle master curves of the neat bitumen at different short-term aging conditions.

Table 6.8 MSCR results of the neat bitumen at different short-term aging conditions.

Aging condition	Average recovery (%)		Average J_{nr} (1/kPa)	
	0.1 kPa	3.2 kPa	0.1 kPa	3.2 kPa
RTFOT	1.40	No recovery	3.90	4.44
Oven 1h	0.09	No recovery	5.59	6.22
Oven 2h	1.55	No recovery	3.49	3.94
Oven 3h	4.74	No recovery	2.61	3.07
Oven 4h	6.75	0.29	1.86	2.04

Since mechanical tests only give averaged properties of the bitumen sample, FTIR tests were also performed to compare the oxidation products that directly related to aging. Figure 6.20 shows the comparison of carbonyl and sulfoxide indices of the neat bitumen at different short-term aging states. It is clear that the oven aging with a duration of 2 hours generated similar oxidation products as the standard RTFOT did. With the validation from both rheological and chemical properties of aged bitumen, it was decided to use the modified static oven aging for 2 hours in replacement of the standard RTFO aging procedure for all the binders.

(a)   (b)
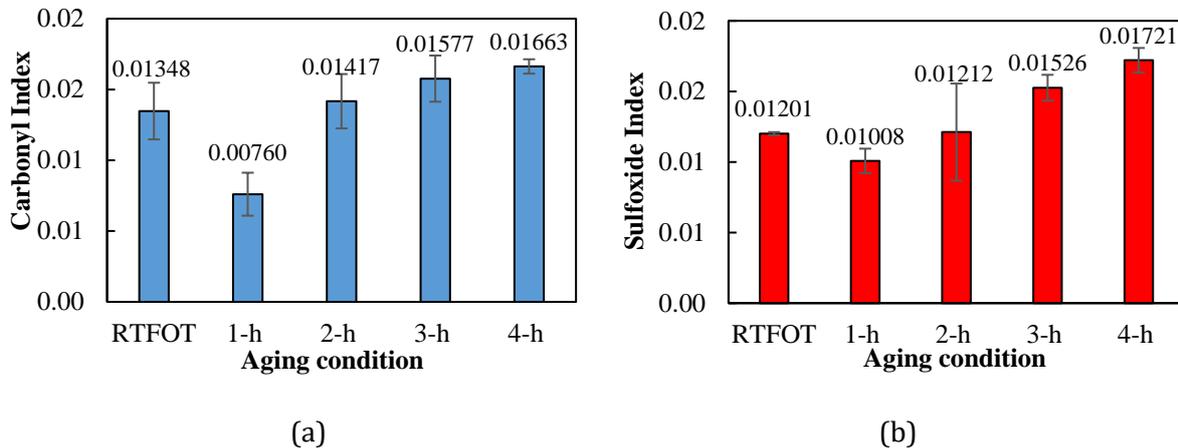
Figure 6.20 (a) Carbonyl index and (b) sulfoxide index of the neat bitumen at different short-term aging conditions.

6.5.5 FTIR analysis

Aging causes chemical composition changes in bitumen. It is worthy to mention that there are no polybutadiene peaks at 965 cm^{-1} indicating the =C-H in phase out-of-plane bending of *trans*-1,4-butadiene observed for all the CRMB binders. Figure 6.21 presents the typical FTIR spectra of base bitumen and CRMB, in which no peaks at 965 cm^{-1} were detected for CRMB. This is because the ATR mode FTIR can only detect a very thin film of the bitumen sample about 2 μm while the rubber particle size is too large to be detected (Yan *et al.* 2018).
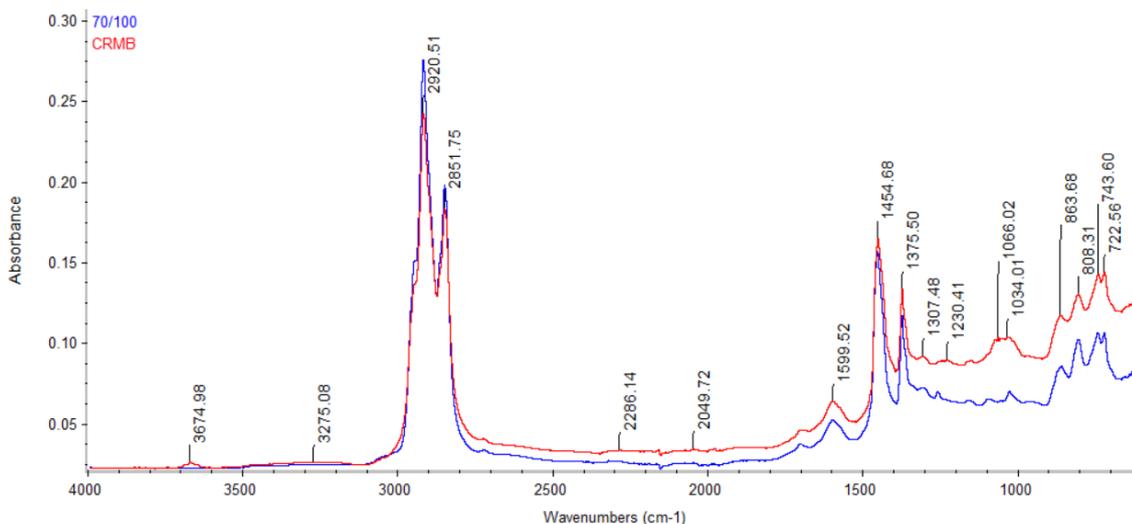
Figure 6.21 FTIR spectra of base bitumen and CRMB.

Figure 6.22 shows the aliphaticity and aromaticity indices of binders at different aging states. The aliphatic structures usually exist in the light fractions of bitumen. During the aging process, light components of bitumen volatiles and aliphatic chains form aromatic rings. The reduction of aliphalticity with aging was observed for all binders in Figure 6.22a. Due to the low reactivity of aliphatic compounds, the reduction of aliphaticity is not obvious in aging. It is also noteworthy that the aliphaticity index of unaged CRMB decreases with the increase of CRM content. This is because the rubber particles absorb the light fractions of bitumen during the interaction process. The absorption of light fractions may continue during aging, resulting in a decrease of the aliphaticity index. The aromaticity index denotes the aromatization of bitumen molecules. Two mechanisms including aromatization of perhydro aromatic rings and aromatization of alkyl substituted naphthenic rings take place during this process (Petersen 2009). The aromaticity of neat bitumen increased after aging, which confirms that the formation of aromatics is associated with an equivalent reduction of the aliphatic structures. However, this is not the case for CRMB binders. In contrast, the aromaticity of all the CRMB binders first decreased at the short-term aging stage and then increased at the long-term aging stage. This finding is also consistent with previous studies (Nivitha *et al.* 2015). This is possibly because CRM continued to interact with bitumen during the short-term aging through the absorption of aromatics and swelling (Ghavibazoo *et al.* 2015). In addition, some aromatic rings fuse to produce more asphaltenes. At the long-term aging stage, rubber polymer degradation may happen and generate more aromatic hydrocarbons through the chain scission process. In addition, the processing oil containing aromatic components together with the earlier absorbed light fractions in rubber may be released from the rubber particles into bitumen. These mechanisms contribute to the increase of aromaticity during the long-term aging stage.

(a)

(b)
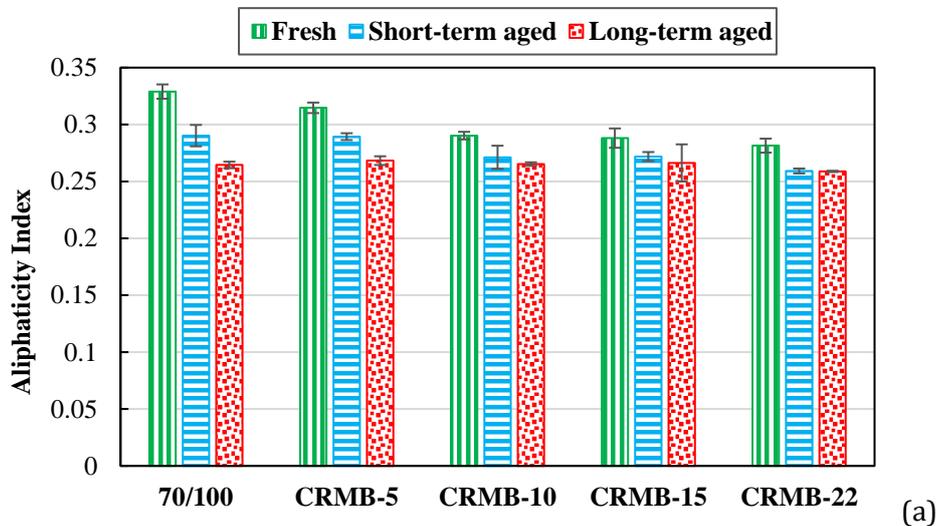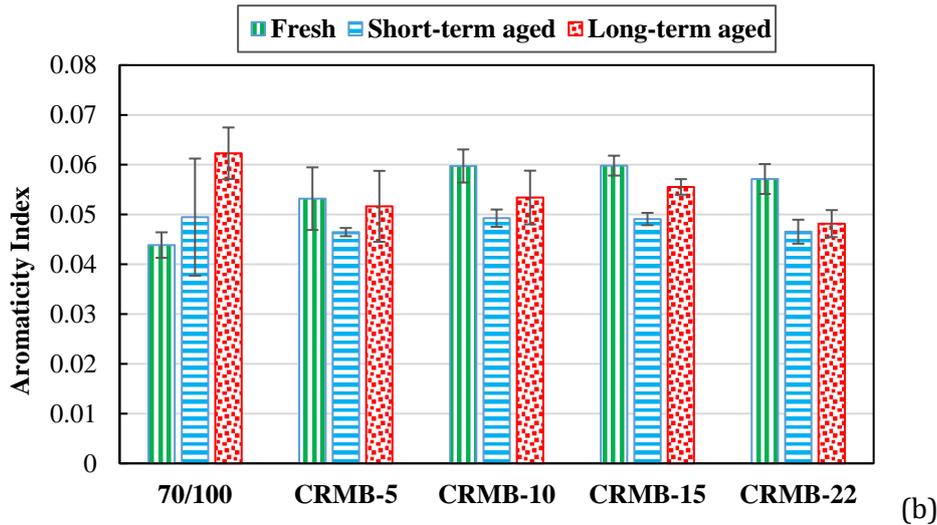
Figure 6.22 (a) Aliphaticity index and (b) aromaticity index of binders at different aging conditions.

Ketones and sulfoxides are the main oxidation products of bitumen aging. The ketone functional group, the major component of the carbonyl absorption region in FTIR, is formed primarily from the oxidation of benzyl carbons in side chains attached to highly condensed aromatic ring systems. Sulfoxides are derived from the oxidation of sulfides. Figure 6.23 shows that the values of the carbonyl and sulfoxide indices consistently increase for all binders during aging. However, when increasing the CRM content of CRMB, the increase of both carbonyl and sulfoxide functional groups become less after aging, indicating decreased bitumen oxidation. The improvement of aging resistance due to crumb rubber modification can be attributed to three mechanisms. Firstly, light fractions of bitumen are absorbed by rubber particles, which means there are less reactive bitumen molecules available to be oxidized. Besides, these early absorbed low molecular weight constituents may be released into bitumen during the aging stage, compensating for the lost components due to aging. Furthermore, the presence of antioxidants in the oily component of crumb rubber retard the oxidation process. Thirdly, polymer chains from the rubber network can also function as retardants to hinder the penetration of oxygen molecules into bitumen. Under this circumstance, polymer chains are preferably attacked by oxygen, so the reaction of polar bitumen molecules with oxygen is delayed.

(a)
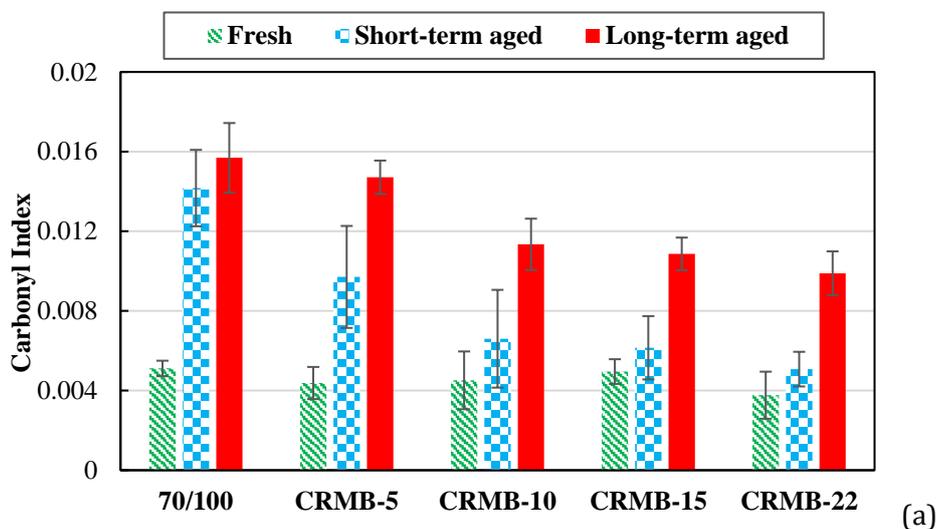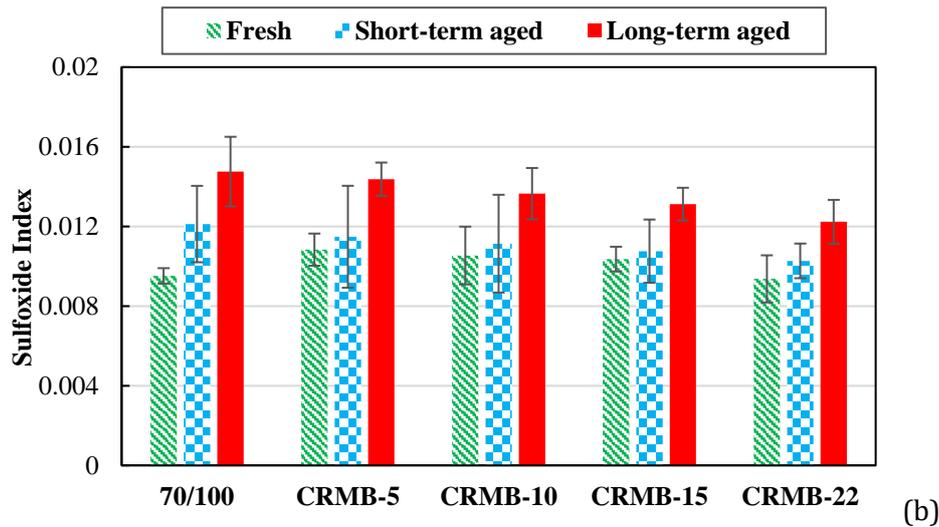
Figure 6.23 (a) Carbonyl index and (b) sulfoxide index of binders at different aging conditions.

6.5.6 Aging effects on the rheological properties of binders

6.5.6.1 *Frequency sweep test*

Aging is known to alter the rheological properties of bitumen, causing an increase in complex modulus and a decrease in phase angle at certain frequencies. Figure 6.24 shows the complex modulus and phase angle master curves of neat bitumen and CRMB with different CRM contents in both fresh and aged states based on the CAM model. Generally, with the increase of aging extent (from short- to long-term), the complex modulus master curve shifts upwards while the phase angle master curve shifts downwards, which indicates stiffer and more elastic response of bitumen after aging. The gaps between the complex modulus master curves of different aging states become smaller with the addition of CRM into bitumen. When the CRM content reaches 22%, the complex modulus master curves of fresh and aged CRMBs are almost overlapped, indicating less aging influence. The phase angle master curves of all CRMB binders show the characteristic plateau in the intermediate frequency domain. This unique feature represents the presence of polymer (rubber) in the bitumen. At high CRM contents of 15% and 22%, the phase angle master curves of CRMBs in the fresh and aged states were interlaced, which shows the complexity of the chemical structure of (aged) CRMB. It is believed the degradation of rubber polymer and the oxidation of bitumen components take place simultaneously for high-content CRMB. The softening effect to the binder from polymer degradation compensates the stiffening effect from bitumen oxidation, as a result that the mechanical properties of CRMB binders vary insignificantly after aging. Due to the inconsistency of complex modulus and phase angle over the frequency range at different aging states, it is unreasonable to define an aging index based on solely selected point values of complex modulus or phase angle at a certain frequency.
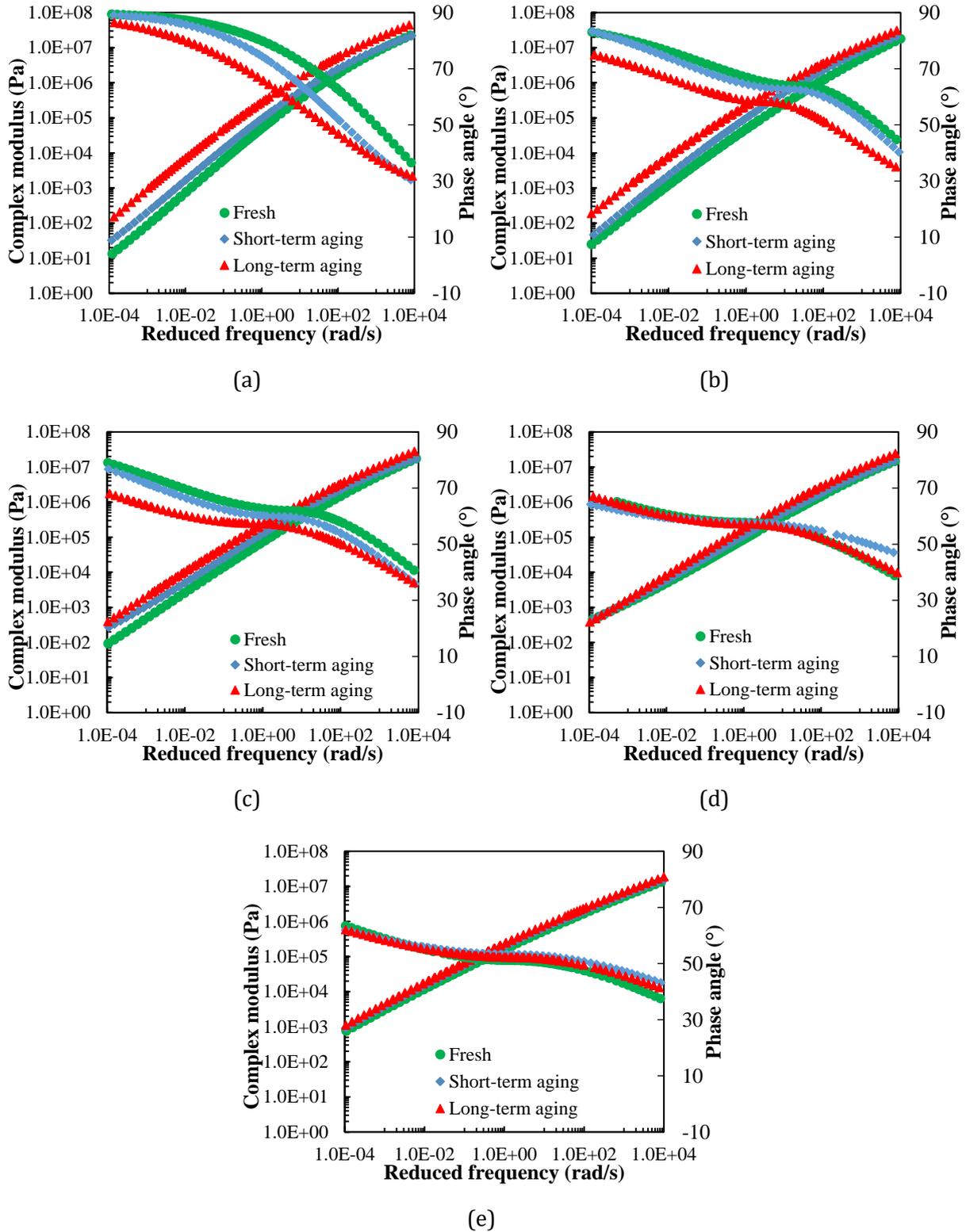
Figure 6.24 Complex modulus and phase angle master curves of (a) neat bitumen (b) CRMB-5 (c) CRMB-10 (d) CRMB-15 and (e) CRMB-22 at different aging conditions.

To further quantitatively characterize the aging effect, a series of parameters based on the rheological properties are summarized in Table 6.9. The crossover frequency and the rheological index R were captured from the CAM model. The R-index is directly proportional to the width of the relaxation spectrum and is a measure of the shear rate dependency of bitumen (Anderson *et*

al. 2011). In addition, the original Superpave rutting factor ($G^*/\sin\delta$) at the high temperature of 64 °C (corresponding to the testing temperature of MSCR) and angular frequency of 10 rad/s, as well as the G-R parameter ($G^* \cdot (\cos\delta)^2/\sin\delta$) at an intermediate temperature of 15 °C and angular frequency of 0.005 rad/s were derived from the built master curves. The G-R parameter is an indicator of the ductile behavior or brittleness, which can be used to assess the non-load associated cracking of binder (Mensching *et al.* 2015).

Table 6.9 Fitted and derived parameters from the master curves of binders at different aging states.

Sample code	Aging condition	Crossover frequency (rad/s)	R index	$G^*/\sin\delta$ (kPa)	G-R parameter (kPa)
	unaged	1844.93	1.44	1.65	0.19
70/100	short-term aged	395.51	1.36	2.85	0.74
	long-term aged	70.63	1.32	7.76	12.76
	unaged	1847.22	3.22	2.77	1.96
CRMB-5	short-term aged	488.80	3.05	3.14	6.43
	long-term aged	284.84	2.91	9.05	37.90
	unaged	580.49	3.61	4.85	8.71
CRMB-10	short-term aged	580.17	1.94	7.60	14.51
	long-term aged	580.88	1.77	13.79	48.36
	unaged	800.00	5.27	9.00	13.05
CRMB-15	short-term aged	799.52	3.67	10.23	16.82
	long-term aged	799.50	3.41	14.64	30.15
	unaged	1336.25	5.82	11.53	20.28
CRMB-22	short-term aged	1331.96	5.66	12.42	27.86
	long-term aged	1330.56	5.49	19.86	28.94

For neat bitumen and CRMB-5, aging causes a decrease of the crossover frequency while it has insignificant influence on the crossover frequencies of other CRMB binders. For each binder, the R-index decreases after aging, meaning a smaller relaxation spectrum and increased sensitivity to frequency change. The aging causes an increase of the rutting factor for each binder. The G-R parameters of all the binders show an increasing trend with aging, which means the binders become more brittle and thus vulnerable to cracking. It is noteworthy that both short-term and long-term aging results in a gradual change of the R-index of binders, while long-term aging seems to have more severe impacts on the change of rutting factors and G-R parameters than short-term aging does.

6.5.6.2 *MSCR test*

The MSCR test, which can capture the nonlinear viscoelastic properties of bitumen, was also employed to investigate the aging effect. It was found that MSCR test method is sensitive to the microstructure of polymer modified bitumen and used to determine the presence of elastic response. Therefore, it is anticipated that the results can be used to more effectively characterize the microstructural changes of CRMB at different aging conditions. The average values of MSCR

test results at 64 °C from three replicates for each binder at different aging states are summarized in Table 6.10.

Table 6.10 Summary of MSCR test results and J_{nr} based aging indices of binders at different aging states.

Sample code	Aging condition	J_{nr} (1/kPa)		Percent recovery (%)		Aging index
		0.1 kPa	3.2 kPa	0.1 kPa	3.2 kPa	
70/100	unaged	7.568	8.271	0.000	0.000	
	short-term aged	3.489	3.938	1.550	0.000	**2.100**
	long-term aged	0.937	1.093	10.010	2.800	**7.564**
CRMB-5	unaged	1.884	3.053	19.985	0.640	
	short-term aged	1.336	1.780	22.350	3.725	**1.715**
	long-term aged	0.403	0.605	40.210	18.010	**5.044**
CRMB-10	unaged	0.733	1.433	41.580	8.040	
	short-term aged	0.466	0.914	48.120	15.468	**1.569**
	long-term aged	0.219	0.349	55.360	33.260	**4.106**
CRMB-15	unaged	0.164	0.539	70.577	25.350	
	short-term aged	0.142	0.413	76.317	32.447	**1.306**
	long-term aged	0.140	0.327	76.339	38.790	**1.647**
CRMB-22	unaged	0.027	0.226	87.170	30.815	
	short-term aged	0.022	0.182	91.435	41.657	**1.241**
	long-term aged	0.059	0.143	72.800	47.360	**1.579**

It is clear that the crumb rubber modification of bitumen significantly decreases the non-recoverable creep compliance and increase the percent recovery of neat bitumen, which means improved resistance to permanent deformation. This improvement intensifies with the increase of CRM content. The increase in percent recovery implies the increased elasticity of bitumen. Regarding different binders, the aging process influenced the binder creep-recover property in different ways. In general, the aged binders show higher resistance to permanent deformation than the fresh binders, as evidenced by the smaller J_{nr} values and superior percent recover at all stress levels. To more directly investigate the aging effect on the binder, the following aging index (AI) based on the J_{nr} values at 3.2 kPa stress level was defined (Equation (6.35)). A higher aging index indicates a higher degree of susceptibility towards aging effect and vice versa.

$$\text{AI} = \frac{J_{nr,3.2\text{kPa}_{unaged}}}{J_{nr,3.2\text{kPa}_{aged}}} \tag{6.35}$$

Based on the AI values in Table 6.10, it is observed that at both short-term and long-term aging conditions, CRMBs with higher CRM contents have lower AI values comparing to the neat bitumen, indicating less susceptible to aging effect. These findings coincide with the observations from FTIR results.

6.5.7 Chemo-mechanics of aging

As a result of the chemical changes of bitumen during aging, the mechanical properties of aged bitumen change as well. In previous studies, efforts have been made to correlate the oxidation products, mainly ketone and sulfoxide, with the mechanical parameters of bitumen, e.g., softening point, viscosity, complex shear modulus, phase angle, etc. (L. D *et al.* 2019, Mullapudi *et al.* 2019). This so-called chemo-mechanics correlation will be beneficial to understand the dependence of mechanical properties of binders on their chemical composition. While ketone formation is well correlated to asphaltene formation on oxidation, sulfoxide formation does not contribute to asphaltene formation because sulfoxide derived from the oxidation of sulfides are less polar than asphaltene (Apostolidis *et al.* 2017). Asphaltenes have been proven to be primarily responsible for the viscosity increase (stiffening effect) on aging. Petersen et al. (Petersen and Glaser 2011) reported that the alcohols, which are formed concurrently with the sulfoxides from the same hydroperoxide precursors as the ketones, have a similar effect on bitumen viscosity increase as do the ketones. This dual oxidation mechanism (formation of ketone and sulfoxide) contributes to the age hardening of bitumen. The sum of carbonyl index and sulfoxide index was used as the combined chemical aging index of bitumen after aging (Cavalli *et al.* 2018). It is noteworthy that although aromaticity index of a binder is closely related to its mechanical properties (Soenen and Redelius 2014), the relationship between aromaticity level and aging state is not well-defined as the carbonyl or sulfoxide index (Tarsi *et al.* 2018). Therefore, the correlation was not done between aromaticity and mechanical parameters. In the presented study, six mechanical parameters, namely non-recoverable creep compliance and percent recovery at 3.2 kPa from MSCR tests, R index and crossover frequency from master curves, rutting factor and G-R parameter, were correlated with the combined chemical aging index through statistical analysis in Figure 6.25. Among all the mechanical parameters, J_{nr} gives the best correlation with the combined chemical aging index in terms of both short-term and long-term aging. The percent recovery and $G^*/\sin\delta$ show better correlations with the chemical aging index for long-term aging than short-term aging. However, the other three parameters did not correlate well with aging due to the insensitivity of these parameters to capture the aging effect on binders. It seems that mechanical parameters in the nonlinear viscoelastic region can better differentiate the CRMB binders before and after aging.

(a)   (b)

(c)

(d)

(e)

(f)
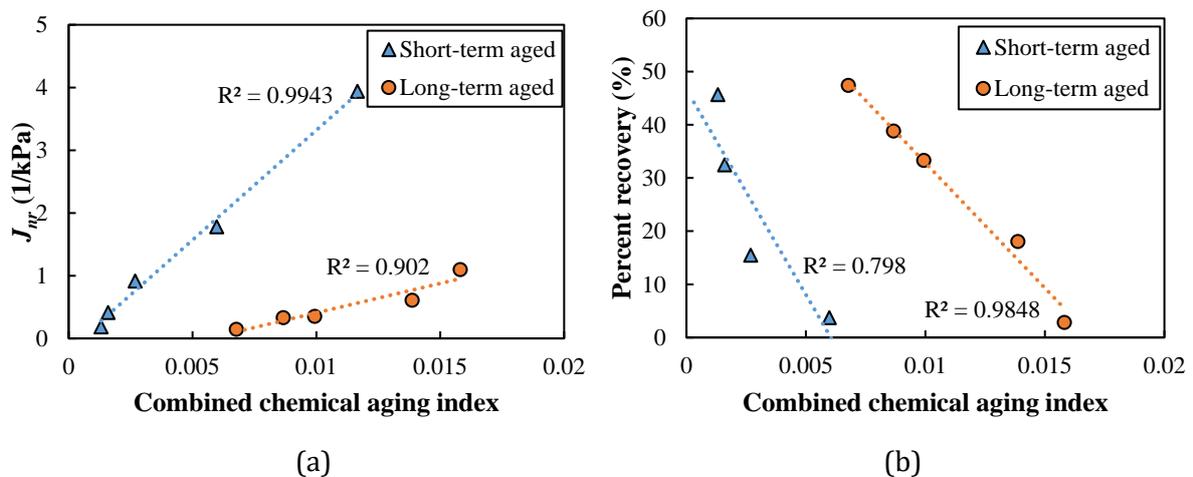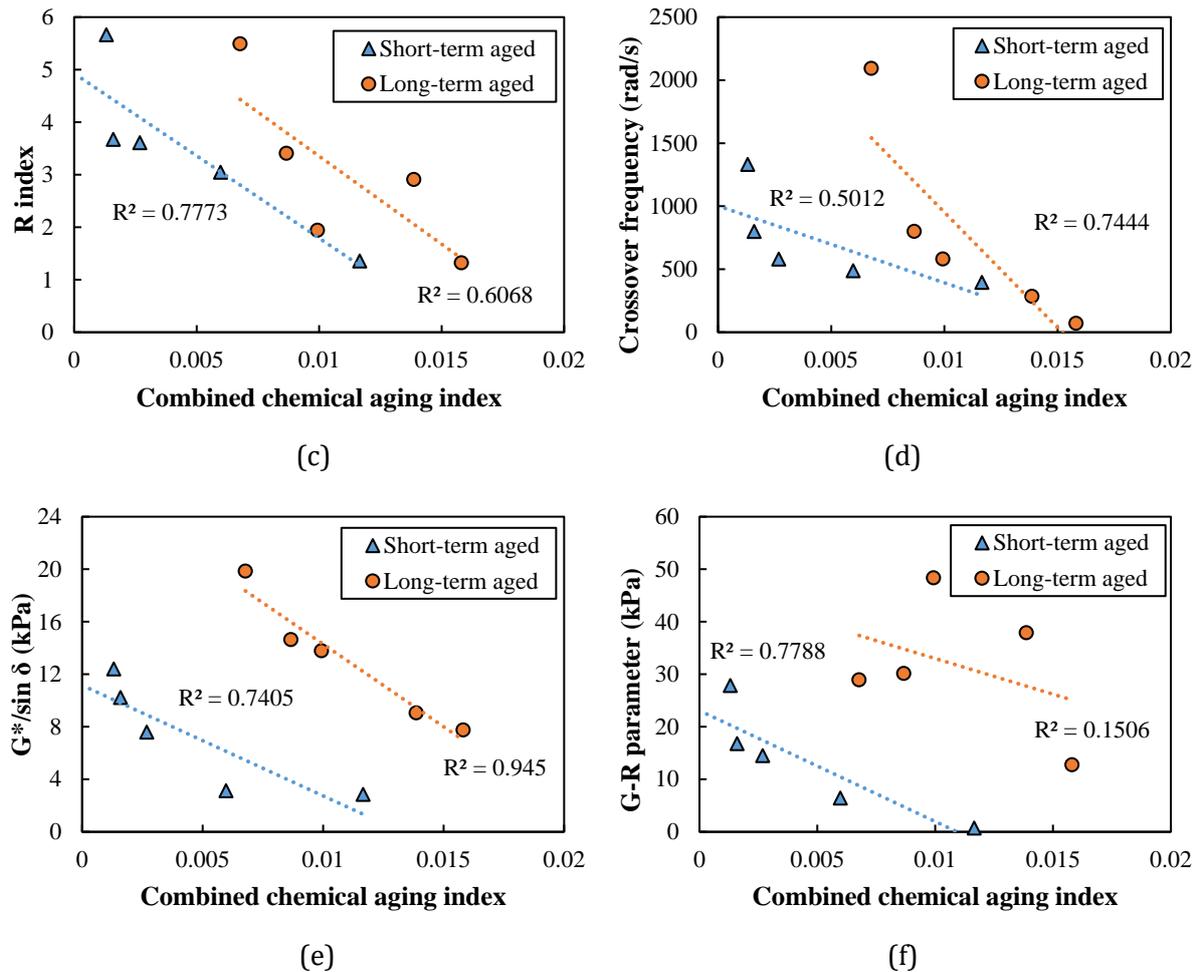
Figure 6.25 Correlation between chemical aging index from FTIR and rheological parameters of bitumen (a) non-recoverable creep compliance (b) percent recovery (c) rheological index (d) crossover frequency (e) rutting factor and (f) G-R parameter.

6.5.8 Summary

This subchapter investigated the effects of laboratory short-term and long-term aging on the chemistry and rheology of CRMB. The following conclusions can be drawn based on the test results:

- The modified static oven aging of bitumen sample with a thickness of 1.25 mm at 163 °C for 2 hours can be an alternative to the standard RTFO aging procedure. The oven aging can be used to create short-term aged CRMB binders in the laboratory without difficulty.

- During the aging process, the aliphaticity index of all binders decreased but the reduction was insignificant. The aromaticity index of neat bitumen increased with the aging extent, while the aromaticity of all the CRMB binders first decreased after the short-term aging then increased after long-term aging. Both carbonyl and sulfoxide indices for each binder increased during aging. However, CRMB binders produced less carbonyl and sulfoxide functional groups than neat bitumen did after aging. The decrease in the oxidation products was intensified with the increase of CRM content.

- Aging causes the binder to become stiffer and alters the rheological properties of all binders, i.e., increase in complex modulus, decrease in phase angle, decrease in non-recoverable creep compliance and increase in recovery ability.

- The addition of CRM into bitumen improved the aging resistance as reflected by the lower carbonyl and sulfoxide indices as well as after aging the less changed rheological parameters of CRMB comparing to neat bitumen. CRMB with higher CRM content showed higher resistance against aging, and thus against stiffening and embrittlement.

- The non-recoverable creep compliance and percent recovery from MSCR tests show better correlations with the combined chemical aging index (sum of carbonyl and sulfoxide indices) than the parameters derived from the linear viscoelastic region do.

This study demonstrated that bitumen modified by crumb rubber shows improved aging resistance, which is beneficial for the long-term performance of rubberized asphalt pavement.

6.6 Storage stability

6.6.1 Introduction

Storage instability of PMB is actually a phase separation process at a microscopic scale during which polymer modifiers separate from bitumen matrix due to the different natures of polymer and bitumen (Polacco *et al.* 2015). If considering PMB as a binary blend which comprises a bitumen-rich phase and a polymer-rich phase, the dynamic asymmetry between these two phases directly drives the phase separation process. There are many factors controlling this dynamic asymmetry within PMB. The density difference between polymer and bitumen is believed to be one of the important causes of storage instability in three-dimensional reality (Zhu *et al.* 2016). More fundamental effects may come from the differences in microstructural composition, physio-chemistry (molecular weight, glass transition temperature, polarity and solubility) for polymer and bitumen which contributes to the incompatibility (Zhu and Kringos 2015). Solubility parameters are often used to interpret and predict the compatibility between bitumen and polymer modifiers (Zhu *et al.* 2019). In terms of CRMB, more specifically, raw material properties (bitumen and CRM characteristics, CRM content, additives) and the interaction conditions determine the storage stability. It is reported that CRMs of small size obtained through ambient grounding result in more storage stable CRMB binders (Sienkiewicz *et al.* 2017). Poor storage stability has negative influence on the overall binder properties and increases the handling difficulty of storage and transport, consequently, influence the durability of asphalt pavements. It also results in difficulties for the binder system to be transported by pipelines (Sienkiewicz *et al.* 2017). Since storage stability directly influence the usage and performance of CRMB, understanding the mechanism and influence of other factors (e.g., rubber content and warm-mix additives) is thus of great importance for both production optimization and quality control.

Besides controlling the preparation conditions of CRMB, there are generally two types of methods to improve storage stability of CRMB. One way is to add various types of chemical compounds into CRMB to form bonds between different components of binders and/or form a polymer network structure (Sienkiewicz *et al.* 2017). The other way is achieved by surface treatment of CRM. Thermochemical, thermo-mechanical, microwave, ultrasonic, biological, and plasma methods were used to activate the CRM (Xiao *et al.* 2018, Hosseinnezhad *et al.* 2019). Furaldehyde or acrylic acid was also reported to activate the surface of CRM (Kocevski *et al.* 2012).

6.6.2 Methods for characterizing storage stability of CRMB

Generally, three main techniques have been applied to characterize phase separation behaviours in bituminous binders: microscopy, chromatography/spectroscopy and mechanical testing (Bahia *et al.* 1998). Optical observations are usually conducted using a fluorescence microscope (FM). Images obtained from FM allows direct and rapid visualization of the relative amount and morphology of both polymer-rich phase and bitumen-rich phase based on their different UV excitation responses (Polacco *et al.* 2015). While FM is very popular and successful in characterizing most PMB binders (colloidal dispersion system), it is not very suitable for CRMB binders (colloidal suspension system). This is because prepared samples subjected to FM observations usually require a thickness of less than 0.1 mm. However, the size of CRM particles within the bitumen matrix is usually bigger than the required sample thickness. Even though other sample preparation methods (e.g., "cooling and fracture" per EN 13632) may overcome this problem (Polacco *et al.* 2015), a large proportion of carbon black inside CRM impedes the fluorescent effect of rubber which makes it difficult to obtain readable morphology. Gel permeation chromatography (GPC) has been adopted to obtain the information of molecular weight distributions of bitumen-rich phase and polymer-rich phase (Putman and Amirkhanian 2010, Zhao *et al.* 2013). Through comparing different phases at a molecular level, the molecular sizes of polymer and bitumen, which is an indicator of compatibility, can be predicted and hence the storage stability. Fourier transform infrared spectroscopy (FTIR) can also be utilized to determine changes in the polymer content by measuring the change of peaks of the corresponding functional groups (Yu *et al.* 2014). However, inconsistent results from FTIR are often reported (Hofko *et al.* 2018). The complexity of equipment, strictness of sampling procedure and difficulty in quantifying results of these techniques hinder their widespread use.

The most common way to evaluate the stability of modified binders is the cigar tube test which simulates the phase separation process in the field in the absence of continuous agitation. The mechanical properties of samples from the different tube sections after conditioning are measured and compared to give an indication of the storage stability. The actual performance of modified binders after storage or the effect of storage conditions on their properties can be directly measured through mechanical testing. In addition, since the densities of bitumen and rubber are different, it is expected to distinguish these two phases by X-ray computed tomography (CT) (Kutay *et al.* 2015). The obtained X-ray CT scan images can reflect the bitumen and rubber phases with different greyscale levels, which can further give insights into storage stability based on the distribution of rubber particles in different positions. This study adopted both mechanical testing method and X-ray CT visualizing technique to evaluate the storage stability of CRMB binders.

6.6.3 Objectives and approach

The present study aims to develop a robust methodology to evaluate the storage stability of CRMB with warm-mix additives using both mechanical and morphological tests. Specific objectives include:

- investigating the effects of rubber content and warm-mix additives on storage stability of CRMB binders. Both mechanical tests (dynamic shear rheometer, DSR) and morphological tests (X-ray CT scan) were conducted on the samples from different parts of the tube after conditioning.

- having a preliminary understanding of the dynamic asymmetry between the bitumen-rich phase (BP) and the rubber-rich phase (RP). The glass transition temperature difference between bitumen and CRM was analyzed by Differential Scanning Calorimetry (DSC) test. Rheological tests were also carried out on the extracted liquid phase (i.e., BP) of CRMB and the swollen rubber phase (i.e., RP) to gain some insights into the dynamic asymmetry.

6.6.4 Experimental design and methods

A detailed testing program of different binders to investigate storage stability is shown in Figure 6.26. There are two testing phases for the experimental design. At Phase 1, six types of CRMB binder samples at the fresh state were subjected to the tube storage stability tests. Multiple stress creep and recovery (MSCR) tests were conducted at 64 °C on samples collected from different parts of the tube after conditioning. The high-temperature performance grade (H-PG) of the neat bitumen is 64 °C and all the H-PGs of all CRMB binders are higher than 64 °C. The choice of this testing temperature for MSCR was expected to differentiate the mechanical properties of all collected samples. Storage stability index was proposed based on the MSCR parameters. X-ray CT scan tests were also conducted on the collected samples from different positions of the tube to gain more insights into the rubber particle distribution in the bitumen matrix. At Phase 2, frequency sweep tests were conducted on the liquid phase of CRMB and swollen rubber samples, which represent the bitumen phase and rubber phase, respectively. The linear viscoelastic behaviours of the bitumen phase and rubber phase were compared in an attempt to link to the phase separation phenomena.
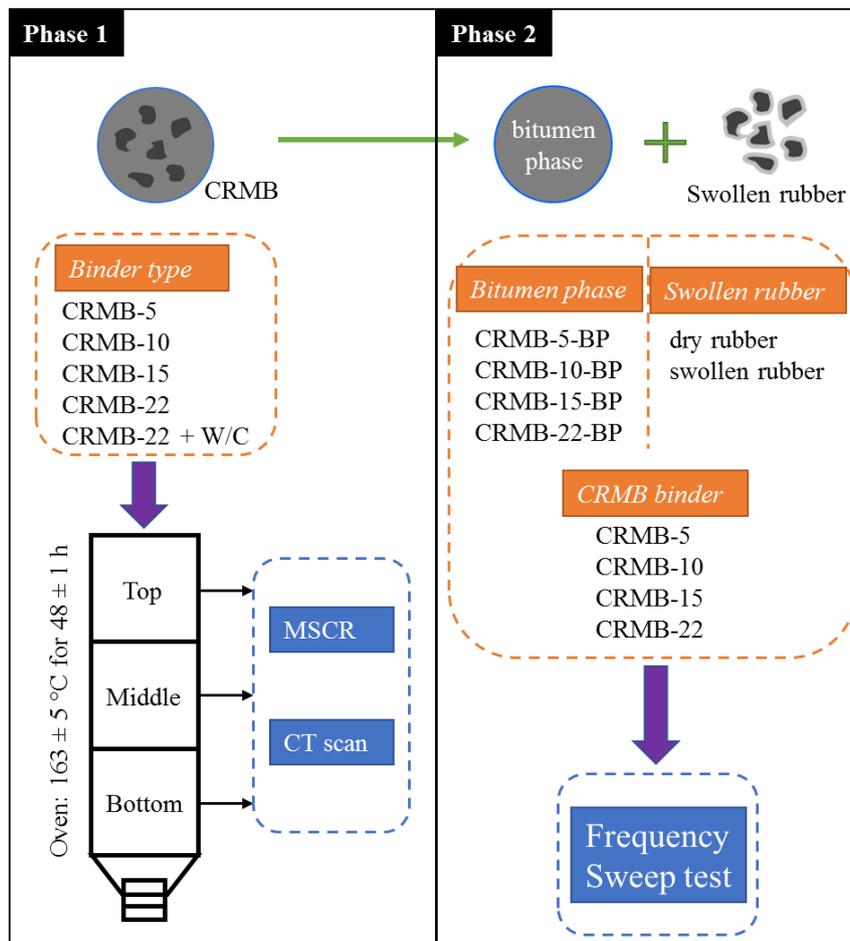
Figure 6.26 Experimental testing plan for different binders.

6.6.4.2 *Storage stability test*

The well-known "tube test" was employed as the storage stability test. During the test, an aluminium foil tube with standard dimensions was filled with hot binder carefully to avoid bringing in air bubbles. The tubes covered with a lid were vertically placed in an oven at 163 ± 3 °C for 48 ± 1 h. After conditioning, settling tubes were moved to a freezer for 2 h. After cooling, the tubes were equally cut into three parts and samples from each part were collected by removing the metal and stored after stirring homogenously. The binder samples from different parts of the tube were subjected to both rheological tests by DSR and X-ray CT scan tests.

6.6.4.3 *Mechanical and morphological tests*

Six types of CRMB binder samples at the fresh state were subjected to the tube storage stability tests. Multiple stress creep and recovery (MSCR) tests were conducted at 64 °C on samples collected from different parts of the tube after conditioning. The high-temperature performance grade (H-PG) of the neat bitumen is 64 °C and all the H-PGs of all CRMB binders are higher than 64 °C (Wang *et al.* 2020g). The choice of this testing temperature for MSCR was expected to differentiate the mechanical properties of all collected samples. Storage stability index was proposed based on the MSCR parameters. X-ray CT scan tests were also conducted on the collected samples from different positions of the tube to gain more insights into the rubber particle distribution in the bitumen matrix.

Binder samples collected from different parts of the tube in the storage stability test were stirred uniformly and poured into special glass bottles with a volume of approximately 5 ml. Then these bottles containing the binders were scanned by a micro X-ray CT. Its resolution is 0.025 mm in all directions. The bitumen and rubber phases are distinguishable in the obtained 2D scan images based on the greyscale values (Figure 6.27). It was intended to reconstruct the 3D images of the binder samples based on the slice images using specific software. However, after the interaction process, a gel-like material was formed surrounding the rubber particles, resulting in a vague boundary between bitumen and rubber phases (Wang *et al.* 2020a, Wang *et al.* 2020b). Besides, the density difference between bitumen and rubber became smaller after the swelling process because of the absorption of bitumen components by rubber. It was found the resultant 3D models of binder samples were biased and cannot reflect the true amounts of rubber in bitumen. Therefore, quantitative analysis was only performed based on the 2D CT scan images.
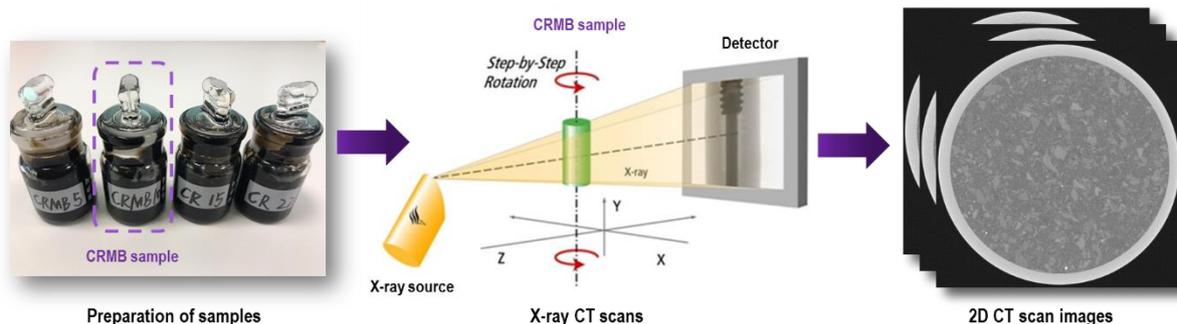
Figure 6.27 X-ray CT scan test for binder samples after the storage stability test.

6.6.5 Storage stability index

From previous studies, it is known that the MSCR parameters are sensitive to the microstructural change of PMB and can be used to evaluate the elastic behavior of binders (D'Angelo and Dongré

2009). Phase separation of CRMB will result in significant changes in the polymer network and hence the elastic behaviors of CRMB. The non-recoverable creep compliance J_{nr} from MSCR tests is expected to be more effective than the traditional rutting parameter G*/sinδ to capture the microstructural change of CRMB after storage. Originally, a storage stability index is defined as the ratio between the J_{nr} of the sample taken from a given distance from the bottom of the settling tube and the same parameter measured on an unconditioned CRMB sample. To demonstrate this idea, the tubes for storing CRMB-22 with/without additives were cut into five equal parts. Samples from all parts were measured. The stability index as a function of settling tube height for three types of binders is shown in Figure 6.28.
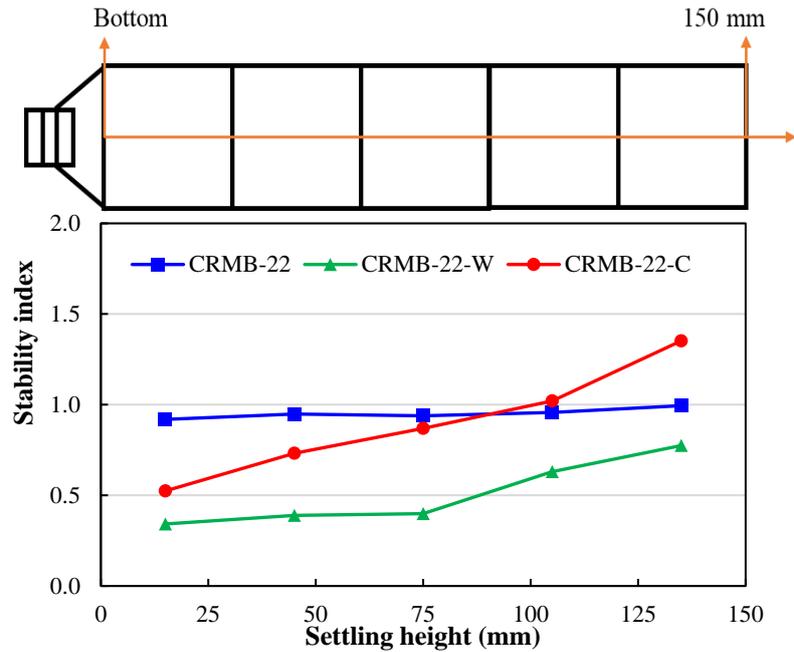
Figure 6.28 Stability index as a function of tube settling height.

It can be found that the stability index of CRMB-22 is close to 1 over the whole range of tube heights, indicating a stable binder. For CRMB-22-W and CRMB-22-C, the storage stability index increases as the tube height increases. This implies that CRMB binders with warm-mix additives are less stable than the common CRMB. The reasons for this will be explained in the next sub-section. In addition, it is worthy to note that the stability indexes of CRMB-22 and CRMB-22-W at different positions are all lower than 1, indicating decreased J_{nr} values comparing to the unconditioned CRMB binders. This fact indicates that binders after conditioning in the oven for 48 h are stiffer than the fresh binders despite the occurrence of potential phase separation. Since the conditioning temperature is 163 °C, bitumen-rubber interaction may continue taking place and potential aging may happen, together changing the mechanical property of binders. Comparing to CRMB-22, the J_{nr} value of CRMB-22-W decreased more, which implies that the wax-based additive may promote the rubber-bitumen to improve the mechanical property.

To quantitatively compare the storage stability of different binders, a proper separation index (SI) which can address the difference between different parts of the tube needs to be developed. The above analysis demonstrates that the mechanical parameter from a fresh binder is not a suitable reference because bitumen-rubber interaction and potential aging may occur during the conditioning. Therefore, the following SI calculated by the non-recoverable creep compliance J_{nr}

values of samples collected from different parts was proposed. The standard storage stability test was used by cutting the tube into three equal parts.

$$\text{SI} = \frac{|J_{nr,\text{t}} - J_{nr,\text{b}}|}{J_{nr,\text{avg}}} \tag{6.36}$$

where $J_{nr,\text{t}}$ and $J_{nr,\text{b}}$ represent the values from the top and bottom sections of the tube, respectively. $J_{nr,\text{avg}}$ is the averaged J_{nr} among the samples from the three equal parts of a tube. Using $J_{nr,\text{avg}}$ of the sample after conditioning can eliminate the bias brought by sample difference due to the interaction and potential aging. A smaller SI value is preferred to achieve higher storage stability of binders.

6.6.6 Effect of rubber content and warm-mix additives

Figure 6.29 shows the separation index of different binders. It is interesting to notice from Figure 6.29 that with the increase of rubber content, the CRMB binder has lower SI indicating higher storage stability. CRMB-22 is the most storage stable binder. In terms of warm-mix additives, the effects of both additives on the SI of CRMB are quite similar. The addition of additives significantly degrades the storage stability indicated by the higher SI values.
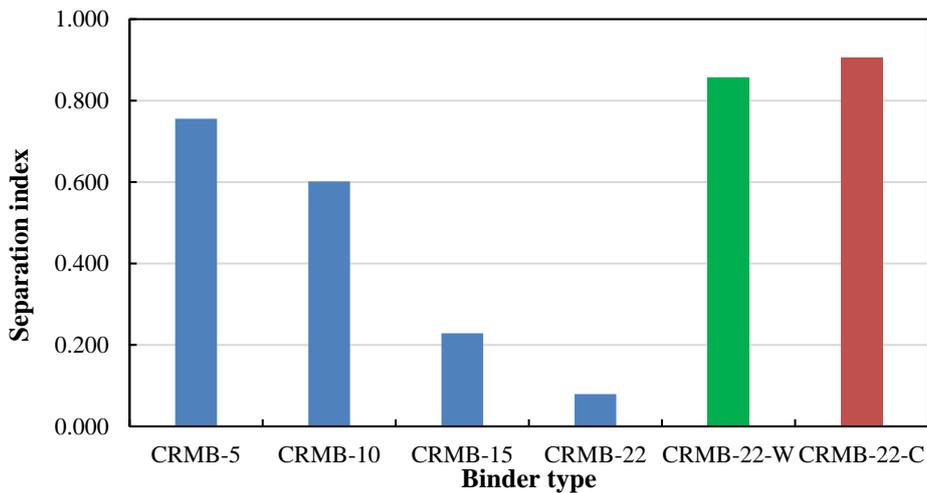
Figure 6.29 Separation index of different binders.

With respect to the phase behaviors of CRMB at high storage temperatures, it can be approximately regarded as a suspension system where rubber particles are suspended in the low-viscosity bitumen medium. According to the Stoke's law, the phase separation in CRMB is driven by the sedimentation velocity of rubber particles in the fluid bitumen. The sedimentation velocity (v) is quantified by Equation (6.37) by considering the gravity force equals to the drag force (frictional force) on rubber particles in the bitumen of a Newtonian fluid state (Ghavibazoo *et al.* 2013):

$$v = \frac{2}{9} \frac{r^2 \Delta \rho g}{\eta} \tag{6.37}$$

Where r is the radius of rubber particle; $\Delta \rho$ is the difference of density between rubber particle and bitumen; η is the viscosity of bitumen; and g is the gravitational acceleration. As implied in Equation (6.37), the sedimentation velocity of rubber particles is proportional to the square of its radius and the density difference between rubber and bitumen, and inversely related to the

viscosity of bitumen. Considering the density of rubber particles (1.15 ± 0.05 g/cm³) is relatively higher than bitumen (1.02 g/cm³), rubber particles tend to settle due to the gravitational force. Therefore, to reduce the sedimentation rate of rubber particles, efforts should be made to decrease the sedimentation velocity, which can be realized through: (1) using finer rubber particles; (2) decreasing the density difference between CRM and bitumen, which is difficult for supplied raw materials; (3) increasing the viscosity of bitumen or residual bitumen (liquid phase of modified bitumen).

Looking back to the storage stability test results in Figure 6.29, increasing rubber content leads to more stable CRMB binders. This is because CRMB with increased volume of rubber has a higher viscosity which hinders the settling of CRM particles (Zhu *et al.* 2017). The states of CRM particles dispersed in bitumen were schematically shown in Figure 6.30. When Rubber content is low, CRM particles absorb only small amounts of light fractions from bitumen and do not change the property of residual bitumen significantly. In addition, the stiffening effect of CRM on the improvement of binder viscosity is relatively weak because of the low content. Since the distance between particles is relatively large, the inter-particle interaction/force can be ignored. The drag force on the particles is insufficient to balance the gravitational force, so that particles will descend due to the higher density. When rubber content is higher, CRM particles significantly change the property of residual bitumen and make it more viscous. The increase of CRM particle volume in the binder after swelling reduces the inter-particle distance. With sufficient inclusions of CRM particle, a potential network can be built as shown in Figure 6.30.
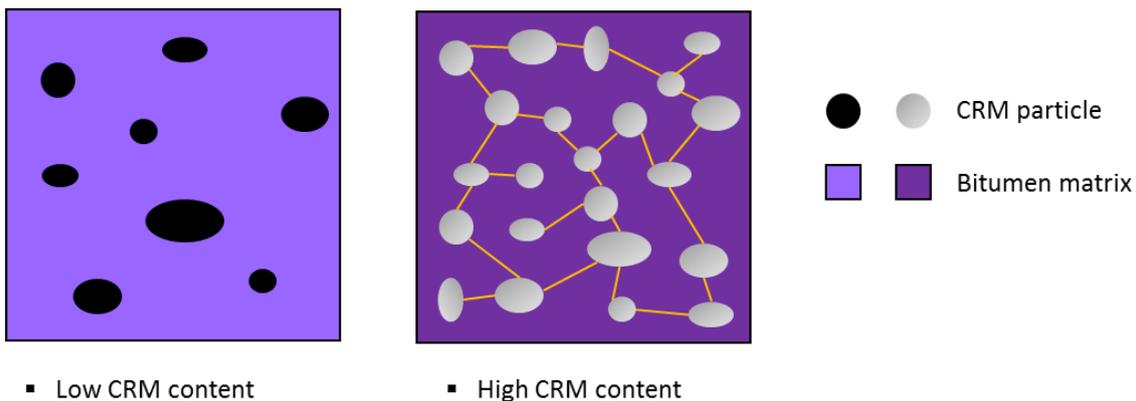
Figure 6.30 Schematic representation of CRM particles suspended in the bitumen matrix. (Note: Different colours represent different states of CRM particle and bitumen; The lines connecting rubber particles were imagined for illustration purpose).

The high viscosity of liquid bitumen and the formed polymer network restrain the movement of CRM particles. Furthermore, it is speculated that when rubber content is high enough, the liquid phase of the binder has similar viscoelastic properties as the swollen rubber, which is verified in the following part. This resemblance further improves the mechanical compatibility between the bitumen-rich phase and rubber-rich phase and consequently increases the storage stability of the binder. By contrast, the addition of warm mix additives decreased the viscosity of CRMB-22 and hence made it easier for CRM particles to descend.

6.6.7 CT scan test results

Mechanical testing is an indirect method to characterize the storage stability of binders. To have more insights into the mechanism of storage stability, CT scan tests were performed to obtain the

rubber particle distribution in bitumen from different positions of the tube sample. Figure 6.31 shows the processing steps of the obtained 2D CT scan images.

2D CT scan image   Image cropping   Segmentation   Measurement
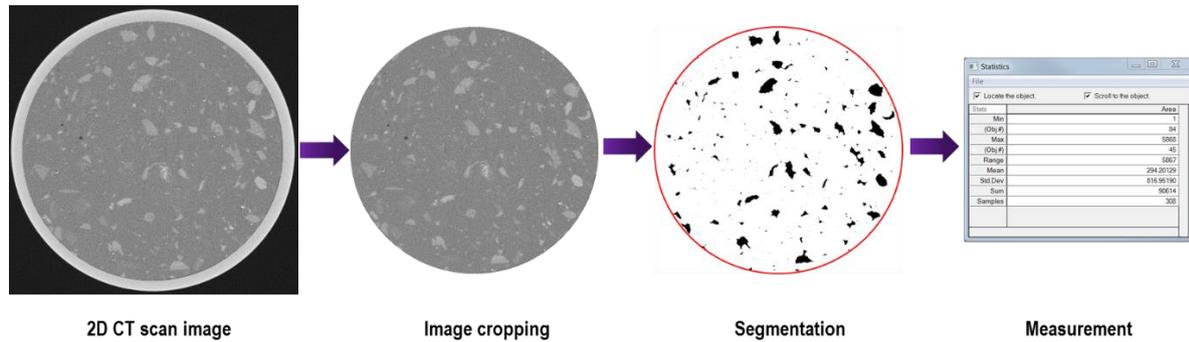
Figure 6.31 CT scan image processing procedure.

The images were first cropped to remove the surrounding container and black background. The brighter parts in the image represent the rubber particles. Segmentation was performed based on the different greyscale values of the bitumen and rubber. A binary image was obtained in which the black islands represent the dispersed rubber particles in the white bitumen domain. Filters were also used to remove the noisy points which may be mistakenly regarded as rubber particles. After the segmentation, the measurement function was applied to calculate the area occupied by rubber particles. The rubber content was further calculated by dividing the total area as displayed by the red circle. The rubber content in different parts of the tube sample was determined by averaging the results from 200 scan images through batch processing using the above procedure. The calculated rubber content varied from different scan images and fluctuated around the averaged value. The obtained rubber content from 2D images maybe deviate from the reality but it is reasonable to compare the values from different samples since a consistent procedure was used.

Another separation index SI_{CT} based on the CT scan results is defined in Equation (6.38).

$$SI_{CT} = \frac{|\phi_t - \phi_b|}{\phi_{avg}} \tag{6.38}$$

where ϕ_t and ϕ_b represent the rubber volume contents of the sample taken from the top and bottom parts, respectively. ϕ_{avg} is the averaged rubber volume content of samples from the three equal parts. The reason for using ϕ_{avg} rather than the original rubber volume content of each binder is because swelling of rubber particles occurring during bitumen-rubber interaction significantly increase the volume of rubber particles. Similar to the previous separation index, a smaller value of the separation index represents higher storage stability of the binder.

Based on the initial dosages of CRM and the densities of CRM and bitumen, the original volume contents of rubber in CRMB-5, CRMB-10, CRMB-15, CRMB-22 are 4.29%, 8.22%, 11.84% and 16.46% respectively. Table 3 summarizes volume fractions of rubber in the binder from different parts and the resulted separation indices. It can be seen clearly that the rubber contents in different parts of the tube are different due to the inhomogeneity of CRMB binders. Because the density of rubber particles is larger than bitumen, rubber particles settle down in the tube during the storage stability test. That is why the rubber content in the bottom is higher. The varying degree of rubber content varies with the type of binder. The average volume fraction of rubber for each binder is approximated twice as high as the original dosage. This confirms the occurrence

of rubber particle swelling in the bitumen matrix (Wang *et al.* 2020f). From the SI_{CT} in Table 6.11, it gives similar findings as the previous SI based on the mechanical properties (J_{nr}). The SI_{CT} value decreases with the increase of rubber content, indicating a more storage stable binder. The addition of warm-mix additives has adverse effects on the storage stability of CRMB binder as reflected by the increased SI_{CT} value.

Table 6.11 Rubber contents of binder and separation index based on CT scan test results.

Binder type	CRMB-5	CRMB-10	CRMB-15	CRMB-22	CRMB-22-W	CRMB-22-C
Top	6.36	14.37	18.35	26.19	25.37	26.25
Middle	8.38	19.46	23.74	30.46	33.35	31.53
Bottom	10.32	22.54	25.56	34.58	40.56	41.26
Average	8.35	18.79	22.55	30.41	33.09	33.01
SI_{CT}	**0.474**	**0.435**	**0.320**	**0.276**	**0.459**	**0.455**

Figure 6.32 compares the separation index from the mechanical test and the CT scan test. There is a high correlation between these two separation indices, which confirms that the mechanical testing (MSCR in this study) is an effective method to differentiate the difference between different parts of the sample to characterize the storage stability. It is noteworthy that the separation indices from CT scan test are closer to each comparing to those from mechanical tests. This means J_{nr} from the MSCR test is more sensitive to the change of rubber content in CRMB binders.
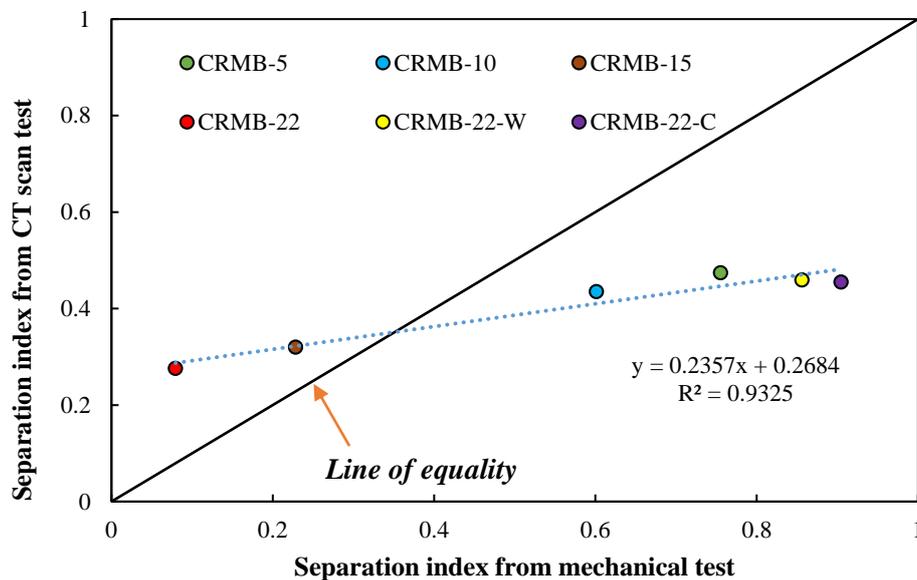
Figure 6.32 Comparison between the separation indices from different tests

In addition, Figure 6.33 shows the CT scan images of CRMB binders with different rubber contents. It verifies the previous assumption of the status of rubber particles in the bitumen matrix as shown in Figure 6.30. When increasing the rubber content, a potential rubber network can be established due to the interparticle interactions with the bitumen, which restrains the movement of the dissociative rubber particles.

(a)	(b)	(c)	(d)
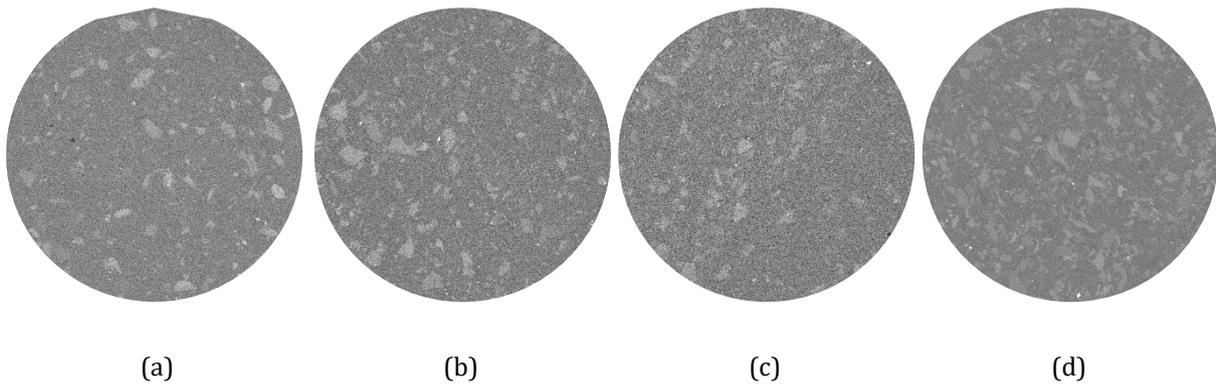
Figure 6.33 CT scan images of (a) CRMB-5, (b) CRMB-10, (c) CRMB-15 and (d) CRMB-22.

6.6.8 Dynamic asymmetry between the components of CRMB

As mentioned earlier, if considering PMB as a binary blend consisting of a bitumen-rich phase and a polymer-rich phase, the dynamic asymmetry between these two phases directly drives the phase separation process. Considering CRMB as a blend of two viscoelastic materials, to better understand the effects of the viscoelasticity of individual component on phase separation dynamics, two questions need to be answered: (1) if there is indeed a dynamic asymmetry between bitumen and rubber within CRMB; and (2) to what extent the dynamic asymmetry affects the phase separation in CRMB. The first question was addressed by investigating the viscoelasticity of CRMB and by analyzing the glass transition temperature (T_g) difference between bitumen and rubber.

6.6.8.1 *Viscoelastic master curves and glass transition temperature*

From the master curves of complex modulus and phase angle of CRMB binders in Figure 5.21a, it can be found in the CRMB system, rubber is presumably a slower phase while bitumen is a faster phase. CRMB with a higher rubber content has a wider relaxation spectrum, which means a more gradual transition from the elastic behaviour to viscous behaviour due to the presence of rubber. A gradual elastic-viscous transition means the system can be more stable when encountering temperature changes.

Both neat bitumen and CRM samples are prepared for DSC tests to determine the glass transition temperatures. Approximately 15 mg of bitumen or CRM is placed in a DSC cup. The cup is sealed with a lid using a special tool to ensure proper contact between the sample and the bottom surface. The cup containing testing materials was placed in the apparatus and conditioned at 25 °C for 5 minutes. Then the temperature was decreased from 25 °C to -60 °C. The measurement started after the isothermal conditioning at -60 °C for 5 minutes, with temperature ramping from -60 to 140 °C at a rate of 20 °C /min (Soenen *et al.* 2013). The heat flows of testing samples were monitored and compared to those of the reference sample (an empty aluminium pan in this study) for further derivations.

The T_g and related thermal parameters of bitumen and CRM are shown in Table 6.12. The Delta C_p parameter reflects the change of heat capacity after glass transition. It is obvious that bitumen and CRM have quite different glass transition temperatures. However, since the large variation of CRM source and complex glass transition phenomena of bitumen, it is difficult to quantitatively characterize the dynamic asymmetry between bitumen and CRM based on their T_gs. Bearing this in mind, the fundamental viscoelastic properties of these two components were investigated in

the following part to see what is the direct contribution to a dynamic symmetry or dynamic asymmetry.

Table 6.12 Glass transition temperatures of bitumen and CRM.

Sample	T_g (°C)	Onset (°C)	End (°C)	Delta C_p (J/g*°C)
70/100	-17.18	-26.81	-9.23	0.118
CRM	-58.37	-61.77	-55.45	0.244

6.6.8.2 *Rheological properties of the bitumen phase and rubber phase*

The bitumen-rubber interaction process alters the volume fractions of rubber and the mechanical properties of both bitumen and rubber. To investigate whether this interaction process has effects on the dynamic asymmetry between BP and RP, FS tests were performed on the extracted liquid bitumen phase and the swollen rubber phases (Wang *et al.* 2020d). It is assumed the rubber particles in CRMB binders with different rubber contents have similar mechanical properties as simulated by the swollen rubber sample. This is because there is a sufficient amount of bitumen in the binder to allow swelling to occur (Airey *et al.* 2004). The master curves of bitumen and rubber before and after swelling were developed in Figure 6.34.
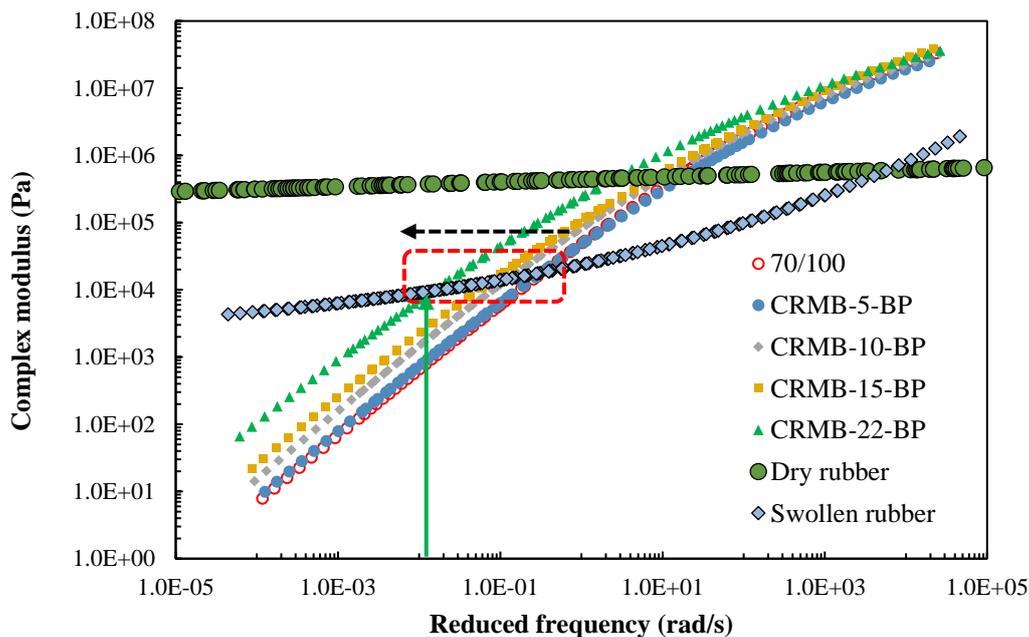
Figure 6.34 Complex modulus master curves of liquid bitumen phase and swollen rubber phase.

Comparing the dry rubber with the swollen rubber, it can be found that dry rubber exhibits obvious elastic behaviors while the swollen rubber shows obvious viscoelasticity and becomes softer than the dry rubber. The complex moduli of swollen rubber are all lower than that of the dry rubber at low frequencies. At high frequencies, the moduli of different samples merge together. In terms of the liquid phases of different CRMB binders, they are stiffer than the neat bitumen because of the loss of light fractions to rubber. Since the mechanical properties of both the bitumen phase and rubber phase are changed after interaction, it is of more interest to analyze

the relative relationship between these two phases. Comparing the bitumen phase with the swollen rubber phase, the swollen rubber sample has lower moduli in the high-frequency region and higher moduli in the low-frequency region. This explains the peculiar viscoelastic response of CRMB. It is important to notice that the crossing points of the master curves of the bitumen phase and swollen rubber phase are located in the relatively low-frequency region. When increasing the rubber content, the crossing point shifts to the lower frequency side. Considering the reference temperature to build the master curve is 30 °C, the crossing point in the low-frequency region corresponds to high temperatures. This means the two phases have similar mechanical properties in the high-temperature region. CRMB with a low rubber content may be stable at lower temperatures (e.g., ambient temperatures) because of the similarity between the bitumen phase and rubber phase as reflected by the crossing over at a relatively high frequency. It may be unstable at higher temperatures (e.g., storage temperatures) because of the dissimilarity between BP and RP. At a fixed low frequency (approximately corresponding to the storage temperature) as indicated by the green arrow in Figure 6.34, no crossing point is reached when the rubber content is low, which means the dynamic asymmetry remains. When increasing the rubber content to a certain value, the crossing point appears and the dynamic asymmetry between the two phases disappears. At this moment, the CRMB binder exhibits as a stable blend during high-temperature storage. This dynamic symmetry between the bitumen phase and the rubber phase is the fundamental reason why CRMB-22 is more storage stable. Since the crossing point of the master curves of two phases is highly dependent on the constituents of CRMB and interaction conditions, it is possible to manipulate these factors to achieve the desired crossover between two phases and hence obtain a storage-stable CRMB blend. In general, bitumen-rubber interaction (mainly swelling) changes both the mechanical properties of bitumen matrix and rubber due to the swelling of rubber by absorbing light fractions of bitumen (Wang *et al.* 2020f). Therefore, by controlling the interaction conditions and selecting the proper raw materials (bitumen and rubber), it is possible to achieve a resemblance between bitumen and rubber phases after the interaction.

6.6.9 Summary

This subchapter investigated the effects of rubber content and warm-mix additives on the storage stability of CRMB binders. The main findings are as follows:

- The mechanical (or other) parameters of fresh CRMB binders cannot be used as a reference in the separation index to evaluate the stability after storage because bitumen-rubber interaction and aging may continue occurring during the storage period. Instead, a parameter taken from the stored samples can serve this purpose.

- Separation indices developed from both MSCR test and CT scan test results reveal that CRMB with a higher rubber content is more storage stable than CRMB with a lower rubber content. The incorporation of both warm mix additives is detrimental to the storage stability of CRMB-22. Based on the results in this study, it is not suggested to add warm mix additives into CRMB during the storage or transport stage.

- When the bitumen-rich phase and rubber-rich phase of CRMB exhibit similar mechanical behaviours, which can be called dynamic symmetry, CRMB will be storage stable. The dynamic asymmetry between binder components drives the phase separation behaviour of CRMB. It is possible to manipulate raw material properties and interaction conditions

to achieve the desired crossover between two phases of CRMB and hence obtain a storage stable CRMB blend.

6.7 References

Abdelrahman, M.A. & Carpenter, S.H., 1999. Mechanism of the interaction of asphalt cement with crumb rubber modifier. *Transportation Research Record: Journal of the Transportation Research Board,* 1661, 106-113.

Airey, G., Rahman, M. & Collop, A.C., 2004. Crumb rubber and bitumen interaction as a function of crude source and bitumen viscosity. *Road Materials and Pavement Design,* 5 (4), 453-475.

Airey, G.D., 2003. State of the art report on ageing test methods for bituminous pavement materials. *International Journal of Pavement Engineering,* 4 (3), 165-176.

Akisetty, C.K., Lee, S.J. & Amirkhanian, S.N., 2010. Laboratory investigation of the influence of warm asphalt additives on long-term performance properties of crm binders. *International Journal of Pavement Engineering,* 11 (2), 153-160.

Anderson, D.A., Christensen, D.W., Bahia, H.U., Dongre, R., Sharma, M.G. & Antle, C.E., 1994. *Binder characterization and evaluation volume 3: Physical characterization.* Washington, D.C., US.

Anderson, D.A. & Kennedy, T.W., 1993. Development of shrp binder specification. *Journal of the Association of Asphalt Paving Technologists,* 62, 481-507.

Anderson, D.A., Le Hir, Y.M., Marasteanu, M.O., Planche, J.P., Martin, D. & Gauthier, G., 2001. Evaluation of fatigue criteria for asphalt binders. *Transportation Research Record,* (1766), 48-56.

Anderson, R.M., King, G.N., Hanson, D.I. & Blankenship, P.B., 2011. Evaluation of the relationship between asphalt binder properties and non-load related cracking. *Journal of the Association of Asphalt Paving Technologists,* 80.

Apostolidis, P., Liu, X., Kasbergen, C. & Scarpas, A.T., 2017. Synthesis of asphalt binder aging and the state of the art of antiaging technologies. *Transportation Research Record: Journal of the Transportation Research Board,* 2633, 147-153.

Bahia, H.U., Hanson, D.I., Zeng, M., Zhai, H., Khatri, M.A. & Anderson, R.M., 2001a. *Characterization of modified asphalt binders in superpave mix design.* Washington D.C.: Board, T.R.

Bahia, H.U., Zhai, H., Onnetti, K. & Kose, S., 1999. Non-linear viscoelastic and fatigue properties of asphalt binders. *Journal of the Association of Asphalt Paving Technologists,* 68, 1-34.

Bahia, H.U., Zhai, H. & Range, A., 1998. Evaluation of stability, nature of modifier, and short-term aging of modified binders using new tests: Last, pat, and modified rtfo. *Transportation Research Record*.

Bahia, H.U., Zhai, H., Zeng, M., Hu, Y. & Turner, P., 2001b. Development of binder specification parameters based on characterization of damage behavior. *Journal of the Association of Asphalt Paving Technologists,* 70, 442-470.

Benedetto, H.D., Delaporte, B. & Sauzéat, C., 2007. Three-dimensional linear behavior of bituminous materials: Experiments and modeling. *International Journal of Geomechanics,* 7 (2), 149-157.

Bonnetti, K.S., Nam, K. & Bahia, H.U., 2002. Measuring and defining fatigue behavior of asphalt binders. *Transportation Research Record,* (1810), 33-43.

Cao, W. & Wang, C., 2018. A new comprehensive analysis framework for fatigue characterization of asphalt binder using the linear amplitude sweep test. *Construction and Building Materials,* 171, 1-12.

Cavalli, M.C., Zaumanis, M., Mazza, E., Partl, M.N. & Poulikakos, L.D., 2018. Effect of ageing on the mechanical and chemical properties of binder from rap treated with bio-based rejuvenators. *Composites Part B: Engineering,* 141, 174-181.

Cortizo, M.S., Larsen, D.O., Bianchetto, H. & Alessandrini, J.L., 2004. Effect of the thermal degradation of sbs copolymers during the ageing of modified asphalts. *Polymer Degradation and Stability,* 86 (2), 275-282.

D'angelo, J. & Dongré, R., 2009. Practical use of multiple stress creep and recovery test. *Transportation Research Record: Journal of the Transportation Research Board,* 2126, 73-82.

D'angelo, J., Kluttz, R., Dongre, R.N., Stephens, K. & Zanzotto, L., 2007. Revision of the superpave high temperature binder specification: The multiple stress creep recovery test. *Journal of the Association of Asphalt Paving Technologists,* 76, 123-162.

D'angelo, J.A., 2009. The relationship of the mscr test to rutting. *Road Materials and Pavement Design,* 10 (sup1), 61-80.

De Visscher, J. & Vanelstraete, A., 2004. Practical test methods for measuring the zero shear viscosity of bituminous binders. *Materials and Structures,* 37 (5), 360-364.

Delgadillo, R. & Bahia, H., 2005. Rational fatigue limits for asphalt binders derived from pavement analysis. *Journal of the Association of Asphalt Paving Technologists,* 78, 97-138.

Erkens, S., Porot, L., Gläser, R. & Glover, C.J., 2016. Aging of bitumen and asphalt concrete: Comparing state of the practice and ongoing developments in the united states and europe. *Transportation Research Board 95th annual meeting.* Washington DC, US: TRB.

Farrar, M., Sui, C., Salmans, S. & Qin, Q., 2015. *Determining the low-temperature rheological properties of asphalt binder using a dynamic shear rheometer (dsr).* Laramie, WY 82072.

Farrar, M.J., Hajj, E.Y., Planche, J.-P. & Alavi, M.Z., 2013. A method to estimate the thermal stress build-up in an asphalt mixture from a single-cooling event. *Road Materials and Pavement Design,* 14 (sup1), 201-211.

Fhwa, 2017. *Four-mm dynamic shear rheometry.* VA.

Gawel, I., Stepkowski, R. & Czechowski, F., 2006. Molecular interactions between rubber and asphalt. *Industrial & Engineering Chemistry Research,* 45 (9), 3044-3049.

Ghavibazoo, A. & Abdelrahman, M., 2013. Composition analysis of crumb rubber during interaction with asphalt and effect on properties of binder. *International Journal of Pavement Engineering,* 14 (5), 517-530.

Ghavibazoo, A., Abdelrahman, M. & Ragab, M., 2013. Effect of crumb rubber modifier dissolution on storage stability of crumb rubber-modified asphalt. *Transportation Research Record: Journal of the Transportation Research Board,* 2370, 109-115.

Ghavibazoo, A., Abdelrahman, M. & Ragab, M., 2015. Evaluation of oxidization of crumb rubber–modified asphalt during short-term aging. *Transportation Research Record: Journal of the Transportation Research Board,* 2505, 84-91.

Hajj, R. & Bhasin, A., 2017. The search for a measure of fatigue cracking in asphalt binders – a review of different approaches. *International Journal of Pavement Engineering,* 19 (3), 205-219.

Hajj, R., Filonzi, A., Rahman, S. & Bhasin, A., 2019. Considerations for using the 4 mm plate geometry in the dynamic shear rheometer for low temperature evaluation of asphalt binders. *Transportation Research Record,* 2673 (11), 649-659.

Hintz, C. & Bahia, H., 2013a. Simplification of linear amplitude sweep test and specification parameter. *Transportation Research Record: Journal of the Transportation Research Board,* 2370, 10-16.

Hintz, C. & Bahia, H., 2013b. Understanding mechanisms leading to asphalt binder fatigue in the dynamic shear rheometer. *Road Materials and Pavement Design,* 14 (sup2), 231-251.

Hintz, C., Velasquez, R., Johnson, C. & Bahia, H., 2011. Modification and validation of linear amplitude sweep test for binder fatigue specification. *Transportation Research Record: Journal of the Transportation Research Board,* 2207, 99-106.

Hofko, B. & Hospodka, M., 2016. Rolling thin film oven test and pressure aging vessel conditioning parameters. *Transportation Research Record: Journal of the Transportation Research Board,* 2574, 111-116.

Hofko, B., Porot, L., Falchetto Cannone, A., Poulikakos, L., Huber, L., Lu, X., Mollenhauer, K. & Grothe, H., 2018. Ftir spectral analysis of bituminous binders: Reproducibility and impact of ageing temperature. *Materials and Structures,* 51 (2).

Hosseinnezhad, S., Kabir, S.F., Oldham, D., Mousavi, M. & Fini, E.H., 2019. Surface functionalization of rubber particles to reduce phase separation in rubberized asphalt for sustainable construction. *Journal of Cleaner Production,* 225, 82-89.

Isacsson, U. & Lu, X., 1995. Testing and appraisal of polymer-modified road bitumens - state-of-the-art. *Materials and Structures,* 28 (177), 139-159.

Jing, R., Varveri, A., Liu, X., Scarpas, A. & Erkens, S., 2019. Laboratory and field aging effect on bitumen chemistry and rheology in porous asphalt mixture. *Transportation Research Record: Journal of the Transportation Research Board*.

Kocevski, S., Yagneswaran, S., Xiao, F., Punith, V.S., Smith, D.W. & Amirkhanian, S., 2012. Surface modified ground rubber tire by grafting acrylic acid for paving applications. *Construction and Building Materials,* 34, 83-90.

Kutay, M.E., Varma, S. & Jamrah, A., 2015. A micromechanical model to create digital microstructures of asphalt mastics and crumb rubber-modified binders. *International Journal of Pavement Engineering,* 18 (9), 754-764.

L. D, P., Falchetto A, C., D, W., L, P. & B, H., 2019. Impact of asphalt aging temperature on chemo-mechanics. *RSC Advances,* 9 (21), 11602-11613.

Lamontagne, J., Dumas, P., Mouillet, V. & Kister, J., 2001. Comparison by fourier transform infrared (ftir) spectroscopy of different ageing techniques: Application to road bitumens. *Fuel,* 80 (4), 483-488.

Lesueur, D., 2009. The colloidal structure of bitumen: Consequences on the rheology and on the mechanisms of bitumen modification. *Adv Colloid Interface Sci,* 145 (1-2), 42-82.

Liang, M., Xin, X., Fan, W., Ren, S., Shi, J. & Luo, H., 2017. Thermo-stability and aging performance of modified asphalt with crumb rubber activated by microwave and tor. *Materials & Design,* 127, 84-96.

Lu, X. & Isacsson, U., 2002. Effect of ageing on bitumen chemistry and rheology. *Construction and Building materials,* 16 (1), 15-22.

Lu, X., Uhlback, P. & Soenen, H., 2017. Investigation of bitumen low temperature properties using a dynamic shear rheometer with 4mm parallel plates. *International Journal of Pavement Research and Technology,* 10 (1), 15-22.

Masad, E.A., Huang, C.-W., Dangelo, J. & Little, D.N., 2009. Characterization of asphalt binder resistance to permanent deformation based on nonlinear viscoelastic analysis of multiple stress creep recovery (mscr) test. *Journal of the Association of Asphalt Paving Technologists,* 78, 535-566.

Mensching, D.J., Rowe, G.M., Daniel, J.S. & Bennert, T., 2015. Exploring low-temperature performance in black space. *Road Materials and Pavement Design,* 16 (sup2), 230-253.

Morea, F., Agnusdei, J.O. & Zerbino, R., 2010. The use of asphalt low shear viscosity to predict permanent deformation performance of asphalt concrete. *Materials and Structures,* 44 (7), 1241-1248.

Mullapudi, R.S., Deepika, K.G. & Reddy, K.S., 2019. Relationship between chemistry and mechanical properties of rap binder blends. *Journal of Materials in Civil Engineering,* 31 (7).

Ninomiya, K. & Ferry, J.D., 1959. Some approximate equations useful in the phenomenological treatment of linear viscoelastic data. *Journal of Colloid Science,* 14 (1), 36-48.

Nivitha, M.R., Prasad, E. & Krishnan, J.M., 2015. Ageing in modified bitumen using ftir spectroscopy. *International Journal of Pavement Engineering,* 17 (7), 565-577.

Oshone, M.T., 2018. *Performance based evaluation of cracking in asphalt concrete using viscoelastic and fracture properties.* University of New Hampshire.

Ouyang, C., Wang, S.F., Zhang, Y. & Zhang, Y.X., 2006. Improving the aging resistance of styrene-butadiene-styrene tri-block copolymer modified asphalt by addition of antioxidants. *Polymer Degradation and Stability,* 91 (4), 795-804.

Petersen, J.C., 2009. *A review of the fundamentals of asphalt oxidation: Chemical, physicochemical, physical property, and durability relationships.* Washington, DC, 0097-8515.

Petersen, J.C. & Glaser, R., 2011. Asphalt oxidation mechanisms and the role of oxidation products on age hardening revisited. *Road Materials and Pavement Design,* 12 (4), 795-819.

Polacco, G., Filippi, S., Merusi, F. & Stastna, G., 2015. A review of the fundamentals of polymer-modified asphalts: Asphalt/polymer interactions and principles of compatibility. *Adv Colloid Interface Sci,* 224, 72-112.

Putman, B.J. & Amirkhanian, S.N., 2010. Characterization of the interaction effect of crumb rubber modified binders using hp-gpc. *Journal of Materials in Civil Engineering,* 22 (2), 153-159.

Rahbar-Rastegar, R., Daniel, J.S. & Dave, E.V., 2018. Evaluation of viscoelastic and fracture properties of asphalt mixtures with long-term laboratory conditioning. *Transportation Research Record: Journal of the Transportation Research Board,* 2672 (28), 503-513.

Rowe, G.M., King, G. & Anderson, M., 2014. The influence of binder rheology on the cracking of asphalt mixes in airport and highway projects. *Journal of Testing and Evaluation,* 42 (5), 20130245.

Safaei, F. & Castorena, C., 2016. Temperature effects of linear amplitude sweep testing and analysis. *Transportation Research Record: Journal of the Transportation Research Board,* 2574, 92-100.

Safaei, F., Lee, J.-S., Nascimento, L.a.H.D., Hintz, C. & Kim, Y.R., 2014. Implications of warm-mix asphalt on long-term oxidative ageing and fatigue performance of asphalt binders and mixtures. *Road Materials and Pavement Design,* 15 (sup1), 45-61.

Schapery, R., 1991. Analysis of damage growth in particulate composites using a work potential. *Composites Engineering,* 1 (3), 167-182.

Schroter, K., Hutcheson, S.A., Shi, X., Mandanici, A. & Mckenna, G.B., 2006. Dynamic shear modulus of glycerol: Corrections due to instrument compliance. *J Chem Phys,* 125 (21), 214507.

Sienkiewicz, M., Borzędowska-Labuda, K., Wojtkiewicz, A. & Janik, H., 2017. Development of methods improving storage stability of bitumen modified with ground tire rubber: A review. *Fuel Processing Technology,* 159, 272-279.

Soenen, H., Besamusca, J., Fischer, H.R., Poulikakos, L.D., Planche, J.-P., Das, P.K., Kringos, N., Grenfell, J.R.A., Lu, X. & Chailleux, E., 2013. Laboratory investigation of bitumen based on round robin dsc and afm tests. *Materials and Structures,* 47 (7), 1205-1220.

Soenen, H. & Redelius, P., 2014. The effect of aromatic interactions on the elasticity of bituminous binders. *Rheologica Acta,* 53 (9), 741-754.

Stempihar, J., Gundla, A. & Underwood, B.S., 2018. Interpreting stress sensitivity in the multiple stress creep and recovery test. *Journal of Materials in Civil Engineering,* 30 (2).

Sui, C., Farrar, M., Harnsberger, P., Tuminello, W. & Turner, T., 2011. New low-temperature performance-grading method. *Transportation Research Record: Journal of the Transportation Research Board,* 2207, 43-48.

Sui, C., Farrar, M., Tuminello, W. & Turner, T., 2010. New technique for measuring low-temperature properties of asphalt binders with small amounts of material. *Transportation Research Record: Journal of the Transportation Research Board,* 2179, 23-28.

Sybilski, D., 1994. Relationship between absolute viscosity of polymer-modified bitumens and rutting resistance of pavement. *Materials and Structures,* 27 (166), 110-120.

Tarsi, G., Varveri, A., Lantieri, C., Scarpas, A. & Sangiorgi, C., 2018. Effects of different aging methods on chemical and rheological properties of bitumen. *Journal of Materials in Civil Engineering,* 30 (3).

Underwood, B.S., Baek, C. & Kim, Y.R., 2012. Simplified viscoelastic continuum damage model as platform for asphalt concrete fatigue analysis. *Transportation Research Record,* (2296), 36-45.

Underwood, B.S., Kim, Y.R. & Guddati, M.N., 2010. Improved calculation method of damage parameter in viscoelastic continuum damage model. *International Journal of Pavement Engineering,* 11 (6), 459-476.

Wang, C., Castorena, C., Zhang, J. & Richard Kim, Y., 2015. Unified failure criterion for asphalt binder under cyclic fatigue loading. *Road Materials and Pavement Design,* 16 (sup2), 125-148.

Wang, C., Zhang, H., Castorena, C., Zhang, J. & Kim, Y.R., 2016. Identifying fatigue failure in asphalt binder time sweep tests. *Construction and Building Materials,* 121, 535-546.

Wang, D., Cannone Falchetto, A., Alisov, A., Schrader, J., Riccardi, C. & Wistuba, M.P., 2019a. An alternative experimental method for measuring the low temperature rheological properties of asphalt binder by using 4mm parallel plates on dynamic shear rheometer. *Transportation Research Record: Journal of the Transportation Research Board,* 2673 (3), 427-438.

Wang, H., Apostolidis, P., Zhu, J., Liu, X., Skarpas, A. & Erkens, S., 2020a. The role of thermodynamics and kinetics in rubber–bitumen systems: A theoretical overview. *International Journal of Pavement Engineering*, 1-16.

Wang, H., Liu, X., Apostolidis, P., Erkens, S. & Scarpas, T., 2019b. Numerical investigation of rubber swelling in bitumen. *Construction and Building Materials,* 214, 506-515.

Wang, H., Liu, X., Apostolidis, P., Erkens, S. & Skarpas, A., 2020b. Experimental investigation of rubber swelling in bitumen. *Transportation Research Record: Journal of the Transportation Research Board,* 2674 (2), 203-212

Wang, H., Liu, X., Apostolidis, P. & Scarpas, T., 2018. Review of warm mix rubberized asphalt concrete: Towards a sustainable paving technology. *Journal of Cleaner Production,* 177, 302-314.

Wang, H., Liu, X., Apostolidis, P., Van De Ven, M., Erkens, S. & Skarpas, A., 2020c. Effect of laboratory aging on chemistry and rheology of crumb rubber modified bitumen. *Materials and Structures,* 53 (2).

Wang, H., Liu, X., Erkens, S. & Skarpas, A., 2020d. Experimental characterization of storage stability of crumb rubber modified bitumen with warm-mix additives. *Construction and Building Materials,* 249.

Wang, H., Liu, X., Van De Ven, M., Lu, G., Erkens, S. & Skarpas, A., 2020e. Fatigue performance of long-term aged crumb rubber modified bitumen containing warm-mix additives. *Construction and Building Materials,* 239.

Wang, H., Liu, X., Zhang, H., Apostolidis, P., Erkens, S. & Skarpas, A., 2020f. Micromechanical modelling of complex shear modulus of crumb rubber modified bitumen. *Materials & Design,* 188.

Wang, H., Liu, X., Zhang, H., Apostolidis, P., Scarpas, T. & Erkens, S., 2020g. Asphalt-rubber interaction and performance evaluation of rubberised asphalt binders containing non-foaming warm-mix additives. *Road Materials and Pavement Design,* 21 (6), 1612-1633.

Wang, H., Lu, G., Feng, S., Wen, X. & Yang, J., 2019c. Characterization of bitumen modified with pyrolytic carbon black from scrap tires. *Sustainability,* 11 (6).

Wang, T., Xiao, F., Amirkhanian, S., Huang, W. & Zheng, M., 2017. A review on low temperature performances of rubberized asphalt materials. *Construction and Building Materials,* 145, 483-505.

Wang, Y. & Richard Kim, Y., 2017. Development of a pseudo strain energy-based fatigue failure criterion for asphalt mixtures. *International Journal of Pavement Engineering,* 20 (10), 1182-1192.

Xiao, F., Yao, S., Wang, J., Wei, J. & Amirkhanian, S., 2018. Physical and chemical properties of plasma treated crumb rubbers and high temperature characteristics of their rubberised asphalt binders. *Road Materials and Pavement Design*, 1-20.

Yan, C., Xiao, F., Huang, W. & Lv, Q., 2018. Critical matters in using attenuated total reflectance fourier transform infrared to characterize the polymer degradation in styrene–butadiene–styrene-modified asphalt binders. *Polymer Testing,* 70, 289-296.

Yu, H., Leng, Z. & Gao, Z., 2016. Thermal analysis on the component interaction of asphalt binders modified with crumb rubber and warm mix additives. *Construction and Building Materials,* 125, 168-174.

Yu, X., Leng, Z. & Wei, T.Z., 2014. Investigation of the rheological modification mechanism of warm-mix additives on crumb-rubber-modified asphalt. *Journal of Materials in Civil Engineering,* 26 (2), 312-319.

Zhang, Y. & Gao, Y., 2019. Predicting crack growth in viscoelastic bitumen under a rotational shear fatigue load. *Road Materials and Pavement Design*, 1-20.

Zhao, S., Bowers, B., Huang, B. & Shu, X., 2013. Characterizing rheological properties of binder and blending efficiency of asphalt paving mixtures containing ras through gpc. *Journal of Materials in Civil Engineering,* 26 (5), 941-946.

Zhu, J., Balieu, R., Lu, X. & Kringos, N., 2017. Numerical prediction of storage stability of polymer-modified bitumen. *Transportation Research Record: Journal of the Transportation Research Board,* 2632, 70-78.

Zhu, J., Balieu, R. & Wang, H., 2019. The use of solubility parameters and free energy theory for phase behaviour of polymer-modified bitumen: A review. *Road Materials and Pavement Design*, 1-22.

Zhu, J. & Kringos, N., 2015. Towards the development of a viscoelastic model for phase separation in polymer-modified bitumen. *Road Materials and Pavement Design,* 16 (sup1), 39-49.

Zhu, J., Lu, X. & Kringos, N., 2016. Experimental investigation on storage stability and phase separation behaviour of polymer-modified bitumen. *International Journal of Pavement Engineering*, 1-10.

7

Micromechanical Modelling of CRMB Viscoelastic Property

Part of this chapter contains published material from "Wang, H., Liu, X., Zhang, H., Apostolidis, P., Erkens, S. & Skarpas, A., 2020. Micromechanical modelling of complex shear modulus of crumb rubber modified bitumen. Materials & Design, 188.

Wang, H., Zhang, H., Liu, X., Erkens, S. & Skarpas, A., 2021. Micromechanics-based Complex Modulus Prediction of Crumb Rubber Modified Bitumen Considering Interparticle Interactions. Road Materials and Pavement Design, 22(sup1), S251-S268."

7.1 Micromechanics-based methods for binder property prediction

A thorough understanding of the interaction conditions and raw material characteristics will guide the material selection and process optimization to obtain the desired binder properties from the modification. One of the vital questions needs to be answered is how to effectively predict the performance of modified binders instead of carrying out the tedious laboratory work. Numerical and analytical models are often used to accomplish this goal. Although considerable work has been done to measure and even predict empirical and fundamental properties of CRMB, very little work has been reported in which rigorous mechanics-based models have been used to investigate the complicated behavior of CRMB (Medina and Underwood 2017). Some empirical models were developed to describe the effect of rubber particles in CRMB. These straightforward models are based on the correlations between rubber related variables (particle size, surface area, etc.) and resultant composite response (Shen *et al.* 2009a, Shen *et al.* 2009b), which are incapable of providing generalized insights into the impact of multi-physical interactions between the constituents. The stiffening or reinforcement mechanisms of rubber in bitumen may stem from volume-filling reinforcement, physiochemical interaction and interparticle interaction. How to properly address these reinforcement mechanisms of CRMB using micromechanical modelling remains a challenge.

Micromechanical models, which can predict fundamental material properties of a composite based on mechanical properties and volume fractions of individual constituents, have been introduced to predict the effective viscoelastic behavior of bituminous materials (Buttlar *et al.* 1999, Yin *et al.* 2008, Underwood and Kim 2014, Zhang *et al.* 2018). Numerical micromechanical models, i.e., finite element models (FEM) and discrete element models (DEM), have been successfully utilized by many researchers (Leon L. Mishnaevsky and Schmauder 2001, Sadd *et al.* 2004, Caro *et al.* 2010, Aragao *et al.* 2011) to predict the properties of a mix with complex compositions. However, these studies also highlighted that FEM/DEM-meshes with detailed information (usually by means of X-ray CT scan) require large-scale computational facilities, which limits the utilization of such models in practice. Alternatively, analytical micromechanical models are expected to provide reliable estimations of mechanical properties of a composite without extensive computational efforts. Analytical micromechanical models developed based on continuum mechanics have increasingly been used to predict the mechanical properties of bituminous materials (Zhang *et al.* 2019). In such models, the detailed information of individual constituents is not required. On the contrary, the constituents having same (very similar) mechanical properties are regarded as one phase; and a composite consists of various phases. For a given macroscopic loading condition, each phase's average stress and strain are evaluated and further utilized to obtain the effective properties of the composite on the basis of the volumetric, mechanical and/or geometrical properties of individual phases.

In the composite system of asphalt mastics or mixtures, fillers and aggregates are usually regarded as inert rigid materials embedded in the bitumen matrix (Shu and Huang 2008). CRMB can be regarded as a binary composite in which bitumen is the matrix while rubber particles are the inclusions. However, unlike asphalt mastic or mixture, the composite system of CRMB is more complicated due to the interaction between rubber particles and bitumen which changes both the mechanical properties and volume fractions of individual constituents. In general, bitumen-rubber interaction (mainly swelling) has four consequences from a micromechanics-based point of view: (1) changing the component proportions and thus the mechanical properties of bitumen matrix due to the absorption of light fractions by rubber and the potential released components

from rubber; (2) changing the mechanical properties of rubber due to the formation of a gel-like structure; (3) changing the volume content of rubber due to swelling (the so-called effective volume fraction); (4) changing the interfacial properties between bitumen and rubber due to aforementioned factors (Wang *et al.* 2020c). Therefore, the accurate determination of input parameters from constituents would be a challenge and directly influence the accuracy of the model prediction. Practically speaking, if the predictions of mechanical properties of CRMB from the known properties and blend percentages of the constituent phases by using micromechanical models are applicable and possess certain levels of accuracy, it can save the time and cost for the tedious laboratory work, which enables a more appropriate selection of source materials (bitumen and rubber type), enhanced material development (binder preparation conditions) and improved design of binders (rubber content and particle gradation).

7.2 Objective and approach

This chapter consists of two stages. The first stage aims to examine the applicability and prediction accuracy of four common micromechanical models (the dilute model (DM), the Mori-Tanaka model (MTM), the self-consistent model (SCM), the generalized self-consistent model (GSCM)) for predicting the complex shear modulus of CRMB with different rubber contents. To achieve the first goal, the following subtasks were done to obtain accurate input parameters for micromechanical models:

- Frequency sweep tests using a DSR were conducted on neat bitumen and CRMB binders with four different rubber contents. The obtained complex modulus data are compared with the model predicted values to examine the performance of different micromechanical models.

- Frequency sweep tests were conducted on both extracted liquid phases of CRMBs and swollen rubber samples to obtain more representative rheological properties of bitumen matrix and rubber inclusion in the composite system of CRMB.

- The finite element method was employed to estimate the volume change of rubber in bitumen after swelling thus obtaining the effective volume content of rubber in CRMB.

After obtaining the input parameters for micromechanical models, they were implemented into different micromechanical models to predict the complex modulus. The predicted results were then compared with the experimental data. An overview of the research steps taken in the first stage is presented in Figure 7.1.
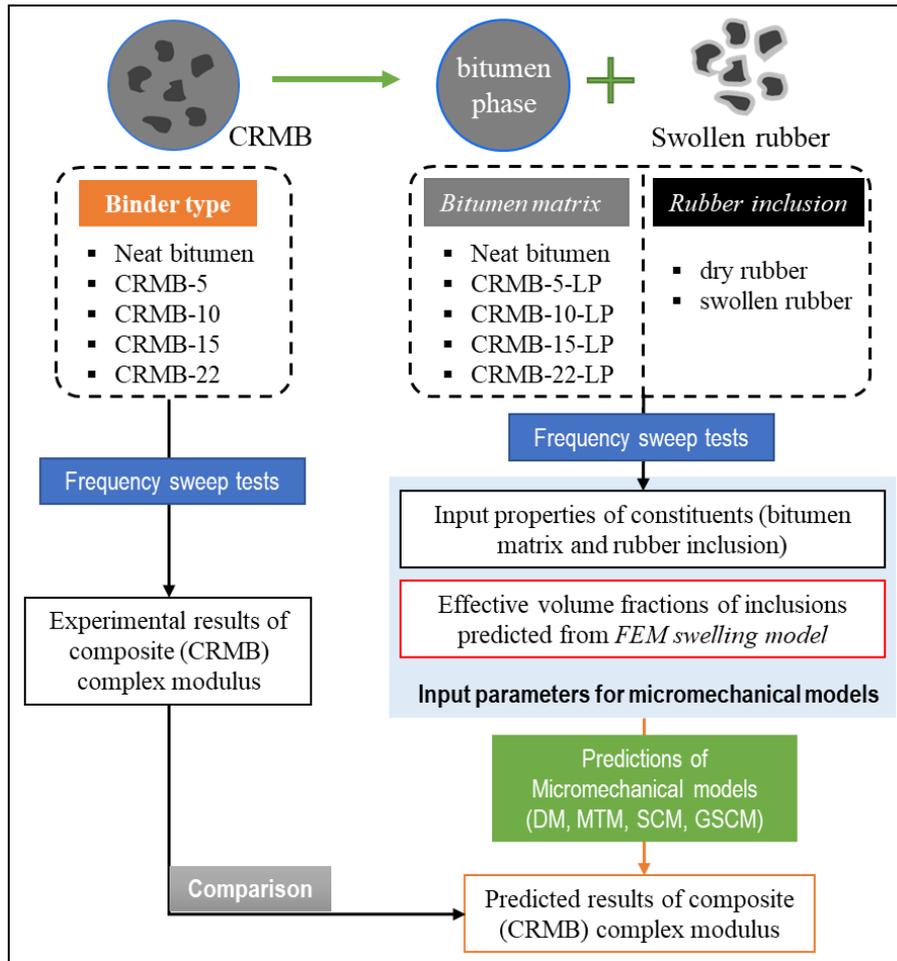
Figure 7.1 Flowchart of research steps in the first-stage study.

The second stage aims to further improve the prediction accuracy by amending the GSCM which performs best among the current micromechanical models. Three different strategies were used in the second-stage study as shown in Figure 7.2. Firstly, mathematical calibration was done on the GSCM by introducing a calibration factor. Then, the (n+1)-phase model was applied to the CRMB system by considering the multilayered properties of swollen rubber particles. Lastly, a new reinforcement mechanism was introduced to account for the interparticle interaction effect. To this end, the reinforcing effect due to polymer chain entanglement was added to the current micromechanical models. The constitutive models of this reinforcement were derived based on the difference between experimental data and micromechanical prediction results.
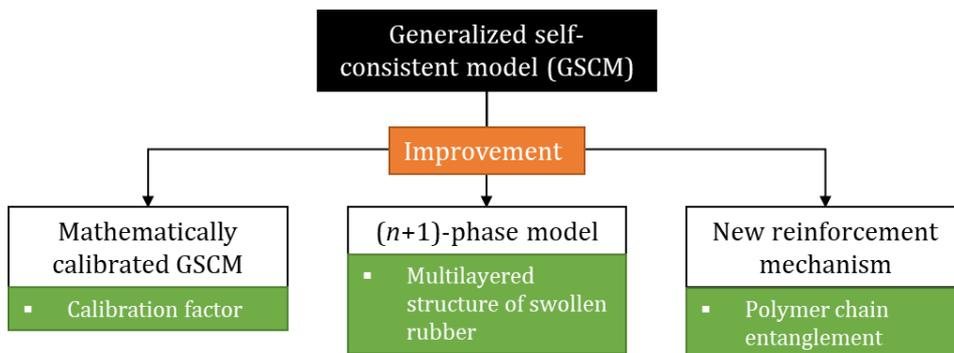
Figure 7.2 Strategies used for improving the prediction accuracy in the second-stage study.

7.3 Micromechanical models

7.3.1 Homogenization concept

Homogenization theory was developed to estimate the effective properties of a heterogeneous composite based on the microstructural description and the local behaviors of its constituents (Yin and Zhao 2016). In this theory, a representative volume element (RVE) is chosen to represent the overall properties of the composite. In an RVE of the CRMB composite system, the constitutive equations of each phase (bitumen and rubber) are shown in Equations (7.1) and (7.2). The interface between the two phases is assumed to be perfectly bonded so that the stress and displacement continuities are satisfied. The average stress and strain of the composite can be related to the average stress and strain of each phase in combination with each volume fraction in Equations (7.3) and (7.4) (Yin and Zhao 2016).

$$\langle \boldsymbol{\sigma} \rangle_b = \mathbf{C}_b : \langle \boldsymbol{\varepsilon} \rangle_b \tag{7.1}$$

$$\langle \boldsymbol{\sigma} \rangle_r = \mathbf{C}_r : \langle \boldsymbol{\varepsilon} \rangle_r \tag{7.2}$$

$$\langle \boldsymbol{\sigma} \rangle_c = (1 - \phi)\langle \boldsymbol{\sigma} \rangle_b + \phi \langle \boldsymbol{\sigma} \rangle_r \tag{7.3}$$

$$\langle \boldsymbol{\varepsilon} \rangle_c = (1 - \phi)\langle \boldsymbol{\varepsilon} \rangle_b + \phi \langle \boldsymbol{\varepsilon} \rangle_r \tag{7.4}$$

where $\langle \boldsymbol{\sigma} \rangle$, $\langle \boldsymbol{\varepsilon} \rangle$ are the average stress and strain; $\mathbf{C}$ is the stiffness tensor; ϕ is the volume fraction of rubber phase; the subscripts "b", "r" and "c" represent the bitumen phase, rubber phase, and CRMB composite respectively. Considering the relationship between $\langle \boldsymbol{\sigma} \rangle_c$ and $\langle \boldsymbol{\varepsilon} \rangle_c$, the effective stiffness tensor of the composite $\mathbf{C}_c$ can be defined as

$$\langle \boldsymbol{\sigma} \rangle_c = \mathbf{C}_c : \langle \boldsymbol{\varepsilon} \rangle_c \tag{7.5}$$

By substituting Equations (7.1), (7.2) and (7.3) into Equation (7.5), the stiffness tensor of the composite can be related to the stiffness tensors of each phase by:

$$\mathbf{C}_c : \langle \boldsymbol{\varepsilon} \rangle_c = (1 - \phi)\mathbf{C}_b : \langle \boldsymbol{\varepsilon} \rangle_b + \phi \mathbf{C}_r : \langle \boldsymbol{\varepsilon} \rangle_r \tag{7.6}$$

If the volume fraction and stiffness tensor of each phase are known, to calculate the effective stiffness tensor, a strain localization tensor $\mathbf{A}$ needs to be introduced to relate the homogenized strain tensor to the local strain tensor of a phase as shown in Equations (7.7) and (7.8).

$$\langle \boldsymbol{\varepsilon} \rangle_b = \mathbf{A}_b : \langle \boldsymbol{\varepsilon} \rangle_c \tag{7.7}$$

$$\langle \boldsymbol{\varepsilon} \rangle_r = \mathbf{A}_r : \langle \boldsymbol{\varepsilon} \rangle_c \tag{7.8}$$

Therefore, the value of $\mathbf{C}_c$ can be further derived by combining Equations (7.6), (7.7) and (7.8) as

$$\mathbf{C}_c = (1 - \phi)\mathbf{C}_b : \mathbf{A}_b + \phi \mathbf{C}_r : \mathbf{A}_r \tag{7.9}$$

It is easy to find the strain localization tensor of each phase having the following relationship with the corresponding volume fraction:

$$(1 - \phi)\mathbf{A}_b + \phi\mathbf{A}_r = \mathbf{I} \tag{7.10}$$

where $\mathbf{I}$ or I_{ijkl} is the unit fourth-order tensor. In general, the volume fractions (ϕ) and mechanical properties of the constituents ($\mathbf{C}_r$ and $\mathbf{C}_b$) are available or can be obtained through laboratory tests. The key point of the homogenization process is to obtain the strain localization tensor that once known, the effective stiffness tensor of the composite $\mathbf{C}_c$ can be calculated by combining Equations (7.9) to (7.10) as

$$\mathbf{C}_c = \mathbf{C}_b + \phi(\mathbf{C}_r - \mathbf{C}_b){:}\mathbf{A}_r \tag{7.11}$$

Various micromechanical models were developed to calculate the localization tensor $\mathbf{A}_r$ based on Eshelby's pioneering work on elastic solutions for a spherical or elliptical inclusion being embedded in an infinite matrix as shown in Figure 7.3 (Eshelby 1957, Eshelby 1959). The essence of Eshelby's equivalent inclusion method is that the particle–matrix heterogeneous domain is transferred to a homogeneous domain same as the matrix material but with an eigenstrain acting in the particle phase to represent inhomogeneity. By using the equivalent inclusion idea, Eshelby solved the inhomogeneity problem by relating the strain of the inclusion $\langle \boldsymbol{\varepsilon} \rangle_r$ and the strain at infinity $\langle \boldsymbol{\varepsilon} \rangle_0$ as Equation (7.12)

$$\langle \boldsymbol{\varepsilon} \rangle_r = \mathbf{A}_r{:}\langle \boldsymbol{\varepsilon} \rangle_0 \tag{7.12}$$

with

$$\mathbf{A}_r = [\mathbf{I} + \mathbf{S}_b{:}(\mathbf{C}_b)^{-1}{:}(\mathbf{C}_r - \mathbf{C}_b)]^{-1} \tag{7.13}$$

where $\mathbf{S}_b$ is known as the Eshelby's fourth-order tensor. It is a function of both the mechanical properties of the matrix and the mechanical and geometrical properties of the inclusion. Assuming matrix and inclusions as isotropic materials and spherical inclusions, $\mathbf{S}_b$ is calculated as

$$\mathbf{S}_b = \frac{3K_b}{3K_b + 4G_b}\mathbf{I}^{\mathrm{v}} + \frac{6(K_b + 2G_b)}{5(3K_b + 4G_b)}\mathbf{I}^{\mathrm{d}} \tag{7.14}$$

with

$$\mathrm{I}_{ijkl}^{\mathrm{v}} = \frac{1}{3}\delta_{ij}\delta_{kl}; \ \mathrm{I}_{ijkl}^{\mathrm{d}} = \frac{1}{2}\left(\delta_{ik}\delta_{jl} + \delta_{il}\delta_{jk}\right) - \frac{1}{3}\delta_{ij}\delta_{kl} \tag{7.15}$$

where K_b and G_b are the bulk modulus and shear modulus of the bitumen matrix, respectively; $\mathbf{I}^{\mathrm{v}}$ and $\mathbf{I}^{\mathrm{d}}$ are the volumetric part and the deviatoric part of the four-order tensor, respectively. δ_{ij} is the Kronecker's delta. For isotropic masterials, the stiffness tensor for each material phase can be written in terms of bulk modulus and shear modulus. Using the two isotropic tensors $\mathbf{I}^{\mathrm{v}}$ and $\mathbf{I}^{\mathrm{d}}$, the stiffness tensor can be written as

$$\mathbf{C}_b = 3K_b\mathbf{I}^{\mathrm{v}} + 2G_b\mathbf{I}^{\mathrm{d}} \tag{7.16}$$

$$\mathbf{C}_r = 3K_r\mathbf{I}^{\mathrm{v}} + 2G_r\mathbf{I}^{\mathrm{d}} \tag{7.17}$$

$$\mathbf{C}_c = 3K_c\mathbf{I}^{\mathrm{v}} + 2G_c\mathbf{I}^{\mathrm{d}} \tag{7.18}$$

where K and G are the bulk modulus and shear modulus of the material, respectively. The elastic theory used here can be extended to viscoelastic materials according to the elastic-viscoelastic correspondence principle (Hashin 1970). The following sections will introduce four commonly used micromechanical models (Yin *et al.* 2008) in the context of the CRMB composite system.

$\langle \boldsymbol{\varepsilon} \rangle_0$

Infinite bitumen matrix

$\mathbf{C}_r, \langle \boldsymbol{\varepsilon} \rangle_r$ Rubber inclusion

$\mathbf{C}_b$
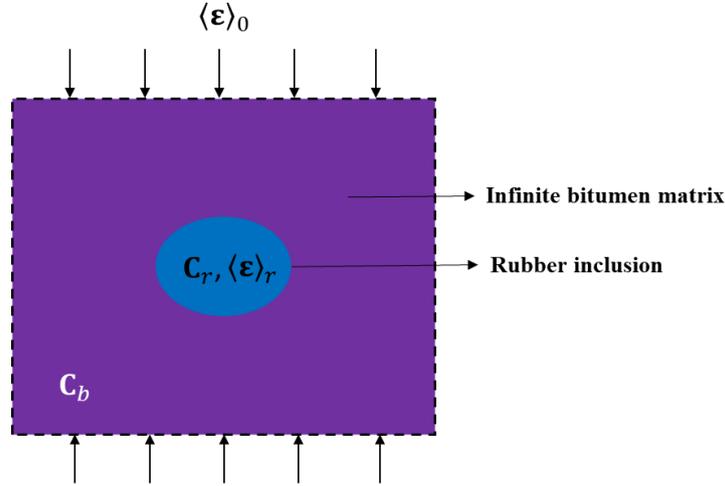
Figure 7.3 Schematic representation of Eshelby's inhomogeneity problem in two-dimension.

7.3.2 Dilute model

In the dilute model (DM) (Eshelby 1957), particles are embedded in an infinite matrix that the particle interactions can be disregarded due to the dilute distribution of particles. The strain localization tensor of rubber can be directly obtained from the Eshelby's solution:

$$\mathbf{A}_r{}^{\mathrm{DM}} = [\mathbf{I} + \mathbf{S}_b : (\mathbf{C}_b)^{-1} : (\mathbf{C}_r - \mathbf{C}_b)]^{-1} \tag{7.19}$$

where $\mathbf{S}_b$ is the Eshelby's tensor obtained from the properties of the bitumen matrix and rubber inclusion. With the known parameters of $\mathbf{S}_b$, $\mathbf{C}_b$, and $\mathbf{C}_r$ defined in Equations (7.14), (7.16) and (7.17) respectively, the expression of $\mathbf{A}_r{}^{\mathrm{DM}}$ can be easily derived. As pointed out earlier, the critical step of the homogenization process is to obtain the strain localization tensor that once known, the effective stiffness tensor of the composite $\mathbf{C}_c$ can be calculated using Equation (7.11). Assuming both phases are isotropic and the inclusions are spherical, the effective bulk modulus and shear modulus of the composite can be written as follows by combining Equations (7.14) and (7.15). The detailed derivation steps can be found in Appendix I.

$$K_c = K_b + \frac{\phi(K_r - K_b)(3K_b + 4G_b)}{3K_r + 4G_b} \tag{7.20}$$

$$G_c = G_b + \frac{5\phi G_b(G_r - G_b)(3K_b + 4G_b)}{3K_b(2G_r + 3G_b) + 4G_b(3G_r + 2G_b)} \tag{7.21}$$

The Dilute model is only suitable for composites with small volume fractions of inclusions in which the interaction between stress/strain fields disturbed by different inclusion particles (known as "inter-particle interaction") was neglected.

7.3.3 Mori-Tanaka model

In the Mori-Tanaka model (MTM), each particle is embedded in a matrix with a uniform strain the same as the average strain of the matrix, Figure 7.4 (Mori and Tanaka 1973). Therefore, the interactions between inclusions are considered. The strain localization tensor of rubber can be calculated from the Eshelby's solution:

$$\mathbf{A}_r{}^{MT} = \mathbf{A}_r{}^{DM} : \left[(1 - \phi)\mathbf{I} + \phi \mathbf{A}_r{}^{DM} \right]^{-1} \tag{7.22}$$

Correspondingly, assuming both phases are isotropic and the inclusions are spherical, the effective bulk modulus and shear modulus of the composite can be calculated as

$$K_c = K_b + \frac{\phi(K_r - K_b)(3K_b + 4G_b)}{3K_b + 4G_b + 3(1 - \phi)(K_r - K_b)} \tag{7.23}$$

$$G_c = G_b + \frac{5\phi G_b(G_r - G_b)(3K_b + 4G_b)}{5G_b(3K_b + 4G_b) + 6(1 - \phi)(G_r - G_b)(K_b + 2G_b)} \tag{7.24}$$

$\langle \boldsymbol{\varepsilon} \rangle_b$
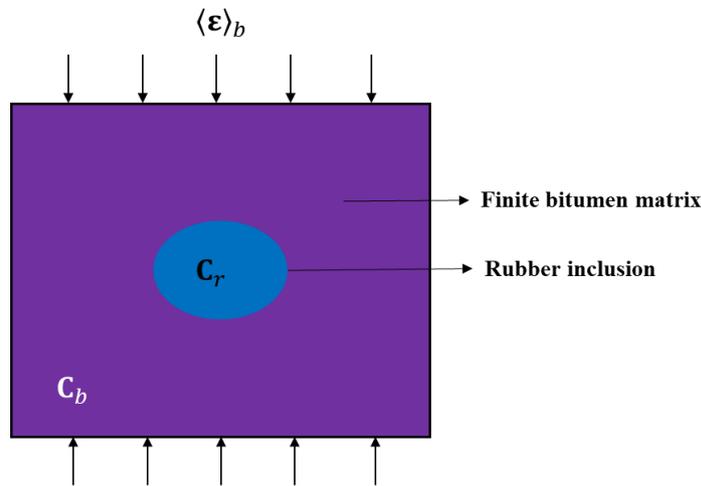
Figure 7.4 Schematic illustration for the M-T model.

7.3.4 Self-consistent model

The self-consistent scheme was proposed to improve the prediction accuracy by considering the interparticle interactions. In the self-consistent model (SCM), each inclusion is assumed to be embedded in an infinite homogenous medium whose mechanical properties are the same as the composite as shown in Figure 7.5 (Hill 1965). The strain localization tensor of rubber is expressed as:

$$\mathbf{A}_r{}^{SC} = [\mathbf{I} + \mathbf{S}_c : (\mathbf{C}_c)^{-1} : (\mathbf{C}_r - \mathbf{C}_c)]^{-1} \tag{7.25}$$

where $\mathbf{S}_c$ is the Eshelby's tensor obtained from the properties of CRMB composite. It is noted that the effective stiffness tensor $\mathbf{C}_c$ is implicitly given when calculating it. Therefore, it needs to be solved using a recursive method by assuming an initial value equal to that of the matrix. Regarding isotropic phases and spherical inclusions, the effective bulk modulus and shear modulus of the composite can be solved as

$$K_c = K_b + \frac{\phi(K_r - K_b)(3K_c + 4G_c)}{3K_r + 4G_c} \tag{7.26}$$

$$G_c = G_b + \frac{5\phi G_c(G_r - G_b)(3K_c + 4G_c)}{3K_c(3G_c + 2G_r) + 4G_c(2G_c + 3G_r)} \tag{7.27}$$
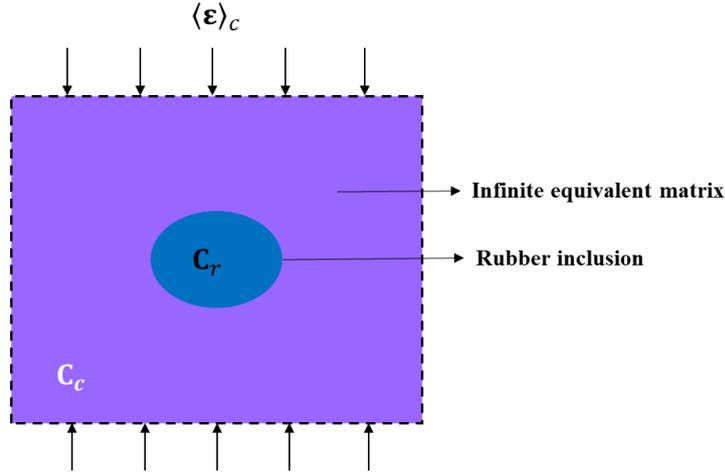
Figure 7.5 Schematic illustration for the SC model

7.3.5 General self-consistent model

The general self-consistent model (GSCM) assumes a spherical particle embedded in a spherical annulus of the matrix material, which in turn is embedded in an infinite medium with the effective mechanical properties of the composite (Figure 7.6). The effective bulk modulus of the composite can be calculated by Equation (7.28). The effective shear modulus of the composite follows a quadratic equation (Equation (7.29)).

$$K_c = K_b + \frac{\phi(K_r - K_b)(3K_b + 4G_b)}{3K_b + 4G_b + 3\phi(K_r - K_b)} \tag{7.28}$$

$$A\left(\frac{G_c}{G_b}\right)^2 + B\left(\frac{G_c}{G_b}\right) + C = 0 \tag{7.29}$$

Coefficients A, B, and C are related to the mechanical properties and volume fraction of each phase. The detailed formulations of these parameters are as follows (Christensen and Lo 1979).

$$\begin{aligned}
A = {} & 8\left(\frac{G_r}{G_b} - 1\right)(4 - 5v_b)\eta_1\phi^{\frac{10}{3}} - 2\left[63\left(\frac{G_r}{G_b} - 1\right)\eta_2 + 2\eta_1\eta_3\right]\phi^{\frac{7}{3}} + 252\left(\frac{G_r}{G_b} - 1\right)\eta_2\phi^{\frac{5}{3}} \\
& - 25\left(\frac{G_r}{G_b} - 1\right)(7 - 12v_b + 8v_b{}^2)\eta_2\phi + 4(7 - 10v_b)\eta_2\eta_3
\end{aligned} \tag{7.30}$$

$$\begin{aligned}
B = {} & -4\left(\frac{G_r}{G_b} - 1\right)(1 - 5v_b)\eta_1\phi^{\frac{10}{3}} + 4\left[63\left(\frac{G_r}{G_b} - 1\right)\eta_2 + 2\eta_1\eta_3\right]\phi^{\frac{7}{3}} - 504\left(\frac{G_r}{G_b} - 1\right)\eta_2\phi^{\frac{5}{3}} \\
& + 150\left(\frac{G_r}{G_b} - 1\right)(3 - v_b)v_b\eta_2\phi + 3(15v_b - 7)\eta_2\eta_3
\end{aligned} \tag{7.31}$$

$$\begin{aligned}
C = {} & 4\left(\frac{G_r}{G_b} - 1\right)(5v_b - 7)\eta_1\phi^{\frac{10}{3}} - 2\left[63\left(\frac{G_r}{G_b} - 1\right)\eta_2 + 2\eta_1\eta_3\right]\phi^{\frac{7}{3}} + 252\left(\frac{G_r}{G_b} - 1\right)\eta_2\phi^{\frac{5}{3}} \\
& + 25\left(\frac{G_r}{G_b} - 1\right)(v_b{}^2 - 7)\eta_2\phi - (5v_b + 7)\eta_2\eta_3
\end{aligned} \tag{7.32}$$

in which

$$\eta_1 = \left(\frac{G_r}{G_b} - 1\right)(49 - 50v_b v_r) + 35\frac{G_r}{G_b}(v_r - 2v_b) + 35(2v_r - v_b) \tag{7.33}$$

$$\eta_2 = 5v_r\left(\frac{G_r}{G_b} - 8\right) + 7(G_r + G_b + 4) \tag{7.34}$$

$$\eta_3 = \frac{G_r}{G_b}(8 - 5v_b) + (7 - 5v_b) \tag{7.35}$$

where G_b and G_r are the shear modulus of the bitumen matrix and rubber inclusion, respectively. v_b and v_r are the Poisson's ratio of the bitumen matrix and rubber inclusion, respectively.
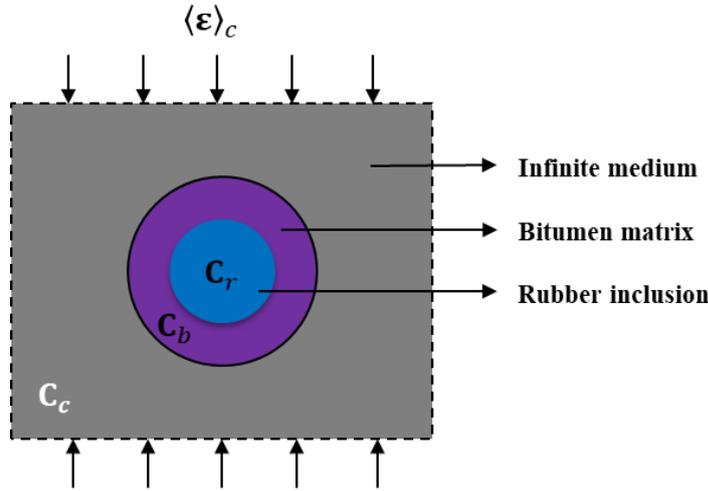
Figure 7.6 Schematic illustration for the GSC model

7.3.6 (n+1)-phase model

The GSC model was further generalized to the (n+1)-phase model by accounting for the inclusions coated with an indefinite number of layers (Figure 7.7). In the (n+1)-phase model, an n-layered spherical inclusion surrounded by the matrix material (phase n) is embedded in an infinite medium (Herve and Zaoui 1993). Phase 1 with a radius of R_1 constitutes the central core while phase r lying within the shell is limited by the spheres with radii of R_{r-1} and R_r. The effective shear modulus of the composite using the (n+1)-phase model can also be solved by a quadratic equation as Equation (7.29). The corresponding coefficients are related to the mechanical properties (e.g., Poisson's ratio) and volume fraction of each phase.

The (n+1)-phase model is generally utilized when additional phases are required to be modeled between the inclusion and the matrix. For instance, the additional phase can be an actual coating material for the inclusion or the inclusion has a multilayered structure due to the physiochemical interactions between different phases. As discussed in the previous chapters, swelling of rubber particles in bitumen results in a multilayered structure of the swollen rubber particles before reaching the equilibrium state (Wang *et al.* 2020a). Intuitively, the different layers with the rubber particles have different mechanical properties where the outer layer is softer than the inner layer due to the ingression of bitumen components. In the current model, phase n is the bitumen matrix while phase 1 to r are the multilayers of swollen rubber particles. Therefore, the (n+1)-phase model may be a good alternative to model the mechanical behaviors of CRMB, which was tried in the second-stage study.
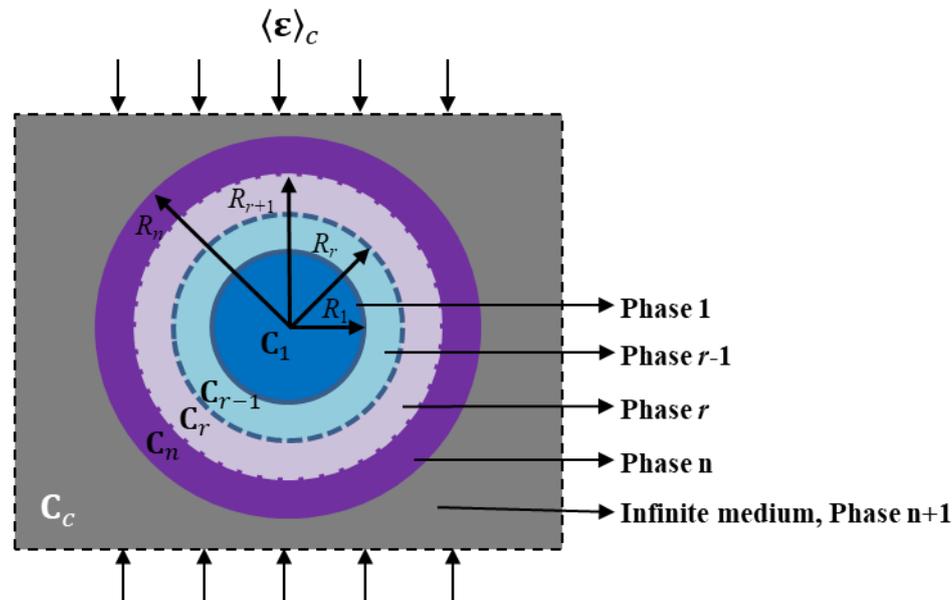
Figure 7.7 Schematic illustration for the (n+1)-phase model.

7.4 Determination of input parameters from tests

7.4.1 Input parameters for micromechanical models

The CRMB binders were produced in the laboratory by blending different percentages of CRMs with base bitumen at 180 °C for 30 minutes according to the mixing procedure in Chapter 5. Four CRM contents including 5%, 10%, 15% and 22 % by mass of base bitumen were used. These CRMBs were labeled as CRMB-5, CRMB-10, CRMB-15, and CRMB-22. As described in the previous section, to effectively predict the mechanical properties of CRMB with micromechanical models, the mechanical properties of both bitumen matrix and rubber inclusion are required. In addition, the volume fraction of each phase also needs to be determined.

Since the nature of both bitumen and rubber phases changed after the bitumen-rubber interaction, it is of vital importance to measure the representative rheological properties of actual bitumen matrix and rubber inclusion in the CRMB system. Dedicated laboratory tests were performed to obtain these input parameters. The effective volume fraction of rubber after swelling was determined by the finite element method. The Poisson's ratios of rubber phase and bitumen phase were assumed to be 0.45 and 0.49, respectively (Aurangzeb *et al.* 2016).

7.4.2 Extraction of liquid phase of CRMB

To obtain the mechanical properties of the bitumen matrices of CRMB binders, the liquid phase of CRMB was extracted by removing the insoluble CRM particles from the bitumen matrix. In this regard, the required amount of fresh CRMB binders was heated to 165 °C and drained through a mesh sieve (0.063 mm) in the oven at 165°C for 20 min (Wang *et al.* 2018a). To allow for a fast and uniform filtration, the heated CRMB samples were manually flattened on the mesh before the drainage. The residual (drained) binder designated as CRMB-X-LP (X represents the rubber content) was collected on an aluminum pan. The extracted liquid phase was stored in the refrigerator immediately to prevent any unwanted aging or reaction and was subjected to DSR testing later.

7.4.3 Preparation of swollen rubber sample

The cylindrical rubber samples were cut from waste truck tires as shown in Figure 7.8. A uniform rubber slice of 2 mm thickness was cut from the tire tread (metal fiber-free) using the water jet cutting technology. Then, laser cutting was applied on the slice to obtain the rubber cylinders with a diameter of 8 mm. These cylindrical rubber samples (2 mm-thickness and 8 mm-diameter) were subjected to the swelling test at 180 °C for 36 h. Based on previous studies (Wang *et al.* 2020b), the rubber sample is believed to reach the swelling equilibrium after 36 h immersion in the hot bitumen at 180 °C. The swollen rubber samples were cleaned from bitumen by wiping with absorbent paper while hot and brushing for a few seconds with cold trichloroethylene gently. All the samples were brushed until there were no significant bitumen imprints left on the white absorbent paper. Through this process, the sample consistency was controlled. The obtained swollen rubber sample is a gel-like material with light-fractions inside the rubber network. Since the geometry of cylindrical rubber samples changed after swelling, a special drill tool with an inner diameter of 8 mm was used to trim the swollen sample into the desired diameter. A fast punching force was applied on top of the drill to minimize the creep deformation of swollen rubber samples at room temperature. This is because if pressing the drill slowly, a truncated cone-like sample will be produced instead of a cylindrical one. No absorbed bitumen was squeezed out of rubber. DSR tests were performed on both dry (unswollen) and swollen rubber samples.
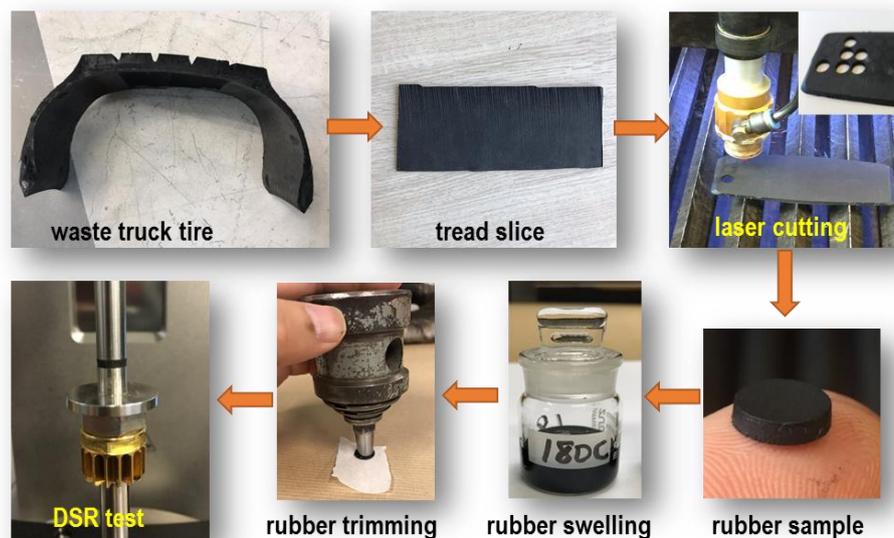
Figure 7.8 Preparation of cylindrical dry rubber and swollen rubber samples.

7.4.4 Dynamic Shear Rheometer test to obtain rheological parameters

A dynamic shear rheometer (Anton Paar) was utilized to obtain the rheological parameters (complex shear modulus and phase angle) of both binder samples and rubber samples following the standard test method. Frequency sweep tests of CRMB and liquid phase binder samples were carried out with a parallel-plate geometry (25 mm diameter and 1 mm gap) from 0.1 to 100 rad/s at temperatures of 10, 30, 50 and 70 °C. Before the frequency sweep tests, strain amplitude sweep tests were conducted to identify the linear viscoelastic (LVE) range and all the measurements were carried out at a strain level of 0.1% under strain-controlled mode.

The rheological and mechanical properties of rubber before and after swelling were tested by DSR using the 8-mm parallel plates. The unreacted (dry) cylindrical rubber sample can be directly placed between the parallel plates of the DSR. Before the placement, a special glue was applied on the surface of the bottom plate and the top surface of the rubber sample to achieve a proper bonding between rubber and plates. Due to the good adhesion between the plates and swollen rubber, no glue was used. For both dry and swollen rubber samples, a manual adjustment was applied to the gap between the plates until the normal force is close to zero. Frequency sweep tests of rubber samples were performed from 0.1 to 100 rad/s over a temperature range of -10~130 °C with an increment of 20 °C. According to previous study, the measurements were carried out at a strain level of 1% under strain-controlled mode (Zegard *et al.* 2016). The viscoelastic parameters (complex modulus and phase angle) of each sample were collected and analyzed.

7.5 Input parameters for micromechanical models

7.5.1 Constitutive modelling of linear viscoelasticity

After obtaining the rheological properties of bitumen matrix and rubber inclusion through DSR tests, time temperature superposition principle was applied to build their master curves of LVE properties in terms of complex modulus and phase angle at a particular reference temperature. The master curves can be constitutively modelled by mathematical models and mechanical element models. Many empirical algebraic equations have been developed to describe the viscoelastic behavior of bituminous materials, such as Christensen and Anderson (CA) model, Christensen, Anderson and Marasteanu (CAM) model, polynomial model, Sigmoidal model, generalized logistic sigmoidal model, etc. (Yusoff *et al.* 2011). Although mathematical model parameters can be adjusted to fit the experimental data well, they usually lack fundamental physical implications. By contrast, mechanical models represented by a combination of mechanical analogies (i.e., springs and dashpots) are established through vigorous derivations and can be related to the microstructural features of materials.

Typical mechanical element models include Maxwell model, Kelvin model, standard linear solid model, Burgers model, generalized Maxwell model and generalized Kelvin model, etc. (Yusoff *et al.* 2011). With increased number of model elements, generalized Maxwell model can achieve ideal results in simulating rheological behaviors of viscoelastic liquid-type materials. Generalized Kelvin model is more suitable for simulating viscoelastic solid-type materials. However, with the increase of the number of mechanical elements, the computational efforts in the analysis process will increase significantly (Park and Schapery 1999). Therefore, to reduce the number of parameters involved, the so-called variable or parabolic dashpot was introduced to replace the linear dashpot to formulate the fractional-order mechanical models. The mechanical response characteristic of the parabolic element is in between those of the linear spring and linear dashpot as shown in Figure 7.9a (Olard and Di Benedetto 2003). The addition of the parabolic element not only improves the ability to describe the LVE properties, but also provides a continuous spectrum. With the aid of the parabolic element, several classic models were developed in the past several decades to describe the LVE properties of bituminous materials, such as Huet model, Huet-Sayegh model and 2S2P1D model, etc. (Wu *et al.* 2018). The arrangement of the mechanical analogies of above fractional models are shown in Figure 7.9.
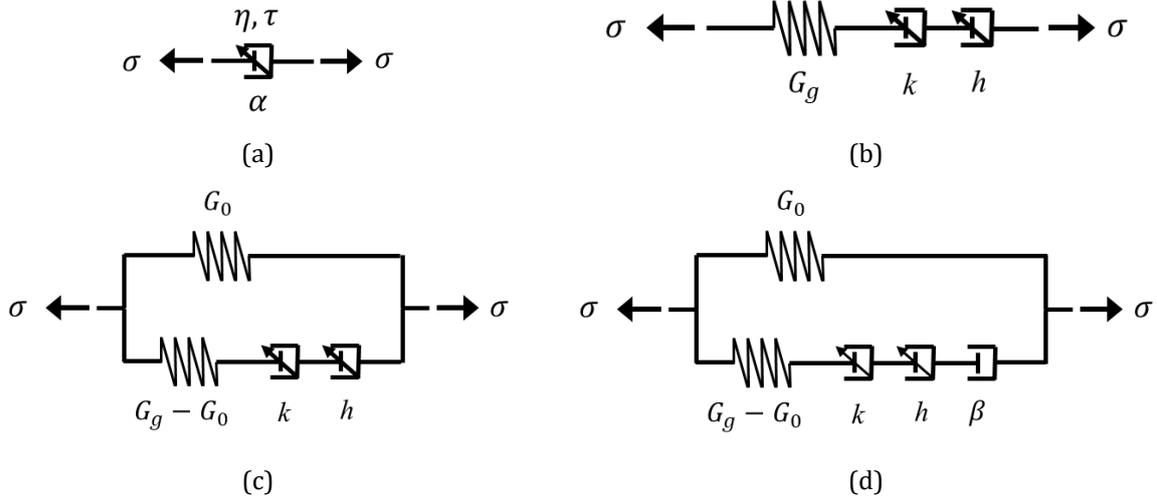
Figure 7.9 Schematic representations of (a) parabolic dashpot (b) Huet model; (c) Huet-Sayegh model; (d) 2S2P1D model.

Huet model consists of a combination of a spring and two parabolic elements (k and h) in series as illustrated in Figure 7.9b. Huet model can be generalized by adding a spring of small rigity in parallel to form Huet-Saygh model. The 2S2P1D model, which stands for two springs, two parabolic elements and one dashpot, is equivalent to append a linear dashpot in line with the parabolic dashpots and spring within the HS model. The analytical expressions of complex modulus of Huet, Huet-Sayegh and 2S2P1D models are shown in Equations (7.36) to (7.38), respectively.

$$G^*(\omega) = \frac{G_g}{1 + \delta(i\omega\tau)^{-k} + (i\omega\tau)^{-h}} \tag{7.36}$$

where G^* is the complex modulus; ω is the angular frequency; G_g is the glassy modulus when $\omega \to \infty$; h, k are exponents such as $1 > h > k > 0$; δ is a dimensionless constant; i is the complex number; τ is the characteristic time, which varies with temperature.

$$G^*(\omega) = G_0 + \frac{G_g - G_0}{1 + \delta(i\omega\tau)^{-k} + (i\omega\tau)^{-h}} \tag{7.37}$$

where G_0 is the static modulus when $\omega \to 0$. Obviously, if the G_0 equals to zero, then the Huet-Sayegh model is identical to the Huet model.

$$G^*(\omega) = G_0 + \frac{G_g - G_0}{1 + \delta(i\omega\tau)^{-k} + (i\omega\tau)^{-h} + (i\omega\beta\tau)^{-1}} \tag{7.38}$$

where $\beta = \eta/(G_g - G_0)\tau$, is a dimensionless constant, which can be used for describing the viscous flow of the material. η is the Newtonian viscosity.

Generally, the complex modulus G^* can be expressed by storage modulus G' and loss modulus G'' as follows:

$$G^*(\omega) = G' + iG'' \tag{7.39}$$

By separating the variables, Equations (7.37) and (7.38) can be converted into a form which is analogous to Equation (7.39) as

$$G^*(\omega) = \left[G_0 + \frac{(G_g - G_0) \times (1 + A)}{(1 + A)^2 + B^2}\right] + \left[\frac{(G_g - G_0) \times (-B)}{(1 + A)^2 + B^2}\right] i \tag{7.40}$$

For the Huet-Sayegh model, variables A and B are defined as below (Pronk 2005):

$$A(\omega) = \delta(\omega\tau)^{-k} \times \cos\left(\frac{k\pi}{2}\right) + (\omega\tau)^{-h} \times \cos\left(\frac{h\pi}{2}\right) \tag{7.41}$$

$$B(\omega) = -\delta(\omega\tau)^{-k} \times \sin\left(\frac{k\pi}{2}\right) - (\omega\tau)^{-h} \times \sin\left(\frac{h\pi}{2}\right) \tag{7.42}$$

For the 2S2P1D model, variable A can be defined as same as that of the Huet-Sayegh model. However, variable B is defined below (Olard and Di Benedetto 2003)

$$B(\omega) = -(\omega\beta\tau)^{-1} - \delta(\omega\tau)^{-k} \times \sin\left(\frac{k\pi}{2}\right) - (\omega\tau)^{-h} \times \sin\left(\frac{h\pi}{2}\right) \tag{7.43}$$

7.5.2 Rheological properties of bitumen matrix and rubber inclusion

7.5.2.1 *Master curves of viscoelasticity*

As mentioned above, the nature of both bitumen and rubber phases changed after the bitumen-rubber interaction. Therefore, it is of vital importance to measure the representative rheological properties of actual bitumen matrix and rubber inclusion in the CRMB system.

In the present study, a modified Christensen-Anderson-Marasteanu (CAM) model and Williams-Landel-Ferry (WLF) equation for shift factors fitting were used to develop complex modulus and phase angle master curves of binders based on the frequency sweep test results (Wang *et al.* 2018b). The complex modulus and phase angle master curves of the liquid phases of CRMB binders, which are considered as the actual bitumen matrices, are presented in Figure 7.10. It can be seen that the liquid phases of CRMB binders are stiffer and more elastic than the neat bitumen as reflected by the increased complex modulus and decreased phase angle. With the increase of rubber content, the improvement of the viscoelasticity of the liquid phase of CRMB is more obvious. At higher rubber content, more light fractions of bitumen were absorbed by rubber particles during the interaction process, which in turn increases the proportions of asphaltenes. The asphaltenes were reported to be primarily responsible for the increase of stiffness and elasticity (Petersen and Glaser 2011). Besides, with the current extraction method, micro rubber particles (smaller than 0.063 mm) may be released into the liquid phase and thus stiffen the liquid phase.
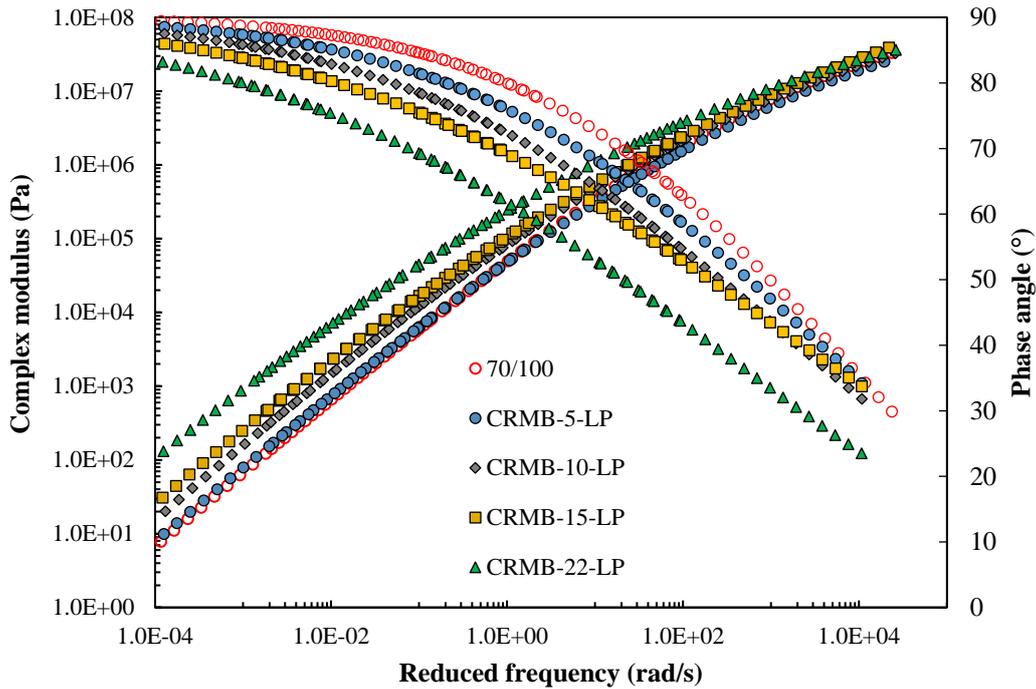
Figure 7.10 Complex modulus and phase angle master curves of bitumen matrices at the reference temperature of 30 °C

From the frequency sweep test data, it was found that rubber is not a rheologically simple material so that common rheological models for bitumen are not suitable for it. Therefore, the master curves were established using a generalized logistic function in Equation (7.44) (Rowe *et al.* 2009) and the WLF equation for shift factors fitting to obtain smooth curves.

$$\log A = \delta + \frac{\alpha}{\left[1 + \lambda e^{(\beta + \gamma(\log \omega))}\right]^{1/\lambda}} \tag{7.44}$$

where A is either complex shear modulus or phase angle. δ is the lower asymptote; α is the difference between the values of upper and lower asymptote; λ, β and γ define the shape between the asymptotes and the location of the inflection point. Based on the time-temperature superposition principle, the master curves of complex modulus and phase angle of dry and swollen rubber samples at a reference temperature of 30 °C were built in Figure 7.11.
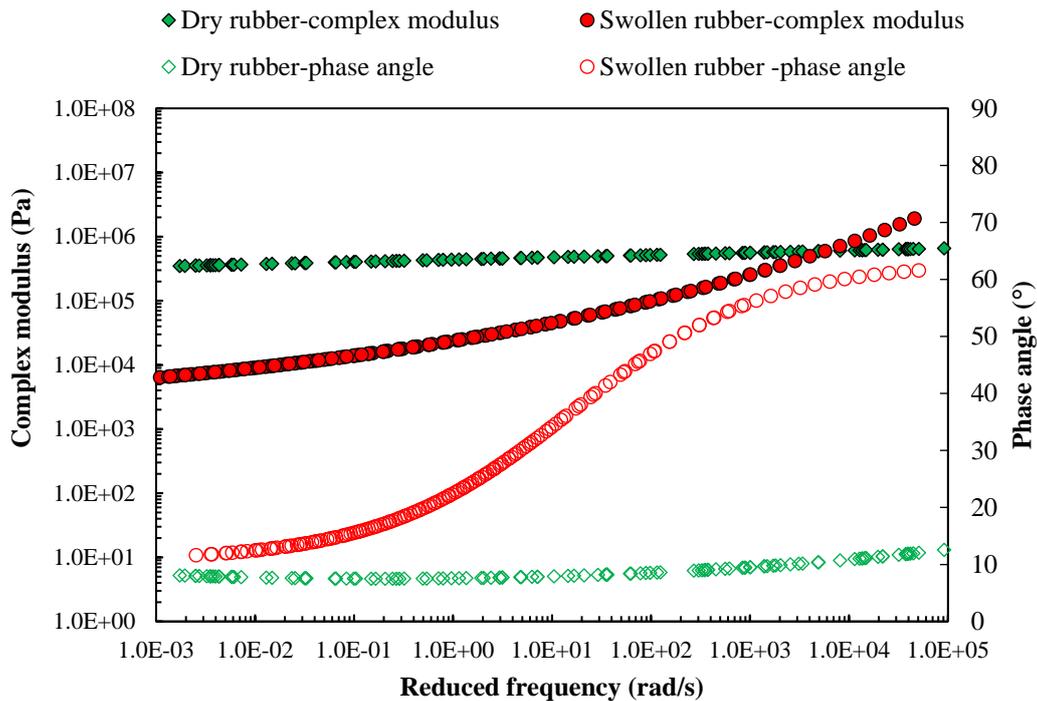
Figure 7.11 Complex modulus and phase angle master curves of rubber inclusions at the reference temperature of 30 °C.

It can be seen that dry rubber exhibits obvious elastic behaviors whose complex modulus and phase angle are almost frequency independent. However, rubber after swelling shows obvious viscoelasticity. It is noteworthy that the phase angles of swollen rubber samples increase with the increase of frequency, which is contradictory to the common behaviors of bitumen. This is the unique nature of rubber polymers. Actually, the phase angle of rubber usually experience an increase stage and then a decrease stage over a large frequency range (Santangelo and Roland 1998). The complex moduli of swollen rubber were lower than the dry rubber in the low-frequency range. At high frequencies, the moduli of them crossed. At the dry state, rubber polymer chains are entangled or crosslinked to each other, forming tightly folded coils, which contributes to the rubber elasticity (Mark 1981). When the rubber polymer chain segments start to absorb bitumen molecules, the folded polymer coils start unfolding, causing the swelling and loosening of the network (Wang *et al.* 2020a). Consequently, this polymer network swelling process will decrease the complex modulus at a macroscopic scale.

From the previous results, it is obvious that the actual bitumen matrix and rubber inclusion are significantly different from the neat bitumen and dry rubber, respectively. It is important to obtain the representative complex modulus data to be served as the input parameters for the micromechanical models in order to have more accurate predictions.

7.5.2.2 *Mechanical constitutive models of bitumen matrix*

As pointed before, the change of the viscoelastic properties of CRMB liquid phase has a strong relationship with the rubber content. Therefore, it is desirable to quantitatively relate the rubber content to the constitutive model parameters of bitumen matrix. Mechanical constitutive models were used to model the viscoelastic behaviors of bitumen matrix since they have fundamental physical meanings. Taking CRMB-22-LP as an example, Figure 7.12 compares the experimental

results with model predictions for both complex modulus and phase angle. The model parameters are summarized in Table 7.1.
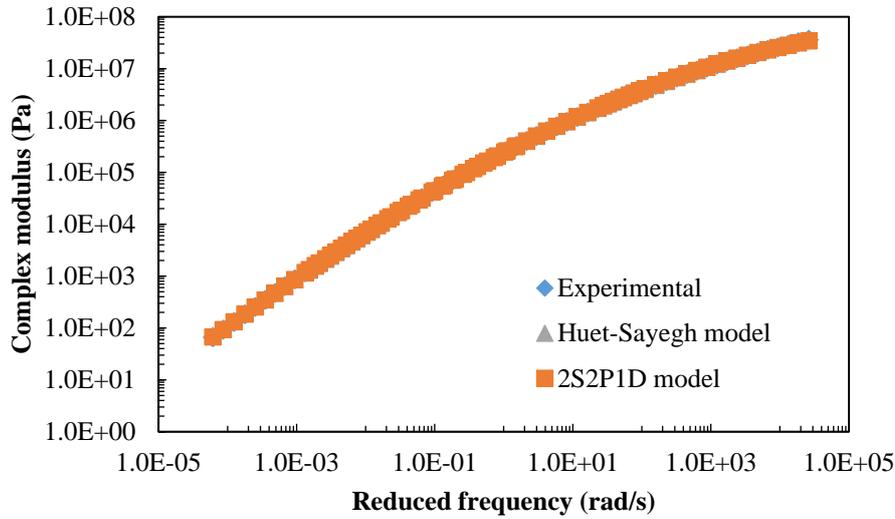
(a)
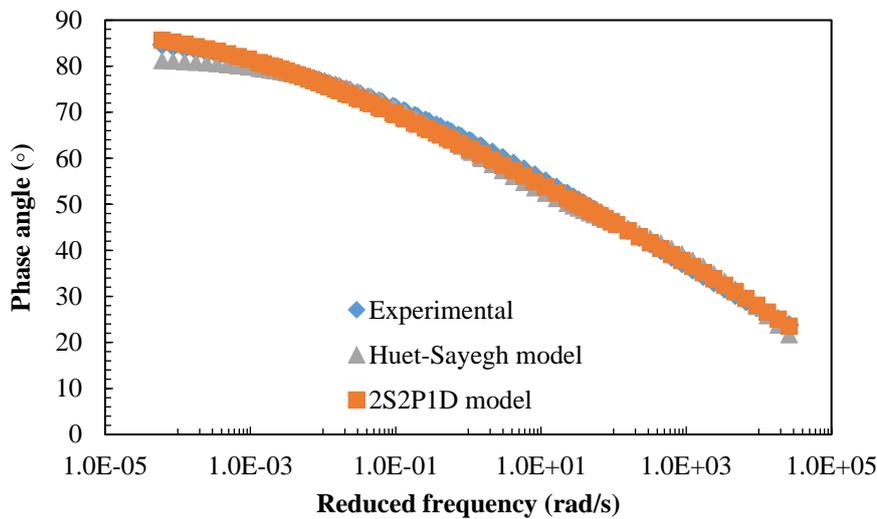
(b)

Figure 7.12 Comparison of Huet-Sayegh model and 2S2P1D model for the rhelogical properties of CRMB-22-LP: (a) complex modulus; (b) phase angle.

Table 7.1 Model parameters for CRMB-22-LP.

Model	G_0 (Pa)	G_g (Pa)	k	h	δ	τ	β	f_{error}
Huet-Sayegh	0	6.29E+07	0.4943	0.9101	10.2923	4.99E-03	-	0.136
2S2P1D	0	8.57E+07	0.3855	0.7018	3.6941	4.30E-04	35.1501	0.035

Only Huet-Sayegh and 2S2P1D models were compared since Huet model is only a special case of Huet-Sayegh model. In the model fitting process, the sum of the squred errors for the storage modulus and loss modulus were minimized as shown in Equation (7.45).

$$f_{error} = \sum_{i=1}^{n} \left[\left(\frac{G'_{m,i}}{G'_{e,i}} - 1 \right)^2 + \left(\frac{G''_{m,i}}{G''_{e,i}} - 1 \right)^2 \right] \tag{7.45}$$

where f_{error} is the sum of the squared errors; $G'_{m,i}$ and $G''_{m,i}$ are storage and loss moduli predicted by the model at the ith frequency, respectively; $G'_{e,i}$ and $G''_{e,i}$ are storage and loss moduli from experiments at the ith frequency, respectively.

As shown in Table 7.1, the values of f_{error} for the 2S2P1D and Huet-Sayegh models are respectively 0.035 and 0.136. From Figure 7.12, it can also be found that 2S2P1D model predicts better than the Huet-Sayegh model, especially at very low frequencies. Huet-Sayegh model has been often reported to describe the rheological properties of asphalt mixtures, while the 2S2P1D can been used for both solid asphalt mixtures and flowable bituminous binders (Yusoff *et al.* 2011). Particularly for binders, for which G_0 equals to zero, Huet-Sayegh model is equivalent to a parabolic dashpot element while 2S2P1D model is equivalent to a linear dashpot element at very low frequencies. Obviously, binders behave like Newtonian fluids at very low frequencies (very high temperatures), for which a linear dashpot is more suitable than the parabolic dashpot to describe their response. This explains why 2S2P1D model has better prediction performance than Huet-Sayegh model.

7.5.2.3 *Relationship between rubber content and model parameters of bitumen matrix*

2S2P1D model was used to model all the bitumen matrices. To further explore the relationship between constitutive model parameters and rubber content, model parameters for each binder were summarized in Table 7.2 and the correlations between 2S2P1D model parameters and rubber content were also presented in Figure 7.13.

Table 7.2 2S2P1D model parameters for CRMB liquid phases.

Binder type	G_0 (Pa)	G_g (Pa)	k	h	δ	τ	β
70/100	0	1.01E+09	0.0001	0.6155	13.5173	4.13E-07	194
CRMB-5-LP	0	8.46E+08	0.0267	0.6211	12.9696	5.13E-07	190
CRMB-10-LP	0	7.67E+08	0.2397	0.6345	7.2144	1.48E-06	150
CRMB-15-LP	0	2.33E+08	0.3101	0.6515	2.5400	1.49E-05	83
CRMB-22-LP	0	8.57E+07	0.3855	0.7018	3.6941	4.30E-04	35

It can be clearly seen from Figure 7.13 that G_g, δ and β decrease with the rubber content, while the other three parameters, τ, k and h, increase with the rubber content.

G_g is the glassy modulus at very high frequencies or very low temperatures. It is known that parameters k and h are related to the fractional/variable dashpot. When k or $h \rightarrow 0$, the fractional dashpot is equal to a linear spring, while when k or $h \rightarrow 1$, the fractional dashpot is equal to a linear dashpot. Parameter τ is the characteristic time, it is an intrinsic time criterion to characterize the viscoelastic behavior of materials. Here, it denotes the retardation time of the parabolic element in 2S2P1D model, which is the time delay for the elastic behavior to occur. Therefore, with these well-correlated relationships between model parameters and rubber content, it is possible to predict the bitumen matrix properties based on the neat bitumen properties and rubber content.

(a)

(b)

(c)

(d)

(e)

(f)
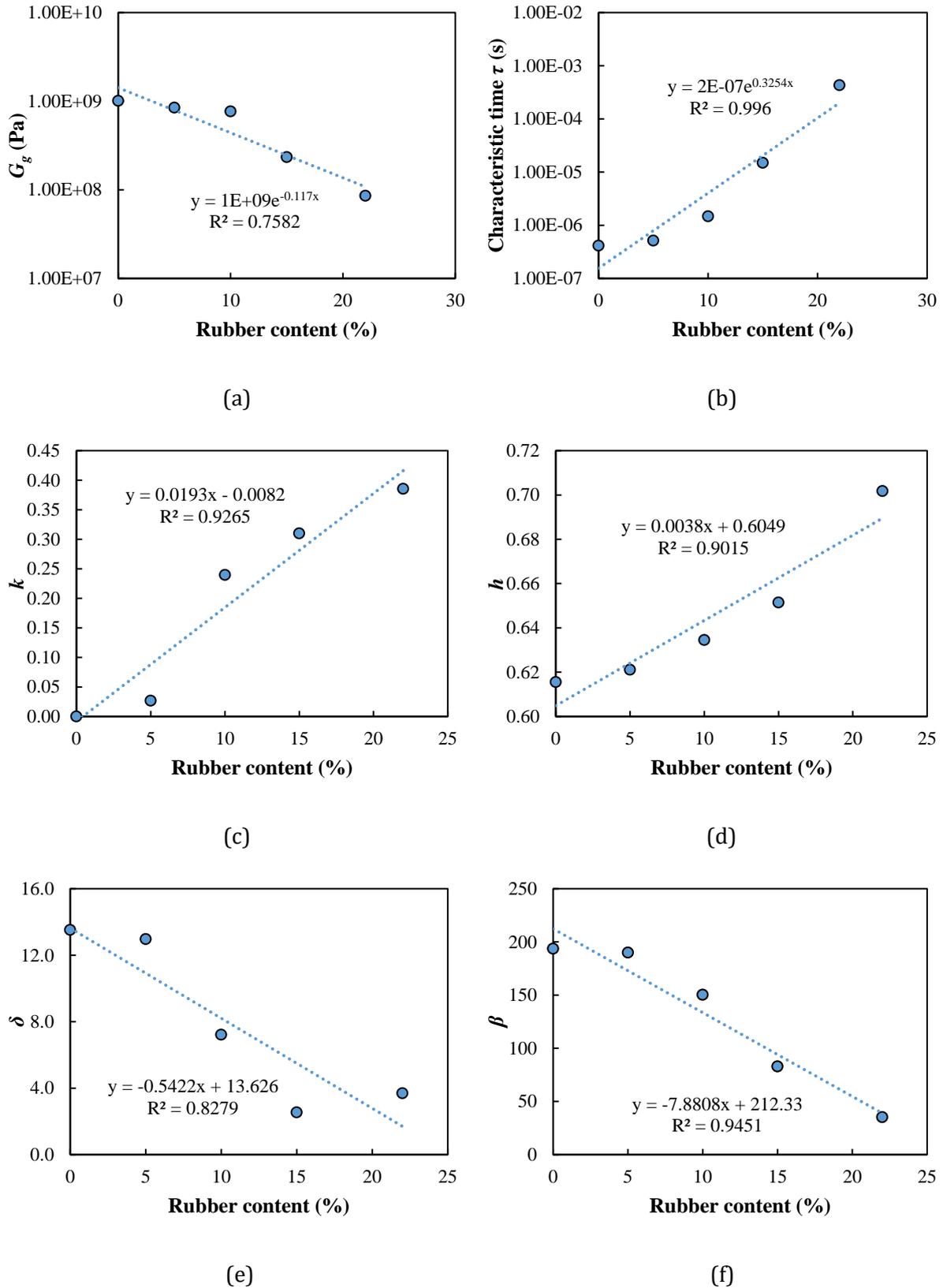
Figure 7.13 Correlation between 2S2P1D model parameters for bitumen matrices and rubber content.

7.5.3 Estimation of effective volume content of rubber in CRMB

An important step in micromechanical modelling is to identify the effective volume content of inclusion to ensure an accurate prediction of mechanical properties. As pointed out by many studies, rubber particles experience volume expansion during the interaction process. How to quantify the precise volume increase remains a challenge. Due to the ambiguity of boundaries between bitumen and rubber phases after interaction in the binder, it is difficult and expensive to use scanning electron microscopy or X-ray computed tomography to evaluate the volume change of rubber particles (Kutay *et al.* 2015). Besides, it is unreasonable to assume a unified swelling ratio for all rubber particles in the binder since rubber particles of different sizes may have different swelling status and thus swelling ratios. Therefore, this study proposed a finite element method to estimate the effective volume content of rubber in CRMB.

A finite element model capable of simulating the multiphysics swelling phenomenon was developed in Chapter 4. It is the diffusion of light fractions of bitumen into rubber polymer network that causes the swelling. The rubber swelling phenomenon essentially consists of mass diffusion and volume expansion (mechanical deformation). The essential theories for mass diffusion and large deformations based on the balance equations driving the solvent diffusion and the force equilibrium, and the constitutive equations for rubber particles were presented in Chapter 4. The above equations were implemented to the finite element model to study the diffusion-induced volume expansion phenomenon of rubber in bitumen. The model can predict the swelling ratio of rubber particles of different sizes given the type of bitumen and rubber as well as the interaction temperature. The simulation results were validated by the experimental results (Wang *et al.* 2019). The following procedures were followed to calculate the effective rubber volume.

- ***Step 1***: Particle size grouping. Based on the gradation of CRM used in this study, the rubber particles were separated into six groups according to the sieve size (Figure 7.14). Since the particle size distribution retained on a sieve usually follows a standard Gaussian distribution, the rubber particles retained on a certain sieve are assumed to have the same size equal to the average size of the passing sieve and retaining sieve. For instance, 7% of rubber particles retained on the 0.5-mm sieve are assumed to have a uniform size of (0.71+0.5)/2=0.605 mm.
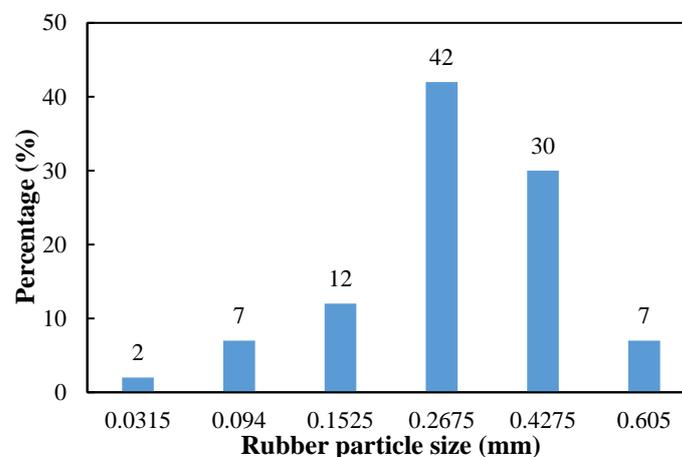
Figure 7.14 The discrete particle size distribution of CRM.

- **Step 2**: Finite element model development. A square two-dimensional domain of 8 × 8 mm meshed with triangular elements was built. Six spherical rubber particles of different sizes in step 1 were embedded in a bitumen matrix as shown in Figure 7.15a. Plane strain conditions were assumed in the lateral mesh directions and no flux was imposed. The initial solvent concentration within the rubber was set as zero, which is the strain-free reference concentration. The periphery boundaries of the rubber particle contacted directly to the bitumen were set to have the same concentration as the surrounding bitumen matrix (Figure 7.15b). Based on the laboratory tests on the materials used in this study, the following model input parameters were used (Wang *et al.* 2020b). The equilibrium swelling concentration is 628.14 kg/m^3. The diffusion coefficient of bitumen into rubber at 180 °C is 3.787 × 10^{-11} m^2/s. The swelling coefficient of rubber at 180 °C is 5.584 × 10^{-4} m^3/kg. The above input parameters were derived from the test results in Chapter 3.

<center>(a)   (b)</center>
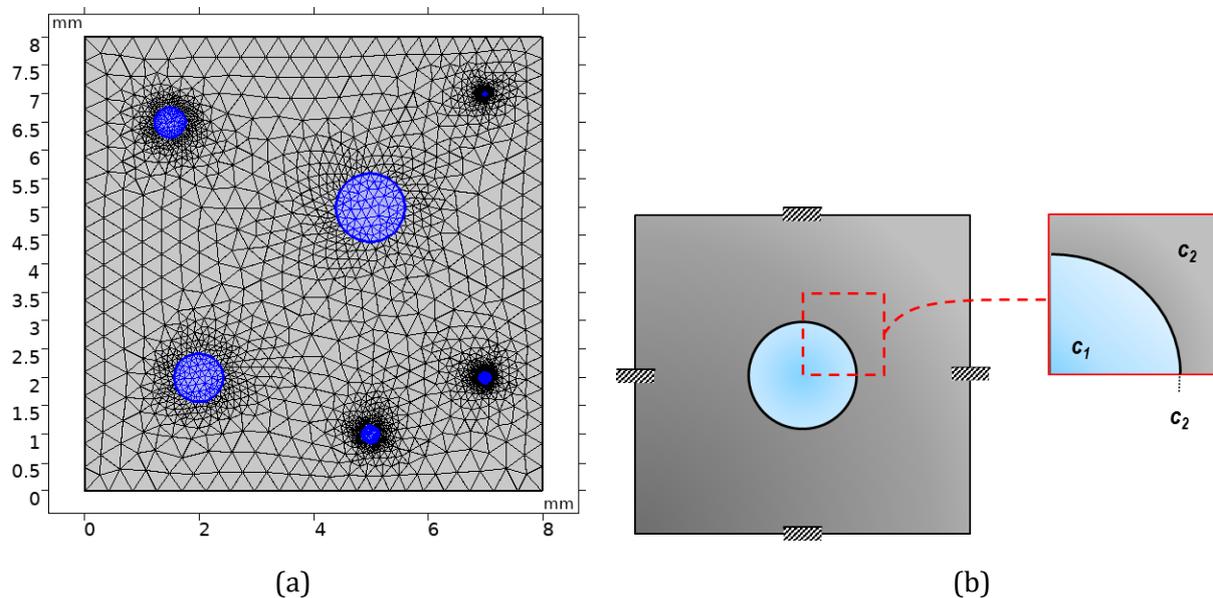
Figure 7.15 (a) Geometry and mesh of the modelling domain: multiple rubber particles of varying sizes; (b) Schematic plot of boundary conditions.

- **Step 3**: Numerical study analysis. The simulation results including the diffusion and deformation fields of swelling of rubber particles with six different sizes at 1800 s (corresponding to the same binder mixing time in the laboratory sample preparation) are presented in Figure 7.16a and Figure 7.16b (COMSOL Multiphysics 2018). It can be seen from the concentration contour that small particles (0.0315, 0.094, 0.1525 and 0.2675 mm) are fully saturated with bitumen molecules while big particles (0.4275 and 0.605 mm) still have a concentration gradient along the direction from outer to inner. The particle size influences the diffusion process and hence the swelling equilibrium.
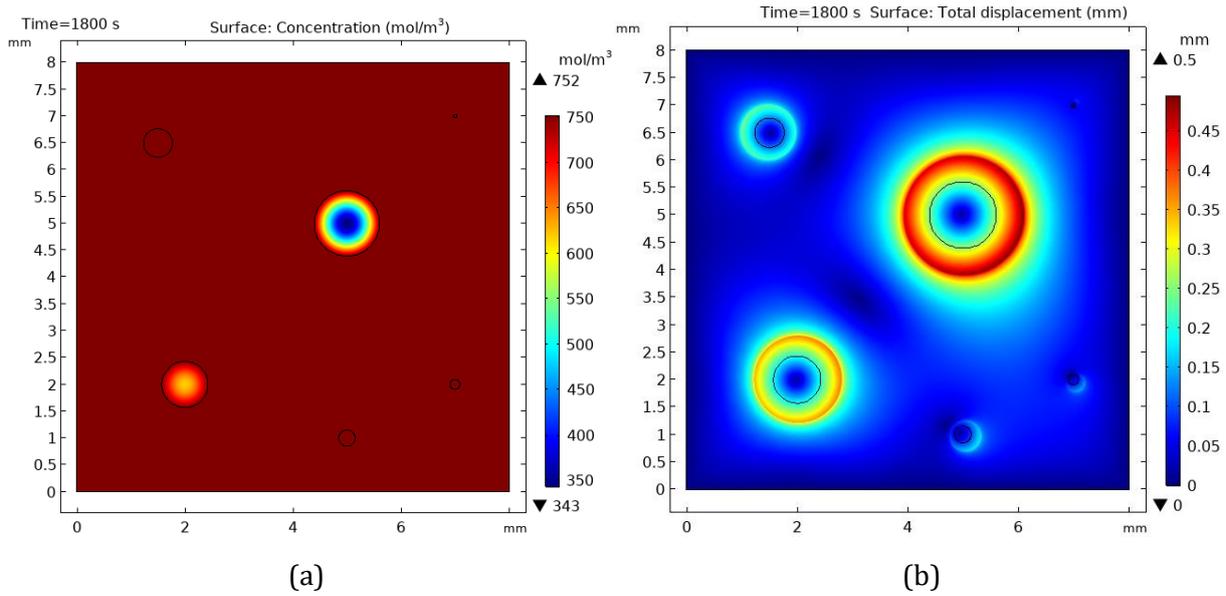
Figure 7.16 Simulation results of rubber swelling in bitumen at 180 °C: (a) concentration and (b) total displacement of rubber particles at t = 1800 s.

- ***Step 4***: Swelling ratio calculation. The black circle in Figure 7.16b represents the original rubber size. Based on the area change of the rubber circle during swelling in the 2D domain, the swelling ratio, defined as the difference between swelling area at time t and the original area (t =0) divided by the original area, was plotted in Figure 7.17. The area of swollen rubber particle was calculated using the surface integral based on the deformed geometry. Swelling of rubber particles occurred faster at the earlier stage and then slowed down. Small particles reached the swelling equilibrium in very short times while it took more time for big particles to reach the equilibrium. The swelling ratios of rubber particles of different sizes at 1800 s were captured from the graph and summarized in Figure 7.18. Combining with the particle size distribution percentage in Figure 7.14, the total effective volume content of rubber V_{eff} can be calculated using the following equation.

$$V_{eff} = \phi \cdot \sum_{i=1}^{n} p_i \cdot s_i \tag{7.46}$$

where ϕ is the original volume fraction of rubber in the binder; p_i is the percentage of the ith particle size group based on the sieve size; s_i is the swelling ratio corresponding to the ith particle size; n is the total number of representative particle size. The original volume contents of rubber in CRMB-5, CRMB-10, CRMB-15, CRMB-22 are calculated as 4.29%, 8.22%, 11.84% and 16.46% respectively based on the densities of bitumen and rubber. The weighted averaged swelling ratio of rubber in CRMB is approximately 2.126. The corresponding effective volume contents of rubber estimated by the above method are 13.40%, 25.69%, 37.02%, and 51.45%, respectively. The estimated volume contents of rubber will be implemented in the micromechanical models in the following section.
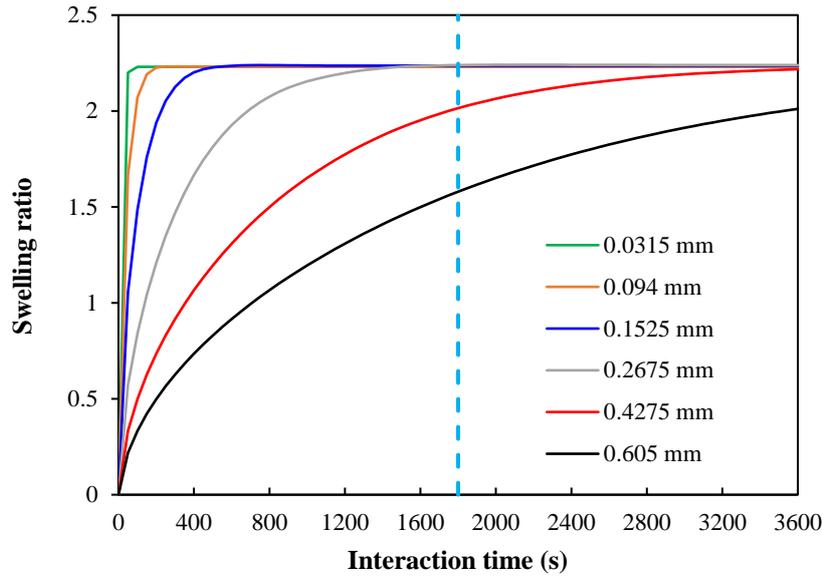
Figure 7.17 Swelling ratio evolution with time of different sized particles.
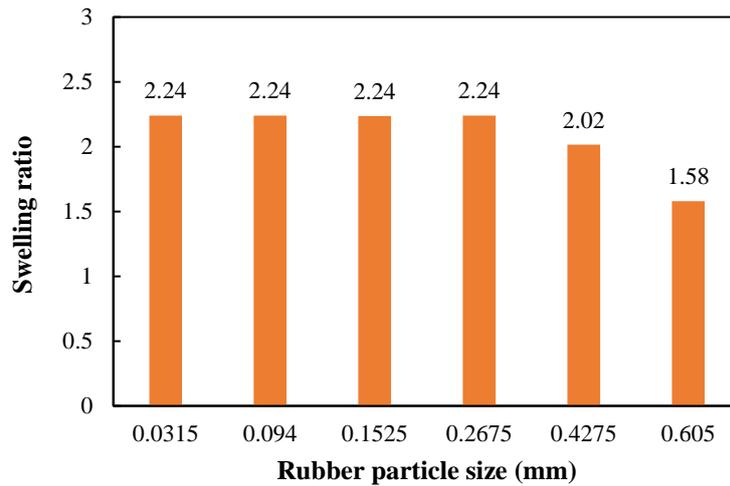
Figure 7.18 The swelling ratios of rubber particles of different sizes at 1800 s.

7.6 Prediction performance of current micromechanical models

7.6.1 Comparison of different micromechanical models

As mentioned before, micromechanical models can predict the mechanical properties of a composite based on mechanical properties and volume fractions of individual constituents. With the obtained complex shear moduli of bitumen matrix and rubber inclusion as well as the effective volume concentration of rubber, the complex shear moduli of CRMB can be predicted using different micromechanical models. The Poisson's ratios of rubber phase and bitumen phase were assumed to be 0.45 and 0.49, respectively (Aurangzeb *et al.* 2016).

For comparison purposes, the predicted complex moduli of CRMB from different micromechanical models using both raw and processed constituent parameters as the inputs are presented in

Figure 7.19 and Figure 7.20 respectively. Raw constituent parameters mean the mechanical properties of neat bitumen and dry rubber, and the initial volume fraction of rubber without considering the swelling effect. Processed constituent parameters mean the mechanical properties of liquid-phase bitumen and swollen rubber and the effective volume fraction of rubber considering the swelling effect. It can be found from Figure 7.18 that most of the rubber particles have reached the swelling equilibrium while for the large rubber particles, a swelling gradient exists from the outer layer to the inner core of rubber. This means a large rubber particle (unsaturated) may not be a uniform continuum. However, for simplicity, all rubber particles here adopted the mechanical properties of the swollen rubber obtained through the DSR tests as the processed input mechanical parameters for the micromechanical models.

(a)   (b)

(c)   (d)
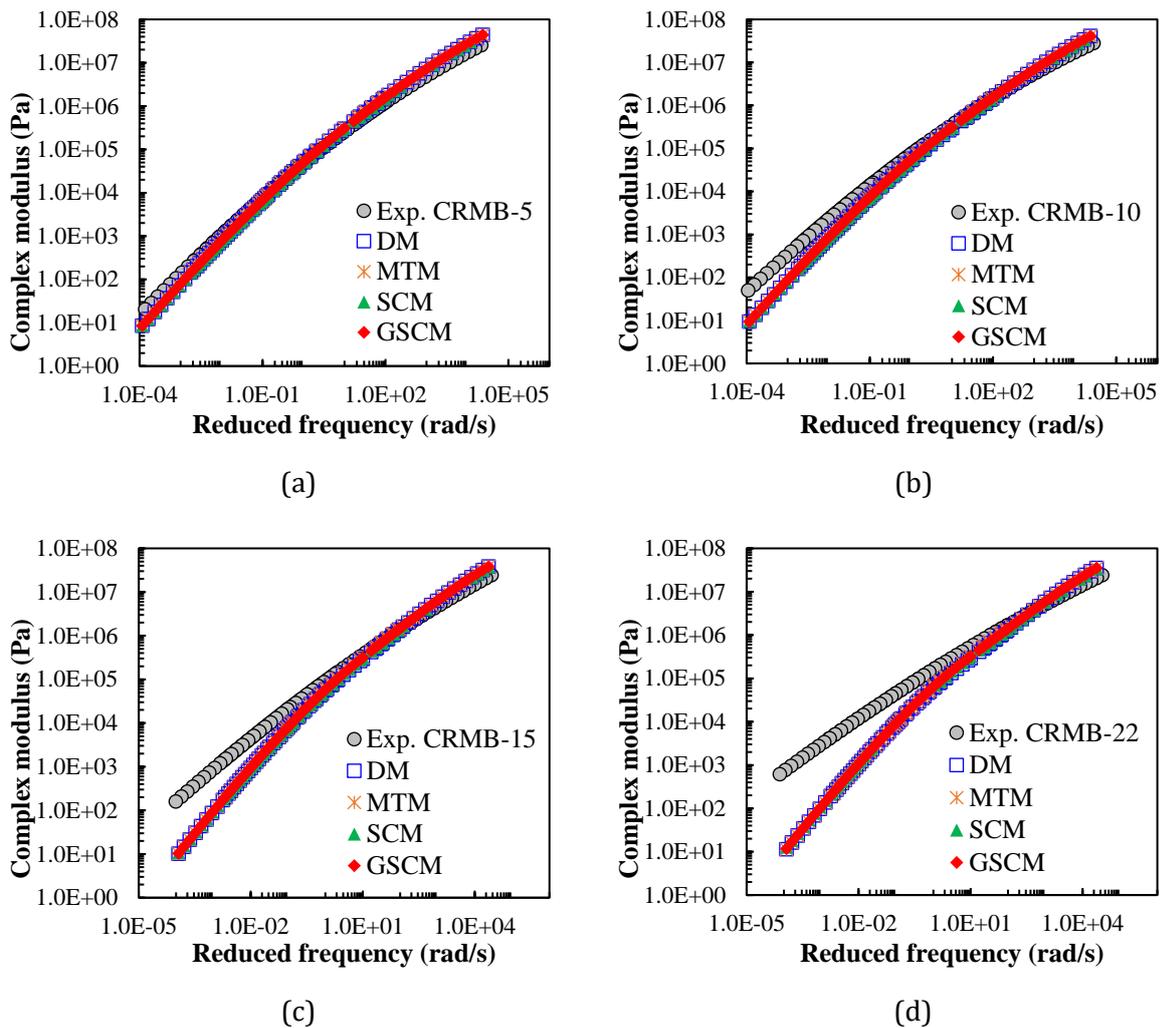
Figure 7.19 Micromechanical model predicted complex moduli of CRMB using the original constituent parameters.

From Figure 7.19, it can be seen that when the volume concentration of rubber is low (CRMB-5 in Figure 7.19a), the predicted complex moduli from models are quite close to the experimental values. This is because the models are more dependent on the matrix properties and the bitumen matrix property was not influenced significantly by rubber at low concentrations. With the increase of rubber concentration, the model predicted results started to deviate from the experimental data. The deviation became more obvious at high concentrations. This essentially

demonstrates that using the original constituent properties will yield biased predictions from the micromechanical models.
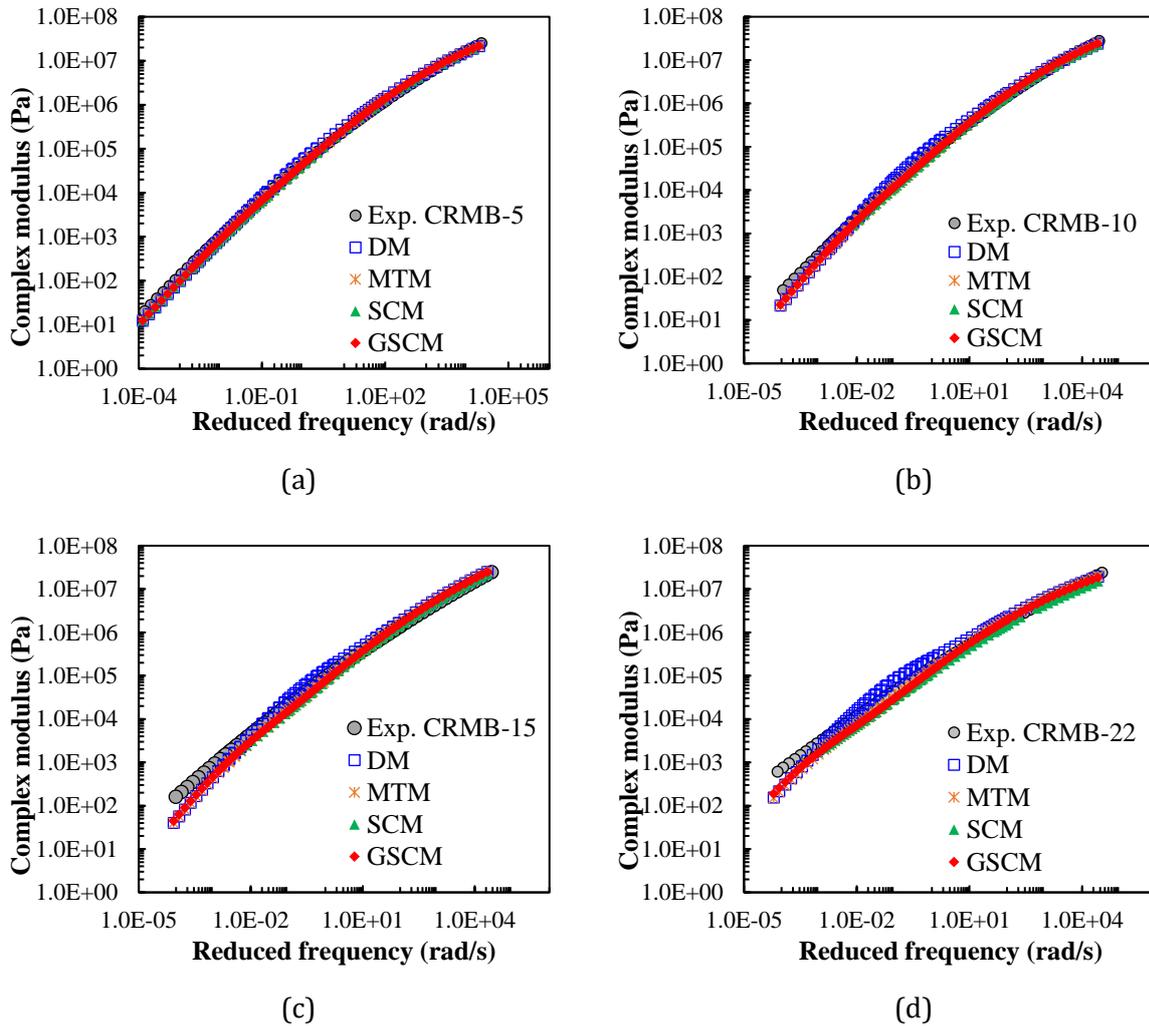
Figure 7.20 Micromechanical model predicted complex moduli of CRMB using the calibrated constituent parameters.

In contrast, using the processed constituent parameters of CRMB yield more accurate complex modulus predictions as shown in Figure 7.20. While all the micromechanical models perform well at low rubber concentrations, biased complex moduli were predicted at high rubber concentrations. This would be the same reason as explained before. For CRMB with high rubber contents, all the models still yield accurate predictions in the high-frequency range while they underestimated the complex modulus in the low-frequency range.

Among the four models, MTM, SCM, and GSCM yield similar predictions but GSCM has the highest prediction accuracy. This finding also coincides with the results on determining the effective viscoelastic properties of highly-filled composite materials (Pichler and Lackner 2009). The DM overestimated the complex modulus in the middle-frequency range for all the four CRMB binders, especially at high rubber concentrations. This stems from the initial assumption of DM which ignores the particle interactions. It is known that the low-frequency range corresponds to the high-temperature range in the master curve frame. The rubber particles will be more active in CRMB at high temperatures since the bitumen phase is softer. The underestimation of complex

modulus at high temperatures may be originating from the fact that the current models cannot fully capture the interparticle interactions. At high temperatures, the CRMB system behaves like a colloidal suspension system. The mechanical difference between bitumen matrix and rubber inclusion becomes larger as can be seen in Figure 7.11. Interparticle interactions including hydrodynamic interaction and colloidal forces play more important roles in determining the mechanical response of the composite system (Tadros 2011).

To sum up, four common micromechanical models are applicable for predicting the complex shear modulus of CRMB with different rubber contents. However, the micromechanical models using the processed constituent parameters (the liquid phase of CRMB binder and swollen rubber properties) yield much more accurate predictions of complex modulus of CRMB than the raw constituent parameters do. All the micromechanical models give reasonable predictions when the rubber concentration is low. However, when increasing the rubber content, micromechanical models yield biased predictions in the low-frequency range. This is associated with the fact these models are primarily developed to account for the stiffening effect resulting from the embedded inclusions in a matrix with minimal or limited particle interactions. which is the case of dispersed suspensions (Yin *et al.* 2008, Zhang *et al.* 2018). Under this circumstance, the behavior of the suspension is dominated by the matrix phase. Therefore, to remedy the underestimation of complex modulus of CRMB at lower frequencies, the interparticle interactions need to be further addressed in the second-stage study.

7.6.2 Model modification based on GSCM

As pointed out by the first-stage study, model calibrations need to be properly addressed to remedy the underestimation of complex modulus of CRMB with high CRM contents at lower frequencies. Therefore, the emphasis for the second-stage study will be placed on further improving the model prediction accuracy by model calibration. Particularly, for the micromechanical models, model calibration can be done either by mathematics or by fundamentally changing the model formula based on the physical mechanism. Firstly, mathematical calibration was done on GSCM to improve the model prediction accuracy. Secondly, the multilayered structure of swollen rubber particles, which was neglected in the GSCM, was considered by using the (n+1)-phase model as a modification of GSCM. To address this issue more efficiently, only binder CRMB-22 was investigated.

7.6.3 Mathematical calibration

Since the underestimation of complex modulus of CRMB at lower frequencies was because of the insufficient consideration of interparticle interaction, the following simple mathematical calibration was done by multiplying the original GSCM predicted value by a calibration factor as shown in Equation (7.47).

$$G^*{}_{cal} = G^*{}_{GSCM} \cdot [1 + \xi_{in}(f)] \qquad (7.47)$$

where $G^*{}_{cal}$ is the calibrated complex shear modulus; $G^*{}_{GSCM}$ is the complex shear modulus predicted by the GSCM; $\xi_{in}(f)$ is the calibration/interaction factor, which is frequency-dependent at a certain temperature.

Figure 7.21 presents the ratios of measured and predicted complex moduli for different CRMB binders. With the increase of rubber content, the calibration curve changes from flat to curvy

around the line of ordinate equal to 1, indicating more significant calibrations need to be done. Second-order polynomials were used to fit the calibration factors. The frequency-dependent calibration factor was formulated in the following form

$$\xi_{in}(f) = a(\log f - b)^2 + c \tag{7.48}$$

where a, b and c are fitting parameters, which are related to the volume fractions of rubber. Table 7.3 summarizes the calibration factor equations. It can be noticed that parameter b is positively related to the rubber content. Therefore, parameter b can be used as an indicator of the volume fraction of particles that participate in the interactions, or as an indicator of interparticle interaction degree.

(a)

(b)

(c)

(d)
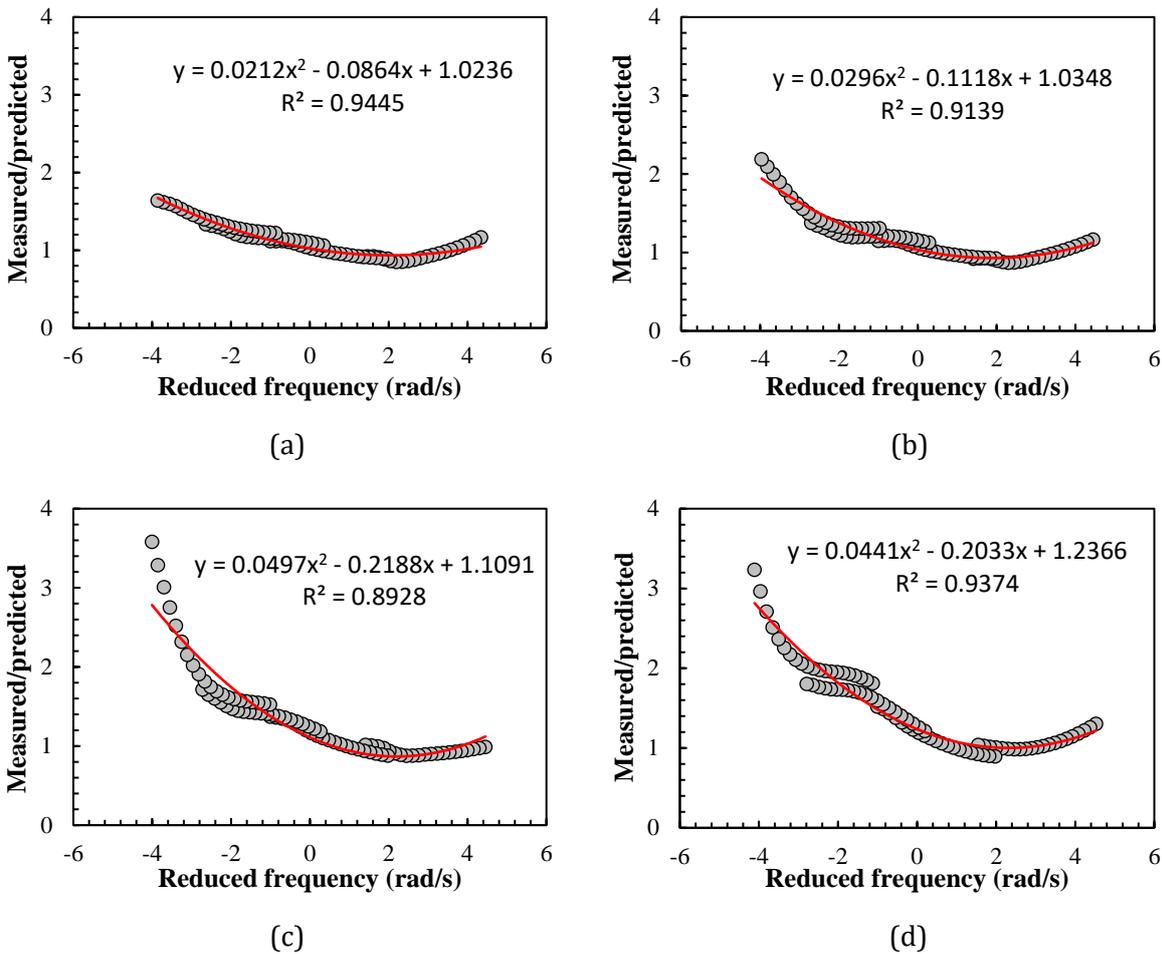
Figure 7.21 Calculation of calibration factors for (a) CRMB-5 (b) CRMB-10 (c) CRMB-15 (d) CRMB-22 based on GSCM.

Table 7.3 Calibration factors for different binders based on GSCM.

Binder type	Formula of $\xi_{in}(f)$	a	b	c
CRMB-5	$\xi_{in}(f) = 0.021(\log f - 1.785)^2 - 0.044$	0.021	1.785	-0.044
CRMB-10	$\xi_{in}(f) = 0.03(\log f - 1.889)^2 - 0.071$	0.030	1.889	-0.071
CRMB-15	$\xi_{in}(f) = 0.05(\log f - 2.201)^2 - 0.132$	0.050	2.201	-0.132
CRMB-22	$\xi_{in}(f) = 0.044(\log f - 2.305)^2 + 0.002$	0.044	2.305	0.002

Figure 7.22 shows the comparison between GSCM and mathematically calibrated GSCM predicted results for CRMB-22. The effectiveness of this modification is also valid for other CRMB binders and the comparison is neglected here. Obviously, the mathematically calibrated model using the calibration formula shown in Table 7.3 gives almost perfect predictions as compared to the experimental data. Mathematical model calibration is simple and efficient to achieve high prediction accuracy. Its disadvantage is the lack of universality and explanation for fundamental mechanisms. It needs to be re-calibrated for every new type of CRMB.
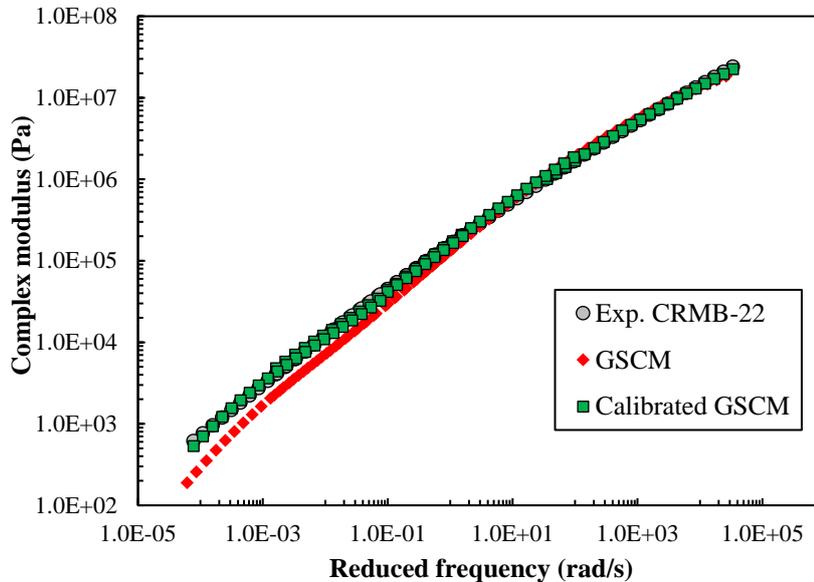
Figure 7.22 Comparison between GSCM and mathematically calibrated GSCM for CRMB-22.

7.6.4 (*n*+1)-phase model for the CRMB system

The schematic illustrations of the (*n*+1)-phase model for the CRMB system are presented in Figure 7.23. Figure 7.23a shows the three-phase model (GSCM) in the context of CRMB, where the fully swollen rubber particles surrounded by the bitumen matrix are embedded in an infinite medium with the effective mechanical properties of CRMB. Figure 7.23b added an additional phase of dry rubber as the core to form the 4-phase model. This is because the inner cores of large rubber particles maybe not swollen after limited mixing time. Figure 7.23c further divided the rubber particle into three layers: dry rubber, half-swollen rubber, fully swollen rubber. The mechanical properties of dry rubber and swollen rubber can be directly taken from Figure 7.11. The mechanical properties of half-swollen rubber were obtained by adjusting the properties of dry rubber and swollen rubber.

| (a) | (b) |

(c)
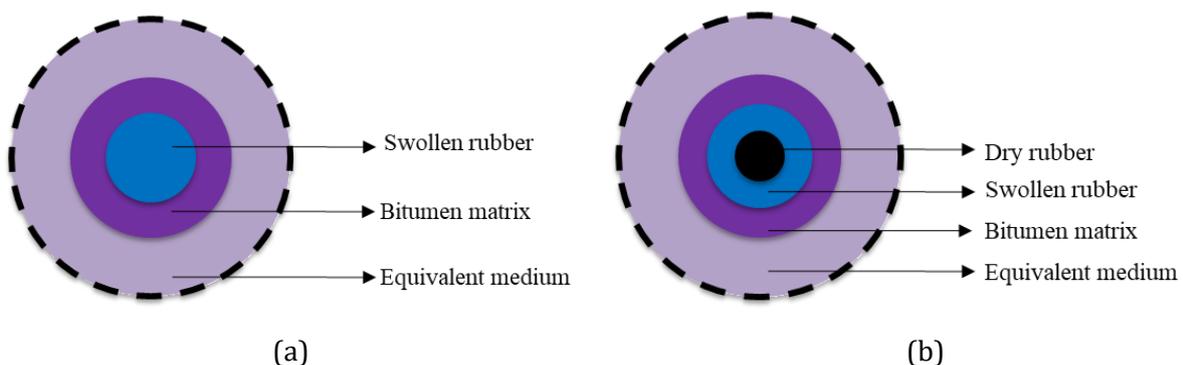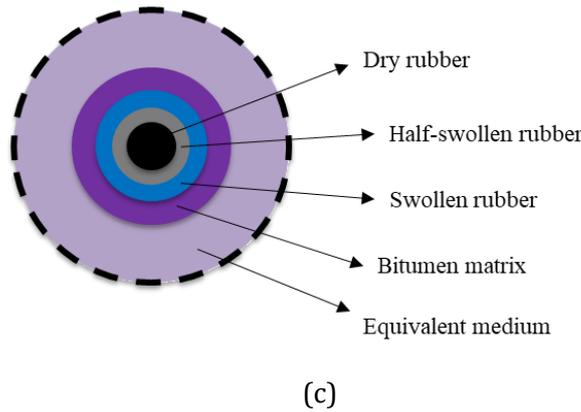
Figure 7.23 Schematic illustrations of the (n+1)-phase model for CRMB system (a) 3-phase, GSCM; (b) 4-phase; (c) 5-phase.

- *Input parameters for the (n+1)-phase model*

Mechanical properties and volume fractions of individual constituents are required to perform the micromechanical analysis. For the (n+1)-phase model, mechanical properties of bitumen matrix, dry rubber inclusion, swollen rubber inclusion were obtained by previous laboratory tests. The mechanical properties, particularly the complex modulus master curve, of half-swollen rubber was obtained by averaging the properties of dry rubber and swollen rubber as shown in Figure 7.24.
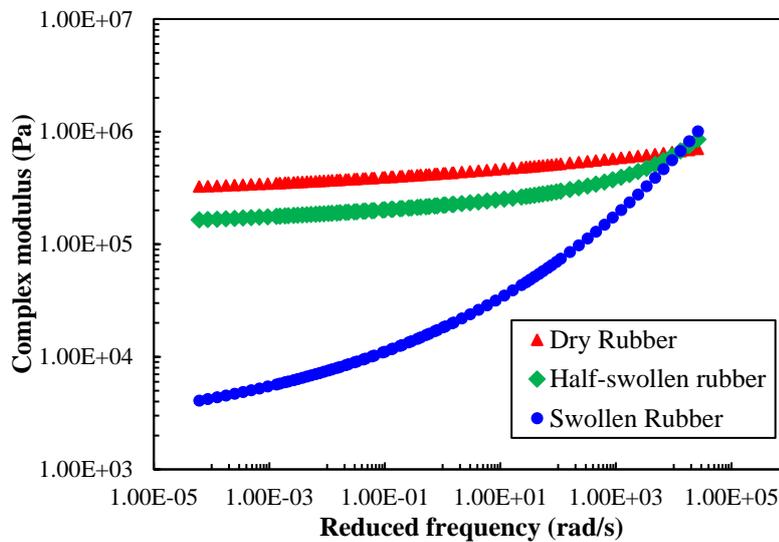
Figure 7.24 Complex modulus master curves of rubber inclusions at a reference temperature of 30 °C.

From the previous FE analysis, the effective volume contents of rubber in CRMB-22 is 35%. To properly apply the (n+1)-phase model on the binder, it is crucial to have the volume fractions of different phases. Although it is possible to have an idea about to what extent each sized rubber particle has swelled by FE simulation, it is complicated to calculate the exact volume fractions of different layers of rubber because of the existence of swelling gradient from the outer layer to the inner core. Therefore, parametric analysis was performed by assuming several different volume fraction combinations of rubber inclusion. Table 7.4 and Table 7.5 respectively shows the volume fraction of each phase used in the 4-phase model and 5-phase model.

Table 7.4 Volume fraction of each phase for the 4-phase model.

Volume fraction	Case 1	Case 2	Case 3	Case 4
Dry rubber V_{dr}	5%	10%	15%	20%
Swollen rubber V_{sr}	30%	25%	20%	15%
Bitumen matrix V_b	65%	65%	65%	65%

Table 7.5 Volume fraction of each phase for the 5-phase model.

Volume fraction	Case 1	Case 2	Case 3	Case 4
Dry rubber V_{dr}	15%	10%	5%	5%
Half-swollen rubber V_{hsr}	10%	10%	10%	5%
Swollen rubber V_{sr}	10%	15%	20%	25%
Bitumen matrix V_b	65%	65%	65%	65%

7.6.4.2 *Prediction results of the (n+1)-phase model*

With the available input parameters, a Matlab code was programmed to implement the complex equations in the (*n*+1)-phase model (Herve and Zaoui 1993) to calculate the predicted results. The predicted complex modulus master curves at 30 °C, for different cases, are shown in Figure 7.25. From Figure 7.25a, the predicted results using the 4-phase model yield slightly more accurate predictions than the 3-phase GSCM. An interesting finding is that increasing the dry rubber volume fraction increases the prediction accuracy. From Figure 7.25b, 4 case studies gave very much similar prediction results. In general, (*n*+1)-phase models considering the multilayer properties of rubber as inputs slightly increase the prediction accuracy, especially at intermediate frequencies. However, the underestimation of complex modulus at lower frequencies by these models remains unsolved.
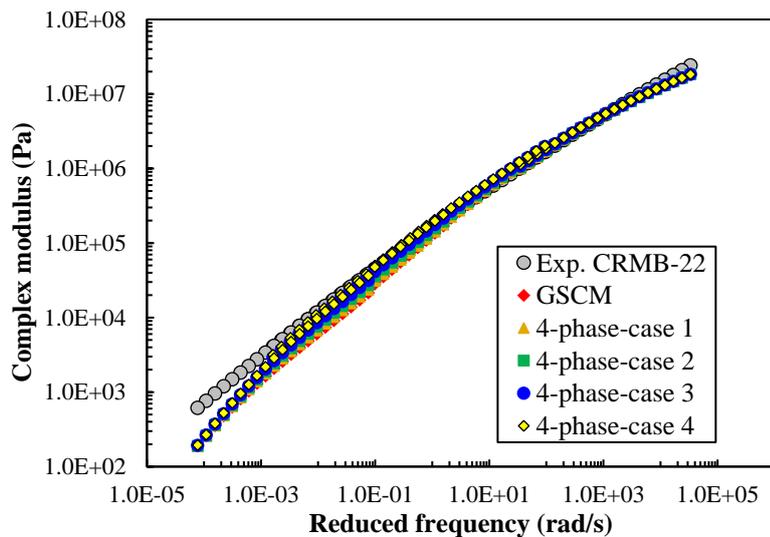
(a)
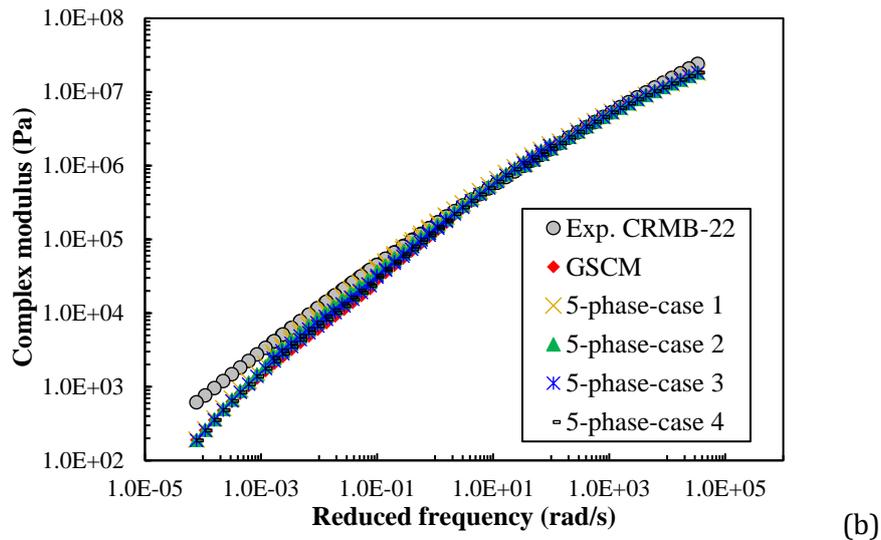
Figure 7.25 Complex modulus master curves of CRMB-22 predicted by (a) 4-phase model and (b) 5-phase model.

7.7 Micromechanical models considering interparticle interactions

7.7.1 Possible explanations for the limitations of previous models

As explained earlier, MTM, SCM, GSCM and (n+1)-phase model all failed to accurately predict the complex shear modulus of CRMB with high rubber contents at high temperatures (corresponding to low frequencies in the master curve). The reason is that these models do not explicitly account for the interparticle interactions at high concentrations. All the rubber particles, as equivalent inclusions, were taken as one phase for MTM, SCM and GSCM, and several disassociated phases for the (n+1)-phase model. The particle's relative configuration (orientations and locations, etc.), and geometrical properties (e.g., size, shape, angularity, surface morphology, etc.) were not considered. Therefore, methods that can more properly address the interparticle interactions by considering the above factors should be investigated.

Generally, there are three stiffening mechanisms for particulate filled composites: volume-filling effect, physiochemical interaction and particle interaction. For the CRMB system in the current study, volume-filling reinforcement is the stiffening caused by the presence of rubber inclusion in the bitumen matrix where the stress/strain fields are disturbed because of the inconsistent mechanical properties of rubber and bitumen. Physiochemical stiffening is due to the swelling of rubber in bitumen, which absorbs the bitumen components and increases the effective volume concentration of rubber inclusion. Interparticle interaction is a broad concept. The interparticle-interaction effect increases with increasing rubber content in bitumen, as rubber particles may come into contact and form a polymer network. The inability of accounting the polymeric network because of particle interaction was shown by the underestimation of complex modulus of previous models. In the previous models, the volume-filling reinforcement and the physiochemical effects were considered as described in the first-stage study. The interparticle interactions were only partially considered without taking the particle's configuration and interrelation into considerations. Therefore, new reinforcement mechanism, which bring in the effect of interparticle interaction, will be introduced in the following section.

7.7.2 Viscoelastic property prediction of CRMB-22 with GSC

It has been pointed out that current micromechanical models underestimated the complex modulus of CRMB at low frequencies or high temperatures. To look into this issue, the GSC model prediction results for CRMB-22 at individual temperatures were compared with the experimental data as shown in Figure 7.26. Besides, the phase angle results of CRMB were also compared since viscoelasticity cannot be defined without the consideration of phase angle. Phase angle is also helpful to understand the mechanism of the matrix-inclusion interaction at high temperatures.
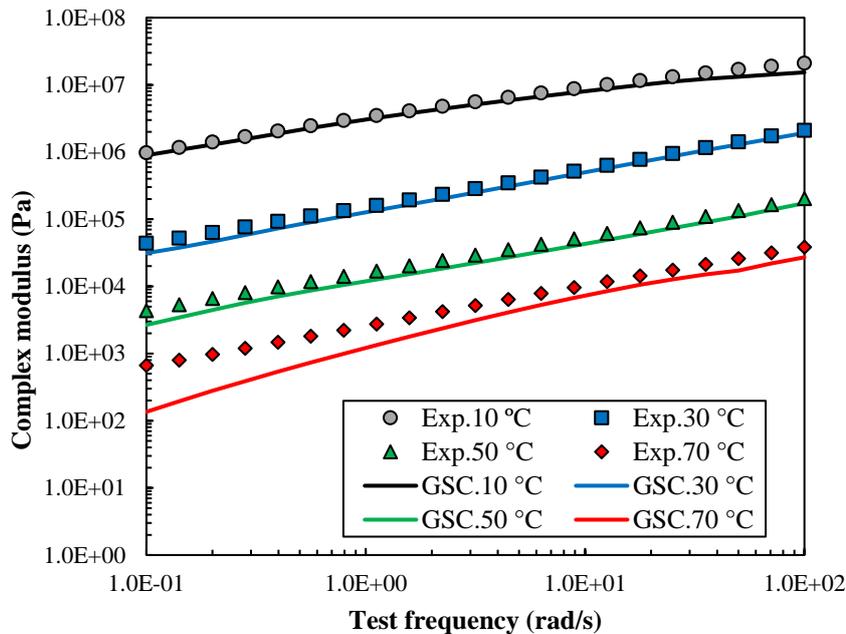
(a)
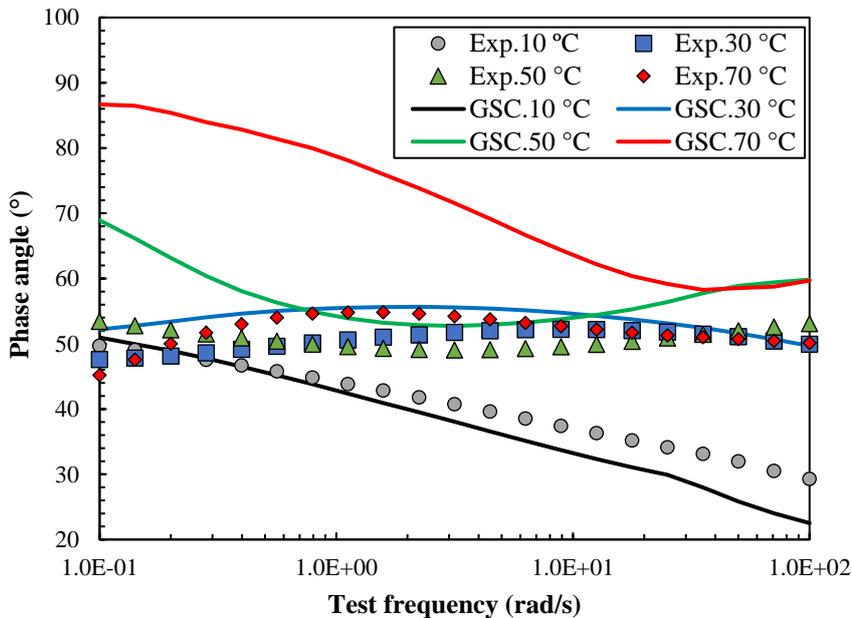
(b)

Figure 7.26 GSC model prediction results for CRMB-22 at each temperature (a) complex modulus; (b) phase angle.

It can be seen from Figure 7.26 that both complex modulus and phase angle are generally accurately predicted at low temperatures. With the increase of temperature, underestimation of complex modulus was observed, while phase angle prediction results at high temperatures are significantly higher than experimental results. The discrepancy between model prediction and experimental results becomes larger at higher temperatures. Besides, it is noteworthy that the phase angle results of CRMB are atypical when compared with unmodified bitumen. It is believed that the presence of rubber particles in the bitumen matrix significantly change the viscoelastic properties of CRMB.

7.7.3 Polymer chain entanglement effect of CRMB system

7.7.3.1 *Reasons for the inaccurate predictions for the CRMB system*

To address the reasons for the inaccurate model predictions for the CRMB system, the interrelation between the bitumen matrix and rubber inclusion needs to be carefully analysed. At low temperatures, the mechanical mismatch between rubber particles and bitumen is relatively small and rubber particles are less active due to the limited polymer chain mobility. Therefore, the micromechanical model prediction results at low temperatures are accurate enough even without considering the interparticle interaction effects. However, at high temperatures, bitumen matrix behaves like liquid while rubber inclusion, which is stiffer than bitumen matrix, will play a more dominant role in determining the mechanical properties of CRMB.

(a)   (b)
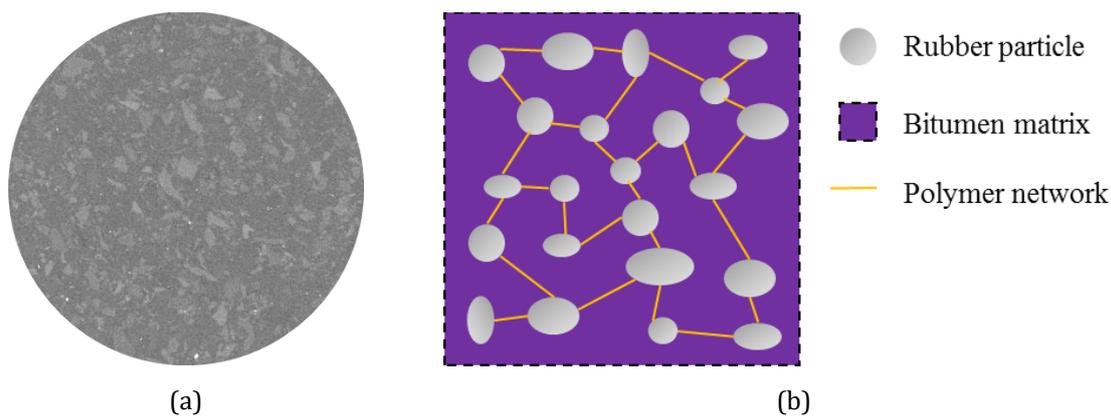
Figure 7.27 (a) CT scan image of CRMB-22. Dark area represents bitumen matrix while light area represents rubber particles; (b) Schematic of polymer network formed by chain entanglement.

From the CT scan image of CRMB-22 in Figure 7.27a, rubber particles are dissociative and do not have direct contacts in the bitumen matrix. Therefore, there is no so-called particle packing effect which is usually seen in asphalt mixture (Zhang *et al.* 2019). However, recalling the surface layer structure of swollen rubber particles in Figure 2.8, the disentangled rubber polymer chains on the surface of rubber particles may form a 3-D polymer network (Figure 7.27b) because these disentangled chains from neighbouring particles may entangle again (Rubinstein and Colby 2003).
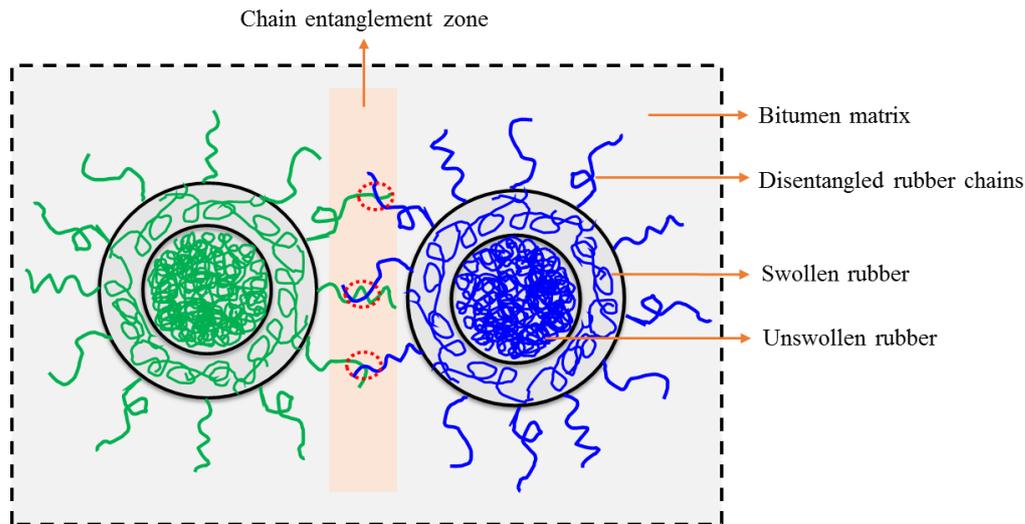
Figure 7.28 Illustration of rubber polymer chain entanglement. Color green and blue represent two rubber particles.

Figure 7.28 illustrates the phenomenon of rubber polymer chain entanglement between two neighbouring rubber particles. The improved mobility of disentangled rubber polymer chains at high temperatures will increase the chances for chain entanglement to occur. Besides, at higher rubber concentrations, the chain entanglement effect will be more significant. This potentially formed rubber polymer network due to chain entanglement effects will restrain the movement of the dissociative rubber particles, which offers extra elasticity and stiffening effect to the CRMB system {Rubinstein, 2002 #2338}, hence reducing the phase angle and increasing the complex modulus. Therefore, to further improve the prediction accuracy of micromechanical models, new reinforcement mechanism, which is caused by the chain entanglement effect, must be considered.

7.7.3.2 *Constitutive models of entangled polymer network*

Since polymer chain entanglement occurs at a molecular scale, it is almost impossible to directly measure the mechanical and volumetric properties of the entangled polymer network. Assuming the discrepancy between experiment and micromechanical prediction is originated from the entangled polymer network, the constitutive models of this reinforcement can be derived based on the difference between experimental data and micromechanical prediction results. The rationale of calibrating the current micromechanical model is by adding a network element to the existing model in parallel from a constitutive modelling point of view.

Huet model was used to fit the mechanical properties of the entangled polymer network based on the difference between experiment and model prediction. The fitted viscoelastic properties of the entangled polymer network for CRMB with different rubber contents are shown in Figure 7.29. For comparison reason, the Huet model fitted results for the dry rubber sample were also plotted in Figure 7.29. It can be seen from Figure 7.29a that complex modulus curves of the network are merged at high frequencies, which means no significant corrections on the model predicted complex moduli need to be done at high frequencies (low temperatures). At low frequencies (high temperatures), the original prediction needs significant corrections due to underestimation. For CRMB with a higher rubber content, a stiffer network is required to remedy the underestimation. The complex moduli of both dry rubber and network increase with the frequency.

Besides, with the increase of rubber content, a more elastic (smaller phase angle) network is observed in Figure 7.29b. It is noteworthy that the phase angle of the entangled network is independent of frequency, which is similar to dry rubber. Compared to the entangled polymer networks, dry rubber is stiffer and more elastic. Generally speaking, the entangled polymer network with a higher rubber content tends to behave like the dry rubber. From the microstructural point of view, dry rubber can be regarded as a much more condensed polymer network as the one considered here. The mechanical similarity between dry rubber and entangled networks implies the possibility of relating the model parameters of networks to that of dry rubber.

(a)

(b)
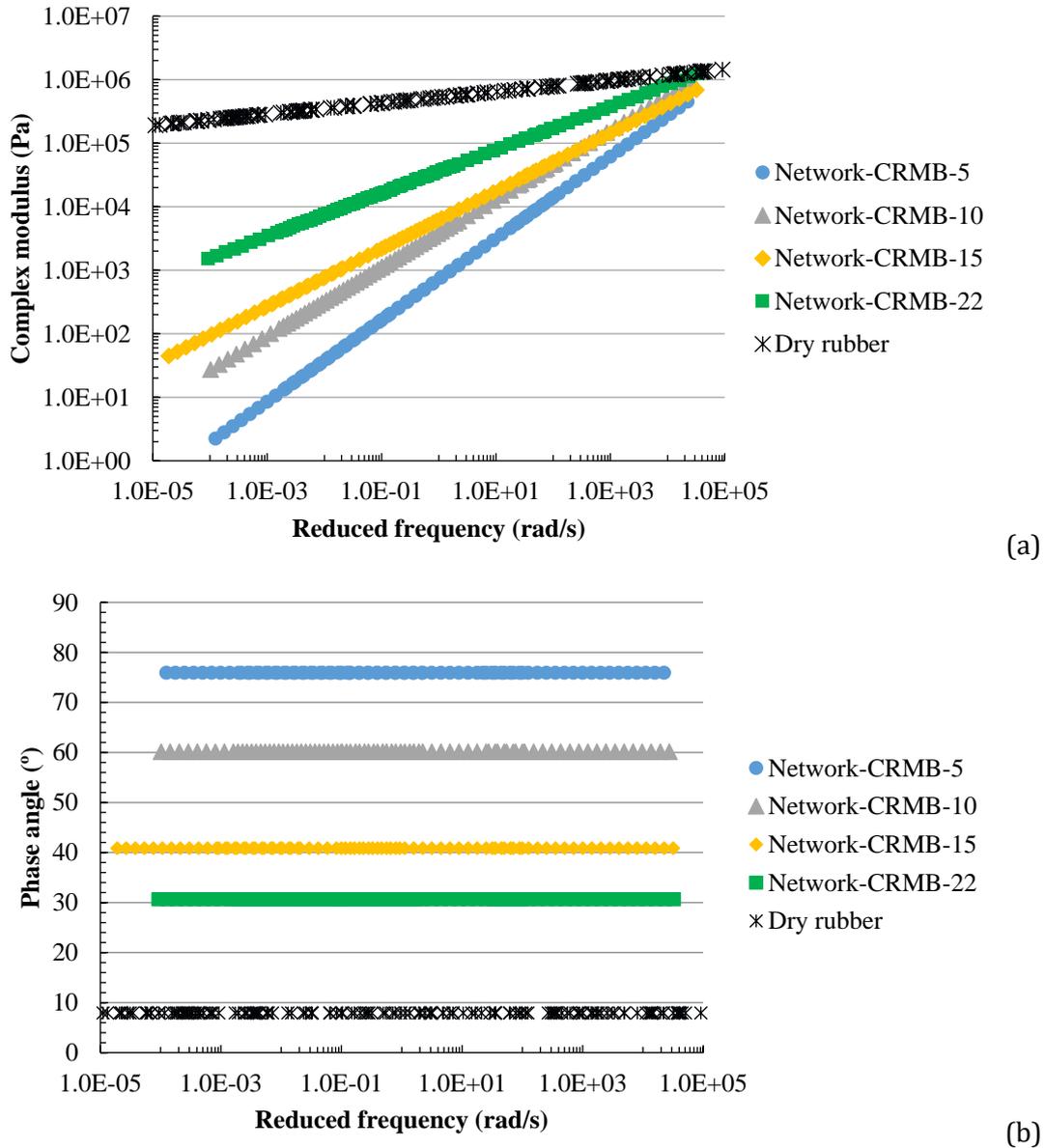
Figure 7.29 Constitutive models of entangled polymer network (a) complex modulus (b) phase angle at a reference temperature of 30 °C.

7.7.3.3 *Relationship between rubber content and model parameters of entangled polymer network*

Similar to what has been done to the bitumen matrix, it is also desirable to relate rubber content to model parameters of entangled polymer network. This is because once built these

relationships, the mechanical properties of networks can be predicted based on the rubber content. Huet model parameters for the entangled polymer network and dry rubber were summarized in Table 7.6. Since the phase angle of the network is independent of frequency, the phase angle values of different networks were also listed in Table 7.6 to have a more intuitive comparison. The correlations between model parameters and rubber content were also presented in Figure 7.30.

Table 7.6 Huet model parameters for the entangled polymer network and dry rubber.

Material	G_g (Pa)	k	h	δ	τ	Phase angle (°)
Network-CRMB-5	1.05E+10	0.6429	0.6429	4577.3	3.55E-06	75.9
Network-CRMB-10	1.59E+10	0.5388	0.5388	80378.7	6.65E-04	60.2
Network-CRMB-15	1.86E+11	0.4541	0.4541	1653891.4	1.70E-03	40.9
Network-CRMB-22	1.91E+11	0.3404	0.3404	631253.6	1.91E-03	30.6
Dry rubber	1.11E+11	0.0883	0.0932	82727.0	2.46E-05	7.9

(a)

(b)

(c)

(d)
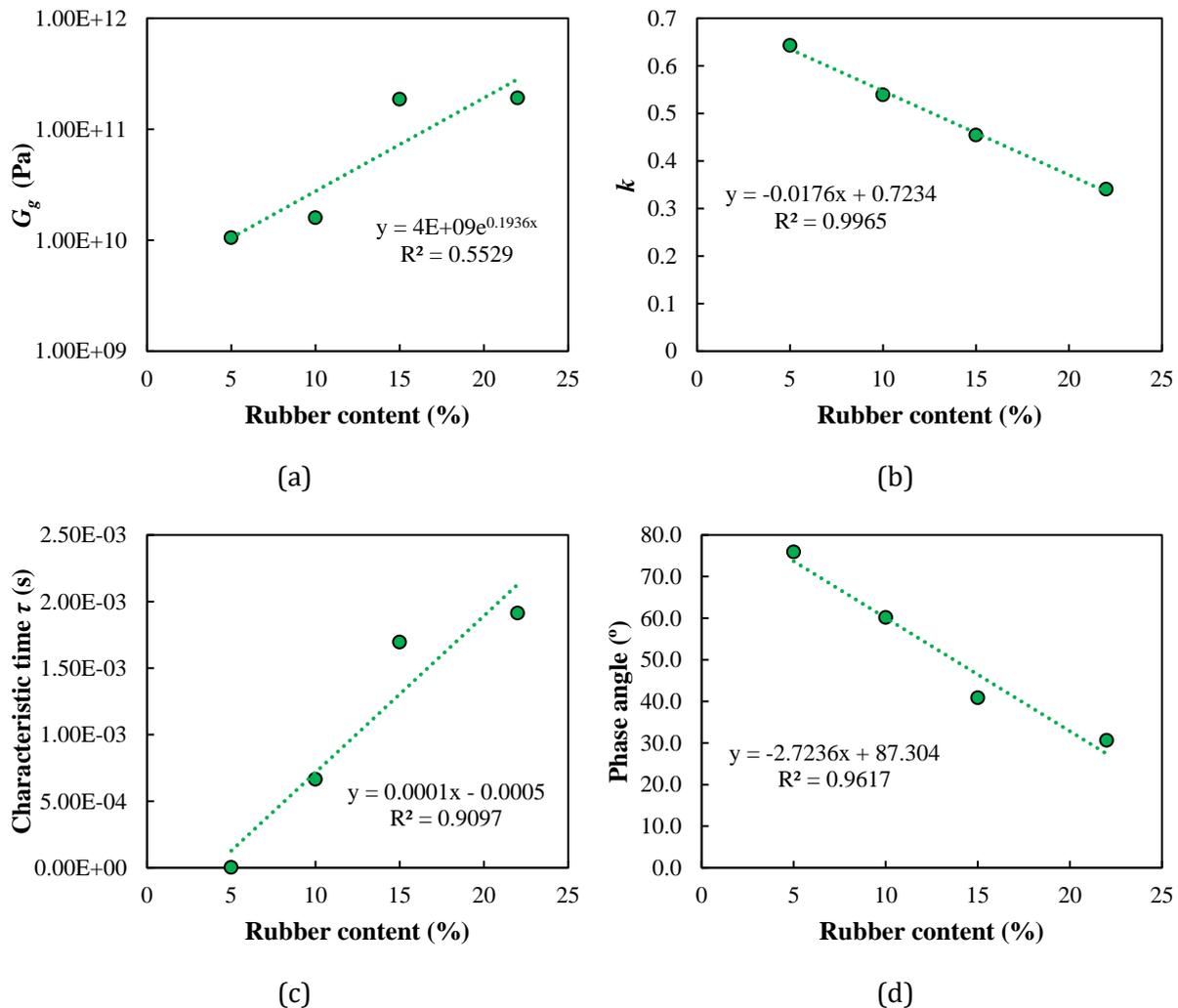
Figure 7.30 Correlation between Huet model parameters for entangled polymer network and rubber content.

It can be clearly seen from Figure 7.30 that G_g and τ increase with the rubber content, while k, h and phase angle decrease with the rubber content. With the increase of rubber content, the entangled network is more elastic as reflected by the decreased parameters k, h and phase angle. It also shows more significant delayed elasticity since the retardation time τ increases. It is noteworthy that parameters k and h of dry drubber are very close to zero, indicating a decisively elastic nature. Although there is resemblance between the mechanical properties of dry rubber and networks, it is difficult to find quantitative relationships between the model parameters of them because the network and dry rubber are in totally different physical states. Besides, the measured dry rubber sample is filled with carbon black and other additives. It cannot be directly compared with the network which is supposed to comprise entangled polymer chains. Nevertheless, with the relationships presented in Figure 7.30, it is possible to predict the mechanical properties of the network based on the rubber content with a certain accuracy.

7.7.4 Calibrated micromechanical model prediction results

As mentioned before, the strategy of calibrating the current micromechanical model is by adding a network element to the existing model in parallel from a constitutive modelling point of view as shown in Figure 7.31. The constitutive elements in black color represent the response of the current GSC model, while the constitutive elements in orange represents the additional response from the entangled polymer networks. By integrating these two responses, the current micromechanical model was calibrated.
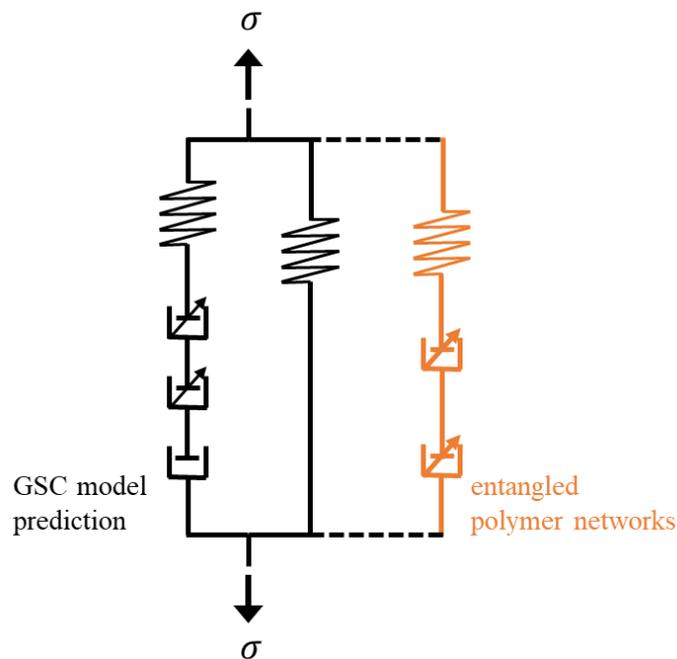
Figure 7.31 Strategy of considering the network effect on the GSC model prediction.

Technically, after obtaining the constitutive models of the entangled polymer networks, the extra reinforcement mechanism due to chain entanglement effect was added to the current GSC model prediction results through complex number operations. Correspondingly, Figure 7.32 presents the calibrated GSC model prediction results for CRMB-22 at individual temperatures as an example. Comparing to the original prediction results in Figure 7.26, the calibrated GSC model

significantly improves the prediction accuracy for both complex modulus and phase angle, especially at high temperatures.

(a)

(b)
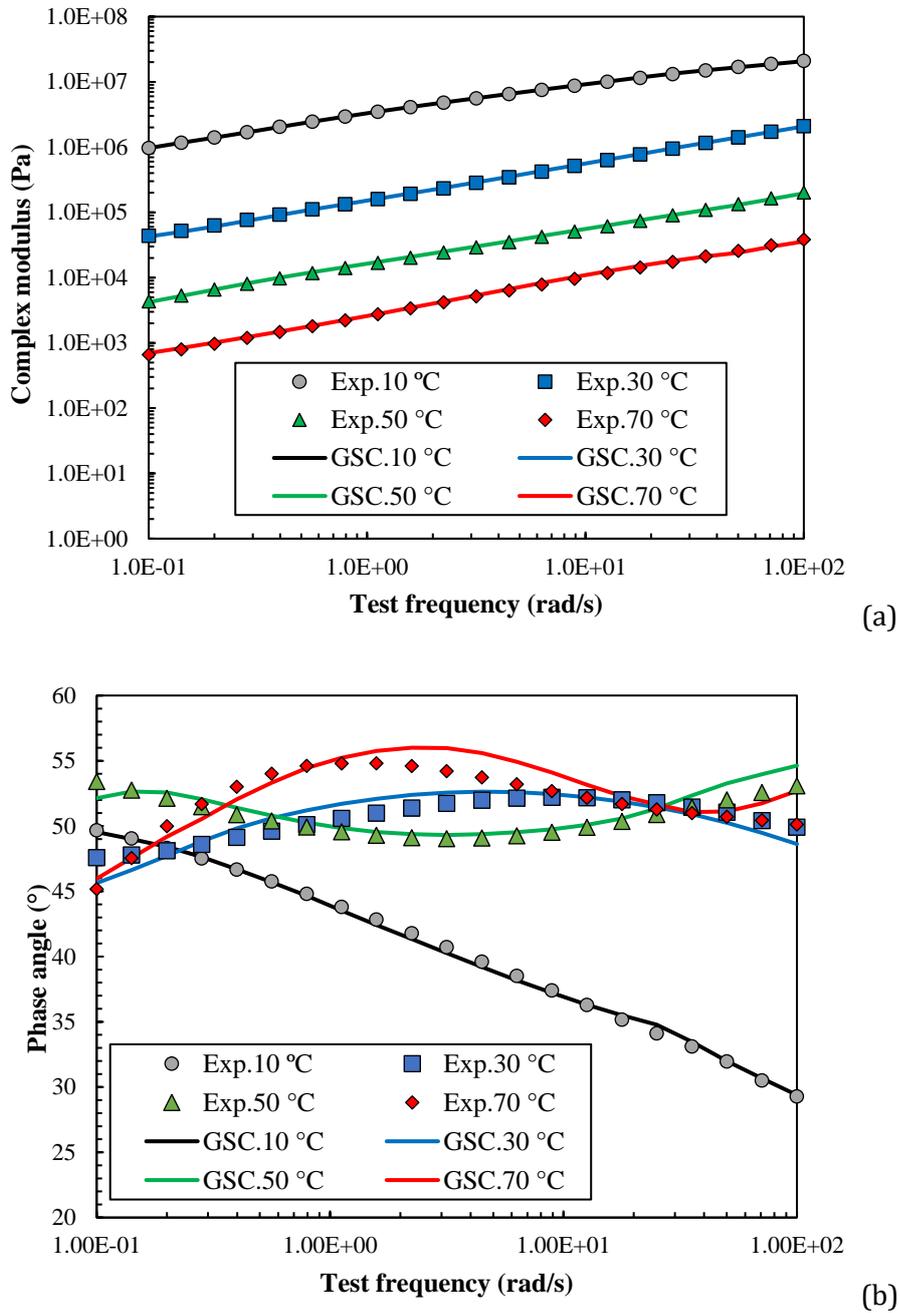
Figure 7.32 Calibrated GSC model prediction results for CRMB-22 at each temperature (a) complex modulus; (b) phase angle.

Since the prediction accuracy was significantly improved at each temperature by calibrating the GSC model with a network element, it is more convenient to compare the experimental and model prediction results in the framework of master curve. Figure 7.33 presents the complex modulus and phase angle master curves at a reference temperature of 30 °C from both experiment and model predictions. For illustration purpose, the master curves of the entangled polymer network were also plotted to give an indication on how this extra element can influence the model prediction results. The network element exactly remedies the GSC model prediction inaccuracy,

either underestimation or overestimation, at different frequencies. It can be seen from Figure 7.33a that underestimation of complex modulus at low frequencies from GSC model was rectified after adding the network element. The phase angle master curve predicted from the calibrated GSC model in Figure 7.33b is more accurate after bringing in the elastic element to the original GSC model.
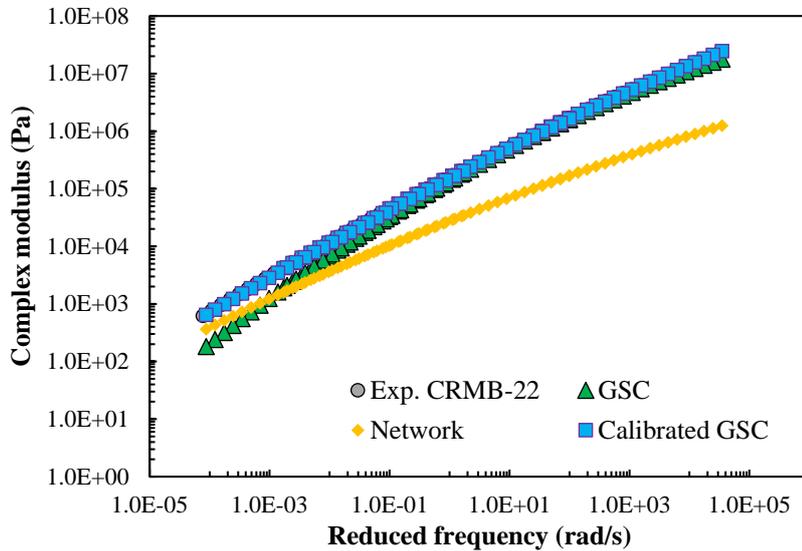
(a)
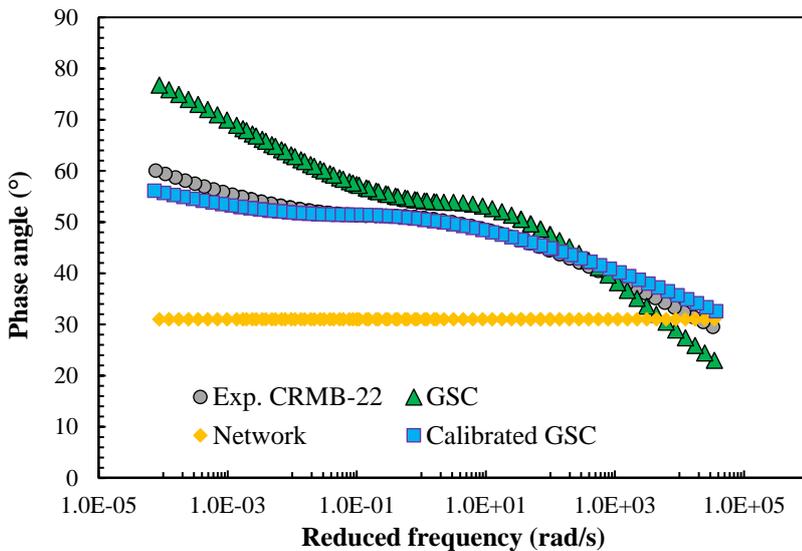
(b)

Figure 7.33 Experimental and model predicted results for CRMB-22 at a reference temperature of 30 °C. (a) complex modulus (b) phase angle.

In addition, the calibrated GSC model prediction results for other CRMB binders are also shown in Figure 7.34. As expected, the calibrated GSC model shows superior prediction performance for both complex modulus and phase angle. In summary, there are three main steps involved in the model calibration process:

- **Step 1.** Micromechanical prediction using GSC model based on the bitumen matrix properties and rubber inclusion.

- *Step 2.* Fitting the constitutive model of the polymer network based on the difference between GSC predicted data and experimental data.

- *Step 3.* Calibration/correction of GSC model by adding the networking element.
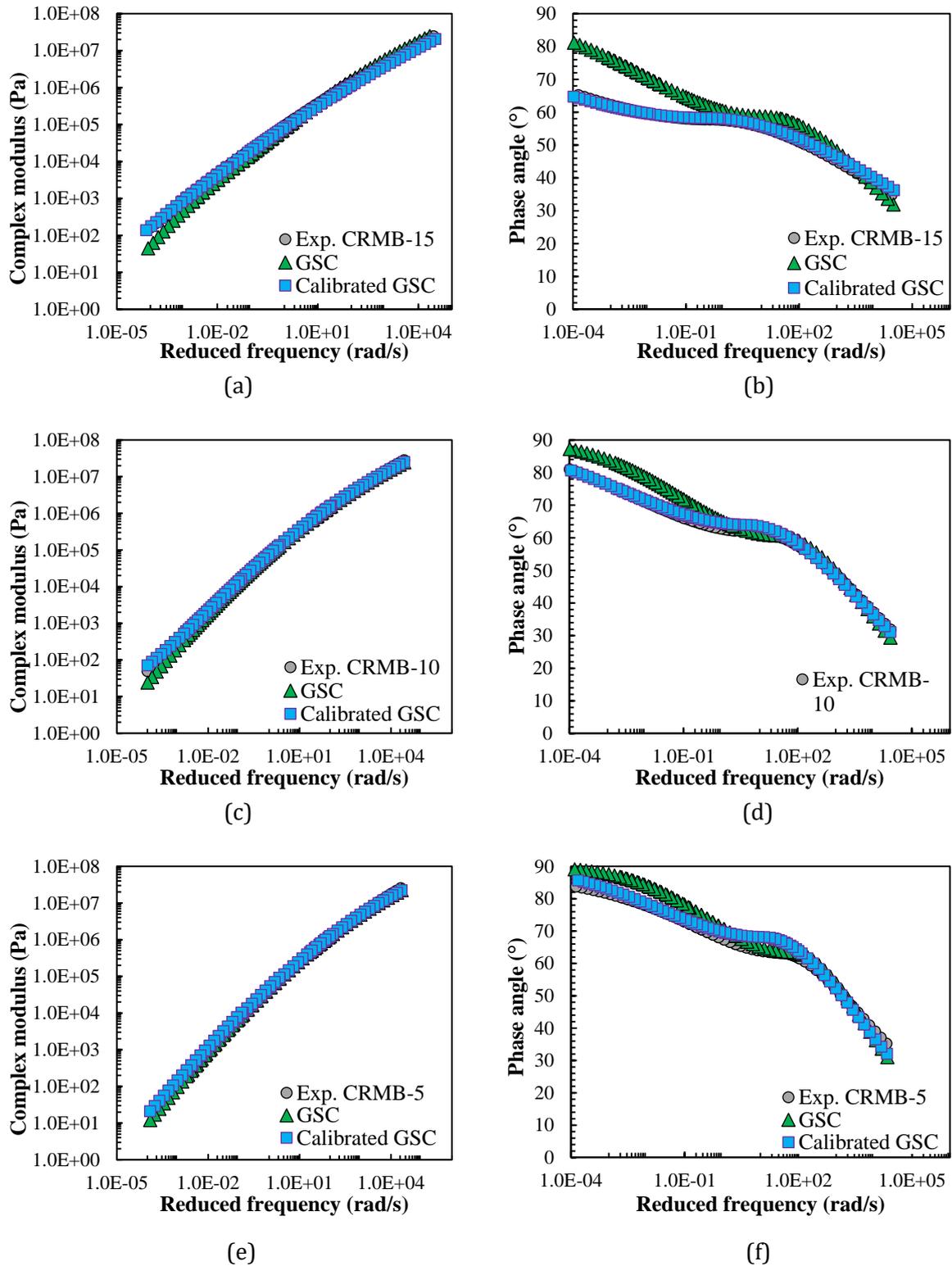
Figure 7.34 Experimental and model predicted results at a reference temperature of 30 °C. (a) complex modulus of CRMB-15; (b) phase angle of CRMB-15; (c) complex modulus of CRMB-10; (d) phase angle of CRMB-10; (e) complex modulus of CRMB-5; (f) phase angle of CRMB-5.

7.8 Viscoelastic property prediction framework for CRMB

As emphasized in Section 7.1, from a practical point of view, it is desirable to predict the CRMB viscoelastic properties based on the ingredient properties and recipe. With the mentioned two-stage study, the linear viscoelastic (LVE) property prediction framework for CRMB is illustrated in Figure 7.35.
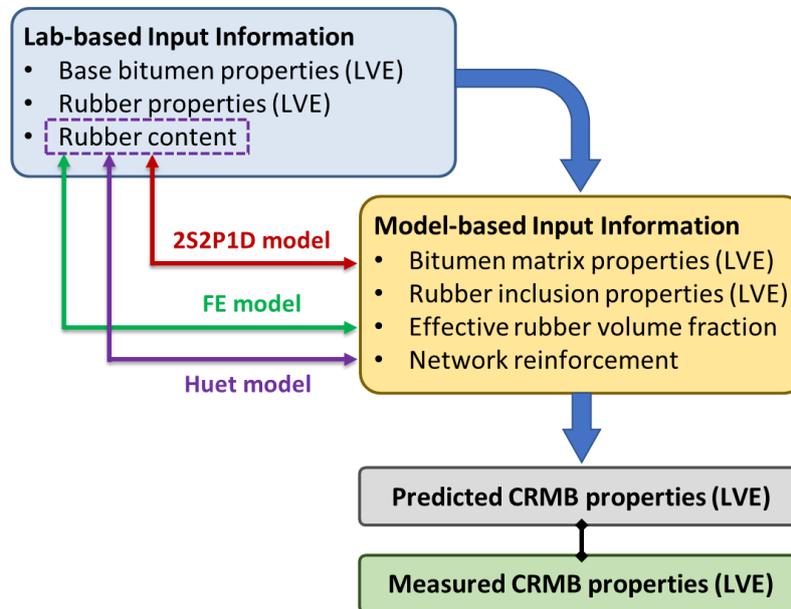
Figure 7.35 Viscoelastic properties determination framework for CRMB.

As for the micromechanical modelling, the LVE properties of bitumen matrix and rubber inclusion, and the volume fraction of rubber need to be provided as the input parameters. At a given processing condition (temperature and time) for preparing CRMB, the bitumen matrix properties can be predicted from the base bitumen properties based on the rubber content. The effective rubber volume fraction can be predicted through the FE swelling model simulation. The constitutive model of the entangled polymer network, which is used to calibrate the micromechanical model, can also be estimated based on the rubber content. At a given condition, rubber inclusion properties depend on the properties of both base bitumen and dry rubber as well as their chemo-physical interaction. It is difficult to directly link them together, but empirical relationships can be built to predict the rubber inclusion properties. In general, the LVE property prediction framework shown in Figure 7.35 is feasible and quite promising. After knowing the properties of base bitumen and rubber as well as the rubber content, the LVE properties of the resulting CRMB at a given processing condition can be estimated with experimental evidence and numerical iterations.

7.9 Summary

This chapter conducted a two-stage study on the micromechanical modelling of CRMB. The first-stage study aimed to predict the complex modulus of CRMB with more representative constituent parameters. Frequency sweep tests using DSR were performed on both binders and individual constituents (bitumen matrix and rubber inclusion). The finite element method was used to estimate the effective volume concentration of rubber. The main conclusions from the first-stage study can be drawn:

- The liquid phases of CRMB binders (real bitumen matrices) are stiffer and more elastic than the neat bitumen as reflected by the increased complex modulus and decreased phase angle.
- Dry rubber exhibits obvious elastic behaviors whose complex modulus and phase angle are almost frequency independent. Swelling significantly alters the rubber properties, making it softer and more viscous.
- Estimated from the numerical swelling model, the volume concentration of rubber after mixing with bitumen increases to 3.126 times as the blended rubber percentage.
- Using the liquid phase of CRMB binder and swollen rubber properties as the micromechanical model input yields more accurate predictions. The used four micromechanical models predict well at higher frequencies while underestimating the complex modulus at lower frequencies. Among the four used models, GSCM has the highest prediction accuracy.

The second-stage study aimed to further improve the prediction accuracy by amending the GSCM which performs best among the current micromechanical models. Firstly, mathematical calibration was done on the GSCM by introducing a calibration factor. Then, the (n+1)-phase model was applied to the CRMB system by considering the multilayered properties of swollen rubber particles. Lastly, a new reinforcement mechanism called chain entanglement effect was introduced to account for the interparticle interaction effect. The main conclusions from the second-stage study can be drawn:

- Mathematical model calibration is simple and efficient to achieve high prediction accuracy. Its disadvantage is the lack of universality and explanation for fundamental mechanisms. It needs to be re-calibrated for every new type of CRMB.
- The (n+1)-phase models considering the multilayer properties of rubber as input, slightly increase the prediction accuracy, especially at intermediate frequencies. However, the underestimation of complex modulus at lower frequencies by these models remains.
- The polymer chain entanglement effect accounts for the underestimation of complex modulus and lack of elasticity (overestimation of phase angle) for CRMB at high temperatures/low frequencies.
- The mechanical properties of bitumen matrix and entangled polymer network can be determined based on the rubber content.
- The introduction of the entangled polymer network to the GSC model significantly improved the prediction accuracy for both complex modulus and phase angle in the whole frequency range.

In summary, by incorporating the physio-chemical interaction mechanism into the currently available models, a new dedicated micromechanical model for predicting the viscoelastic properties of CRMB has been developed. The predicted viscoelastic properties can thereafter be used as inputs for a better mix design.

7.10 References

Aragao, F.T.S., Kim, Y.R., Lee, J. & Allen, D.H., 2011. Micromechanical model for heterogeneous asphalt concrete mixtures subjected to fracture failure. *Journal of Materials in Civil Engineering,* 23 (1), 30-38.

Aurangzeb, Q., Ozer, H., Al-Qadi, I.L. & Hilton, H.H., 2016. Viscoelastic and poisson's ratio characterization of asphalt materials: Critical review and numerical simulations. *Materials and Structures,* 50 (1).

Buttlar, W., Bozkurt, D., Al-Khateeb, G. & Waldhoff, A., 1999. Understanding asphalt mastic behavior through micromechanics. *Transportation Research Record: Journal of the Transportation Research Board,* (1681), 157-169.

Caro, S., Masad, E., Bhasin, A. & Little, D., 2010. Micromechanical modeling of the influence of material properties on moisture-induced damage in asphalt mixtures. *Construction and Building Materials,* 24 (7), 1184-1192.

Christensen, R. & Lo, K., 1979. Solutions for effective shear properties in three phase sphere and cylinder models. *Journal of the Mechanics and Physics of Solids,* 27 (4), 315-330.

Comsol Multiphysics, 2018. Mems pressure sensor drift due to hygroscopic swelling. *COMSOL Application Gallery.*

Eshelby, J., Year. The elastic field outside an ellipsoidal inclusioned.^eds. *Proceedings of the Royal Society of London A: Mathematical, Physical and Engineering Sciences.* The Royal Society, 561-569.

Eshelby, J.D., Year. The determination of the elastic field of an ellipsoidal inclusion, and related problemsed.^eds. *Proceedings of the Royal Society of London A: Mathematical, Physical and Engineering Sciences.* The Royal Society, 376-396.

Hashin, Z., 1970. Complex moduli of viscoelastic composites—i. General theory and application to particulate composites. *International Journal of Solids and Structures,* 6 (5), 539-552.

Herve, E. & Zaoui, A., 1993. N-layered inclusion-based micromechanical modelling. *International Journal of Engineering Science,* 31 (1), 1-10.

Hill, R., 1965. A self-consistent mechanics of composite materials. *Journal of the Mechanics and Physics of Solids,* 13 (4), 213-222.

Kutay, M.E., Varma, S. & Jamrah, A., 2015. A micromechanical model to create digital microstructures of asphalt mastics and crumb rubber-modified binders. *International Journal of Pavement Engineering,* 18 (9), 754-764.

Leon L. Mishnaevsky, J. & Schmauder, S., 2001. Continuum mesomechanical finite element modeling in materials development: A state-of-the-art review. *Applied Mechanics Reviews,* 54 (1), 49-67.

Mark, J.E., 1981. Rubber elasticity. *Journal of Chemical Education,* 58 (11), 898-903.

Medina, J.R. & Underwood, B.S., 2017. Micromechanical shear modulus modeling of activated crumb rubber modified asphalt cements. *Construction and Building Materials,* 150, 56-65.

Mori, T. & Tanaka, K., 1973. Average stress in matrix and average elastic energy of materials with misfitting inclusions. *Acta metallurgica,* 21 (5), 571-574.

Olard, F. & Di Benedetto, H., 2003. General "2s2p1d" model and relation between the linear viscoelastic behaviours of bituminous binders and mixes. *Road Materials and Pavement Design,* 4 (2), 185-224.

Park, S.W. & Schapery, R.A., 1999. Methods of interconversion between linear viscoelastic material functions. Part i - a numerical method based on prony series. *International Journal of Solids and Structures,* 36 (11), 1653-1675.

Petersen, J.C. & Glaser, R., 2011. Asphalt oxidation mechanisms and the role of oxidation products on age hardening revisited. *Road Materials and Pavement Design,* 12 (4), 795-819.

Pichler, C. & Lackner, R., 2009. Upscaling of viscoelastic properties of highly-filled composites: Investigation of matrix–inclusion-type morphologies with power-law viscoelastic material response. *Composites Science and Technology,* 69 (14), 2410-2420.

Pronk, A.C., 2005. The huet-sayegh model: A simple and excellent rheological model for master curves of asphaltic mixes. *R. Lytton Symposium on Mechanics of Flexible Pavements.* Baton Rouge, Louisiana, United States.

Rowe, G., Baumgardner, G. & Sharrock, M., 2009. Functional forms for master curve analysis of bituminous materials. *Advanced Testing and Characterisation of Bituminous Materials, Vols 1 and 2*, 81-+.

Rubinstein, M. & Colby, R.H., 2003. *Polymer physics*: Oxford university press New York.

Sadd, M.H., Dai, Q.L., Parameswaran, V. & Shukla, A., 2004. Microstructural simulation of asphalt materials: Modeling and experimental studies. *Journal of Materials in Civil Engineering,* 16 (2), 107-115.

Santangelo, P.G. & Roland, C.M., 1998. Temperature dependence of mechanical and dielectric relaxation incis-1,4-polyisoprene. *Macromolecules,* 31 (11), 3715-3719.

Shen, J., Amirkhanian, S., Xiao, F. & Tang, B., 2009a. Influence of surface area and size of crumb rubber on high temperature properties of crumb rubber modified binders. *Construction and Building Materials,* 23 (1), 304-310.

Shen, J., Amirkhanian, S., Xiao, F. & Tang, B., 2009b. Surface area of crumb rubber modifier and its influence on high-temperature viscosity of crm binders. *International Journal of Pavement Engineering,* 10 (5), 375-381.

Shu, X. & Huang, B., 2008. Micromechanics-based dynamic modulus prediction of polymeric asphalt concrete mixtures. *Composites Part B: Engineering,* 39 (4), 704-713.

Tadros, T., 2011. Interparticle interactions in concentrated suspensions and their bulk (rheological) properties. *Adv Colloid Interface Sci,* 168 (1-2), 263-77.

Underwood, B.S. & Kim, Y.R., 2014. A four phase micro-mechanical model for asphalt mastic modulus. *Mechanics of Materials,* 75, 13-33.

Wang, D., Li, D., Yan, J., Leng, Z., Wu, Y., Yu, J. & Yu, H., 2018a. Rheological and chemical characteristic of warm asphalt rubber binders and their liquid phases. *Construction and Building Materials,* 193, 547-556.

Wang, H., Apostolidis, P., Zhu, J., Liu, X., Skarpas, A. & Erkens, S., 2020a. The role of thermodynamics and kinetics in rubber–bitumen systems: A theoretical overview. *International Journal of Pavement Engineering*, 1-16.

Wang, H., Liu, X., Apostolidis, P., Erkens, S. & Scarpas, T., 2019. Numerical investigation of rubber swelling in bitumen. *Construction and Building Materials,* 214, 506-515.

Wang, H., Liu, X., Apostolidis, P., Erkens, S. & Skarpas, A., 2020b. Experimental investigation of rubber swelling in bitumen. *Transportation Research Record: Journal of the Transportation Research Board,* 2674 (2), 203-212.

Wang, H., Liu, X., Apostolidis, P. & Scarpas, T., 2018b. Rheological behavior and its chemical interpretation of crumb rubber modified asphalt containing warm-mix additives. *Transportation Research Record: Journal of the Transportation Research Board,* 2672 (28), 337-348.

Wang, H., Liu, X., Zhang, H., Apostolidis, P., Scarpas, T. & Erkens, S., 2020c. Asphalt-rubber interaction and performance evaluation of rubberised asphalt binders containing non-foaming warm-mix additives. *Road Materials and Pavement Design,* 21 (6), 1612-1633.

Wu, Q., Wang, C., Liang, R., Liu, Y., Cheng, J. & Kang, Y., 2018. Fractional linear viscoelastic constitutive relations of anhydride-cured thermosetting rubber-like epoxy asphalt binders. *Construction and Building Materials,* 170, 582-590.

Yin, H. & Zhao, Y., 2016. *Introduction to the micromechanics of composite materials* Boca Raton, Florida: CRC Press.

Yin, H.M., Buttlar, W.G., Paulino, G.H. & Benedetto, H.D., 2008. Assessment of existing micro-mechanical models for asphalt mastics considering viscoelastic effects. *Road Materials and Pavement Design,* 9 (1), 31-57.

Yusoff, N.I.M., Shaw, M.T. & Airey, G.D., 2011. Modelling the linear viscoelastic rheological properties of bituminous binders. *Construction and Building Materials,* 25 (5), 2171-2189.

Zegard, A., Helmand, F., Tang, T., Anupam, K. & Scarpas, A., 2016. Rheological properties of tire rubber using dynamic shear rheometer for fem tire-pavement interaction studies. *8th International Conference on Maintenance and Rehabilitation of Pavements.* Singapore: Research Publishing Services, 535-544.

Zhang, H., Anupam, K., Scarpas, A. & Kasbergen, C., 2018. Comparison of different micromechanical models for predicting the effective properties of open graded mixes. *Transportation Research Record,* 2672 (28), 404-415.

Zhang, H., Anupam, K., Scarpas, A., Kasbergen, C. & Erkens, S., 2019. Effect of stone-on-stone contact on porous asphalt mixes: Micromechanical analysis. *International Journal of Pavement Engineering*, 1-12.

8

Conclusions and Recommendations

8.1 Conclusions

The motivation for this research was to develop a fundamental understanding of the bitumen-rubber interaction mechanism, with a view to developing a set of tools and methodologies that can be used to optimize the design of crumb rubber modified bitumen and to predict its properties.

In this dissertation, the interaction mechanism between bitumen and rubber was reviewed from the viewpoint of polymer science; both experimental and numerical investigations of rubber swelling in bitumen were performed; the preparation procedures of CRMB were optimized and its chemo-physio-mechanical properties were characterized; long-term performance of binders were systematically evaluated; micromechanical models were used to predict the viscoelastic properties of binders. On the basis of these, the following conclusions regarding the research questions proposed in Chapter 1 can be drawn.

8.1.1 Bitumen-rubber interaction mechanism

This part intends to answer RQ1. The interaction between rubber and bitumen plays a very important role in controlling the properties of rubberized bituminous binders. From the viewpoint of polymer science, in the binary binder system, bitumen can be regarded as the low-molecular-weight solvent while rubber can be regarded as the polymer with high molecular weight. The bitumen-rubber interaction at high temperatures is generally a rubber dissolution process (which consists of swelling and chain disentanglement) and a chemical degradation process. In principle, the rubber swelling process can be systematically modelled by the Flory-Rehner theory in combination with the diffusion theory. The chain disentanglement of the swollen polymer network is a subsequent process to swelling. The chemical degradation of rubber in bitumen mainly includes the chain scission reactions which are observed as devulcanization and depolymerization. Admittedly, it is of great difficulty to do quantitative analysis on the model in the context of rubber swelling in bitumen since both rubber and bitumen are very complex systems instead of pure substances. However, the fundamental knowledge in polymer-solvent interaction is still of great importance to understand the interaction process and guide the material selection and process optimization to obtain desired binder properties.

The effects of interaction conditions (temperature, time and mixing energy) and raw material characteristics (rubber type, particle size, particle content, pre-treatment, etc.) were analysed based on the proposed theoretical framework in subsection 2.4. These critical factors can fundamentally alter the bitumen-rubber interaction parameters, and consequently the binder properties. In view of the diversity of raw materials (bitumen and rubber) and varying demands of binder properties, it is difficult to draw any universal conclusion. However, the following recommendations are made in terms of specific application scenarios.

- Temperature is the dominant factor that determines the product type of rubberized binders. Different CRMB products can be produced by manipulating the interaction temperature ranges which correspond to different interaction mechanisms.

- To maximize the swelling effect of rubber in bitumen, bitumen with more maltenes (soft grade bitumen) and tire rubber with high natural rubber components should be chosen to create similarity in solubility parameters.

- Devulcanized rubber is encouraged to be used in bitumen modification to eliminate the acrid smell and to improve the mechanical property and storage stability of rubberized binders.

8.1.2 Rubber swelling in bitumen

This part intends to answer RQ2. Various laboratory tests were carried out to investigate the kinetics of bitumen diffusion into cylindrical rubber samples cut from scrap truck tires, the equilibrium swelling characteristics of rubber and the mechanical properties of rubber before and after swelling at different high temperatures.

- Through FTIR results, no rubber dissolution (or too inconspicuous to be detected) during interaction with naphthenic oil takes place in the temperature range from 160 to 200 °C. This supports that rubber did not dissolve into bitumen in the same temperature range. Aliphatic compounds from bitumen preferentially diffused into rubber during the swelling process.

- Through bitumen sorption tests, the corrected diffusion coefficients of Pen 70/100 bitumen into truck tire rubber are determined as 15.15×10^{-6}, 37.87×10^{-6} and 109.12×10^{-6} mm^2/s at 160, 180 and 200 °C, respectively. The diffusion coefficient increases with the increase of temperature in an Arrhenius form.

- The volume expansion of rubber during swelling was captured by the CT scan images. Rubber swells faster at the earlier stages then the expansion rate slows down. The swelling ratio of rubber increased from 1.97 at 160 °C to 3.03 at 200 °C after 36 h interaction.

- Through DSR tests, swollen rubber becomes softer compared to the dry rubber and exhibits obvious viscoelastic behaviors. With the increase of temperature, the softening and viscous effect are more significant.

A coupled diffusion-expansion model was developed to address the multiphysics of swelling which consists of mass diffusion and volume expansion. In this model, a one-way coupling was introduced between concentration and mechanics to predict the swelling behavior of rubber in bitumen.

- There is a good correlation between the simulation results and the previously reported experimental results. The developed model can effectively predict the swelling behavior of rubber in bitumen.

- Under the same condition, truck-tire rubber can absorb more bitumen and cause more swelling than car-tire rubber.

- Temperature is a crucial factor affecting the swelling process. With the increase of temperature, the diffusion coefficient increases and the equilibrium swelling time decreases.

- In general, high penetration grade bitumen with higher aromatic fractions is more compatible with rubber and therefore increases the swelling extent of rubber.

- Under the same condition, small rubber particles swell faster and reach the equilibrium swelling at an earlier stage than large rubber particles.

- Rubber particle concentration seems have no effects on the swelling in this simulation.

8.1.3 CRMB preparation and property characterization

This part intends to answer RQs 3&4. Rheological and chemical characterization on CRMB binders prepared at different mixing conditions was carried out to determine the optimized interaction condition. Warm-mix additives (wax-based) were incorporated in CRMB using different procedures. The influence of preparation procedure on CRMB containing warm-mix additives was investigated from both rheological and thermal characteristics.

- The bitumen-rubber interaction is highly mixing temperature and time-dependent. With the increase of interaction temperature, the swelling and degradation of rubber particles successively occurred.
- The optimum bitumen-rubber interaction condition was determined at the mixing temperature of 180°C for 30 min, which produces CRMB binders with a lower non-recoverable compliance and a higher percent recovery.
- In terms of the incorporation of warm-mix additives, both types of warm-mix additives were added to the prepared CRMB using the hot-mix method for the current study.

The rheological behaviour and its chemical interpretation from the perspective of activation energy and molecular weight distribution were also investigated.

- CRMB and binders with wax additives show apparent shear-thinning behaviours at certain temperatures. The incorporation of CRM into base bitumen dramatically increases the complex viscosity. It also improves the rheological properties of base bitumen with enhanced stiffness and elasticity provided by the cross-linking polymer network. Wax-based additive increases the complex viscosity and complex modulus, and decreases the phase angle of bitumen due to the stiffening effect of the unique microcrystalline lattice structure at service temperatures. The chemical type of the additive has an insignificant effect on the rheological properties at the in-service temperatures.
- Binders modified by either CRM or wax-based additive have decreased flow activation energies, indicating lower thermal susceptibility. The higher CRM content, the lower activation energy of binder can be achieved.
- The phase-angle inversion method provides adequate and comparable molecular weight distributions, and this simply implemented method offers new perspectives in the interpretation of rheological data to monitor the change in the molecular structure of bitumen. Both CRM and the wax-based additive increased the average molecular weight of bitumen. The chemical-based additive had an insignificant effect on the molecular weight distribution of bitumen.

8.1.4 Binder performance evaluation of CRMB

This part intends to answer RQ5. A unified DSR method with different instrument accessories (4-, 8- and 25-mm diameter plates) was used for binder performance characterization from low to high temperatures.

- CRMB binders have superior rutting, fatigue, and thermal cracking resistance due to rubber modification. The improvement of high-, intermediate- or low-temperature performance is more prominent at higher rubber concentrations.

- Warm-mix additives have different effects on high-, intermediate- or low-temperature performance. Generally, the wax-based additive improves the rutting resistance while has adverse effects on the intermediate- and low-temperature performance. By contrast, chemical-based additive slightly impairs the high-temperature rutting resistance while improves the intermediate- and low-temperature performance.

- In terms of the critical cracking temperature, the low-temperature PG of 70/100 based binders is creep stiffness controlled while CRMB binders are *m*-value controlled. Rubber modification changes the controlling mechanism of low-temperature performance.

- The stiffening of the bitumen phase and the inclusion of swollen rubber particles in the bitumen matrix together contribute to the peculiar viscoelastic response of CRMB, i.e., stiffer and more elastic at high temperatures, softer and more elastic at low temperatures. This modification mechanism explains the superior rutting and thermal cracking resistance of CRMB.

The aging characteristics and storage stability of CRMB were also investigated.

- During the aging process, the aliphaticity index of all binders decreased but the reduction was insignificant. The aromaticity index of neat bitumen increased with the aging extent, while the aromaticity of all the CRMB binders first decreased after the short-term aging then increased after long-term aging. Both carbonyl and sulfoxide indices for each binder increased during aging. However, CRMB binders produced less carbonyl and sulfoxide functional groups than neat bitumen did after aging. The decrease in the oxidation products was intensified with the increase of CRM content.

- Aging causes the binder to become stiffer and alters the rheological properties of all binders, i.e., increase in complex modulus, decrease in phase angle, decrease in non-recoverable creep compliance and increase in recovery ability.

- The addition of CRM into bitumen improved the aging resistance as reflected by the lower carbonyl and sulfoxide indices as well as after aging the less changed rheological parameters of CRMB comparing to neat bitumen. CRMB with higher CRM content showed higher resistance against aging, and thus against stiffening and embrittlement.

- The non-recoverable creep compliance and percent recovery from MSCR tests show better correlations with the combined chemical aging index (sum of carbonyl and sulfoxide indices) than the parameters derived from the linear viscoelastic region do.

- The mechanical (or other) parameters of fresh CRMB binders cannot be used as a reference in the separation index to evaluate the stability after storage because bitumen-rubber interaction and aging may continue occurring during the storage period. Instead, a parameter taken from the stored samples can serve this purpose.

- Separation indices developed from both MSCR test and CT scan test results reveal that CRMB with a higher rubber content is more storage stable than CRMB with a lower rubber content. The incorporation of both warm mix additives is detrimental to the storage stability of CRMB. Based on the results in this study, it is not suggested to add warm mix additives into CRMB during the storage or transport stage.

- When the bitumen-rich phase and rubber-rich phase of CRMB exhibit similar mechanical behaviours, which can be called dynamic symmetry, CRMB will be storage stable. The

dynamic asymmetry between binder components drives the phase separation behaviour of CRMB. It is possible to manipulate raw material properties and interaction conditions to achieve the desired crossover between two phases of CRMB and hence obtain a storage-stable CRMB blend.

8.1.5 Micromechanical modelling for predicting viscoelastic properties of CRMB

This part intends to answer RQ6. A two-stage study on the micromechanical modelling of CRMB was conducted to predict the viscoelastic properties of CRMB. The first-stage study aims to predict the complex modulus of CRMB with more representative constituent parameters.

- The liquid phases of CRMB binders (real bitumen matrices) are stiffer and more elastic than the neat bitumen as reflected by the increased complex modulus and decreased phase angle.
- Dry rubber exhibits obvious elastic behaviors whose complex modulus and phase angle are almost frequency independent. Swelling significantly alters the rubber properties, making it softer and more viscous.
- Estimated from the numerical swelling model, the volume concentration of rubber after mixing with bitumen increases to 2.126 times as the blended rubber percentage.
- Using the liquid phase of CRMB binder and swollen rubber properties as the micromechanical model input yields more accurate predictions. The used four micromechanical models predict well at higher frequencies while underestimating the complex modulus at lower frequencies. Among the four used models, GSCM has the highest prediction accuracy.

The second-stage study aimed to further improve the prediction accuracy by amending the GSCM which performs best among the current micromechanical models.

- Mathematical model calibration is simple and efficient to achieve high prediction accuracy. Its disadvantage is the lack of universality and explanation for fundamental mechanisms. It needs to be re-calibrated for every new type of CRMB.
- The (n+1)-phase models considering the multilayer properties of rubber as input slightly increase the prediction accuracy, especially at intermediate frequencies. However, the underestimation of complex modulus at lower frequencies by these models remains.
- The polymer chain entanglement effect accounts for the underestimation of complex modulus and lack of elasticity (overestimation of phase angle) for CRMB at high temperatures/low frequencies.
- The mechanical properties of bitumen matrix and entangled polymer network can be predicted based on the rubber content.
- The introduction of the entangled polymer network to the GSC model significantly improved the prediction accuracy for both complex modulus and phase angle in the whole frequency range.

8.2 Recommendations

The performance of CRMB is governed by a set of parameters such as raw material properties (e.g., bitumen type and composition, rubber type, particle size, gradation and dosage), interaction conditions and whether additives were incorporated. The variability of the aforementioned parameters introduces a high level of complexity to the problem and causes additional difficulties in optimizing the design of CRMB. In the following, recommendations are made for the

continuation of this research on the basis of the obtained results. Moreover, general guidelines and suggestions are given for practitioners.

8.2.1 Recommendations for future research

- In this research, the Flory-Rehner theory was used to qualitatively explain the rubber swelling process in bitumen. Quantitative analysis can be performed on the blend of pure rubber materials (i.e., nature rubber and SBR) and typical bitumens given that interaction parameters can be accurately obtained. Besides, the main focus of this research is on the traditional wet-processed CRMB. Terminal blend type CRMB, which has gained more and more interests, should be systematically investigated with emphasis on the chemical degradation process (devulcanization and depolymerization).
- In terms of rubber swelling test, further research can be extended to more material combinations (e.g., bitumen with different chemical compositions and car tire rubber) to establish a database of interaction parameters (e.g., diffusion coefficients, swelling coefficients). The non-Fickian diffusion behaviours of bitumen into rubber may be addressed. The multilayer structure of swollen rubber is worth to be further investigated with more advanced characterization tools.
- Spherical rubber particles were assumed in the developed 2-D numerical model. The microstructure of real CRMB samples considering the geometrical properties and configuration of rubber particles can be implemented in the numerical model through 3-D reconstruction of X-ray CT scan images. A coupled diffusion-flow model can be developed to consider the fluid flow phenomena in the CRMB blend due to mixing in reality.
- GPC tests for various types of asphalt binders at both unaged and aged states should be conducted to produce a more accurate calibration equation for the phase angle inversion method.
- This research used different fatigue failure criteria for analyzing the TS and LAS test results, a unified failure criterion (e.g., PSE-based analysis) can be applied to the analysis process of both tests in the future. Fatigue performance at the mastic and mixture levels should be also evaluated to verify the findings at the binder level.
- Future research should be undertaken to investigate the aging effects on the chemo-physical properties of rubber polymer in bitumen and the possible rule of carbon black to have a better understanding of the aging mechanism of CRMB. Then, the rejuvenation of aged CRMB can be done accordingly.
- Practical methods (e.g., adding chemical compounds and surface treatment of CRM) can be applied to further improve storage stability of CRMB after considering the findings in this study.
- More mechanistic-empirical relationships between raw material parameters (i.e., base bitumen properties, dry rubber particle properties, rubber content) and interacted material parameters in CRMB at given conditions (i.e., bitumen matrix properties, rubber inclusion properties and effective rubber content) can be established to ensure a more efficient and more accurate viscoelastic property prediction framework for CRMB.

8.2.2 Recommendations for practitioners

There are several types of CRMB products available in the market and have been used in different engineering practices. For given raw material combinations (bitumen and rubber), there is no

exclusive optimized condition for preparing CRMB. The optimized preparation conditions really depend on the desired properties of CRMB from the practitioners, for instance, maximized mechanical properties, storage stable, etc. Based on the findings of this research, it has been established that the bitumen-rubber interaction governs the properties and performance of CRMB. Through material selection and preparation procedure optimization, practitioners can control or dictate the property development of CRMB by controlling the bitumen-rubber interaction. For example, generally speaking, rubber swelling should be maximized to achieve high-viscosity and better mechanical properties of CRMB. By contrast, chemical degradation of rubber should be dominated to achieve a storage stable CRMB system.

Moreover, nowadays, more and more sustainable materials and technologies have been applied in the pavement practice, such as warm mix asphalt (WMA), recycled asphalt pavement (RAP), etc. The use of these materials can reduce the energy consumptions and reserve more natural resources. Nevertheless, the introduction of these materials necessitates an understanding of their roles in affecting the bitumen-rubber interaction, so that the desirable characteristics are attained without compromising or even improving the properties of CRMB.

Therefore, it is recommended that the determination of bitumen-rubber interaction parameters (e.g., solubility parameters, diffusion coefficients, swelling coefficients, dissolution rates, etc.) should become part of the standard practice in the rubberized asphalt industry. To this end, the pavement engineering community should focus on the development of easily implementable testing protocols, similar to those available for bitumen grading tests, which designate the test conditions, sample preparation and provide the analytical tools to determine the parameters related to bitumen-rubber interaction. This information can serve as a screening tool for the selection of tire rubber, bitumen, as well as modifiers and additives, hence enabling the development of CRMB binder designs with improved and desired characteristics. The obtained interaction parameters also give insights into the engineering performance of CRMB, such as high-, intermediate- and low-temperature performance, aging resistance, storage stability, etc. More importantly, once this information becomes available, practitioners can use the proposed viscoelastic property prediction framework for CRMB to predict the mechanical properties of CRMB with minimized laboratory efforts. The predicted viscoelastic properties can thereafter be used as an input for a better mix design.

Furthermore, with the development of devulcanization technologies in rubber industry, devulcanized rubber is encouraged to be used in bitumen modification to eliminate the acrid smell and to improve the mechanical property and storage stability of rubberized binders.

Appendix I

Dilute model

The main equations related to the Dilute model are listed below:

$$\mathbf{A}_r{}^{\mathrm{DM}} = [\mathbf{I} + \mathbf{S}_b : (\mathbf{C}_b)^{-1} : (\mathbf{C}_r - \mathbf{C}_b)]^{-1} \qquad\qquad \text{I.1}$$

$$\mathbf{C}_c = \mathbf{C}_b + \phi(\mathbf{C}_r - \mathbf{C}_b) : \mathbf{A}_r \qquad\qquad \text{I.2}$$

with

$$\mathbf{S}_b = \frac{3K_b}{3K_b + 4G_b}\mathbf{I}^{\mathrm{v}} + \frac{6(K_b + 2G_b)}{5(3K_b + 4G_b)}\mathbf{I}^{\mathrm{d}} \qquad\qquad \text{I.3}$$

and

$$\mathbf{C}_b = 3K_b\mathbf{I}^{\mathrm{v}} + 2G_b\mathbf{I}^{\mathrm{d}} \qquad\qquad \text{I.4}$$

$$\mathbf{C}_r = 3K_r\mathbf{I}^{\mathrm{v}} + 2G_r\mathbf{I}^{\mathrm{d}} \qquad\qquad \text{I.5}$$

$$\mathbf{C}_c = 3K_c\mathbf{I}^{\mathrm{v}} + 2G_c\mathbf{I}^{\mathrm{d}} \qquad\qquad \text{I.6}$$

From the definitions of $\mathbf{I}^{\mathrm{v}}$ and $\mathbf{I}^{\mathrm{d}}$ defined in Equation (7.15), it can be found these two four-order isotropic tensors satisfy the following relation for the double dot product:

$$\mathbf{I}^{\mathrm{v}} : \mathbf{I}^{\mathrm{v}} = \mathbf{I}^{\mathrm{v}}; \ \mathbf{I}^{\mathrm{d}} : \mathbf{I}^{\mathrm{d}} = \mathbf{I}^{\mathrm{d}}; \ \mathbf{I}^{\mathrm{v}} : \mathbf{I}^{\mathrm{d}} = \mathbf{0}; \ \mathbf{I}^{\mathrm{d}} : \mathbf{I}^{\mathrm{v}} = \mathbf{0}; \text{and } \mathbf{I}^{\mathrm{v}} + \mathbf{I}^{\mathrm{d}} = \mathbf{I} \qquad \text{I.7}$$

Therefore, substituting Equations (I.3), (I.4) and (I.5) into Equation (I.1), we can obtain

$$\mathbf{A}_r{}^{\mathrm{DM}} = \left\{ \mathbf{I} + \left[\frac{3K_b}{3K_b + 4G_b}\mathbf{I}^{\mathrm{v}} + \frac{6(K_b + 2G_b)}{5(3K_b + 4G_b)}\mathbf{I}^{\mathrm{d}} \right] : \left(\frac{1}{3K_b}\mathbf{I}^{\mathrm{v}} + \frac{1}{2G_b}\mathbf{I}^{\mathrm{d}} \right) : \left[(3K_r - 3K_b)\mathbf{I}^{\mathrm{v}} + (2G_r - 2G_b)\mathbf{I}^{\mathrm{d}} \right] \right\}^{-1} \quad \text{I.8}$$

$$= \left\{ \mathbf{I} + \left[\frac{1}{3K_b + 4G_b}\mathbf{I}^{\mathrm{v}} + \frac{3(K_b + 2G_b)}{5(3K_b + 4G_b)G_b}\mathbf{I}^{\mathrm{d}} \right] : \left[(3K_r - 3K_b)\mathbf{I}^{\mathrm{v}} + (2G_r - 2G_b)\mathbf{I}^{\mathrm{d}} \right] \right\}^{-1}$$

$$= \left\{ \mathbf{I}^{\mathrm{v}} + \mathbf{I}^{\mathrm{d}} + \left[\frac{3K_r - 3K_b}{3K_b + 4G_b}\mathbf{I}^{\mathrm{v}} + \frac{6(K_b + 2G_b)(G_r - G_b)}{5(3K_b + 4G_b)G_b}\mathbf{I}^{\mathrm{d}} \right] \right\}^{-1}$$

$$= \frac{3K_b + 4G_b}{3K_r - 3K_b + 3K_b + 4G_b}\mathbf{I}^{\mathrm{v}} + \frac{5(3K_b + 4G_b)G_b}{6(K_b + 2G_b)(G_r - G_b) + 5(3K_b + 4G_b)G_b}\mathbf{I}^{\mathrm{d}}$$

$$= \frac{3K_b + 4G_b}{3K_r + 4G_b}\mathbf{I}^{\mathrm{v}} + \frac{5(3K_b + 4G_b)G_b}{3K_b(2G_r + 3G_b) + 4G_b(3G_r + 2G_b)}\mathbf{I}^{\mathrm{d}}$$

Substituting Equation (I.8) into Equation (I.2) yields the following equation

$$3K_c\mathbf{I}^{\mathrm{v}} + 2G_c\mathbf{I}^{\mathrm{d}} = 3K_b\mathbf{I}^{\mathrm{v}} + 2G_b\mathbf{I}^{\mathrm{d}} + \phi[(3K_r - 3K_b)\mathbf{I}^{\mathrm{v}} + (2G_r - 2G_b)\mathbf{I}^{\mathrm{d}}] : \mathbf{A}_r \qquad \text{I.9}$$

$$3K_c\mathbf{I}^{\mathrm{v}} + 2G_c\mathbf{I}^{\mathrm{d}} = 3K_b\mathbf{I}^{\mathrm{v}} + 2G_b\mathbf{I}^{\mathrm{d}} + \phi\frac{(3K_b + 4G_b)(3K_r - 3K_b)}{3K_r + 4G_b}\mathbf{I}^{\mathrm{v}}$$

$$+ \phi\frac{5(3K_b + 4G_b)G_b(2G_r - 2G_b)}{3K_b(2G_r + 3G_b) + 4G_b(3G_r + 2G_b)}\mathbf{I}^{\mathrm{d}}$$

$$3K_c\mathbf{I}^{\mathrm{v}} + 2G_c\mathbf{I}^{\mathrm{d}} = \left[3K_b + \phi\frac{3(3K_b + 4G_b)(K_r - K_b)}{3K_r + 4G_b}\right]\mathbf{I}^{\mathrm{v}} + \left[2G_b + \phi\frac{10G_b(3K_b + 4G_b)(G_r - G_b)}{3K_b(2G_r + 3G_b) + 4G_b(3G_r + 2G_b)}\right]\mathbf{I}^{\mathrm{d}}$$

Therefore, extracting the terms corresponding to $\mathbf{I}^{\mathrm{v}}$ and $\mathbf{I}^{\mathrm{d}}$ respectively from above equation, we can obtain

$$K_c = K_b + \frac{\phi(K_r - K_b)(3K_b + 4G_b)}{3K_r + 4G_b} \qquad\qquad \text{I.10}$$

$$G_c = G_b + \frac{5\phi G_b(G_r - G_b)(3K_b + 4G_b)}{3K_b(2G_r + 3G_b) + 4G_b(3G_r + 2G_b)} \qquad\qquad \text{I.11}$$

Summary

A sustainable pavement, which can minimize environmental impacts through the reduction of energy consumption, natural resources and associated emissions while meeting all performance conditions and standards, is in urgent need to combat the climate change. The current scenario of depleting crude oil, reduced quarry zones, and stringent environmental regulations has driven the use of waste materials and by-products in pavement applications. The utilization of crumb rubber from scrap tires for bitumen modification has become a common engineering practice since last century.

The chemical and physical interaction between bitumen and rubber plays an important role not only in the property development of crumb rubber modified bitumen (CRMB), but also in its storage, transport, and construction. Besides, more and more sustainable materials and technologies, such as warm mix asphalt (WMA), have been applied in the pavement practice. Therefore, it is of vital importance to understand the interaction mechanisms between the constituent materials.

The motivation for this research was to develop a fundamental understanding of the bitumen-rubber interaction mechanism, with a view to developing chemo-physio-mechanical methodologies and test procedures that can be used to optimize the design of CRMB and to predict its properties.

After the introductory chapter, a literature review on bitumen-rubber system is carried out to provide the theoretical basis of following chapters. Laboratory swelling tests of rubber in bitumen determines the necessary parameters for the numerical rubber swelling model. The mass diffusion and volume expansion phenomena of the rubber are incorporated in a multiphysics model to predict the rubber swelling in bitumen. With the further understanding of bitumen-rubber interaction mechanisms, both experimentally and numerically, the preparation procedures of CRMB are optimized and its chemo-physio-mechanical properties are characterized. Furthermore, long-term performance of binders, which are concerned by practitioners, are evaluated systematically. Micromechanical modelling utilizes the previous determined parameters of constituents and provides a robust prediction of the viscoelastic properties. Finally, the thesis is concluded by providing a summary of findings and conclusions and giving an outlook for future research and practice to enable more successful and extensive applications of rubberized asphalt materials.

The experimental and modelling approaches discussed throughout this thesis are anticipated to represent a significant contribution towards the development of multiphysics methodologies for characterizing and modelling CRMB. The fundamental basis of these methodologies should then lend to the design optimization and performance prediction of other polymer modified binders in general.

Curriculum Vitae

Haopeng Wang 王昊鹏

Dec. 1991	Born in Huai'an, Jiangsu Province, China

Education

Aug. 2009 - Jun. 2013	Bachelor of Engineering (with Honour), Highway and Bridge Engineering
	School of Transportation, Southeast University, China
Sep. 2013 - Jun. 2016	Master of Science, Highway and Railway Engineering
	School of Transportation, Southeast University, China
Sep. 2016 - Sep. 2021	PhD candidate, Pavement Engineering
	Faculty of Civil Engineering and Geosciences, Delft University of Technology, The Netherlands
Oct. 2020 - Sep. 2021	Visiting PhD student, Pavement Engineering
	Department of Civil and Environmental Engineering, The Hong Kong Polytechnic University, Hong Kong

Awards

2018	*Best Poster Award*
	The 8th International Association of Chinese Infrastructure Professionals (IACIP) Annual Meeting 2018, Washington D.C., USA
2019	*Best Presentation Award*
	The 8th International Transportation PhD Student Symposium, Aachen, Germany
2020	*Outstanding Graduate Student Award*
	International Association of Chinese Infrastructure Professionals (IACIP)
2021	*Outstanding Service by a Student Member Award*
	Academy of Pavement Science and Engineering (APSE)
2021	*Outstanding Graduate Student Award*
	Wang Binggang Foundation
2021	*Marie Skłodowska-Curie Individual Fellowships*
	Horizon 2020, European Commission

List of relevant publications

Journal Publications

1. **Wang, H.**, Liu, X., Apostolidis, P., Wang, D., Leng, Z., Lu, G., Erkens, S. and Skarpas, A. (2021). Investigating the High- and Low-temperature Performance of Warm Crumb Rubber Modified Bituminous Binders using Rheological Tests. *Journal of Transportation Engineering, Part B: Pavements*. DOI: 10.1061/JPEODX.0000326 (*Q2*)

2. **Wang, H.**, Liu, X., Varveri, A., Zhang, H., Erkens, S., Skarpas, A., and Leng, Z. (2021). Thermal aging behaviors of the waste tire rubber used in bitumen modification. *Progress in Rubber Plastics and Recycling Technology*. DOI: 10.1177/14777606211038951 (*Q4*)

3. **Wang, H.**, Zhang, H., Liu, X., Skarpas, A., Erkens, S., and Leng, Z. (2021). Micromechanics-based complex modulus prediction of crumb rubber modified bitumen considering interparticle interactions. *Road Materials and Pavement Design*, 22, sup1, 1-18. *(Q1)*

4. **Wang, H.**, Liu, X., Apostolidis, P., Erkens, S., Skarpas, A. and Zhu, J. (2020). The Role of Thermodynamics and Kinetics in Rubber-Bitumen Systems: A Theoretical Overview. *International Journal of Pavement Engineering*. *(Q1)*

5. **Wang, H.**, Liu, X., Apostolidis, P., van de Van, M., Erkens, S. and Skarpas, A. (2020). Effect of Laboratory Aging on Chemistry and Rheology of Crumb Rubber Modified Bitumen. *Materials and Structures*, 53, 26. *(Q2)*

6. **Wang, H.**, Liu, X., Erkens, S. and Skarpas, A. (2020). Experimental Characterization of Storage Stability of Crumb Rubber Modified Bitumen with Warm-mix Additives. *Construction and Building Materials*, 249, 118840. *(Q1)*

7. **Wang, H.**, Liu, X., Apostolidis, P., Erkens, S. and Skarpas, A. (2020). Experimental Investigation of Rubber Swelling in Bitumen. *Transportation Research Record: Journal of the Transportation Research Board*, 2674(2), 203-212. *(Q3)*

8. **Wang, H.**, Liu, X., Zhang, H., Apostolidis, P., Erkens, S. and Skarpas, A. (2020). Micromechanical Modeling of Complex Shear Modulus of Crumb Rubber Modified Bitumen. *Journal of Materials and Design*, 188, 108467. *(Q1)*

9. **Wang, H.**, Liu, X., van de Van, M., Lu, G., Erkens, S. and Skarpas, A. (2020). Fatigue performance of long-term aged crumb rubber modified bitumen containing warm-mix additives. *Construction and Building Materials,* 239, 117824. *(Q1)*

10. **Wang, H.**, Liu, X., Apostolidis, P., Erkens, S. and Scarpas, T. (2019). Numerical investigation of rubber swelling in bitumen. *Construction and Building Materials,* 214, 506-515. *(Q1)*

11. **Wang, H.**, Lu, G., Feng, S., Wen, X. and Yang, J. (2019). Characterization of Bitumen Modified with Pyrolytic Carbon Black from Scrap Tires. *Sustainability,* 11(6), 1631. *(Q2)*

12. **Wang, H.**, Liu, X., Zhang, H., Apostolidis, P., Scarpas, T. and Erkens, S. (2018). Asphalt-rubber interaction and performance evaluation of rubberised asphalt binders containing non-foaming warm-mix additives. *Road Materials and Pavement Design*, 1-22. *(Q1)*

13. **Wang, H.**, Liu, X., Apostolidis, P. and Scarpas, T. (2018). Non-Newtonian Behaviors of Crumb Rubber-Modified Bituminous Binders. *Applied Sciences,* 8(10), 1760. *(Q2)*

14. **Wang, H.**, Liu, X., Apostolidis, P. and Scarpas, T. (2018). Review of warm mix rubberized asphalt concrete: Towards a sustainable paving technology. *Journal of Cleaner Production,* 177, 302-314. *(Q1)*

15. **Wang, H.**, Liu, X., Apostolidis, P. and Scarpas, T. (2018). Rheological Behavior and Its Chemical Interpretation of Crumb Rubber Modified Asphalt Containing Warm-Mix Additives. *Transportation Research Record: Journal of the Transportation Research Board,* 2672(28), 337-348. *(Q3)*

16. Zhu, J., Balieu, R. and **Wang**, H. (2019). The use of solubility parameters and free energy theory for phase behaviour of polymer-modified bitumen: a review. *Road Materials and Pavement Design*, 1-22. *(Q1)*

Refereed Conference Publications

1. **Wang, H.**, Apostolidis, P., Zhang, H. Liu, X., Erkens, S. & Scarpas, A. (2020). Dissolution simulation of polymers in bitumen. In Advances in Materials and Pavement Prediction (AM3P 2020), August 5-7, 2020, San Antonio, Texas, US.

2. **Wang, H.**, Jirawat, B., Liu, X., Erkens, S. and Skarpas, A. (2019) Experimental characterization of storage stability of crumb rubber modified bitumen. In the 8th European Asphalt Technology Association Conference (EATA 2019), June 3-5, 2019, Granada, Spain.

3. **Wang, H.**, Apostolidis, P., Liu, X. and Scarpas, A. (2018) Modeling of rubber swelling in bituminous binders. Proceedings of Advances in Materials and Pavement Performance Prediction (AM3P 2018), April 16-18, 2018, Doha, Qatar.

Editor of Books

1. Chen, X., Yang, J., Oeser, M., and **Wang, H.** (Eds.). (2020). Functional Pavements: Proceedings of the 6th Chinese-European Workshop on Functional Pavement Design (6th CEW 2020, October 18-21, 2020, Nanjing, China). CRC Press.

Propositions

Associated with the dissertation

Crumb rubber modified bitumen: Experimental characterization and modelling

of

Haopeng WANG

1. The chemical and physical interaction between bitumen and rubber, or polymers in general, governs the property development of modified binders. It is possible to achieve desired binder properties by properly selecting the production conditions.
   This proposition pertains to this dissertation [Chapter 5].
2. Measuring rheological properties of binders helps us bridge the gap between molecular structure and binder performance.
   This proposition pertains to this dissertation [Chapter 5].
3. Performance based specifications for binders are only appreciated when the development of material models is matured. For example, linear viscoelastic properties of binders are inadequate to characterize the high-temperature performance, which involves plastic damage.
   This proposition pertains to this dissertation [Chapter 6].
4. The accuracy of micromechanics model inputs is of vital importance to the model prediction accuracy. This is problematic, since measuring these inputs accurately is challenging.
   This proposition pertains to this dissertation [Chapter 7].
5. As a researcher, when you believe you know everything in your field, it is time to read more literature.
6. Comparing to other disciplines, the general public as well as funding agencies have underestimated the importance of pavement engineering, so do pavement engineers.
7. To advance pavement engineering as an academic discipline, science must be put prior to engineering in research efforts.
8. Multidisciplinary research is very popular at the moment, but it is only meaningful when the researcher really comprehends the different disciplines.
9. "Nothing in life is to be feared, it is only to be understood. Now is the time to understand more, so that we may fear less." [*Marie Skłodowska Curie*]
10. Climate change is real but should not be used for political gain.

These propositions are regarded as opposable and defendable, and have been approved as such by the promotors Prof. dr. ir. S.M.J.G. Erkens and Prof. dr. A. Scarpas, and co-promotor Dr. X. Liu.